Role and regulation of the p53-homolog p73 in the transformation of normal human fibroblasts

Dissertation zur Erlangung des
naturwissenschaftlichen Doktorgrades
der Bayerischen Julius-Maximilians-Universität Würzburg

vorgelegt von
Lars Hofmann

aus
Aschaffenburg

Würzburg 2007

Eingereicht am

Mitglieder der Promotionskommission:
Vorsitzender: Prof. Dr. Dr. Martin J. Müller
Gutachter: Prof. Dr. Michael P. Schön
Gutachter : Prof. Dr. Georg Krohne

Tag des Promotionskolloquiums:

Doktorurkunde ausgehändigt am

Erklärung

Hiermit erkläre ich, dass ich die vorliegende Arbeit selbständig angefertigt und keine anderen als die angegebenen Hilfsmittel und Quellen verwendet habe. Diese Arbeit wurde weder in gleicher noch in ähnlicher Form in einem anderen Prüfungsverfahren vorgelegt. Ich habe früher, außer den mit dem Zulassungsgesuch urkundlichen Graden, keine weiteren akademischen Grade erworben und zu erwerben gesucht.

Würzburg,

Lars Hofmann

Content

Summary

The prototyical tumor suppressor p53 is able to arrest cells after DNA damage or as a response to oncogene expression. The transactivation-competent (TA) isoforms of the more recently discovered p53 family member p73 also prevent tumors, but the underlying mechanisms are less well understood. The work presented here addressed this issue by using a cell culture model of tumorigenesis in which normal human diploid fibroblasts are stepwise transduced with oncogenes. Cells in pretransformed stages were shown to harbour high levels of TAp73 mRNA and protein. This positive regulation was probably a result of pRB inactivation and derepression of E2F1, a key activator of TAp73. Consequences for such cells included an increased sensitivity to the cytostatic drug adriamycin, slower proliferation and reduced survival at high cell density, as demonstrated by rescue experiments using siRNA-mediated knockdown of TAp73. In order to identify potential effector pathways, the gene expression profile of siRNA treated, matched fibroblast cell lines with high and low TAp73 levels were compared in DNA microarrays. These findings support the notion of TAp73 up-regulation as an anti-proliferative defense mechanism, blocking the progress towards full transformation. This barrier could be overcome by the introduction of a constitutively active form of Ras which caused a switch from TAp73 to oncogenic ΔNp73 expression, presumably through the phosphatidylinositol 3-kinase (PI3K) pathway. In summary, the results presented emphasize the tumor-suppressive function of TAp73 and indicate that its downregulation is a decisive event during the transformation of human cells by oncogenic Ras mutants.

Zusammenfassung

Der gut untersuchte Tumorsuppressor p53 vermag das Wachstum von Zellen nach DNA-Schädigung oder Onkogenaktivierung zu arretieren. Die transaktivierungsfähigen (TA) Isoformen von p73, eines kürzlich entdeckten Mitgliedes der p53-Familie, können ebenfalls die Tumorentstehung verhindern. Die Mechanismen sind hier aber noch sehr unvollkommen verstanden. Zu deren Untersuchung wurde in der vorliegenden Arbeit ein Zellkulturmodell der Tumorentstehung verwendet, bei dem normale humane diploide Fibroblasten schrittweise mit bestimmten Onkogenen transduziert wurden. Zellen in unvollständig transformierten Stadien hatten hohe Spiegel an TAp73-mRNA und -Protein. Diese positive Regulation war vermutlich eine Folge von pRB-Inaktivierung und der Derepression von E2F1, einem der wichtigsten Aktivatoren von TAp73. Beobachtete Konsequenzen für solche Zellen waren höhere Empfindlichkeit für Zytostatika wie Adriamycin, langsameres Wachstum und geringere Überlebensfähigkeit bei hoher Zelldichte, was durch Rescue-Experimente mit siRNA-vermitteltem TAp73-Knock down gezeigt werden konnte. Um mögliche Effektor-Signalwege zu identifizieren, wurden die Genexpressionsprofile von siRNA-behandelten Fibroblastenlinien, die sich nur im TAp73-Spiegel unterschieden, in DNA microarrays verglichen. Die Befunde daraus lassen den Schluss zu, dass die Hochregulation von TAp73 einen antiproliferativen Schutzmechanimus darstellt, der die vollständige Transformation verhindert. Diese Barriere konnte überwunden werden durch die zusätzliche Präsenz von aktiviertem Ras, das einen Wechsel der Expression von TAp73 zu der von onkogenem ΔNp73 bewirkte. Dies ist vermutlich abhängig vom Phosphatidylinositol-Signalweg. Zusammenfassend wurde die Rolle von TAp73 als Tumorsuppressor weiter gefestigt, da die Niederregulierung des Proteins eine zentrale Rolle in der Transformation menschlicher Zellen durch onkogene Ras-Mutanten spielt.

1. Introduction

1.1. Molecular basics of cancer

Cancer is the general term for malignant neoplasia, which may be of epithelial (carcinomas; most common) or mesenchymal (sarcomas) origin. There are three main classes of conditions which may cause cancer in humans:

- Environmental factors (chemical mutagens, irradiation, UV light; but also nutrition, life style, social status, cultural practice, professional occupation etc.)
- Infections with viruses like human papilloma virus (HPV) or various herpes viruses causing Burkitt's lymphoma, Karposi sarcoma etc.
- Genetic disposition.

It is estimated that up to 90% of all cancers directly result from environmental factors (Boyle, 1999). All cancers, regardless of their causes, are derived from normal body cells which have been converted to tumor cells through a succession of several rare genetic events in a multistage process called (malignant) transformation.

Normal somatic cells have a limited replicative life span that is genetically determined (Hayflick limit). They are also restrained in their growth by contact with their extracellular milieu, that is, neighboring cells and stroma. On a statistical basis cells acquire mutations that make them grow better or, in terms of Darwinian evolution, confer on them a selective advantage. The afflicted genes almost always encode proteins involved in regulating cell proliferation, survival or DNA damage repair. The odds to acquire a transforming mutation are greatly increased in presence of the factors listed above. Accumulation of four to six such lesions in a human cell eventually gives rise to a macroscopic tumor (Dix, 1989; Fearon and Vogelstein, 1990). However, multiple mechanisms have arisen to forestall uncontrolled cell division (Lowe *et al.*, 2004). Some of these are devices within the cell, such as those that limit cell cycle progression, whereas others are social signals that prompt a cell to remain within its supportive microenvironment. Additionally, in a healthy individual and barring gross risk factors, transforming cells are detected and eliminated by the immune system. In combination, these tumor-suppressing mechanisms are remarkably effective; on average, cancers arise less than once in a human lifetime, despite trillions of potential target cells. For these reasons, cancer in humans usually develops over many decades and primarily correlates with old age (Peto *et al.*, 1975).

Today we know over a 100 different types of cancer. There are thousands of known molecular alterations associated with the malignant phenotype, and their number increases unabated

thanks to applications like genome-wide transcriptional profiling, proteomics, and functional genetic library screens (Balmain, 2001). Despite this complexity, there are a number of features that are shared by all cancer cells of solid tumors (**Fig. 1**) (reviewed in Hanahan and Weinberg, 2000). They exhibit deregulated growth uncoupled from external signals, unlimited replicative life span (immortality), and the ability to recruit blood vessels (angiogenesis). Cells at this stage are capable to form a mass called a benign tumor. The most aggressive, "malignant" neoplastic lesions are in addition invasive, i.e. the growing tumor breaks down tissue boundaries by spreading through adjacent basement membranes. Finally, single cells or small clusters disseminate, enter the blood stream or lymphatic system and form independent daughter tumors (metastases) close or distant to the original site.

Two more features might be added to the list as "accessory". First, already in early stages of transformation cancer cells are usually found in a state of genomic instability. This condition manifests itself in aneuploidy and/or chromosome translocations. It increases the mutability of tumor cell genomes and thus, greatly facilitates the acquisition of the six "main" characteristics (**Fig. 1**). Second, dysfunctional epigenetic control like aberrant DNA methylation or histone acetylation can also contribute to the tumorigenic process.

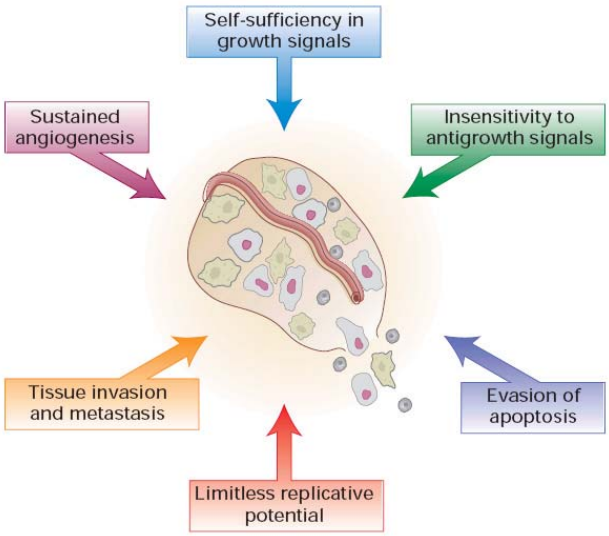

Fig. 1 The six "hallmarks of cancer". This set of capabilities is believed to be acquired by most, if not all types of human tumors, albeit through various mechanistic strategies. Modified after Hanahan & Weinberg (2000).

The development of similar traits in cancer cells irrespective of their origin is dictated by severe selective pressure imposed upon them by the host defense and the nutritional requirements of the growing tumor. This likeness gives rise to the hope that cancer pathology will not always be describable only in elaborate phenomenological terms, but there will be one day a unifying theory of transformation involving a limited number of affected regulatory pathways. Indeed,

from the copious wealth of scientific data collected over the past decades concepts have begun to emerge (Hahn and Weinberg, 2002b).

1.2. Early research on tumorigenesis

The history of molecular oncology dates back almost 100 years (Knudson, 2001). Theodor Boveri (1914) was the first to propose a genetic basis for cancer, an idea that was developed from his work in Würzburg on chromosomal abnormalities of somatic cells. Tumorigenesis was long thought to be a multi-step process. Research on its molecular foundation started in the 1960s with DNA tumor viruses such as polyoma virus, human papilloma virus (HPV) strains 16 and 18, simian virus 40 (SV40), and adenovirus. A few years later, in the early 1970s, attention was also paid to acutely transforming retroviruses. Theses early studies already demonstrated that transformation of individual cells could be achieved by a few defined genetic elements, which were called oncogenes. The evolutionary origin of oncogenes carried by the DNA tumor viruses is not clear. When rationalized functionally, it appears that these oncoproteins have evolved to interfere with host cell regulatory circuits in ways that favor viral replication. In uninfected cells, the same circuits regulate cell proliferation and survival. In contrast, the cancer-causing genes of retroviruses were found to be mutant versions of normal growth-controlling genes, which came to be called proto-oncogenes.

Although oncogenic viruses are responsible for only a small portion of human cancers, such studies of tumor virus-encoded proteins in experimental models of cellular transformation, both in animals and in cell culture, have revealed a number of critical intracellular signaling pathways that contribute to spontaneously arising cancers. However, while the value of mouse models for investigating the basic principals of tumorigenesis is undisputed (Balmain, 2002; Berns *et al.*, 1991; Hahn and Weinberg, 2002a), such studies have also revealed profound differences in the molecular tumor biology of the two species (reviewed in Rangarajan and Weinberg, 2003). These differences help to explain what was known already more than 20 years ago: rodent cells are much easier to transform than human cells. Instead of at least six alterations, primary murine cells require only a minimum of two (Land *et al.*, 1983; Rangarajan *et al.*, 2004). Deactivation of either the p53 or the $p16^{INK4a}$/Rb tumor suppressor pathway is an absolute requirement (Serrano *et al.*, 1997). The additional introduction of oncogenes like Ras (Kamijo *et al.*, 1997) or Raf plus Myc (Metz *et al.*, 1995) to permanently activate the Ras-Raf-MAP kinase pathway are sufficient to fully transform mouse cells. Without neutralization of p53 function, mouse cells respond to the introduced oncogenes by undergoing senescence (Serrano *et al.*, 1997).

Despite these successes in rodent models, the introduction of the pairs of oncogenes that transform rodent cells have consistently failed to transform primary human cells to a tumorigenic state. Such human cells only exhibited a limited proliferative capacity and either entered a state similar to replicative senescence or crisis. Senescence occurs upon proliferation of normal human cells and is characterized among other things by an irreversible growth arrest but continued metabolic activity (Dimri *et al.*, 1995; Goldstein, 1990). Having circumvented senescence, for example through SV40 LT expression (Shay and Wright, 1989), such cells continue to proliferate for a period of time but ultimately enter a crisis characterized by widespread cell death. It is now known that unlike murine cells, human cells must bypass these two barriers to become immortalized. They are presumably mounted to block the proliferation of mutant, oncogene-bearing cells. These responses also explain why the formation of a transformed cell clone often depends on the actions of a second introduced gene, the main function of which is to neutralize the antineoplastic defense mechanism that is triggered by the previously introduced one (Weinberg, 1997).

1.3. Developing cell culture models of tumorigenesis

The first and to the date only type of cancer where the etiology is known in detail on a genetic basis are colorectal tumors. In an exemplary investigation Vogelstein and colleagues delineated the events occurring in colon epithelial stem cells during their transformation (Vogelstein *et al.*, 1988). From these findings, a comprehensive model for colorectal carcinogenesis was developed which attempted to reconcile clinical progression with the common genetic changes that are found in the various stages of the disease (Fearon and Vogelstein, 1990). These most frequent changes are loss of the chromosome region containing the familial adenomatous polyposis (FAP), p53 and deleted in colorectal cancer (DCC) genes as well as mutation of the K-Ras gene. It was finally emphasized that decisive for the biological behavior of a colorectal tumor is the assembly of the genetic changes, not the chronological order in which they were acquired. This is regarded today as a universal principal in tumorigenesis (Hanahan and Weinberg, 2000).

However, extrapolations from cancer epidemiology and histopathology can hardly be expected to provide accurate measures of the number of genetic changes that are required to convert normal human cells into cancer cells. More compelling observations might derive instead from direct manipulation of human cells and their transformation into tumor cells (reviewed in Zhao *et al.*, 2004). The call for a "rather simple conceptual framework for understanding how the growth deregulation of cancer cells develops" (Weinberg, 1991) persisted.

The first report of a genetically defined cell culture model for the transformation of primary human cells was published from the group of Robert Weinberg in 1999 (Hahn *et al.*, 1999). They were able to change human embryonic kidney cells (HEK) and foreskin fibroblasts of the BJ strain into something which closely resembled cancer cells. The introduction of only three transforming factors, human telomerase (hTERT), the SV40 Early region (ER) encoding Large T (LT) and small t (st) antigen, and H-RasV12 (constitutively active H-Ras with the G12V point mutation), enabled HEK and BJ cells to grow in soft agar and form progressive tumors in nude mice (**Fig. 2**). Any other combination of two out of these three factors was either not tumorigenic (ER + hTERT) or not even viable due to the onset of senescence (hTERT + H-Ras) or crisis (ER + H-Ras). The transformed cell lines were of polyclonal origin, but the authors could exclude further genetic alterations by comparing cultured cells before and after their passage through nude mice. Polyclonality was preserved; morphology, telomere length, growth rate and tumorigenic potential were identical, demonstrating that no selection within the cell populations took place during tumor outgrowth. It was concluded that the introduction of hTERT, SV40 ER, and H-RasV12 sufficed to fully transform primary human cells.

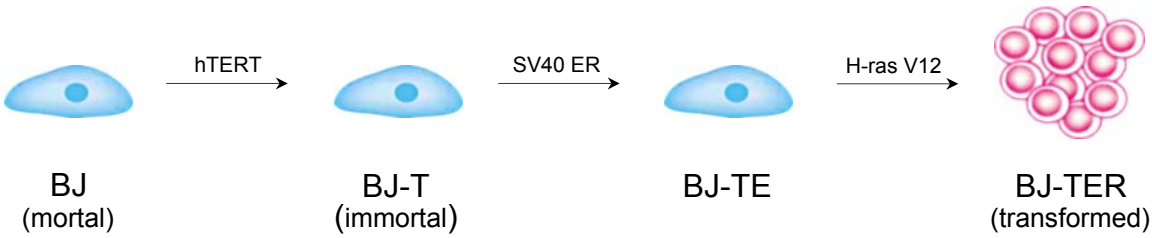

Fig. 2 Cell culture transformation of BJ normal human fibroblasts with defined genetic elements (after Hahn *et al.*, 1999). See text for details.

Fibroblasts like the BJ strain give rise to sarcomas. In 2001, the same group reported an analogous model for human breast carcinoma. They used the same genetic elements to turn human mammary epithelial cells (HMEC) into tumor cells (Elenbaas *et al.*, 2001). Interestingly, in all cases scrutinized a chromosomal rearrangement was detected which invariably resulted in a mild amplification of the c-Myc gene with concomitantly elevated c-Myc protein levels. This is in contrast to the outcomes with BJ and HEK, where no c-Myc activation was observed. It was agued this could reflect tissue-specific differences in the pathways required to be affected for tumorigenicity.

The role of the polypeptides encoded by the SV40 ER in the transformation of BJ and HEK cells was further investigated (Hahn *et al.*, 2002). When dissecting the contribution of the LT and st antigen, it became apparent that the relevant functions of LT are indeed limited to the

inhibition of the p53 and Rb pathway, while st appears to interfere with PP2A signaling (see sect. 1.4.3).

1.4. Key molecules in human cell transformation

The studies discussed above demonstrate that the immortalization and subsequent transformation of some, if not all, cultured human cells require the cooperation of at least four oncogenes. The pathways that are perturbed by the introduction of hTERT, H-Ras, SV40 st, and SV40 LT define a set of genetic changes that are sufficient to program the tumorigenic phenotype. It is worth noting that alterations in the affected principal pathways (p53, RB, Ras and telomerase) are commonly detected in a wide variety of human tumors. The four transforming agents employed in the model system are now discussed in more detail.

1.4.1. hTERT

Human cells lose about 50 to 100bp from the telomeric ends of their chromosomes with each division. This gradual loss of DNA has been implicated in the control of proliferative potential, since cells enter the state of senescence when their telomeres are reduced to a certain minimal length. The enzyme responsible to maintain telomeres is a ribonucleoprotein called telomerase (Harrington *et al.*, 1997; Meyerson *et al.*, 1997; Nakamura *et al.*, 1997). Most murine cells express constitutive telomerase activity (Prowse and Greider, 1995) and maintain extremely long telomeres (Kipling and Cooke, 1990). Unlike mice, adult somatic cells in humans normally do not express telomerase (Kim *et al.*, 1994). However, human tumors invariably have acquired means to protect their chromosome ends from erosion, approximately 90% of these by reactivated telomerase expression (Kim *et al.*, 1994), the remainder through a recombination process termed alternative lengthening of telomeres or ALT (Bryan *et al.*, 1997). In addition, evidence for yet other means to preserve telomere function are accumulating (Argilla *et al.*, 2004; Cerone *et al.*, 2005). This indicates that telomere maintenance is a crucial event in tumor progression and that human cancer cells must acquire this function (Granger *et al.*, 2002). The notion is supported that telomere attrition serves as a mechanism of tumor suppression (Masutomi and Hahn, 2003).

It has been pointed out that also primary cells need to be immortalized *in vitro* in some way prior to transformation (Rhim, 2000). Ectopic expression of the catalytic subunit of human telomerase, hTERT, has become the method of choice here (Bodnar *et al.*, 1998). While transformation per se is also possible in the absence of telomerase activity (Seger *et al.*, 2002), it is essential for tumor *progression* to restore and maintain genomic stability to an extent that permits cell survival. Indeed, transfection with LT alone or in combination with H-Ras is not

sufficient to circumvent crisis in BJ or HEK cells (Hahn *et al.*, 1999). On the other hand, moderate genomic instability with chromosome end-to-end fusion and subsequent telomerase activation actually favors the acquisition of tumorigenic changes (confer Komarova and Wodarz, 2004). Thus, telomere shortening and telomerase activation can act both to suppress and to facilitate tumor development, depending on the timing and context of these related events (Masutomi and Hahn, 2003).

1.4.2. H-RasV12

H-RasV12, a mutant allele of H-Ras (human gene = *HRAS1*), is a 21 kDa-protein which belongs to the Ras family of small GTP-binding proteins. H-Ras and the closely related K-Ras and N-Ras are found constitutively activated mutant forms in 20-30% of all human cancers (Downward, 2003; Shields *et al.*, 2000). Almost all Ras activation in tumors is accounted for by mutations in codons 12, 13 and 61. Amino acid substitutions at these sites, like the G12V mutant allele used in this project, prevent the hydrolysis of GTP, thereby rendering Ras constitutively active (Scheffzek *et al.*, 1997).

Ras proteins occupy overlapping but distinct functions in signal transduction. By stimulating the conversion of the Ras oncoprotein from an inactive GDP-bound to an active GTP-bound state, extracellular signals detected by cell-surface receptors can be transmitted to the cell. In the GTP-bound state, Ras stimulates downstream targets (effectors), which in turn affect numerous activities of the cell, such as proliferation, apoptosis, and differentiation (Shields *et al.*, 2000). In a normal cell the exchange of GDP for GTP is catalyzed by guanine nucleotide exchange factors (GEFs), while the conversion of bound GTP to GDP is facilitated by GTPase activating proteins (GAPs). It is the balance between these proteins that determines the activation state of Ras and its downstream target pathways.

There are at least ten different pathways that are known to be induced by Ras (for an overview, see Malumbres and Barbacid, 2003). The reason why there are so many effectors is because Ras most likely utilizes distinct sets in combinatorial fashion to effect its diverse biological actions. Ras causes a diverse spectrum of responses, the outcome depending on cell type. Fibroblasts and epithelial cells, and rodent and human cells, differ for instance greatly in their susceptibility to transformation. In turn, the complex nature of the transformed phenotype caused by oncogenic Ras might in itself require Ras activation of multiple signaling pathways (Shields *et al.*, 2000). The best-understood and most relevant in the context of cell transformation are the following three effector pathways (Downward, 2003):

- Raf serine/threonine kinases and the activation of the ERK mitogen-activated protein kinases (MAPKs)

- Phosphoinositide 3-kinases (PI3Ks)
- GEFs for the Ral small GTPases (RalGDS, RGL and RGL2/Rlf)

Their concerted activation is believed to promote several of the characteristics of malignant transformation, including increased proliferation, desensitization to apoptosis, induction of angiogenesis, and increased invasiveness. The relative importance of the effectors varies between different cell types, though. The importance of the RAF–MEK–ERK pathway in Ras oncogenic signaling has been firmly established. Yet, recent studies have indicated that this pathway might be preferentially used in rodent cells, whereas the RAL-GDS pathway might be responsible for transformation of various human cell types including fibroblasts (Hamad *et al.*, 2002).

1.4.3. SV40 small t

The SV40 small t antigen (st) forms stable complexes with protein phosphatase 2A (PP2A), thereby partially reducing its enzymatic activity. PP2A is actually a complex heterotrimeric family of enzymes. Its members are composed of a catalytic C subunit, a structural A subunit and one of several B subunits, which serve regulatory or adaptor functions (Millward *et al.*, 1999). St binds to PP2A through its unique C-terminus, which is independent from the presence of LT and, importantly, is indispensable for anchorage independent growth and tumor formation of human fibroblasts in nude mice. Moreover, cells transduced with st needed 33% less time to complete their cell cycle and were more resistant to stress induced by starvation, compared to control cells (Hahn *et al.*, 2002). Chen *et al.* (2004) could demonstrate that the effect of st on human cell transformation derives at least in part from interactions with PP2A complexes containing the B56γ subunit. The underlying molecular mechanism has been elucidated very recently in the publication of the crystal structure of the st antigen complexed with the A subunit of PP2A (Cho *et al.*, 2007). However, the identification of the crucial downstream targets is complicated by the fact that PP2A modulates the activity of more than 30 kinases *in vitro* and forms stable complexes with a large number of cellular or viral proteins (Millward *et al.*, 1999).

1.4.4. SV40 Large T

Finally, the set of four transforming entities is completed with the Large T antigen of simian virus 40 (SV40 LT), one of the best-studied virus-encoded oncoproteins. It contains a number of functional domains mostly connected with manipulation of the host cell cycle and with replication of the viral genome (for an overview, compare **Fig. 19** and sect. 3.2.2/ 3.2.3 in Results).

Although LT is known to bind to and modulate the actions of many host cell proteins (Ali and DeCaprio, 2001), its role in the transformation of human cells appears to lay solely in the inactivation of the retinoblastoma (Rb) and p53 tumor suppressor proteins by direct interaction (Saenz-Robles *et al.*, 2001). However, the specific functions of the Rb and p53 pathways that prevent human cell transformation are still not fully understood.

1.5. Principles of tumor suppression

It has been pointed out that a major effect of Rb and p53 is their anti-cancer activity. Such counterparts to the oncogenes were aptly labeled "anti-oncogenes" or, more commonly today, tumor suppressors. They were originally identified through the study of hereditary cancers (Knudson, 1983). Because heterozygosity (one normal allele) is sufficient for full protection, both alleles of an anti-oncogene, by definition, have to be mutated in tumors. One mutation may be inborn (germ line mutation; two germ line mutations being lethal), or both may be acquired (somatic mutations). Therefore, defects in tumor suppressor genes are inherited in a recessive fashion (Knudson, 1985). This is an important difference to proto-oncogenes, where one activating gain-of-function alteration results in an allele that is inherited dominantly. Knudson (1971) had much earlier summarized his statistical evaluation of childhood retinoblastoma in the "two-hit model". The initial statement was that certain malignancies (mostly cancers where the incidence peaks in infants) require only two steps, or "hits", for tumor development. In the case of retinoblastoma the two hits disable both alleles of the *RB1* gene, thus knocking out the Rb protein, a key regulator of the cell cycle. In later usage the definition of the expression "two hits" shifted in that it was combined with Knudson's other important contribution, the concept of anti-oncogenes. A tumor suppressor is now said to conform to Knudson's two-hit hypothesis if both alleles are frequently mutated or lost in tumors.

Over the past 30 years, many such tumor suppressor genes have been identified (Sherr, 2004). Even more prominent among these than *RB1* is the *TP53* gene. Its product p53 arguably is the most intensely studied protein in science. Its central importance is highlighted by the fact that p53 is functionally deactivated by deletion or mutation in more than 50% of all cancers. p53 is a transcription factor that establishes programs for cell-cycle checkpoints, apoptosis, senescence, and repair in response to a variety of cellular stresses, including DNA damage, hypoxia, and nutrient deprivation. The protein is also induced by many oncogenes, including E1A, Myc and E2F (Fridman and Lowe, 2003; Vogelstein *et al.*, 2000). Moreover, p53 inactivation severely compromises oncogene-induced apoptosis. Consistent with this role in coupling proliferation to cell death, inactivation of p53 potently cooperates with diverse oncogenes to promote transformation *in vitro* and tumorigenesis *in vivo*.

1.6. *p73, a transcription factor of the p53 family*

1.6.1. Gene and protein organization of p73

Since its original identification in 1979 as a binding partner of SV40 LT (Lane and Crawford, 1979; Linzer and Levine, 1979), p53 was long believed to be unique. However, relatively recently two more members have been added to the p53 family: p63 (Osada *et al.*, 1998; Schmale and Bamberger, 1997; Yang *et al.*, 1998) and p73 (Kaghad *et al.*, 1997). All three p53 family members act primarily as transactivators of transcription. They do so by forming homotetramers and docking to promoters of target genes in a sequence specific manner via their DNA binding domains. Consequently, both p63 and p73 share key functional domains with p53, including its N-terminal transactivation domain, C-terminal oligomerization domain, and a conserved DNA-binding domain (**Fig. 3a**).

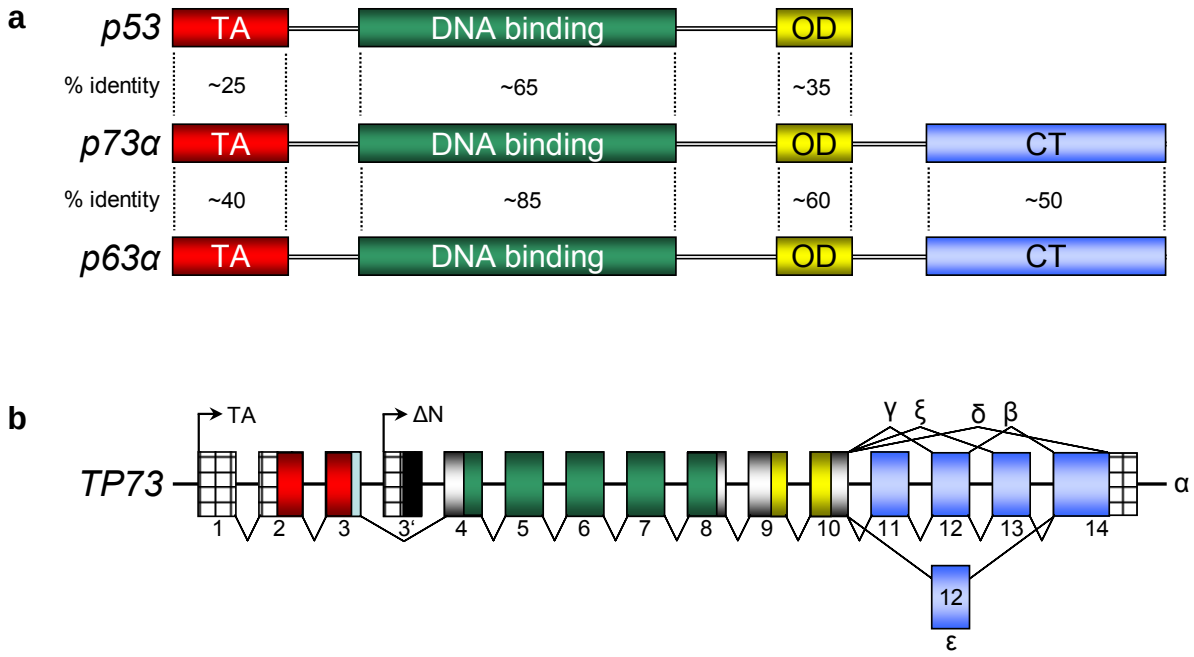

Fig. 3 Structure of the p53 family proteins and the p73 gene. (**a**) Comparison of the domain structure of the three p53 family members. TA, transactivation domain; OD, oligomerization domain; CT, carboxy-terminus. Primary amino acid sequence comparisons between p63 and p73 reveal a high degree of identity. These proteins are both more homologous to each other than to p53. (**b**) Exon-intron arrangement of the p73 gene in the human genome. *TP73* is spread over ~100 kb. The proximal promoter gives rise to the TA isoforms, whereas the distal promoter directs expression of the ΔN isoforms (arrows). The splicing patterns that give rise to the major C-terminal variations in addition to the α isoform (the β, γ, δ, ε and ξ isoforms) are indicated. Solid colors, translated exons- coloring as in panel (a); checkered, non-translated regions (after Stiewe *et al.*, 2004; Yang *et al.*, 2002). Further N-terminal complexity arises from aberrant splicing of TA promoter transcripts (not shown).

However, the *TP63* and *TP73* gene organization is considerably more complex, resulting in a multitude of different isoforms (Melino *et al.*, 2002; Yang *et al.*, 2002). Specifically, the p73 gene encodes several full-length or "TA" proteins that are transactivation competent, pro-apoptotic and therefore tumorsuppressive. They differ in the sequence of their C-terminal end

and are generated through alternative splicing (**Fig. 3b**). The use of an alternative promoter in intron 3 gives rise to the so-called ΔNp73 isoforms (**Fig. 3b**). They lack the N-terminal transactivation domain and can function as dominant negatives, i.e. anti-apoptotic and oncogenic. The p63 gene organization, isoform palette and corresponding physiological effects are quite similar (Mills, 2006).

1.6.2. p53 family proteins have diverse biological functions

Studies using knockout mice revealed that p63 is required for normal epithelial stem cell function and for the proper development of several tissues like the apical ectodermal ridge. $p63^{-/-}$ mice are born alive but have truncated or missing limbs, craniofacial defects and lack epidermal stratification as well as hair follicles, teeth, and mammary glands. Pups die of dehydration and maternal neglect within hours after birth (Mills *et al.*, 1999; Yang *et al.*, 1999).
While the bulk of research on p73 deals with its function in tumor development, an important role in development has been identified as well. Unlike p53 knockout mice, those functionally deficient for p73 were initially reported not to be more tumor-prone than controls (Yang *et al.*, 2000), a finding that was later challenged (Flores *et al.*, 2005). It undisputed, though, that $p73^{-/-}$ mice do exhibit a wide range of neural and infective abnormalities, including hippocampal dysgenesis, hydrocephalus, dysfunctions in pheromone/ hormone signaling and chronic inflammation of eyes, ears, and nose. Resulting bacterial infections are probably secondary to the persisting inflammations and concomitant mucositis, not a consequence of any immunodeficiency. Newborn $p73^{-/-}$ pups show the wasting syndrome and high rates of mortality, mostly due to gastrointestinal and intracranial bleeding. Adults generally fail to produce offspring, apparently both due to failure of the males to copulate and of the females to conceive or gestate (Yang *et al.*, 2000). In conclusion, p73 in development functions primarily in the central nervous system (survival, neurogenesis, spinal fluid homeostasis) and in sensory pathways.
In contrast to its homologs, p53 has no overt role in normal development (Donehower *et al.*, 1992). Then again, a certain degree of functional overlap does accompany the structural similarities of the three proteins. Transcriptional activation of shared target genes leads to the induction of cell-cycle arrest and apoptosis. These cell growth-inhibitory responses are thought to be crucial for the tumor suppressor activities of p53. Given the functional similarity between p53 and p73, it is not unreasonable to suppose that p73 might also be important for the inhibition of cancer development. Indeed, p73 is clearly involved in cancer, although in a distinct way to that of p53.

1.6.3. p73 in cancer development

While p53 is the single most frequently mutated gene in tumors, inactivating mutations of p73 have not been identified (Irwin and Kaelin, 2001b; Stiewe and Putzer, 2002) and p73-deficient mice were not found tumor-prone (Yang *et al.*, 2000). Indeed, there has been much debate and speculation about the possible roles of p73 in tumor suppression. A large number of conflicting experimental and clinical reports assigned to it either an oncogenic or protective effect. This apparent discrepancy is resolved by the dichotomy of the full-length and N-terminally truncated p73 isoforms, a detail early publications were ignorant of (e.g., Kovalev *et al.*, 1998; e.g., Zaika *et al.*, 1999).

The existence of ΔNp73 was reported first in conjunction with the knockout mouse (Yang *et al.*, 2000). ΔNp73 functions as a p53 family antagonist, is expressed at elevated levels in several tumor types (Concin *et al.*, 2004; Stiewe *et al.*, 2002b; Zaika *et al.*, 2002), and high levels correlate with an adverse prognosis in cancer patients (Casciano *et al.*, 2002). Ectopic expression of ΔNp73 transforms NIH3T3 cells to tumorigenicity and facilitates immortalization of primary murine embryo fibroblasts (Petrenko *et al.*, 2003; Stiewe *et al.*, 2002b). The tumor-promoting activity of ΔNp73 can be attributed to its dominant-negative function towards p53 and the other proapoptotic p53 family members (Petrenko *et al.*, 2003; Stiewe *et al.*, 2002a).

In contrast, TAp73 acts p53-like, and there is accumulating evidence for a role as a potent tumor suppressor (Flores *et al.*, 2005 and references therein). Apoptosis is a function thought to be critical for tumor suppression and the response of tumor cells to chemotherapeutic agents. TAp73 does indeed induce apoptosis independent from p53 after DNA damage (Flores *et al.*, 2002; Irwin *et al.*, 2000; Stiewe and Putzer, 2000), albeit this does not appear to be a mechanism common to all tissues (Senoo *et al.*, 2004). Likewise, p73 is a determinant of chemotherapeutic efficacy in humans (see Discussion), irrespective of p53 status (Irwin *et al.*, 2003; Rodicker *et al.*, 2001).

In the light of these findings it appears very likely now that the *TP73* gene encodes two protein forms with opposing functions. TAp73 acts protective through its p53-like tumor suppressive action. In contrast, the ΔNp73 proteins directly and indirectly antagonize the full-length p53 family members, rendering them putative oncogenes.

1.6.4. Regulation of p73

The regulation of TAp73 and ΔNp73 is as opposed as their functions. For this reason it has been suggested they ought to be regarded as separate proteins (Melino *et al.*, 2002). The ΔN-promoter seems primarily responsive to the full-length p53 family members (Melino *et al.*, 2002). In consequence, the availability of active TAp73 under normal conditions is self-limited

through this negative feedback loop. Detailed analysis of the TAp73 promoter revealed a TATA-like box, probably more than three E2F sites, and a number of other putative transcription factor sites (Ding *et al.*, 1999; Irwin *et al.*, 2000; Seelan *et al.*, 2002; Stiewe and Putzer, 2000). Of note, there is no extended homology to the p53 promoter (Ding *et al.*, 1999).

Of particular interest is the regulation of TAp73 by E2F1. This transcription factor plays an important role in the regulation of cell cycle progression by inducing the transcription of genes whose products are directly or indirectly required for entry into the S phase (Phillips and Vousden, 2001). Since E2F1 is frequently deregulated in cancers (Bell and Ryan, 2004), transactivation of pro-apoptotic targets like TAp73 could constitute a p53-independent safety catch against transformation (Flores *et al.*, 2002; Irwin *et al.*, 2000; Pediconi *et al.*, 2003; Stiewe and Putzer, 2000).

A prominent upstream regulator of E2F1 signaling is Rb. It can assemble transcription repression complexes to inhibit the expression of genes that are regulated by E2F1. The promoters of many genes required for cell cycle progression (like cyclin A, cyclin E, cdc2) contain E2F binding sites. Rb therefore acts as an inhibitor of cell proliferation and in addition, functions as a downstream effector in p53- and $p21^{Cip1}$-dependent growth arrest in DNA damage response.

p73 is also activated by certain oncogenes. Adenoviral E1A as well as the cellular proto-oncoproteins E2F1 and c-Myc lead to activation of both p53 and p73 transcription (Zaika *et al.*, 2001). Other important oncogenes discriminate between p53 family members. The SV40 Large T antigen inactivates p53 but does not interact with p63 or p73 (Dobbelstein and Roth, 1998; Kojima *et al.*, 2001; Roth and Dobbelstein, 1999). The same is true for adenoviral E1B55K and the HPV E6 protein (Marin *et al.*, 1998), suggesting that p63 or p73 are not involved in the transformation induced by SV40 and HPV.

The steady-state levels of proteins in general are determined by the rate of their synthesis *vs.* the rate of their degradation. While p53 is tagged for proteasomal destruction by the E3 ubiquitin ligase MDM2/HDM2, specific degradation of p73 seems to be facilitated mainly by the Hect ubiquitin–protein ligase Itch (Rossi *et al.*, 2005). The negative influence of HDM2 on available TAp73 is on the other hand not neglicible, as a recent study demonstrates (Lau *et al.*, 2007). On the whole, p73 degradation is very complex and involves ubiquitin-dependent and -independent proteasome pathways (reviewed in Ozaki and Nakagawara, 2005).

1.6.5. Regulation by p73

While TAp73 directly interacts with a number of proteins, the more fundamental consequence of increased TAp73 stability and expression is its enhanced transactivation activity.

Reminiscent of their partial overlap in gene/ protein sequence, cellular effect, and regulation, p53 and TAp73 have common as well as distinct transcriptional targets. Proteins that are positively regulated by TAp73 include:

- Apoptosis: Bax, CD95, Puma, Perp, Noxa, p53AIP1, scotin
- Cell cycle control: $p21^{WAF1}$, GADD45, 14-3-3σ, $p27^{kip1}$, $p57^{KIP2}$, Cyclin G, CaN19
- Degradation/ inhibition: ΔNp73, MDM2/HDM2
- Differentiation: AQP3, N-CAM, VEGF *(repression)*, Jagged 2
- Diverse/ unknown function: JunB, PIG13, α_1-antitrypsin

(compiled from Fontemaggi *et al.*, 2002; Irwin and Kaelin, 2001a; Lee and La Thangue, 1999; compiled from Melino *et al.*, 2002; Morgunkova, 2005; Ramadan *et al.*, 2005; Zhu *et al.*, 1998)

Specificity of gene activation by TAp73 is thought to be realized by a combination of a) posttranslational modifications, b) coactivators like Yes-associated protein (YAP), and c) subcellular localization (Costanzo *et al.*, 2002; Strano *et al.*, 2005).

1.7. Scope of the project

The cell culture model developed by Hahn and colleagues (see **Fig. 2**) is a useful and versatile tool for molecular cancer research because the different stable cell lines that represent progressing stages of malignancy can be analyzed separately. The model also allows the replacement of the oncogenic factors by others and the subsequent characterization of the cellular effects.

The tumor suppressive function of the p53 family member TAp73 is established to some extent and the roadmap to the major physiological effect, apoptosis, is on hand (if still at a large scale). Yet the continuous stream of data pointing to new interaction partners, transcriptional targets, modes of regulation, or even whole new functions testifies to the incompletion of the picture we have of p73. We therefore decided to adopt the fibroblast model by Hahn *et al.* to study the role and regulation of p73 during the transformation of normal human cells.

Initial biochemical characterization of the four stages BJ, BJ-T, BJ-TE, and BJ-TER revealed a sharp increase of TAp73 transcript and protein levels exclusively in BJ-TE. This result prompted us to issue a hypothetical model explaining the SV40 Large T-induced p73 upregulation and subsequent suppression by H-Ras. Finally, in order to confirm the assumptions made and to identify new potential interaction partners or effectors, the expression profile of human fibroblasts with a stable knockdown of TAp73 was compared with that of control cells in DNA microarrays.

2. Materials and Methods

2.1. Materials and Equipment

2.1.1. Instruments and other technical equipment

Tab. 1 Technical equipment used in this work

Name	Supplier/ Manufacturer
Autoclaves	BPW Hiclave HV-110 ; Systec V-150
Automatic pipettes	Eppendorf Multipette, Multipette plus
Balance	Kern 572
Blotting chamber	Bio-Rad Trans-Blot SD
Casting assembly (protein gel)	Hoefer Dual Gel Caster
Cell culture bench	BDK
Stand-alone centrifuges	Beckman Coulter Avanti J-20 XP, Avanti J-25
Stand-alone centrifuges: rotors	Beckman JA-10, JA 25.15, JA 25.50, JLA 16.250, JS 25.50
Table top centrifuges	Eppendorf centrifuge 5415R, 5417R, 5810R, MiniSpin
Ultracentrifuges	Beckman L7*, LE-70*, Optima TLX**
Ultracentrifuges: rotors	*: Beckman 70.1 TI; **: Beckman TLA 120.2
Electrophoresis chambers	Hoefer HE33 mini, HE 100 SuperSub, mighty small SE260; Biometra Agagel Standard
Electroporation units	Bio-Rad Gene PulserII, Micro Pulser
Film developer	Kodak X-omat 1000
Flow cytometer	BD Biosciences FACSCalibur
Fluorescence imager	Li-Cor Biosciences Odyssey
Fluorescence microscope	Zeiss Axiovert 200 w/ power supply Leistungselektronik Jena ebq100 isolated and CCD-camera Photometrics CoolSnap cf
Freezers (-20°C)	Liebherr Premium
Freezers (-80°C)	Heraeus HeraFreeze
Gel documentation	Herolab E.A.S.Y 440K
Ice preparation	Scotsman AF 200
Incubators (bacteria)	Heraeus B6, B12
Incubators (cell culture)	Heraeus HERAcell 240
Laser scanning cytometer	CompuCyte iCys w/ fluorescent microscope Olympus IX 71, CCD-camera Sony DXC-390P and focus unit Prior Scientific ProScan H29V4
Luminometer	BMG Fluostar Optima
Magnetic stirrers	IKA Werke RCT basic, Ikamag Reo
Micropipettes	Gilson Pipetman P
Microscope	Leica DMIL 090-135.001
Nitrogen tank	MVE Cryosystem 6000
PCR cyclers	Eppendorf Mastercycler Gradient; Applied Biosystems GeneAmp PCR System 9700
PCR hood	Captair Biocap RNA/ DNA
pH-meter	Schott CG 842

Tab. 1 (continued)

Name	Supplier/ Manufacturer
Photometer	Eppendorf BioPhotometer
Pipetting aids	IBS Integra Pipetboy acu; Falcon Express
Plate storage (protein gel)	Amersham Plate Mate SE 100
Plates (protein gel)	Amersham
Power supplies	Bio-Rad PowerPac Basic, PowerPac 200, PowerPac 300, PowerPac HC
Precision balance	Sartorius CP225D
Pump system (cell culture bench)	Vacuubrand BioChem VacuuCenter BVC21
Real time PCR machine	Applied Biosystems Abi Prism 7000
Refrigerators	Liebherr Premium
Roller mixer	Stuart Scientific SRT 2
Rotator drives	Stuart Scientific STR 4; Labor brand L28
Shaking incubator	Kühner ISF-1-W
Sonicator	Bandelin Sonoplus (power supply), UW 2070 (adapter), SH70G + MS72 (horn)
SpeedVac	Eppendorf Concentrator 5301
Thermomixer	Eppendorf Thermomixer comfort
Tilting table	Biometra WT 12
UV workbench	Vilbert Lourmat TFX-20.M
Vortex	Scientific Industries Vortex Genie 2
Water baths	Memmert WB 7, WB 14; Huber Polystat cc1
Water deionizing unit	Elga Purelab ultra

2.1.2. Glass and plastic ware, consumables

Tab. 2 Cell culture plates, glassware, and single use articles

Name	Supplier/ Manufacturer
96well-plate (black, round bottom)	Nunc
96well-plate (white, flat bottom)	Nunc
96well-plate (white, round bottom)	Nunc
Bacteria plates	Greiner
Cell culture plate (60, 100, 150mm)	TPP; Greiner; Sarstedt
Cell culture well plates (6, 12, 24, 96well)	TPP; Greiner; Sarstedt
Cell scraper	Sarstedt
Cryo box	Nalgene Cryo 1°C freezing container
Cryo tubes (bacteria)	Roth Roti-store
Cryo tubes (cell culture)	Nunc
Cuvettes (electroporation: bacteria)	Bio-Rad, Eurogentec
Cuvettes (electroporation: cell culture)	Bio-Rad
Cuvettes (OD determination)	Sarstedt; Eppendorf
Disposable canulae	Braun
Disposable syringe filters	Roth, Sarstedt
Disposable syringes	Primo
Glass beakers, Erlenmeyer beakers, bottles	Schott Duran
Glass pipettes	Hirschmann EM Techcolor
Nitrocellulose membrane	Amersham hybond-ECL
Pipette tips	Various

Tab. 2 (continued)

Name	Supplier/ Manufacturer
Plastic beakers	Vitlab
Reaction caps 1.5, 2ml("Eppis")	Sarstedt
Reaction caps 15, 50ml ("Falcons")	TPP; Greiner; Sarstedt
X-ray film	Kodak; Noras

2.1.3. Enzymes, PCR reagents and size standards

All restriction enzymes were obtained from Fermentas with the exception of PacI and NcoI (New England Biolabs). All DNA and protein ladders, alkalic phosphatase (CIAP), Klenow fragment, T4 DNA ligases, and desoxyribonucleoid triphosphate mix (dNTPs) were purchased from Fermentas as well. Ribonuclease A (RNase A) was ordered from Applichem.

Only reaction buffers of the original supplier were used.

2.1.4. Antibodies

Tab. 3 Antibodies from Western Blots and immunostainings; HRP = horse radish peroxidase

Recognized antigen	Order nr. or Clone	Type	Supplier
Alexa Fluor 488 anti-mouse	Anti- IgG_1	Secondary antibody	Molecular Probes
Alexa Fluor 546 anti-mouse	Anti-IgG_{2b}	Secondary antibody	Molecular Probes
Alexa Fluor 546 anti-mouse IgG	-	Secondary antibody	Molecular Probes
Alexa Fluor 680 anti-mouse IgG	-	Secondary antibody	Molecular Probes
Alexa Fluor 680 anti-rabbit IgG	-	Secondary antibody	Molecular Probes
Anti-mouse IgG, HRP-linked	-	Secondary antibody	Pierce, Amersham
Anti-rabbit IgG, HRP-linked	-	Secondary antibody	Pierce, Amersham
BrdU	Ab-3	Mouse monoclonal	Oncogene
H-Ras	C-20	Rabbit polyclonal	Santa Cruz Biotechnology
p73 (total)	ER-15	Mouse monoclonal	BD Pharmingen
p73 (total)	1.1	Rabbit polyclonal	Custom made
p73α	1.1	Rabbit polyclonal	Custom made
p73α/β	Ab-4 Cocktail	Mouse monoclonal	Dunn Labortechnik
SV40 Early Region	Ab419	Mouse monoclonal	Dr. A. Chestukhin
SV40 Early Region	Pab 108	Mouse monoclonal	Santa Cruz Biotechnology
SV40 LT	Pab 101	Mouse polyclonal	Santa Cruz Biotechnology
SV40 st	Ab-3	Mouse monoclonal	Calbiochem
TAp73	IMG-246	Mouse monoclonal	Imgenex
TAp73	IMG-259	Mouse monoclonal	Imgenex
β-actin	AC-15	Mouse monoclonal	Abcam

2.1.5. Oligonucleotides

Tab. 4 PCR, sequencing and mutagenesis primers used in this project

Int. #	Name	5'→3' sequence	Purpose	5'-modification
15	TAp73_for	GGCTGCGACGGCTGCAGAGC	RT-PCR	
16	TAp73_rev	GCTCAGCAGATTGAACTGGGCCATG	RT-PCR	
21	ΔNp73_for	CAAACGGCCCGCATGTTCCC	RT-PCR	
23	ΔN'p73_for	TCGACCTTCCCCAGTCAAGC	RT-PCR	
24	ΔN'p73_rev	TGGGACGAGGCATGGATCTG	RT-PCR	
118	RTGAPDH_for	AATGGAAATCCCATCACCATCT	Real Time PCR	
119	RTGAPDH_rev	CGCCCCACTTGATTTTGG	Real Time PCR	
164	ΔNp73_rev2	TTGAACTGGGCCGTGGCGAG	RT-PCR	
165	5'GAPDH	CACAGTCCATGCCATCAC	RT-PCR	
166	3'GAPDH	CACCACCCTGTTGCTGTA	RT-PCR	
234	TS	AATCCGTCGAGCAGAGTT	Real Time PCR	
319	ACX	GCGCGG[CTTACC]$_3$CTAACC	Real Time PCR	
455	pBABE-for	TTGAACCTCCTCGTTCGAC	Sequencing	
558	SV40ER_orient	ATATAAGCAGAGCTGGTTTAGTG	Sequencing	
891	LT_mut_11	AAACCTGTTTTGCTCAAAAGAAATGC CATCTA	Mutagenesis: LT E107K	phosphorylated
925	LT_mut_13	TCTGATGAGAAAGGCAGCTTTAAAA AAATGCAAG	Mutagenesis: LT Y34A	phosphorylated
927	LT_mut_20	CCCTGGAATAGTCACCAGTAATGAGT ACAGTGTGC	Mutagenesis: LT M528S	phosphorylated
1046	SV40-LT-AS	GTAAATAGCAAAGCAAGCAAGAG	RT-PCR	
1047	SV40-ST-AS	AGTTTGTCCAATTATGTCACACC	RT-PCR	
1048	SV40-ER-S	CTGTACAAGAAAATGGAAGATGG	RT-PCR	
1089	LT-Mut_26_Seq	TTCATGGTGACTATTCCAGG	Sequencing	
1264	LT_Nterm_aa140	TGAAGGAAAGTCCTTGGGGT	Sequencing	
1265	LT_C-term	GCCTTCAGGTCAGGGAATTA	Sequencing	

2.1.6. Bacterial strains

Tab. 5 Electro-competent bacterial strains used for cloning

Name	Genotype	Vendor
E. coli DH10B	F$^-$ mcrA Δ(mrr-hsdRMS-mcrBC) Φ80lacZΔM15 ΔlacX74 recA1 endA1 araΔ139 Δ(ara, leu)7697 galU galK λ- rpsL (Str^R) nupG	Invitrogen
E. coli E10	(mcrA)183 (mcrCB-hsdSMR-mrr)173 endA1 supE44 thi-1 recA1 gyrA96 relA1 lac Kan^r [F'proAB lacI^{q}ZDM15 Tn5(Tet^r)]	Stratagene
E. coli Top10 F'	F´{lacI^q, Tn10(Tet^R)} mcrA Δ(mrr-hsdRMS-mcrBC) Φ80lacZ ΔM15 ΔlacX74 recA1 araD139 Δ(ara-leu)7697 galU galK rpsL (Str^R) endA1 nupG	Invitrogen
E. coli XL1-blue MRF'	D(mcrA)183 D(mcrCB-hsdSMR-mrr)173 endA1 supE44 thi-1 recA1 gyrA96 relA1 lac [F'proAB lacI^{q}ZDM15 Tn10 (Tet^r)]	Stratagene

2.1.7. Plasmids

Tab. 6 Plasmids/ expression vectors used in this work

Name	Size [bp]	Origin
pAdTrack-LT	11200	This work
pAdTrack-LT(E107K)	11200	This work
pAdTrack-LT(M528S)	11200	This work
pAdTrack-LT(Y34A)	11200	This work
pBABE-neo-T	6490	Morgenstern & Land 1990
pBABE-zeo-smallT	6871	Hahn WC *et al.* 2002
pCMVΔR8.74	11921	courtesy D. Trono
pGL3-Enh-p73pr-mut2/4/5	5355	This work
pGL3-Enh-p73pr-Δpvu-mut2/3/4	5355	This work
pGL3-Enh-p73pr-Δpvu-wt	5355	This work
pLPC-GFPS	6998	Serrano M *et al.* 1997
pLPC-HrasV12	6744	Serrano M *et al.* 1997
pLPCX	5639	Serrano M *et al.* 1997
pLVTHM	11080	Wiznerowicz & Trono 2003
pLVTHM-ns	11140	This work
pLVTHM-p73si#1	11140	This work
pMD2.G	5824	courtesy D. Trono
pRSV-Rev	4174	courtesy D. Trono
pUC19sfiI-LT	4930	This work
pUC19sfiI-LT(E107K)	4930	This work
pUC19sfiI-LT(M528S)	4930	This work
pUC19sfiI-LT(Y34A)	4930	This work
pVSVG	4711	courtesy D. Trono
pWPI-SV40ER #8	13700	This work
pWZL-blast3-hTERT	8600	courtesy R. Pieper
pAdGFP	35000	AG Stiewe
pAdGFP-E2F	37900	AG Stiewe
pZIP-SV-776-1	6617	Jat *et al.* 1986

2.1.8. Eukaryotic cell lines

Tab. 7 Eukaryotic cell lines used in this work. Abbreviations for eukaryotic resistence markers: Blast = blasticidin, G418 = neomycin analog, Puro = puromycin. Figures in the exponents are the final antibiotic concentrations during the selection in µg/ml.

Name	Introduced transgene(s)	Resistance	Source
BJ	-	-	ATCC #CRL-2522
BJ-T	hTERT	Blast^{1}	This work
BJ-TE	SV40 Early Region	Blast^{1} G418^{500}	This work
BJ-TER	H-RasG12V	Blast^{1} G418^{500} Puro$^{0.75}$	This work
DU145	-	-	AG Stiewe
EcoPack	-	-	AG Stiewe
H1299	-	-	AG Stiewe
HA1E	-	-	Counter et al. 1998
HA1ER	-	-	Counter et al. 1998
HEK293	-	-	AG Stiewe

Tab. 7 (continued)

Name	Introduced transgene(s)	Resistance	Source
HEK293T	-	-	AG Stiewe
MCF7	-	-	AG Stiewe
Retropack/ PT-67	-	-	BD Biosciences; Miller & Jen 1996
SAOS	-	-	AG Stiewe
T98G	-	-	ATCC #CRL-1690
VH6	-	-	AG Stiewe
VH6-T	hTERT	-	This work
VH6-TE	SV40 Early Region	-	This work
VH6-TE>ns	Non-silencing siRNA	-	This work
VH6-TE>p73si#1	siRNA p73#1	-	This work
VH6-TER	H-RasG12V	-	This work

2.2. Buffers, media and solutions

All of the following products were purchased from PAA: Dulbecco's Modified Eagle-Medium (DMEM; high glucose), fetal calf serum (FCS), minimum essential (MEM) amino acids (10x), Phosphate buffered saline (PBS). Self-prepared buffers and solutions were made according to the recipes listed below. Unless noted otherwise only deionized water was used (referred to as ddH_2O; source: Elga "Purelab ultra" filter unit). For PCRs, HPLC-grade water (Roth) was used.

2.2.1. Protein detection

Stripping buffer

50mM Tris-HCl pH 6.8
2% SDS
100mM β-mercapto ethanol

RIPA lysis buffer

50mM Tris-HCl pH 7.2
150mM NaCl
0.1% SDS
1% sodium deoxycholate
1% Triton X-100

5x Blotting buffer

970mM glycine
125mM Tris pH 8.3

5x SDS running buffer

125mM Tris

1.25mM glycine

0.5% SDS

10x TBS

150mM NaCl

50mM Tris pH 7.5

TBST0.1/ TBST0.2

15mM NaCl

5mM Tris pH 7.5

0.1/ 0.2% Tween

Blocking buffer

TBS 0.1

10% milk powder

2.2.2. Flow cytometry

Hypotonic propidium iodide-citrate buffer

0.1% sodium citrate

0.1% Triton X-100

50µg/ml propidium iodide

2.2.3. Cell culture

Cytomix preparation for electroporation

120mM KCl

0.15mM $CaCl_2$

10mM K_2HPO_4 / KH_2PO_4 pH 7.6

25mM HEPES pH 7.6

2mM EGTA pH 7.6

10% FCS

100mM ATP

250mM reduced glutathione

2.2.4. Plasmid isolation from bacteria

Puffer 1 (re-suspension buffer)

5mM Tris pH 8.0
10mM EDTA pH 8.0
100µg/ml RNAse A

→ storage at 4°C

Puffer 2 (lysis buffer)

200mM NaOH
1% SDS

Puffer 3 (neutralization buffer)

3 M KAc pH 5.5

GTE buffer

50mM glucose
25mM Tris-HCl pH 8.0
10mM EDTA
4mg/ml lysozyme

→ storage at 4°C

1x SSC

150mM
15mM sodium citrate-HCl pH 7.0

2.2.5. Other self-prepared buffers, media and solutions

LB medium

5g/l NaCl
5g/l yeast extract
10g/l bactotrypton
pH 7.5

5x TBE

445mM Tris
445mM boric acid
10mM EDTA pH 8.0

SB medium

5g/l NaCl

20g/l yeast extract

35g/l bactotrypton

pH 7.5

50x TAE

2M Tris-acetate

50mM EDTA, pH 8.0

2.3. Cell culture

2.3.1. Cell maintenance

All cell lines were maintained at 37°C and 5% CO_2 in Dulbecco's Modified Eagle's Medium (PAA) supplemented with 10% fetal calf serum, 100U/ml penicillin, 100µg/ml streptomycin and 1µg/ml amphotericin B (all frim PAA). Periodically (approximately every other month), 8µg/ml ciprofloxacin (Ciprobay 400®) was added.

2.3.2. Tumorigenicity assay

For soft agar analysis in 6-well plates, $4x10^4$ cells in PBS were mixed with an equal volume of 0.66% agar solution in 2x Eagle's medium (cooled to 40°C) and poured onto a bed of 0.5% agar. On the next day, the agar layers were carefully overlaid with DMEM +10% FCS, which was renewed every 4 to 5 days. After 4 weeks, colonies were microscopically photographed. All of the experiments were performed in triplicate.

2.3.3. Growth curves

To compare growth kinetics among different cell lines, growth curves were prepared by seeding $5x10^4$ cells per 60mm plate. The plates were then counted in triplicate at regular intervals, usually every 2 or 3 days. Cells were fed but not split and counted until widespread cell decay set in.

In a variation of this approach, VH6-TE cells transduced with lentivirus carrying various p73 or non-silencing (ns) siRNAs and a GFP marker were mixed with an equal part of the parental cell line and seeded on 60mm plates in triplicate. The plates were split at equal intervals at a constant 1:4 ratio and the fraction of GFP positive cells was determined by flow cytometry (BD Biosciences FACSCalibur). At each time point, samples from pure cultures of VH6-TE, VH6-TE>p73si#1, and VH6-TE>ns were measured as well to ensure constancy of the original fluorescence intensity during the course of co-culture.

2.3.4. Viability staining

To determine the viability of trypsinized cells, they were mixed with a 1:2 dilution of trypan blue stock solution (Roth). Viable cells are capable to exclude the dye and appear white, with a bright halo. Only those were counted as alive. All other objects of appropriate size and shape were considered dead cells.

2.3.5. Transfection

Eukaryotic cells were transduced chemically by using following reagents according to the manufacturer's protocol: Fugene 6 (Roche), JetPEI (Qbiogene), Lipofectamine 2000 (Invitrogen), Oligofectamine (Invitrogen), PolyFect (Qiagen), SuperFect (Qiagen), TransPEI (Eurogentec). Depending on reagent and experimental technique, either 24-wells (for luciferase assays), 6-wells or 60mm dishes (for virus production) were used.

The protocol for transfection of fibroblasts with polyethylenimine (PEI) derivatives was modified to increase the efficiency and minimize cytotoxic effects. After having placed cells in contact with the DNA/ PEI complexes, plates were centrifuged (280xg/ 5min/ RT) and exposure time was reduced to 2h.

2.3.6. Electroporation

To transduce eukaryotic cells electrically, they were seeded at low density on 150mm plates. Upon reaching about 80% confluence cells were trypsinized, pelleted (200xg/ 10min/ 4°C) and resuspended in 250µl cytomix per plate. 10µg of the plasmid DNA to be transduced was added, everything was given in a pre-chilled electroporation cuvette and incubated on ice for 10min. Electroporation was performed at 250V and at a capacity of 975µF. Before seeding the processed cells on a 150mm plate, they were equilibrated at 37°C for 10min.

2.3.7. Retroviral transduction

The cell lines BJ-T, BJ-TE and BJ-TER were generated by sequential infection of the human diploid fibroblast strain BJ (ATCC CRL-2522) with retroviruses that were produced by transfection of the amphotropic packaging cell line PT67 (Becton Dickinson) with the plasmids pWZL-blast3-hTERT, pZIP-SV776-1 or pLPC-HrasV12 (Hahn *et al.*, 1999; Serrano *et al.*, 1997; Sonoda *et al.*, 2001). Transduced cells were selected with 1µg/ml blasticidin (Merck Biosciences), 400µg/ml G418 (PAA), or 0.75µg/ml puromycin (Becton Dickinson), respectively.

Analogous to the BJ strain, the cell lines VH6-T, VH6-TE, and VH6-TER were generated from the human diploid fibroblast strain VH6 by transduction with lentiviruses which were raised by transfecting 293T cells with pWPI-hERT, pWPI-ER, and pLLP-HrasV12, respectively. Because

the pWPI vectors do not carry any eukaryotic drug resistance markers, VH6 cell lines were not drug selected.

2.3.8. Adenoviral transduction

Adenoviruses based on the pAd-GFP vector were produced as described by the AdEasy protocol found on the homepage of Bert Vogelstein's lab (www.coloncancer.org/adeasy/protocol2.htm and ~/adeasy/adeasy_got_easier). Briefly, Ad293 cells were transfected with the recombined adenoviral construct on 60mm plates (see sect. 2.3.5). The supernatant of this primary infection was used to infect Ad293 on a larger scale (usually eight 150mm plates). Plates were harvested at near-complete infection, as monitored by GFP fluorescence. All cells were combined, pelleted, resuspended in 5ml PBS containing 10% glycerol, and frozen/ thawed three times. Cell trash was spun down at 4°C/ 3000xg for 10min, while the supernatant (containing high titer adenovirus) was aliquoted and stored at -80°C.

Adenoviral titers were determined by infecting 3T3 in DMEM with 2% FCS on 96well plates in tenfold determination with dilution series from 10^{-2} and 10^{-10} of the viral harvests. Plates were monitored for 7-10 days for cytopathic effects (CPE) and the viral titer was calculated from the highest dilutions that still showed CPEs. A titer above $1x10^{8}$ was considered high.

To infect target cells, they were incubated with a minimum of medium containing 2% FCS and 0.5 - 5% adenovirus for 2h. After that, normal medium was added to the regular volume. Efficiency of transduction was estimated by the fraction of GFP positive cells after 3-5 days.

2.3.9. Cell stock freezing

Cells were suspended in DMEM containing 20% FCS and 10% DMSO, aliquoted into cryo tubes and frozen down to -80°C in the “Cryo 1°C freezing container” (Nalgene). The frozen vials were then transferred into liquid nitrogen for long-term storage.

2.4. DNA work

2.4.1. Cloning

To generate expression plasmids, DNA fragments (vector backbone and insert) were prepared by restriction digest. Fragments were liberated and purified from agarose gels (kits by Promega, Qiagen). If the digests did not yield compatible ("sticky") ends, a blunt ligation had to be carried out. For this, the staggered ends of purified vector and insert had to be filled first utilizing the Klenow fragment of DNA polymerase I.

To minimize relegation, the ends of the linearized vector backbone were de-phosphorylated by incubation with 1 to 2 units of CIAP at 37°C for 2 to 3 hours. A ligation reaction typically

contained 1 volume of vector, 7 volumes of insert and 1 unit of T4 ligase, which was incubated at RT for 1 or 2h or typically, at 16 °C overnight. 40µl of electro-competent *E. coli* (**Tab. 5**) were gently mixed with 1 to 2µl of the ligation reaction and in 0.1cm cuvettes electroporated according to supplier recommendations. The treated bacteria were suspended in 0.5 to 1ml LB medium, incubated at 37°C for 30 to 60 min under vigorous shaking, plated on LB-agar plates containing selective antibiotics (100µg/ml ampicillin or 50µg/ml kanamycin) and cultivated overnight at 37°C. For further analysis, single clones were picked from those plates, inoculated in 4 to 5ml LB with antibiotic, subjected to the "miniprep" procedure and a suitable restriction digestion.

For an overview of plasmids constructed in this work, see **Tab. 6** in sect. 2.1.6. Specifically, pUC19sfiI-LT was generated by liberating the Large T cDNA from pBABE-neo-T by BamHI digestion and inserting it in the BamHI site of pUC19sfiI. Point mutations were introduced in pUC19sfiI-LT (QuikChange Multi kit, Stratagene) to yield pUC19sfiI-LT Y34A, -LT E107K, and -LT M528S. The four LT versions were again cut out with BamHI and cloned into the unique BamHI site of the adenoviral pAdTrack-LT vector. Similarly, cloning the BamHI fragment from pZIP-SV-776-1 was ligated with the unique Bam site of pWPI+BamHI (AG Stiewe), resulting in pWPI-SV40ER #8. The pGL3 constructs with various varieties of the p73 promoter from (Seelan *et al.*, 2002) were found to be inadequate for the sensitivity of our luciferase assay systems. Therefore, the NheI/HindIII-fragments containing the respective promoter regions were inserted in the corresponding site of pGL3-Enhancer (purchased from Promega). This gave pGL3-Enh-p73pr-mut2/4/5, pGL3-Enh-p73pr-Δpvu-wt, and pGL3-Enh-p73pr-Δpvu-mut2/3/4.

2.4.2. Plasmid DNA isolation- Miniprep

Small-scale purification of vector DNA from bacteria was achieved using the following standard protocol for the preparation of plasmid DNA by alkaline lysis with SDS. From 5ml fresh overnight culture, 1.5 to 2ml were pelleted (20000xg/ 1min/ 4°C) and re-suspended in 300µl buffer 1. An equal volume buffer 2 was added, followed by 5min incubation on ice, addition of an equal volume of buffer 3 and another 5min on ice. The fluffy white cell trash was spun down (20000xg/ 5min/ 4°C) and the clear supernatant mixed with 700µl isopropanol. DNA was collected (20000xg/ 5min/ 4°C), washed once with 70% ethanol and eluted in 50µl ddH_2O.

If higher DNA purity was required, most notably for sequencing, 2-5ml of fresh overnight bacteria culture was processed using the “NucleoSpin Plasmid” kit by Macherey & Nagel.

2.4.3. Plasmid DNA isolation- Midiprep

For the extraction of plasmid DNA from 20 to 100ml of overnight bacteria culture and increased purity, kits from Quiagen (Plasmid Midi), Macherey & Nagel (Nucleobond PC 100) and Promega (Pure Yield Plasmid Midiprep System) were used, following the respective protocols.

2.4.4. Plasmid DNA isolation- Maxiprep

Plasmid DNA isolation from 100 to 500 ml culture, the largest scale in this work, was performed either using the Quiagen "Plasmid Maxi" kit according to the manufacturer's instructions or the cesium chloride gradient method. The latter is a long-established protocol based on research from the 1960s (Radloff *et al.*, 1967; Waring, 1966).

Transformed *E. coli* grown overnight in 500ml of LB or SB medium were pelleted (5000xg/ 10min/ 4°C), suspended in 40ml GTE buffer and incubated at room temperature for 20min. 80ml of freshly prepared buffer 2 were added and after vigorous mixing everything was incubated on ice for 10min, followed by the addition of 40ml of buffer 3 and another 20min incubation on ice. The precipitated cell trash was spun down (5000xg/ 10min/ 4°C), the supernatant filtered and combined with 0.6 volumes of isopropanol. The pelleted DNA (5000xg/ 10min/ 20°C) was dried and resuspended in 7ml 0.1x SSC buffer. 1g solid CsCl was added per ml of crude DNA solution, incubated for at least 30min on ice and centrifuged at 6000rpm/ 20min/ 4°C. The supernatant was transferred into centrifuge tubes (Beckman), mixed with 20µl of ethidium bromide and centrifuged overnight (55000rpm/ 20°C). Usually a single purple band was visible which was extracted by inserting a disposable syringe fitted with a large-gauge needle into the side of the tube just underneath the band. To eliminate ethidium bromide, the collected clear red fluid was repeatedly mixed with 2-3ml of TE-saturated butanol until the aqueous phase appeared colorless. Three volumes TE buffer and 8 volumes 100% ethanol were added. DNA was then spun down (6000rpm/ 15min/ 4°C), washed with 70% ethanol, dried in a water bath at 65°C, and finally eluted in 500-1000µl 0.1x SSC buffer.

2.4.5. DNA purification- spin columns

Existing DNA was purified with the "Wizard SV Gel and PCR clean-up System" by Promega. Miniprep DNA samples processed like this typically yielded around 5-10µg of purified DNA.

2.4.6. DNA purification- phenol-chloroform extraction

An alternative method to clear DNA from RNA and protein residues is the extraction with phenol and chloroform. For this, the DNA sample is first thoroughly mixed in a 1.5ml reaction cap with the same volume of phenol/ chloroform/ isoamyl alcohol (24:24:1; Roth). To achieve

complete phase separation, the mixture was centrifuged (20000xg/ 3min/ 4°C). The upper phase containing the DNA was transferred into a new cap, mixed thoroughly with an equal volume of chloroform/ isoamyl alcohol (24:1; Roth), and centrifuged as before. Again, the upper phase was transferred into a new cap and 1/20 volume of 5M NaCl and 2.5 volumes of ethanol (100%) were added. If little yield was expected, 1µl of 20 mg/ml solution of glycogen was added as a co-precipitant. DNA was pelleted (20000xg/ 10min/ 4°C), washed with 70% ethanol, pelleted again, and eluted in 30-50µl ddH_2O.

2.4.7. DNA quantification

For most purposes, the concentration of a DNA solution was determined by measuring the OD at 260nm, where one OD is equivalent to 50µg/ml dsDNA.

The purity can be monitored by OD_{280} and OD_{230} measurement, which indicates the protein and RNA content, respectively. The OD ratios of the plasmid solutions used in this work were mostly in the range of 1.85-1.95 ($OD_{260/280}$) and 2.25-2.35 ($OD_{260/230}$; only midi- and maxipreps). The $OD_{260/230}$ values in minipreps varied more widely between 1.25 and 2.5 (with most samples between 1.6 and 2.0), probably depending on which purification method and which kit vendor was used.

For more delicate methods like Real Time PCR, DNA concentrations were determined with the "PicoGreen DNA quantitation" kit (Quiagen) according to the vendor's protocol.

2.4.8. DNA sequencing

Plasmid DNA sequencing was ordered either from Seqlab (Göttingen, Germany) or Agowa (Berlin, Germany). Reactions were prepared according to the respective requirements for hotshot sequencing.

2.4.9. Mutagenesis

All site-directed mutagenesis reactions were performed using the "QuikChange" kit (Stratagene). Procedure was according to protocol except that half the amount (0.5µl) of enzyme mix was used. The concluding DpnI digest was usually extended to several hours at 37°C with a total of 3-4µl (30-40U) of enzyme.

2.5. RNA work

2.5.1. RNA isolation

For the RNA isolation from whole cells the "RNeasy Mini Kit" (Quiagen) or the "NucleoSpin RNA II" kit (Macherey & Nagel) were used. RNA was usually harvested, resuspended in 50 to 100µl of RNAlater (Quiagen), stored at -80°C and extracted according to the vendor protocol.

The optional DNA digestion step in the Quiagen protocol was always carried out using the "RNase-free DNase set" (Quiagen) as described in the manuals.

2.5.2. RNA quantification

Freshly extracted RNA was immediately quantified with the RiboGreen RNA quantitation reagent (Molecular Probes) according to the manual. RNA calibration curves were prepared with the 100 ng/ml RNA Stock (Molecular Probes). All RNA isolates were measured in triplicate with 1 or 2µl RNA per well. Fluorescence of standard curve and RNA samples was read in a Fluostar Optima luminometer (BMG) and the RNA concentrations calculated in Microsoft Excel with the Fluostar plug-in.

2.5.3. cDNA preparation

To make cDNA from fresh or frozen RNA, the following standard recipe was utilized. Per reverse transcriptase (RT) reaction,

0.2 – 2µg	RNA (depending on concentrations)
2µl	RT puffer
2µl	dNTP mix
2µl	random hexamers
0.2µl	RNAse inhibitor
1µl	RT
ad 20µl	H_2O

were mixed, incubated for 1h at 37°C and deactivated for 4 min at 95°C. Since precisely equal amounts of RNA for one set of cDNA syntheses were used, cDNA concentrations were not determined after the RT reaction.

2.5.4. PCR and semi-quantitative RT-PCR

General Reverse Transcription PCR (RT-PCR) protocol: per reaction, mix

2µl	cDNA
3µl	Taq Puffer
0.6µl	dNTP mix
0.6µl	3' primer
0.6µl	5' primer
0.2µl	Taq
ad 28µl	H_2O

Some target genes required the addition of 5% DMSO (see **Tab. 8**). The PCR mixes were then in a Mastercycler Gradient (Eppendorf) or GeneAmp PCR System 9700 (Applied Biosystems) subjected to following general touchdown PCR program:

95 °C	15min	
95 °C x+2°C>x-3°C /-0.5°C per cycle 72 °C	15s 30s 60s	10 cycles
95 °C 64 °C 72 °C	15s 30s 60s	15-35 cycles
72 °C	4min	
4 °C	∞	

"X" is the higher of the two primer melting temperatures. The cycle number for amplification after the touchdown sequence was dependent on transcript abundance of the target. The household gene GAPDH for instance required a mere 15-18 cycles, whereas TAp73 required usually 25-30 cycles. **Tab. 8** supplies the amplicon sizes for the various Real Time and RT-PCRs performed for this project. For primer sequences, refer to **Tab. 4**.

2.5.5. PCR primers and amplicon sizes

Tab. 8 Internal primer numbers and amplicon sizes in bp of the semiquantitative and Real Time PCR primers of this project. Primer sequences are listed in Tab. 4. Nd, not determined.

Target gene	Isoform	Organism	3' primer (int. #)	5' primer (int. #)	Amplicon [bp]	remark
GAPDH	n/a	human	118	119	**58**	Real Time PCR
GAPDH	n/a	human	165	166	**448**	RT-PCR
p73	total	mouse	199	200	**617**	PCR +5% DMSO
p73	TA	mouse	197	198	**464**	PCR +5% DMSO
Telomeric repeat	n/a	Human	319	234	**variable (50+6x)**	Real Time TRAP
p73	ΔN	human	21	164	**nd**	
p73	ΔN'	human	23	24	**215**	
p73	TA	human	15	16	**257**	Real Time PCR
SV40 LT	n/a	SV40	1046	1048	**~317**	
SV40 st	n/a	SV40	1047	1048	**329**	

2.5.6. Real Time PCR

Real Time PCRs were performed in an Applied Biosystems Abi Prism 7000 cycler. For the detection of TAp73 (primer #15 & 16), the following program was used:

50 °C	2min	
95 °C	10min	
95 °C 69 °C 72 °C	15s 30s 60s	10 cycles
95 °C 64 °C 72 °C	15s 30s 60s	40 cycles

The program for GAPDH (primer #118 & 119):

50 °C	2min	
95 °C	10min	
95 °C	15s	40 cycles
60 °C	60s	

To quantify the activity of telomerase in a cell lysate, a Real Time TRAP modified after (see also Kim and Wu, 1997; Wege *et al.*, 2003) was used that included following program (primer ACT & TS = #319 & 234):

25 °C	10min	
95 °C	10min	
95 °C	30s	50 cycles
60 °C	90s	

The sequences for all primers mentioned above are listed in **Tab. 4**.

2.5.7. DNA microarray

5µg RNA (RNeasy Mini Kit, Promega) from proliferating and confluent VH6TE>ns si/ VH6TE >p73si-1 were hybridized according to the supplier's manual (one-cycle target labeling procedure) with a "GeneChip Human Genome U133A 2.0" chip (Affymetrix; detects 14500 human genes). For this a Hybridization Oven 640 and a Fluidics Station 450 (both Affymetrix) were used. The assay was read out on an Affymetrix GeneChip Scanner 3000 with workstation and data evaluation was performed using the free GeneSpring GX software (Agilent Technologies), version 7.3.1. Genes that were regulated according to density were considered for further interpretation when at least one of its signals out of the set of four DNA chips exceeded a threshold of 200 units. No threshold was set for p73si-regulated genes. From the signal intensities, the normalized expression levels were calculated with the standard normalization function in the GeneSpring program.

2.6. Protein work

2.6.1. Western Blot

Western immunoblots were typically conducted as follows. Harvested cells were pelleted (200xg/ 10min/ 4°C), suspended in an appropriate volume of RIPA lysis buffer and incubated on ice for 30min. Supernatants of the final centrifugation step (20,000xg/ 10-20min/ 4°C) were assayed for protein content using the method according to Bradford (1976) with commercially available reagent mixture. Whole cell lysates were either stored at -80°C or, preferentially, were directly used. Lysates representing the same amount of total protein were denatured (boiling for 5min at 95°C in loading buffer), separated by SDS-PAGE and transferred onto a nitrocellulose membrane using a semi-dry technique. A blotting sandwich was prepared as follows: three sheets of Whatman paper for each side were soaked in blotting buffer and placed on the blotting apparatus, followed by the nitrocellulose membrane, the gel and another three sheets of paper soaked in blotting buffer. Blotting was performed for roughly 1min per kDa of molecular weight with about 1.2mA/cm^2. After 1h blocking with 10% milk powder in TBS, the membrane was incubated overnight at 4°C with the appropriate primary antibody followed by extensive washing with three changes of TBST0.1. Finally, blots inoculated for 1h at room temperature with the HRP- or fluorescent dye-conjugated secondary antibodies were washed five times and detected proteins were visualized with ECL or the Odyssey infrared imager, respectively.

After this procedure, membranes were occasionally re-probed for another protein (usually the loading control). In that case, it was necessary to strip the membrane of adhering antibodies. For this it was incubated for 15 to 30min at 50°C in pre-warmed stripping buffer, washed several times with TBS and processed as described above, starting over with the blocking step.

2.7. Cell-based assays

2.7.1. BrdU incorporation assay

The fraction of cells in a population with active DNA synthesis ("S phase index") can be quantified by immunofluorescence staining against bromodeoxyuracil (BrdU). This chemical is a tymidine analog and will be used as a building block for nascent DNA in cells that are in the S phase during the BrdU exposure. These cells later can be visualized with a BrdU-specific antibody.

BJ type fibroblasts were seeded in 12well plates on round coverslips at no more than 5x10^4 per well. After about 36h at standard conditions or in DMEM with 0.1% FCS, cells were incubated overnight with 10µM BrdU in 1ml DMEM with 0.1% or 10% FCS. Wells were washed the next morning three times with PBS. 1-2ml fixative was added, everything incubated for 45min at

RT, then washed again twice. To permeabilize cellular membranes for DAPI (Rundquist, 1993), the samples were denatured in 1-2ml 4N HCl for 10-20min at RT, concluded by three times washing for 5min. Unspecific binding sites were blocked by incubating the coverslips for 45min in a moist chamber with 100µl blocking buffer. After washing in PBS, samples were stained with an 1:100 dilution of BrdU antibody (Ab-3, Oncogene) for one hour (moist chamber, RT), and washed again three times for 5min each. Labeling with fluorescent secondary antibody (1:1000 or higher in blocking buffer) was performed accordingly, but only for 30-45min. The final four washing steps were 1) PBS+DAPI 5min, 2) & 3) PBS 5min each, and 4) ddH_2O.

For long term storage, completely dry samples were mounted on regular cover slips prior to imaging under the fluorescent microscope. Optimal results were obtained with 20µl of ProLong antifade kit (Molecular Probes), but Vectashield Hard*Set (Vector Laboratories) and UltraCruz mounting medium (Santa Cruz) were also used.

3. Results

3.1. Validation of the model system

The aim of this work was the characterization of the regulation of the p73 protein during the malignant transformation of human cells. We took advantage of the fact that the group of Robert Weinberg has recently proposed a cell culture model for the stepwise transition of a normal into a cancer cell (Hahn *et al.*, 1999). The basis for this *in vitro* transformation were normal diploid fibroblasts (**Fig. 4**), which were sequentially transduced with hTERT (human telomerase), the Early Region of the DNA tumor virus SV40 coding for small t and Large T, and the oncogenic allele H-RasV12.

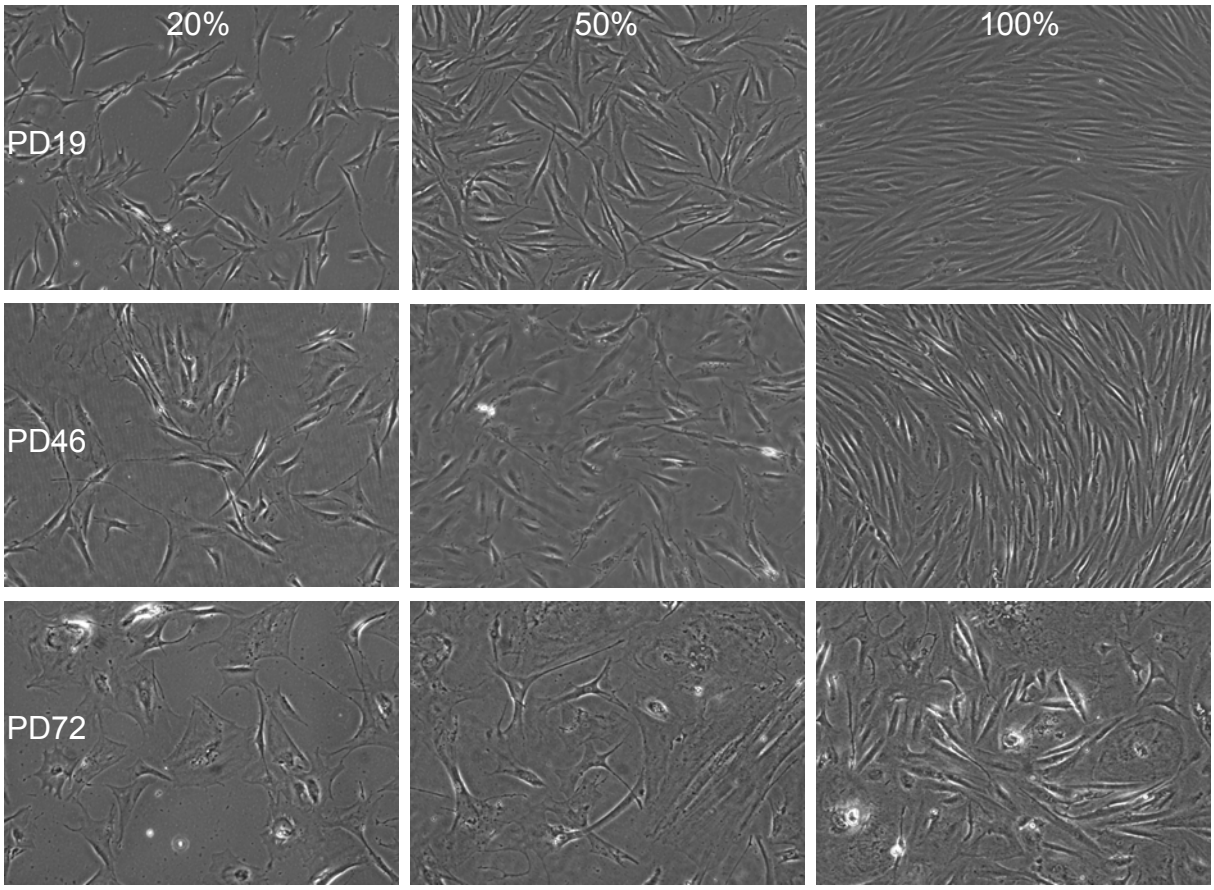

Fig. 4 Normal human diploid fibroblasts, the basis of the cell culture system for transformation. Pictures of the same culture were taken at low, medium and maximum density when it reached population doublings (PD) 19, 46 and 72. Note that at PD 72, many of the fibroblasts have a flat, roundish shape, indicating they have entered replicative senescence. Such aged cells will not form a dense regular layer anymore, irrespective of how long they are kept in culture.

hTERT immortalizes cells by maintaining the telomeric chromosome ends. Otherwise, fibroblasts would enter replicative senescence after approximately 70-80 population doublings (PD; compare **Fig. 4**, lower row). The SV40 small t antigen (st) interferes with protein phosphatase 2A (PP2A) signaling, the SV40 Large T antigen (LT) inhibits both the p53 and Rb

pathway, and H-RasV12 provides permanent growth signals. The alterations in the effected targets or signal pathways were shown to be sufficient to render the last cellular stage of the model system, named -TER, tumorigenic in nude mice (Hahn *et al.*, 1999). In order to create a working platform for this project we sought to establish the system in the laboratory and to adapt it to our purposes.

3.1.1. Western Blot

The introduction of the three genetic elements hTERT, SV40 early region (ER) and oncogenic H-RasV12 was accomplished by way of retroviral gene transfer. Starting from the BJ wild type, this yielded BJ-T, BJ-TE, and BJ-TER, respectively. The expression of SV40 LT (one of the products of the SV40 ER) and of H-RasV12 was verified by Western immunoblot (**Fig. 5**). SV40 LT was found in comparable levels in both BJ-TE and BJ-TER, while high levels of H-Ras were observed only in BJ-TER. Endogenous H-Ras was not detectable under these conditions. The same is true for the small t (st) antigen, the other relevant protein generated from the SV40 ER. Failure to make it visible in Western blots was probably due to lack of sufficiently sensitive antibodies.

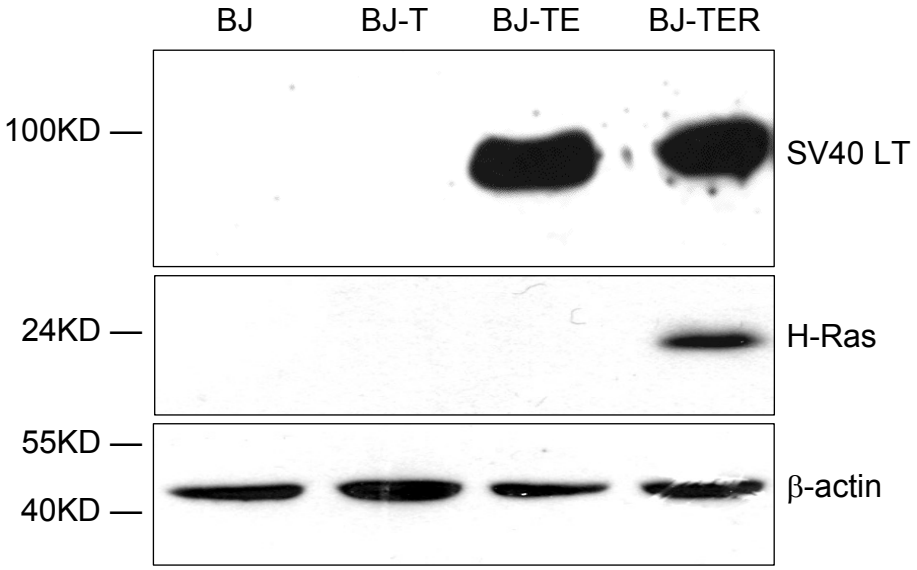

Fig. 5 Immunoblot in lysates from the four principal BJ lines against the SV40 Large T antigen and H-Ras. β-actin serves as loading control. LT could be detected in BJ-TE and -TER cells while elevated H-Ras expression was evident only in BJ-TER. Successful introduction of these transgenes is therefore demonstrated.

3.1.2. Real Time TRAP

The catalytic subunit of human telomerase, hTERT, is generally not active in differentiated cells (Kim *et al.*, 1994). The measurement of hTERT activity can be achieved using the telomeric repeat amplification protocol (TRAP) method. TRAP was originally conceived as a gel-based application, where increasing hTERT activity was visualized as a progressively longer

characteristic band pattern on a DNA gel (Kim *et al.*, 1994; Kim and Wu, 1997). We used a variation of TRAP, which was adapted for Real Time PCR (Wege *et al.*, 2003).

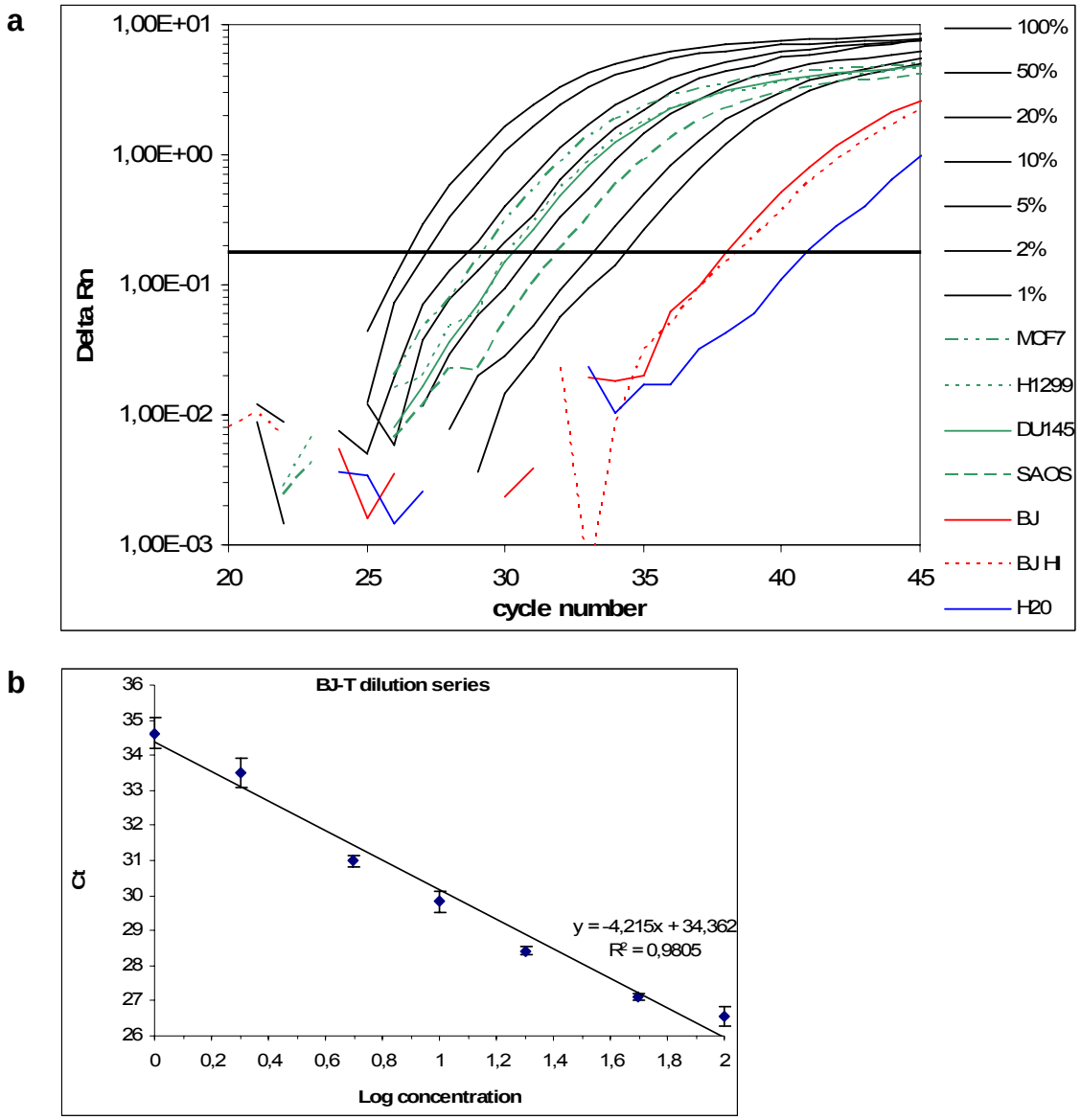

Fig. 6 Real Time PCR of BJ and BJ-T lines for hTERT activity. (**a**) The solid black curves belong to a dilution series prepared from BJ-T lysate, starting with pure lysate (100%; leftmost curve) and finishing with a hundredfold dilution (1%) at the right. These BJ-T derived curves serve as a reference for the measurement of wild type BJ lysate (red solid line), which show far less hTERT activity than even the 1% BJ-T curve. Indeed, the comparison with the heat inactivated BJ (HI, dotted red line) or the water control curve (solid blue line) demonstrate that BJ have hardly appreciable levels of active hTERT. The validity of the reference curves is demonstrated by the inclusion of four different hTERT positive cancer cell lysates (MCF7, H1299, DU145, SAOS; different green lines). All curves are one arbitrarily selected measurement out of a triplicate. The horizontal bar signifies the threshold by which the Ct values are determined. (**b**) Reference curve of BJ-T lysate dilutions generated from the Ct values (mean ± SD) of the black curves from panel (a) and the $\log_{10}$ of the corresponding BJ-T lysate concentrations.

Fig. 6a summarizes the results obtained with Real Time PCR TRAP (RT-TRAP) applied to lysates from BJ and BJ-T cells. As a reference, a dilution series from BJ-T cell lysate was prepared (**Fig. 6a**, black solid curves; **Fig. 6b**), since the hTERT activity in BJ-T presumably is very high. This is indeed the case, if one takes the curves of the telomerase positive cell lines

MCF7, H1299, DU145, and SAOS for comparison. Their specific hTERT activity corresponds to 16.8±1.2%, 10±1.1%, 9.8±2.3%, and 3.5±0.7%, respectively, of the activity found in undiluted BJ-T lysate (**Tab. 9**). In contrast, undiluted BJ lysate exhibited only trace amounts of 0.13±0.06% of the BJ-T activity. This value is unsubstantially higher than the value of 0.1±0.05% for the theoretical zero activity sample, heat inactivated BJ lysate (dotted red curve). The absolute baseline is set by the water control (solid blue curve) with 0.042±0.035%.

Tab. 9 Relative hTERT activity calculated from the Ct values in Fig. 6a. Activity values are the mean of three determinations and are expressed as percent of the activity found in undiluted BJ-T lysate. HI = heat inactivated; SD = standard deviation.

	BJ	***BJ HI***	***H_2O***	***MCF7***	***H1299***	***DU145***	***SAOS***
Activity [%]	0,131	0,101	0,042	16,83	9,97	9,77	3,46
SD	0,064	0,049	0,035	1,15	1,15	0,234	0,654

In summary, two things were proven with this experiment. First, BJ-T cells harbor a high level of ectopic hTERT activity, compared to cancer cells as a positive control. Second, the activity in the wild type BJ cells is practically not detectable since it is hardly above the background of the two negative controls BJ HI and water.

3.1.3. Soft agar test

Because of the profound changes in their molecular circuitry, one of the ways fully transformed cells differ from their precursors is the ability to grow in an anchorage independent fashion. A widely used test to uncover this latter ability is the soft agar assay. Cells are mixed with liquid agar or agarose and plated at low density on an agar bed, preventing this way any substrate contact. Cells are then cultured in this semi-solid material for a couple of weeks, during the course of which those cells with a tumorigenic potential will form clones while all others will merely survive as solitary cells. **Fig. 7** shows the result of the four BJ strain cell lines after they had been subjected to the soft agar assay for approximately three weeks. It is readily apparent that indeed only the TER line with the full set of transforming genetic elements grew out into clones. All other lines remained under these conditions single but viable cells, as determined by the vital stain Hoechst 33342. It should be mentioned here that in some repetitions of this experiment also BJ-TE were noted for having a tendency to develop clones, particularly in setups with higher cell densities.

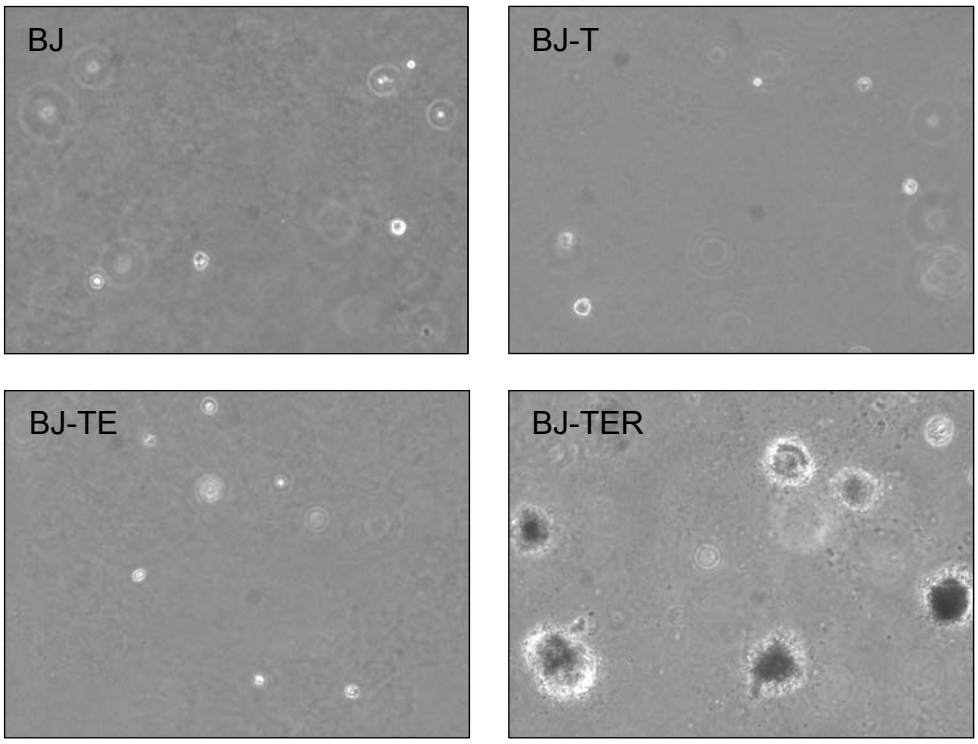

Fig. 7 Soft agar assay to test for anchorage-independent growth. In agreement with expected results only fully transformed TER cells were able to form colonies after about three weeks in agarose under these conditions ($4x10^4$ cells per well, regular feeding). BJ, BJ-T, and BJ-TE lines survive as viable, but single cells. Magnification 100x.

After having provided formal proof of the molecular integrity of the three engineered cell lines BJ-T, BJ-TE, and BJ-TER, they were further characterized to investigate possible changes in their biological properties brought about by their (partial) transformed status. First cell cycle profiles of all four stages of the model system were to be prepared. However, high throughput applications to analyze cellular properties like DNA content previously included flow cytometry and thus, required adherent target cells to be trypsinized and to be kept at least briefly in suspension. This proved to be a major drawback for the fibroblast lines of this work as it was not possible even under mild conditions to gain clean profiles. There are a number of possible explanations for this, excessive stress being one of them.

3.1.4. Cell cycle analysis

The cell cycle profiles shown in **Fig. 8** were obtained using a laser scanning cytometer (CompuCyte/ Olympus). One advantage of this technology is that adherent cells can be measured *in situ*. Therefore, cells of low passages were grown on 24-well plates under normal conditions, fixed while proliferating, and stained with DAPI. The histograms in **Fig. 8a** belong to the four BJ lines. The profiles for BJ and BJ-T are virtually identical. With a prominent, sharp G_1 peak and very little cells in S phase and G_2, they provide a typical example for the cell cycle distribution of slow-growing normal human cells. BJ-TE and BJ-TER cells are again very

much alike in their profiles. Aside from the sharp G_1 peak, they are characterized by a greatly expanded fraction of the S and G_2 phase. There is also a small but significant population of sub-G1 cells which is completely absent in the previous two profiles.

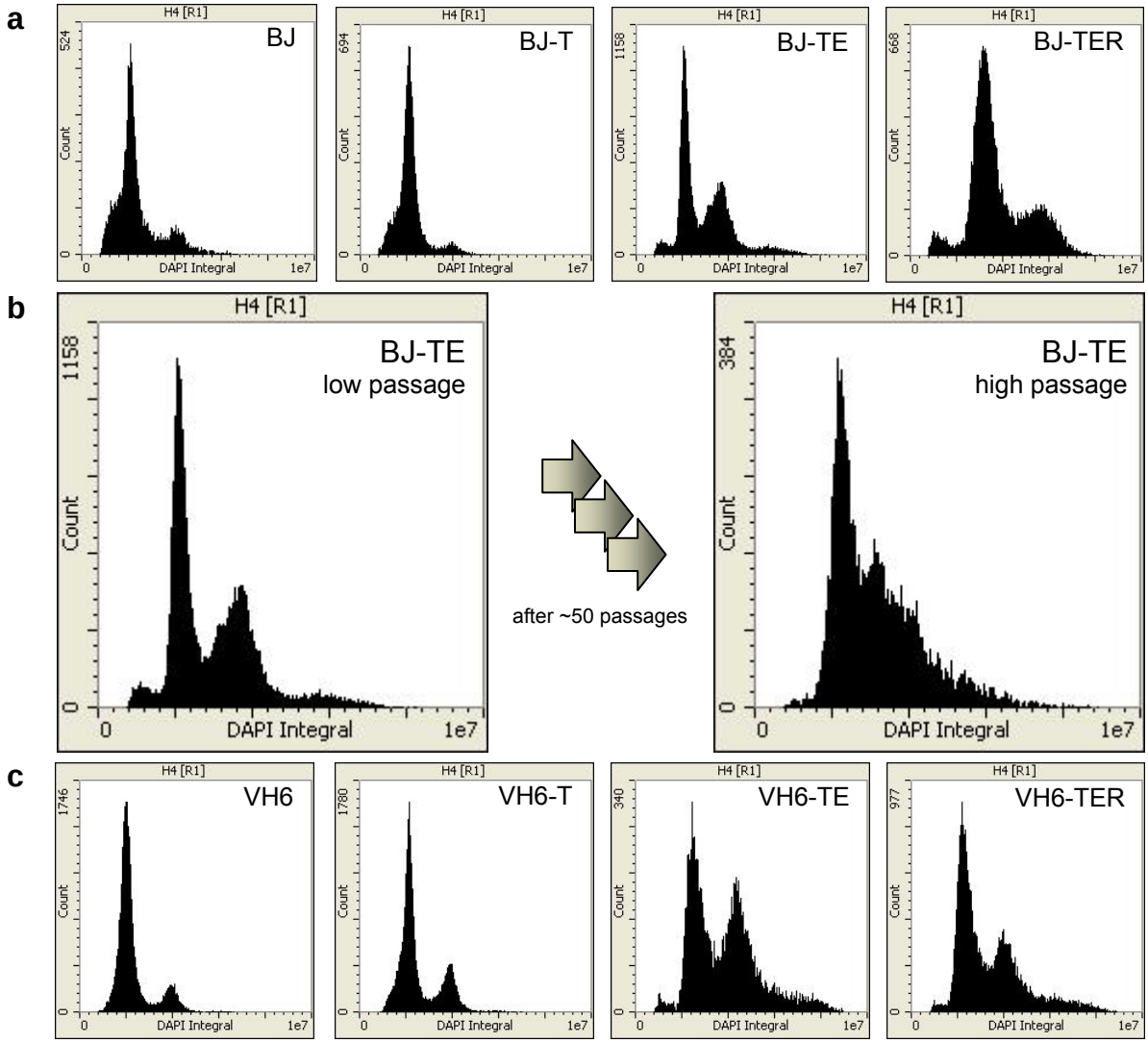

Fig. 8 Cell cycle profiles of human fibroblasts in different stages of experimental transformation. (**a**) All four BJ lines were stained at low passage numbers and sparse density with DAPI and measured while still adherent. BJ and BJ-T have the typical profile of normal proliferating cells with a prominent, sharp G_1 peak and very little S- and G_2-phase cells. BJ-TE are characterized by a marked increase in S- and G_2-phase and a significant sub-G_1 fraction. The profile of BJ-TER cells is in its distribution similar to low-passage BJ-TE but is shifted so far to the right that a complete transition to tetraploidy seems to have occurred. (**b**) The introduction of the SV40 ER into BJ-T alone leads to genomic instability. When BJ-TE cells were continuously cultured, a partial shift of the cell cycle to tetraploidy occurred, resulting in a mixed population of cells. (**c**) Cell cycle profiles for VH6, VH6-T, VH6-TE, and VH6-TER. Samples were treated exactly like described for the BJ strain. The VH6 profiles are very similar to those of the matching BJ lines except that in VH6-TER the shift towards a higher DNA content is less pronounced than in BJ-TER.

The most striking difference between the TE and TER lines is the apparent shift in the fully transformed BJ-TER from a normal diploid to a near-tetraploid set of chromosomes. This duplication seems to be more or less complete because the G_1 peak in BJ-TER exactly fills the spot of the G_2 peak in the BJ-TE histogram. Additionally, the BJ-TER G_1 and G_2 peaks have a

much broader base than the respective BJ-TE peaks. This further supports the assumption of widespread genomic instability in BJ-TER cells because it hints at the existence of other aneuploid cells beside those with a perfect duplication of their chromosome set.

Another interesting observation was made when BJ-TE cells were measured which had been in culture for about 50 passages more than those used in **Fig. 8a**. While not as extensive as BJ-TER, these aged TE also show clear signs of genomic instability. The most prominent sign is what could be interpreted as a second G_1 peak halfway between the regular G_1 and G_2 peaks (**Fig. 8b**). This can only be attributable to the presence of the SV40 ER and is not entirely unexpected given the well-characterized role of the SV40 st and especially the LT antigen in transformation. It appears plausible that the observed transition is progressive in nature, in other words, could be observed in passages less distant than the ones used in **Fig. 8b**. While this issue was not further investigated, care was taken that generally only cell material with low passage numbers was used for experiments.

Like many experiments in this work, this one was performed in parallel in BJ cells and in the corresponding VH6 cells. VH6 is another established laboratory strain of normal diploid human fibroblasts and was used to confirm results with the BJ lines. **Fig. 8c** shows that the respective corresponding derivatives of the VH6 and BJ strains are indeed essentially identical with two exceptions. Firstly, the fraction of G_2 phase cells in VH6-TE and -TER is relative higher. Secondly, the tendency to genomic instability is less readily seen in VH6-TER than in BJ-TER. Since the sensitivity of fibroblasts to the length of exposure to the SV40 ER has just been demonstrated, this might be an issue of difference in passage numbers, i.e., time in culture, between the two TER lines.

The last experiment to investigate the basic properties of the four fibroblast lines is an alternative method to establish the S-phase index, the BrdU staining. Cells are incubated for a short period with the DNA base analogue bromodeoxyuracil (BrdU). Only proliferating cells with active DNA synthesis will incorporate BrdU. The labeled DNA can be visualized by immunofluorescence with a specific BrdU antibody.

An elevation of the S phase index as a marker of increased proliferation (like seen in BJ-TE/ -TER; **Fig. 8**) is a hallmark of malignant transformation (Hanahan and Weinberg, 2000). Hence, the expected outcome of the immunofluorescence staining is a confirmation of the findings above. **Fig. 9** shows representative images of BJ, BJ-T, BJ-TE, and BJ-TER (top to bottom) stained for BrdU (red). Total nuclei are made visible with DAPI (blue). S phase cell nuclei consequently appear bright red to purple in the overlay. Cells were grown for 36h under starvation (0.1% FCS; **Fig. 9a-d**) or normal conditions (10% FCS; **Fig. 9a'-d'**). From those

images it is obvious that starvation arrested cell proliferation in all lines, albeit to varying degrees, as testified by the reduction or absence of BrdU positive cells in the left column of **Fig. 9**. It is also evident that the increase of cells in the S phase from BJ to BJ-TER seen with laser scanning cytometry is mirrored here. This is true both under normal conditions and even more so during starvation.

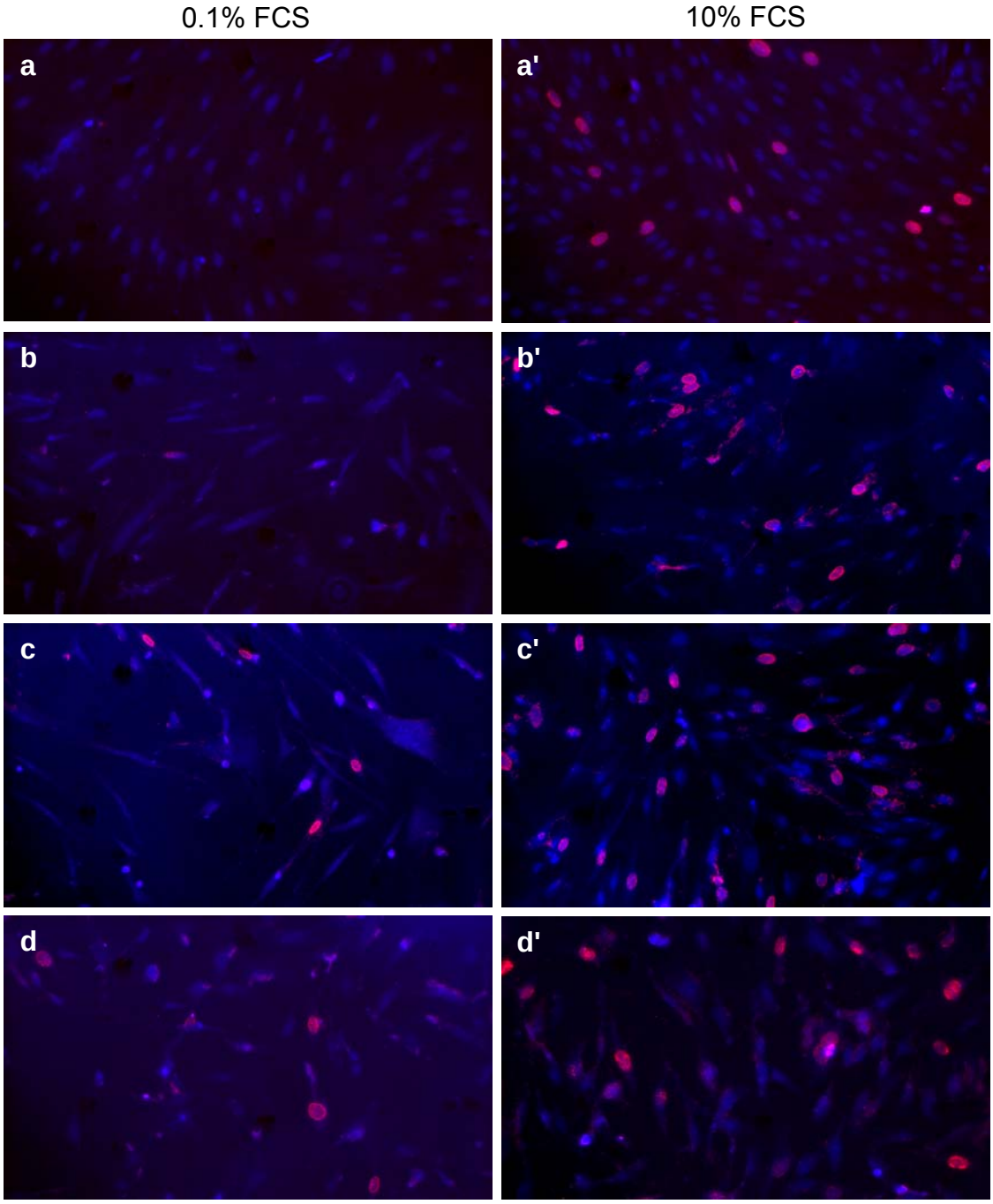

Fig. 9 Representative images of BJ, BJ-T, BJ-TE, and BJ-TER cells stained with an antibody against BrdU after serum starvation (**a-d**) and under normal conditions (**a'-d'**). Cells were cultured for 36h, followed by an overnight incubation with 10µM BrdU. The nuclei of cells which incorporated BrdU (and which were consequently in the S-phase) appear bright red. The total cell number was determined by counterstaining with DAPI (blue).

The S phase indices were quantified by counting at least four different images per treatment and cell line and their statistical differences were determined. Statistics were calculated with the t-test (two-tailed and for unpaired samples). According to **Fig. 10**, significant differences exist between BJ and BJ-TE/ -TER (0.1% FCS) and BJ and BJ-T/ -TE/ -TER (10% FCS). When the two samples of each BJ line are compared with each other, it is interesting to note that in the lines with wild type-like cell cycle profiles, BJ and BJ-T, the different treatments lead to significantly different S phase indices (t-test, $p<0.05$). Those cells are almost completely arrested after serum starvation and have significantly more proliferating cells (10 and 25%, respectively) when properly fed. BJ-TE and BJ-TER in contrast each maintain a very similar fraction of dividing cells of around 25-30%, both with 10% FCS and after 36h starvation. This vitality in the face of severe nutritional stress is probably an effect of the introduced SV40ER in BJ-TE. Indeed, Hahn *et al.* (2002) could show that the minor ER product small t markedly increased the cell proliferation in immortalized BJ and HEK cells. This effect was even more pronounced under serum starvation and was independent from H-Ras. However, H-RasV12 probably contributes in BJ-TER as well, since it provides constitutive internal growth stimuli. Increased cell vigor clearly is advantageous for a developing tumor, particularly before it acquires the ability to recruit blood vessels.

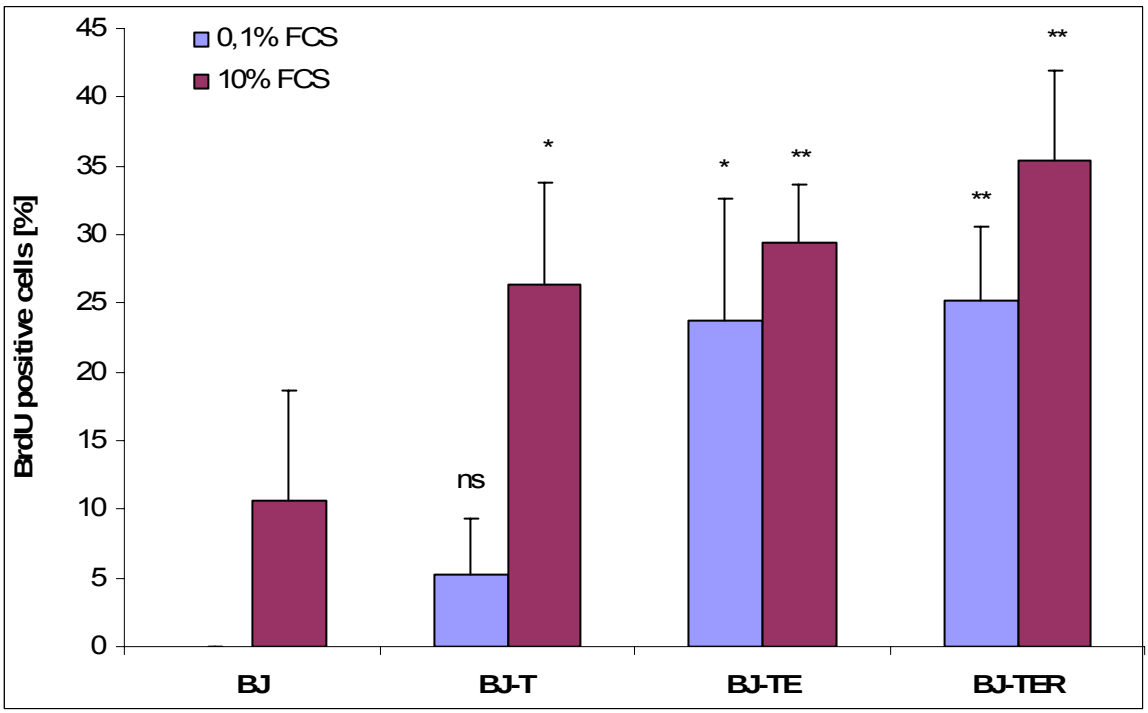

Fig. 10 Quantification of the BrdU staining in the five BJ lines after serum starvation (blue column) and under normal conditions (purple columns). Values represent the mean fraction of BrdU-positive cells (i.e., the S-phase index) with the standard deviation of at least four different counted areas. Significant differences to the respective BJ wild type sample are indicated by asterisks (*: $p<0.05$, **: $p<0.01$; Student's t-test, two-tailed, for unpaired samples).

3.2. Up-regulation of p73 in TE cells

3.2.1. TAp73 is up-regulated in confluent BJ-TE cells

After some of the basic properties of the fibroblast cell lines had been defined, we went on to investigate their p73 status. It has been outlined that the *TP73* gene gives rise to two distinct categories of proteins that differ in their amino terminal end and have opposing functions. The scope of this work was mostly limited to the transcription competent full-length TAp73 isoforms with potential tumor suppressive functions. The regulation of the oncogenic counterpart ΔNp73 within the framework of the fibroblast model system remains to be investigated in more detail.

TAp73 shares many functional and regulatory features with its family member and better understood homolog p53. Both are transcription factors, which upon activation exert their protective effect mostly through sequence-specific target gene activation, resulting in apoptosis (both) or senescence (only p53). Since their cognate promoter sequences overlap, it is hardly surprising that there exists a certain degree of functional redundancy between p53 and p73. In fact, a number of important p53 target genes like $p21^{WAF1}$, $p27^{kip1}$, *BAX*, *HDM2* were shown to be activated by p73 as well (Fontemaggi *et al.*, 2002; Lee and La Thangue, 1999; Zhu *et al.*, 1998). On the other hand, due to its central role as "guardian of the genome", p53 is in almost all tumors either directly or indirectly deactivated, while p73 is hardly ever found mutated there. However, little is known about its regulation in pre-malignant stages or what role indirect means of neutralizing TAp73 might play. It is therefore of interest if in the engineered BJ lines (i.e., at some point along the way to transformation) a change in TAp73 expression occurs.

The first piece of evidence about differential regulation of TAp73 in the fibroblast model system came from the level of transcription. In a Real Time PCR with primers specific for TAp73 (**Fig. 11a)** cDNA from all four BJ lines, harvested either proliferating or 100% confluent, was measured. According to **Fig. 11a,** BJ-T (blue curves), BJ-TE (red), and BJ-TER (light green) all have a similar low levels of TAp73 mRNA like their respective proliferating (broken lines) or confluent (solid lines) BJ wild type control (grey). The only exceptions are confluent BJ-TE cells, which have a mean Ct value of 29.2±0.64 vs. 37.2±1.2 in confluent BJ. That these differences are real is demonstrated in **Fig. 11b**. As a control for balanced cDNA synthesis and equal loading the confluent samples were also tested for their transcript levels of GAPDH, a constitutively expressed housekeeping gene. All curves are almost identical (Ct: 17.64±0.21 for BJ, 17.55±0.1 for BJ-TE) which means that the TAp73 results can be directly compared.

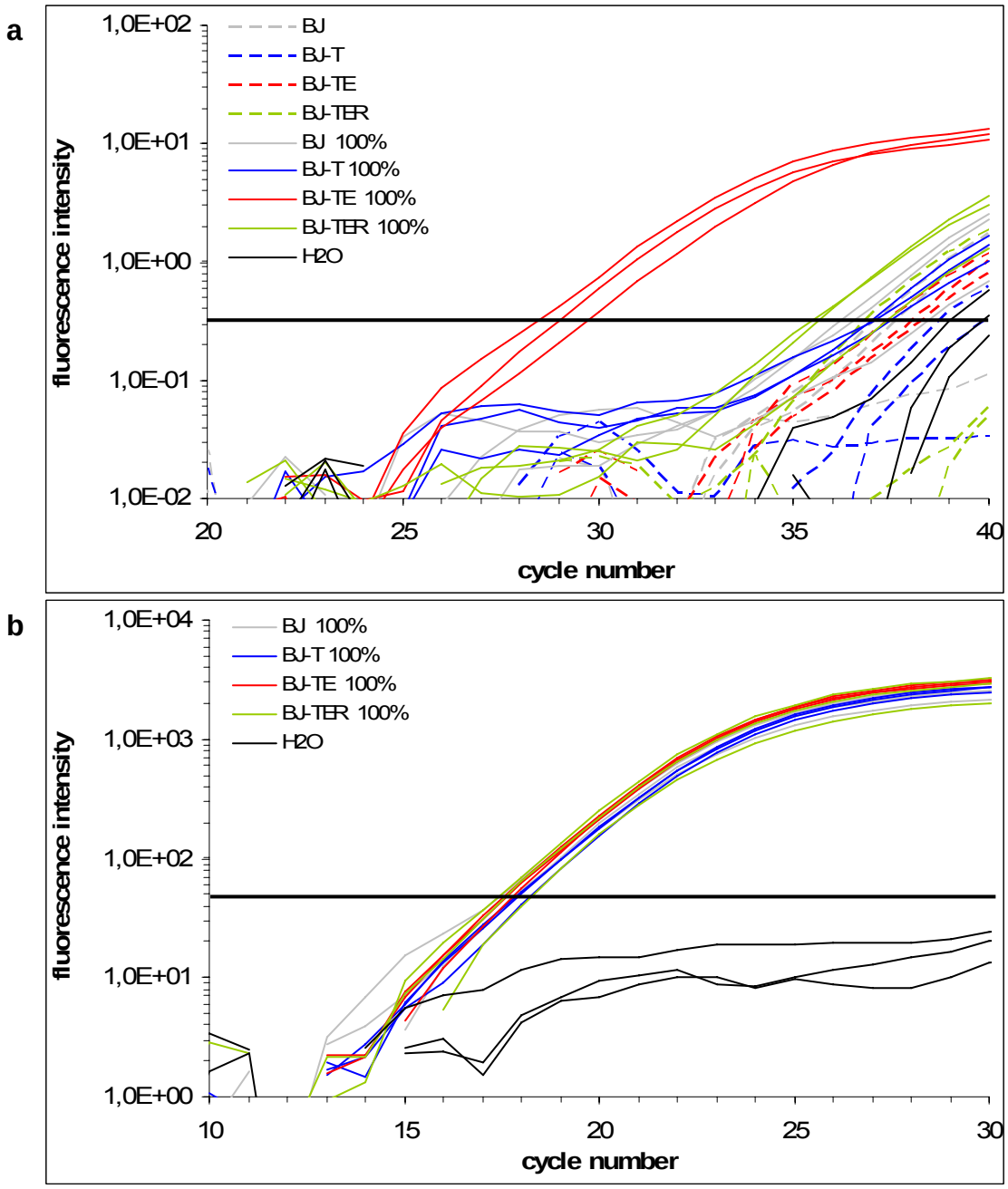

Fig. 11 Real-time PCR for TAp73 (**a**) and GAPDH (**b**) in BJ, BJ-T, BJ-TE and BJ-TER cells. In both graphs colored broken lines are used for samples from proliferating cells and colored solid lines for samples from confluent (arrested) cells. Black solid lines mark the water control. All samples were measured and drawn as triplicates. The horizontal bars signify the threshold by which the Ct values are determined. Note that the scales of the x- and y-axis are different in both graphs. (**a**) It is plainly visible that only confluent BJ-TE cells have relatively much of TAp73 transcript; all other samples, including "BJ-TER 100%", are very close to the low wild type levels. (**b**) Distortions due to unequal reverse transcription or loading of cDNA can be excluded at least for the confluent samples because the all of the curves for the mRNA level of GAPDH, a housekeeping gene, are virtually identical.

The GAPDH data may also be used to normalize the results from **Fig. 11a**. The calculation assumes a duplication of PCR product in each cycle. The difference between the Ct values of BJ 100% and BJ-TE 100% then translates to an about 240-fold TAp73 activation (**Fig. 12**).

Importantly, this activation is almost nullified in BJ-TER 100%, which retain little more than basic TAp73 levels.

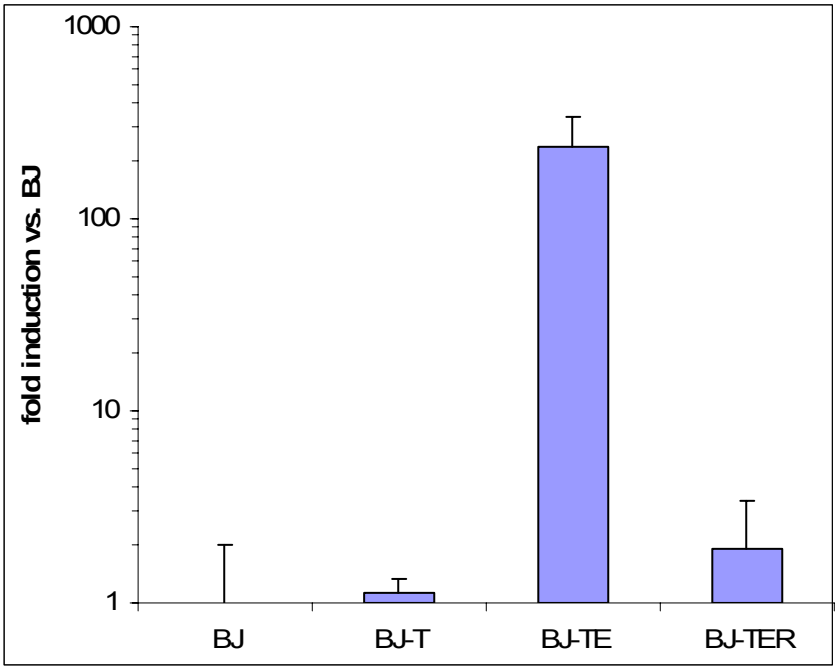

Fig. 12 Semi-log plot of the relative TAp73 induction in the BJ cell lines. Results from the TAp73 Real Time PCR were normalized with the Ct values from the GAPDH Real Time PCR. The TAp73 mRNA level in BJ is defined as one. The data adjustment therefore gives the mean fold induction of TAp73 compared to BJ. Error bars = adjusted SD.

Finally, one randomly selected well out of each of the eight triplicate samples was run on a DNA gel to visualize the described outcome. A picture of the gel (**Fig. 13**) reveals that the amounts of PCR product closely resemble the relationship of the Real Time curves in **Fig. 11a**. Only cDNA from confluent BJ-TE (lane 7) gave significant amount of PCR product. The other three confluent samples (lanes 5, 6, 8) are represented by very faint bands, the strongest of which belonging to BJ-TER (lane 8). There is no trace at all from the four proliferating cell samples (lanes 1-4).

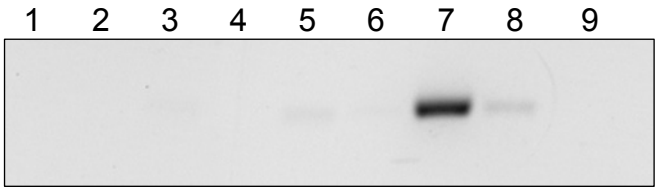

Fig. 13 DNA gel with TAp73 Real Time PCR products. One randomly selected samples out of every triplicate from Fig. 11a was run on a 2% agarose gel. Order of loading: lanes 1-4, BJ/ BJ-T/ BJ-TE/ BJ-TER proliferating; lanes 5-8, BJ/ BJ-T/ BJ-TE/ BJ-TER 100%; lane 9, water control. The "BJ-TE 100%" sample is again the only one with any significant amount of PCR product. A much weaker signal is in addition just visible in lane 8 (BJ-TER 100%).

The elevated transcript levels of TAp73 found only in BJ-TE were also confirmed in semi-quantitative RT-PCR. Comparison of confluent with proliferating samples in **Fig. 14** proves that

the only substantial increase happened when BJ-TE grew dense. The other three BJ lines showed no difference in their TAp73 transcripts irrespective of whether harvested at sparse or high density. Quite in contrast to the dynamics of tumor suppressive TAp73 mRNA, the transcripts of the oncogenic, truncated isoform ΔNp73 seem to be up-regulated only in BJ-TER, in particular if they are still proliferating. However, this interesting lead has not been followed in this work.

As a control for the correct identity of the four cell lines PCRs for the SV40 Large T antigen and for hTERT were performed (**Fig. 14**). The cell lines could be verified, because LT is expressed only in BJ-TE and -TER, while hTERT was found additionally in BJ-T (but not in parental BJ). The hTERT result, as far as BJ/ BJ-T are concerned, is also in good agreement with the outcome of Real Time PCR (confer **Fig. 6** and **Tab. 9**). Equal loading in the RT-PCRs is demonstrated by quantification of GAPDH.

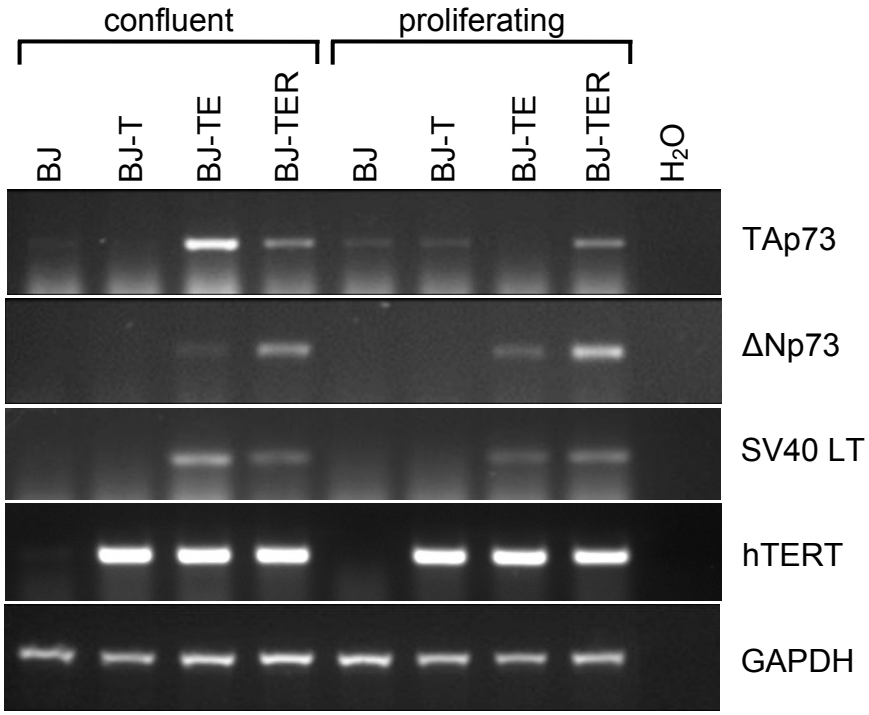

Fig. 14 Semi-quantitative RT-PCR in the four BJ lines, confluent and proliferating. If the TAp73 status at both densities is compared for each cell line, it shows that there are no big changes except for the already observed strong induction in confluent BJ-TE. Conversely, oncogenic ΔNp73 is found up-regulated only in proliferating BJ-TER cells. The proper expression of two introduced transgenes, SV40 LT and hTERT, is demonstrated as well. Equal loading control is provided by the PCR against GAPDH.

An interesting observation is that the density-dependent increase of TAp73 transcript in cells transfected with the SV40 Early Region is not restricted to the fibroblasts of the model system. Connective tissue is derived from the mesodermal germ layer, but the correlation of confluence and TAp73 expression could also be observed in HA1E, cells of endodermal origin (**Fig. 15**).

HA1E are renal epithelial cells, which have been transfected with hTERT and the SV40 LT (Counter *et al.*, 1998).

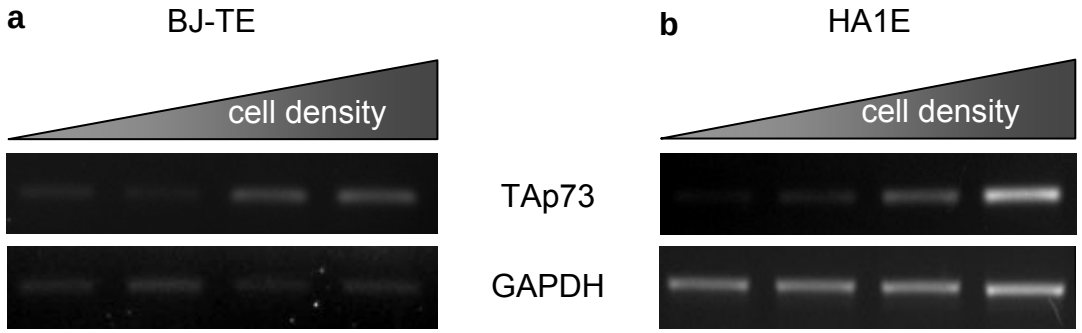

Fig. 15 Semi-quantitative RT-PCR for TAp73 in cell lines of different embryogenic origin. (**a**) BJ-TE as fibroblasts are of mesodermal origin. (**b**) HA1E epithelial cells are derived from the endodermal germ layer. In both cases, the amount of TAp73 transcript correlates directly with the confluence of the culture. Cell density-dependent increase of TAp73 therefore appears to be a general, if not universal regulative mechanism.

Usually findings from the mRNA level should be verified for the protein world. This is advisable because ratios of amounts of transcript are not necessarily preserved between samples of diverse origins due to the confounding influence of posttranscriptional mRNA processing or varying translation efficacy. Therefore the TAp73 protein level was determined by Western blot in confluent samples from all four BJ lines. It is evident from **Fig. 16** that indeed the elevated transcript level found in BJ-TE is translated into a likewise increased amount of TAp73 protein, compared to the other three lines. Given the generally low abundances of p53 proteins and the resulting small absolute differences in endogenous protein levels it is of particular importance here to demonstrate equality in total protein loading. As can be seen in **Fig. 16**, this premise is nicely fulfilled since β-actin levels are very similar in all lanes.

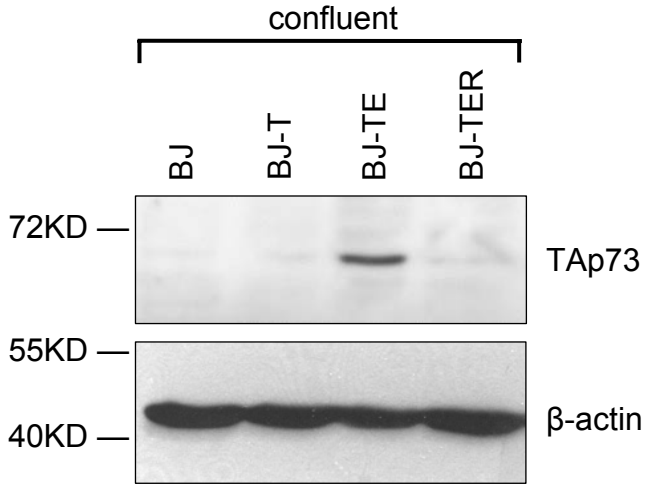

Fig. 16 Western Blot for TAp73 in confluent BJ/ BJ-T/ BJ-TE/ BJ-TER. This experiment confirms that the increase of TAp73 transcripts in BJ-TE is indeed carried over to the protein level. β-actin is included as equal loading control.

3.2.2. SV40 LT, not st, leads to elevated levels of p73 in TE cells

It has been shown above that BJ-TE have markedly increased levels of TAp73 mRNA and protein, compared with BJ, BJ-T and BJ-TER. The only change between BJ-T and BJ-TE is the introduction of the SV40 Early Region, which gives rise to three peptides, the small t antigen (174aa/ 21kDa) , the 17 kT (135aa/ 17kDa) (Zerrahn *et al.*, 1993), and the Large T antigen (708aa/ 94kDa). They are generated by alternative splicing and all share the first 82 residues of the amino terminal end (**Fig. 17**). Two of these, the st and LT antigen, have an extensive track record of publications that investigate or exploit their oncogenic potential in eukaryotic host cells. The third, 17kT, was disregarded here for two reasons. On the one hand, there is no report about a role in transformation to date, and like the group of W. Hahn we did not observe any expression of 17kT (Hahn *et al.*, 2002). Second, one can argue that since it is little more than an N-terminus of the LT protein, it will behave exactly like that: an additional Rb inhibitor. With respect of the regulation of TAp73 in the model system, this raises two questions. First, which polypeptide product of the SV40 ER is responsible for the observed up-regulation of TAp73 in BJ-TE, st or LT? Second, what is the underlying molecular mechanism- what other factors are involved, which pathways are triggered?

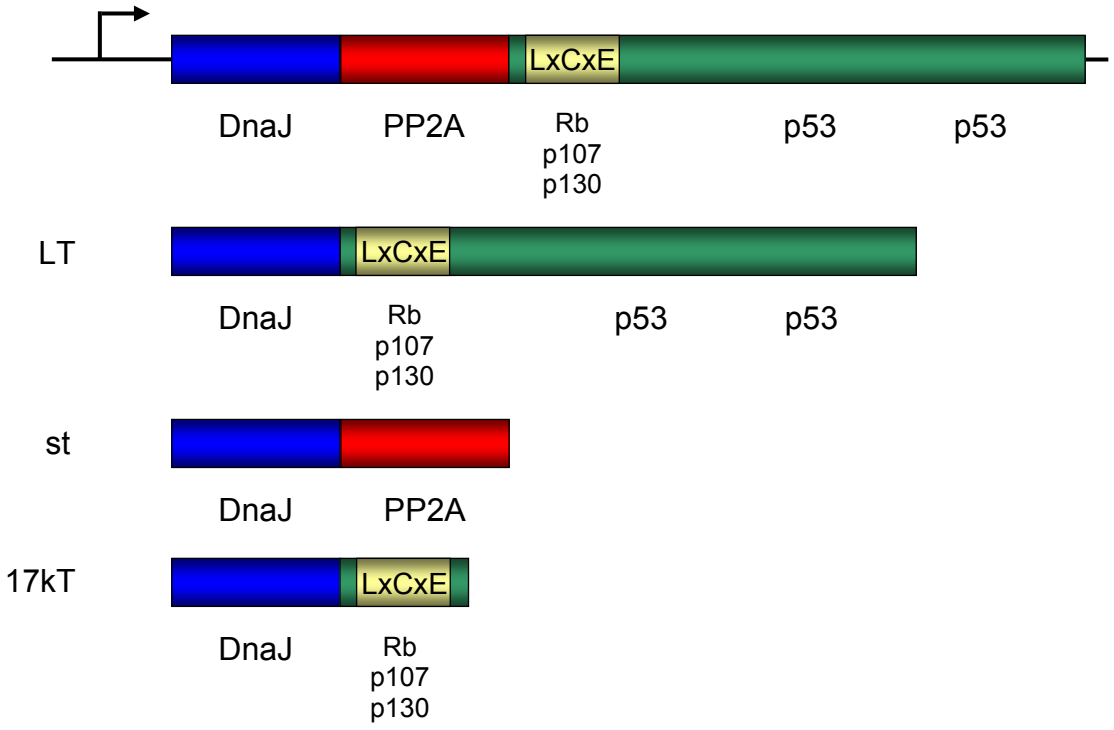

Fig. 17 Viral proteins produced by the SV40 Early Region. The large T antigen, small t antigen and 17 kT protein are generated by means of alternative splicing. They all share the same first 82 residues of the amino terminus, which contains a domain with homology to the DnaJ family of molecular chaperones. LT is the only product with LxCxE motif (Rb binding) and a bipartite region for interaction with p53. The unique C-terminal end of st that specifies PP2A binding is encoded by an intronic region in the LT sequence. The 17kT protein sequence is identical with the first 131 amino acids of LT, followed by four residues (ALLT) from a different reading frame. Redrawn from (Hahn and Weinberg, 2002a).

To answer the question which of those two viral proteins causes the TAp73 peak, VH6-T cells were infected with empty lentivirus or with one harboring st, LT, or ER. Immediately after their transduction, cells were grown to confluence and harvested. RT-PCRs were performed to detect LT, st, TAp73, and GAPDH (loading control).

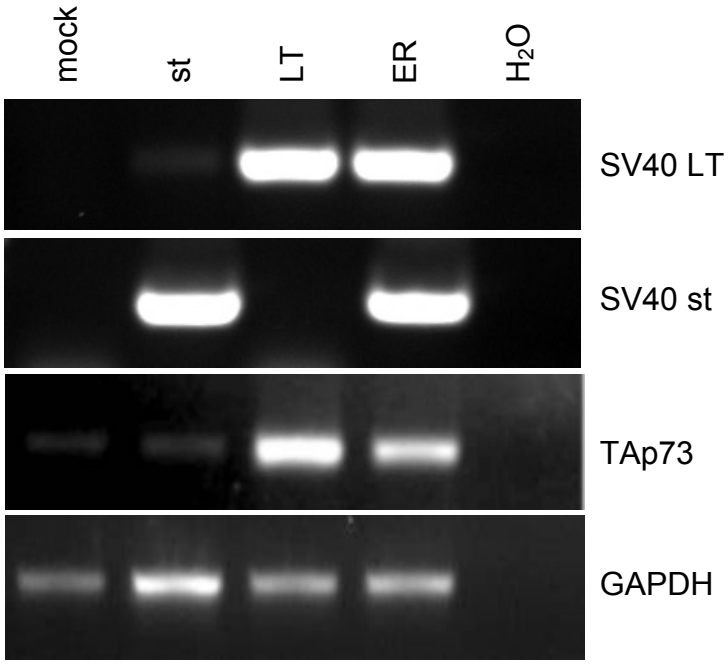

Fig. 18 RT-RCR in confluent VH6-T cells which were stably transduced with lentiviruses carrying empty vector (mock), the small t antigen (st), Large T antigen (LT) or the Early Region (ER) of SV40.

Fig. 18 shows first that st and LT were transcribed in the appropriate lines to high mRNA levels. More importantly, it is obvious that LT alone is responsible for the TAp73 induction, because this effect could be reproduced in the VH6-T cells freshly transduced with LT-virus. Cells infected with an ER-virus were included as a positive control and therefore give a strong TAp73 band as well. Any role of st in facilitating the high TAp73 levels in TE cells can probably be excluded. This is because the fresh VH6-T>st cells in **Fig. 18** do not have more TAp73 transcript than the base level of mock infected cells.

3.2.3. Transcriptional regulation of TAp73

After having established LT as the causative agent of TAp73 induction, we went on to identify the pathway(s) involved and to investigate the possible role of other factors. Likely candidates were found after considering the known partners with which the LT antigen directly interacts (reviewed in Saenz-Robles *et al.*, 2001). **Fig. 19** gives an overview of the functional domains in LT. Highlighted in red are the three domains that were chosen for the next set of experiments (Ali and DeCaprio, 2001; Conzen and Cole, 1995; Zhu *et al.*, 1992). Like other DNA tumor viruses, SV40 has evolved to inactivate both the Rb and p53 tumor suppressors by direct

binding. In fact, p53 was first discovered in complex with LT (Lane and Crawford, 1979; Linzer and Levine, 1979). In addition, the J domain at the extreme N-terminus mediates the inactivation of the Rb and the Rb-related p107 and p130 proteins (Zalvide *et al.*, 1998). Finally, Conzen *et al.* (1997) found evidence for a p53-independent antiapoptotic function which was located in the BH1-like domain. Since p73 also induces apoptosis in several manners which do not require p53 (Ramadan *et al.*, 2005), this domain is an interesting candidate for mediating a connection of LT with p73 signaling.

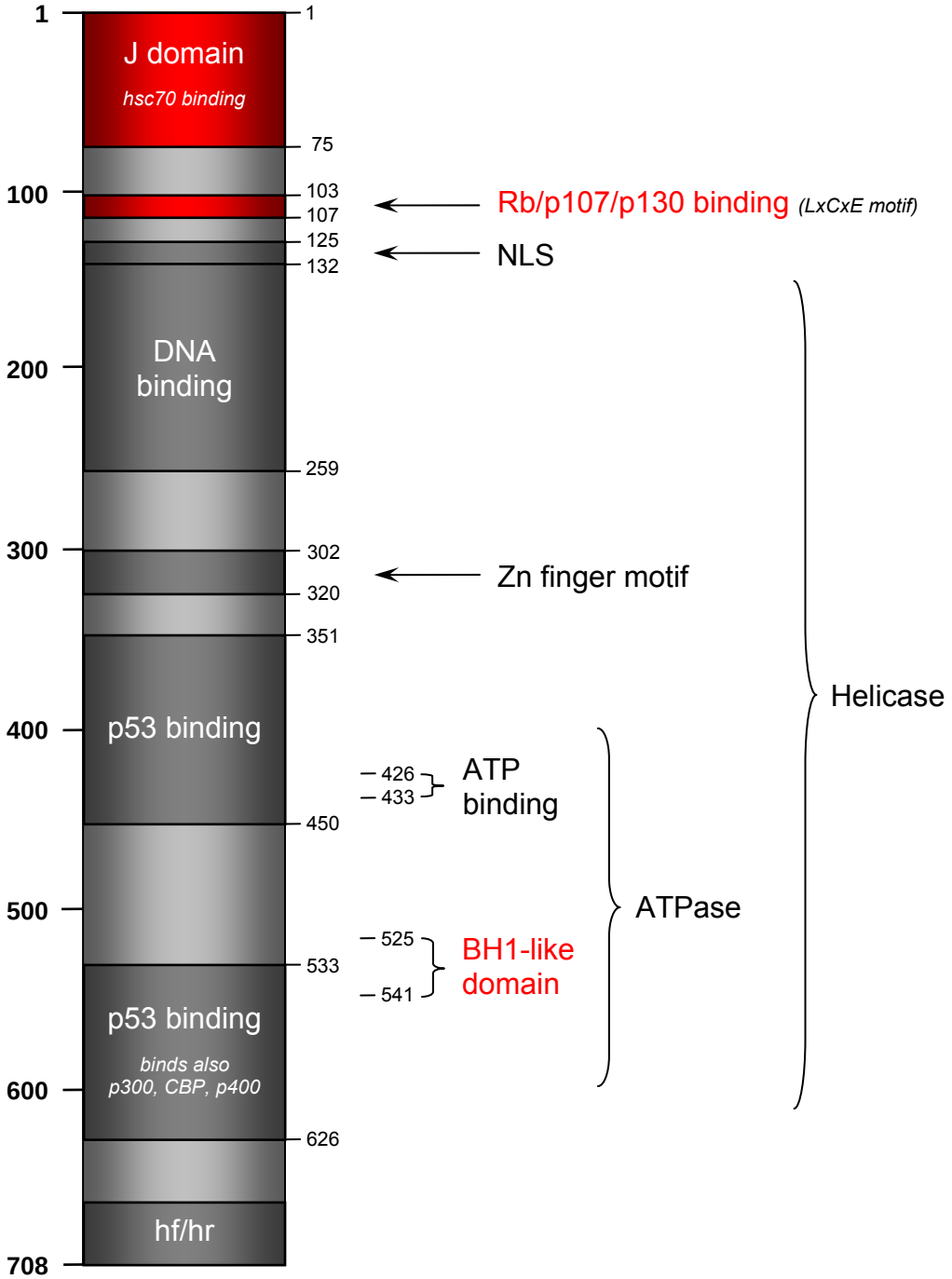

Fig. 19 Selected functional domains and binding sites of the SV40 Large T antigen. Numbers refer to amino acid positions. The domains selected to be deactivated for further studies are highlighted in red. NLS = nuclear localization signal; hf/hr = determines host range. Diagram was compiled from following sources: (Ali and DeCaprio, 2001; Conzen *et al.*, 1997; Zhu *et al.*, 1992), and SwissProt entry #P03070.

To determine which of the three selected functional domains might be important for its transactivation of TAp73, several published point mutations were introduced in LT. Specifically, the Y34A, E107K, and M528S mutants disable the function of the J domain, the LxCxE motif (Rb/p107/p130 binding), and antiapoptotic properties, respectively (Conzen and Cole, 1995; Rundell and Parakati, 2001; Zhu *et al.*, 1992). These LT mutants were cloned into adenoviral vectors and transfected in T98G glioblastoma cells together with reporter constructs expressing luciferase under control of the TAp73 promoter. The outcome of the subsequently performed luciferase assays is shown in **Fig. 20**. Presence of wild type LT leads to a moderate 2.5fold induction of luciferase, compared to the negative control with empty vector. Surprisingly, the E107K and M528S mutants give approximately the same result. In contrast, the LT construct with the J domain mutation, Y34A, is not able to transactivate luciferase expression via the TAp73 promoter. This outcome could be exactly reproduced in H1299 lung cancer cells and in VH6-T.

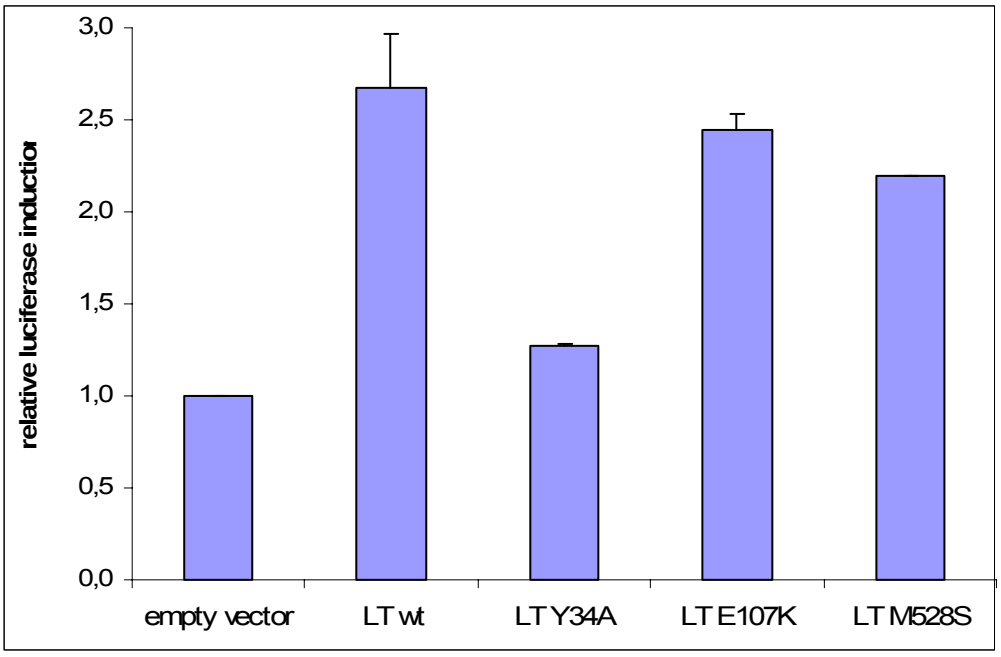

Fig. 20 Result of a luciferase assay in T98G glioblastoma cells. T98G were transfected simultaneously with a reporter plasmid containing luciferase under control of the TAp73 promoter and an empty vector or vector coding for various forms of the SV40 Large T (wt = wild type, Y34A, E107K, M528S = point mutation in the J domain/ Rb binding motif/ BH1-like domain, respectively; confer Fig. 19). Results from duplicate experiments are expressed as fold induction compared to empty vector. Mutations at critical positions of the Rb and BH1-like domains had no effect on p73 promoter driven luciferase expression. However, the LT mutant with the defective J domain was hardly able to transactivate. It can be concluded from this that the J domain might play an important role in the LT mediated up-regulation of TAp73.

The preliminary conclusion from the luciferase assays is that neither the antiapoptotic function nor the Rb binding seem to be involved in the interaction of Large T with the TAp73 promoter. However, a possible role for Rb or its relatives of the pocket protein family, p107 and p130, is still conceivable. It has been pointed out above that the J domain is required to override the

repression of E2F activity by Rb, p107 and p130. The name "J" is derived from the homology to the DnaJ family of molecular chaperones. An immediate function of the LT J domain is the binding of hsc70, a constitutively expressed form of mammalian hsp70; curiously, it was also called "p73" upon discovery (Sawai and Butel, 1989). One possible mechanism by which LT perturbs Rb, p107 and p130 function is to couple ATP hydrolysis by hsc70 with the endothermic disruption of various Rb/p107/p130-E2F transcriptional repressor complexes (compare **Fig. 22**) (Lee and Cho, 2002; Sullivan *et al.*, 2000). Taken together, Rb or p107/p130 are the probable mediators in LT-directed TAp73 up-regulation.

It is important at this point to stress that E2F1 is one of the most important direct activators of p73 transcription (Stiewe and Putzer, 2000). This can be easily demonstrated in cell culture for example by infecting one of the fibroblast lines with an E2F1-adenovirus (**Fig. 21**).

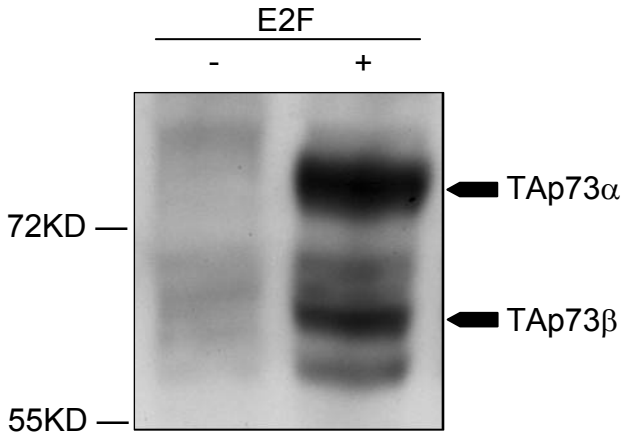

Fig. 21 p73-Western blot of VH6-TE cells infected with AdGFP (-) or AdGFP-E2F (+) adenovirus. Presence of E2F1 leads to a sharp rise in TAp73 levels, best observed in the two most abundant C-terminal isoforms, α and β. The other bands possibly belong to other full-length isoforms.

However, in quiescent cells hypophosphorylated Rb forms a repressor complex with E2F1 and DP-1 on the promoter of p73 (Seelan *et al.*, 2002), preventing its transactivation (**Fig. 22a**). This might explain in part the low abundance of TAp73 in normal (i.e., slowly proliferating) cells like wild type BJ. Rb is a master regulator at the G_1/S phase checkpoint of the cell cycle. In the presence of growth signals, it is deactivated by phosphorylation, which causes its dissociation from the various promoters, allowing expression of the respective genes. Many of these are S phase genes like cyclin E, cyclin A or cdc2 and drive the progression of the cell into mitosis. The increased TAp73 levels in BJ-TE could therefore be explained by the well-documented capability of LT to disrupt Rb/p107/p130-E2F repressor complexes (**Fig. 22b**) (Lee and Cho, 2002). Binding of Rb/p107/p130 by LT results in the effective displacement of Rb family members, given the high level of Large T in TE cells, and E2F1-driven transactivation of TAp73 could ensue then.

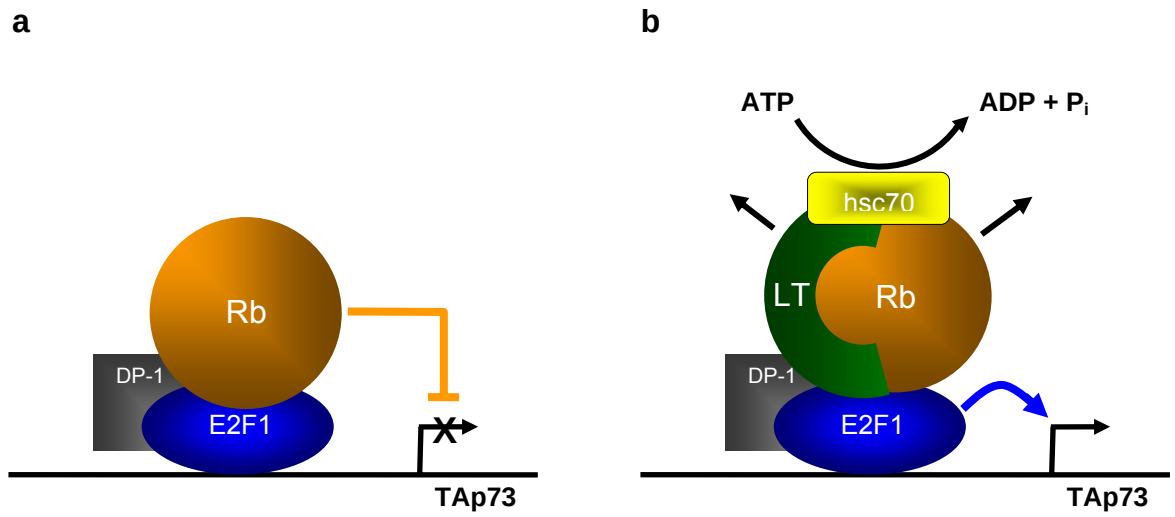

Fig. 22 Model of LT-mediated TAp73 up-regulation. (**a**) Normally transcription factors E2F1 and DP-1 are bound to the TAp73 promoter, which contains at least five E2F binding sites immediately upstream of intron 1. In the absence of proliferative signals, hypophosphorylated Rb and other factors (Abl, Suv39H1, HDAC; omitted for clarity) form a repressor complex around E2F/ DP-1. Expression of the p73 gene cannot commence. (**b**) Hypothetical mechanism of Rb inactivation in TE cells: LT binds to Rb, recruits the co-chaperon hsc70, which stimulates the ATP-driven dissociation of the repressor complex, leaving E2F1 bound to the promoter. Transactivation of TAp73 can now proceed.

Combining both the earlier demonstrated role of LT in TAp73 up-regulation and the requirement of TAp73 transcription on active E2F1, it was decided to test various TAp73 promoter constructs in luciferase assays in the presence and absence of LT. **Fig. 23a** shows the relevant region in the vectors. Five putative E2F binding sites with the consensus sequence TT(C/G)(C/G)CG(C/G) are marked with yellow ovals between -450bp and -160bp relative to the start codon. Aside from the wild type (WT) promoter, two variants called mut2/4/5 and mut2/3/4 were used. They differ in their pattern of mutated E2F sites (crossed-out ovals). Again, these reporter plasmids were transfected into T98G cells together with either empty or wild type LT vector. The outcome of a typical assay is plotted in **Fig. 23b**. The promoter activities are expressed as the ratio of luciferase expressed in the presence over the absence of LT. The mutations of E2F sites 2, 4 or 5 do not seem to influence the promoter efficiency, because mut2/4/5 (red column) leads to an about 2.5fold induction of luciferase, if LT is present. This is identical to the result with non-mutated promoter (blue column). However, if the mut2/3/4 vector (violet column) was used, induction ratio dropped below one, indicating the stimulating effect of LT on transcription was lost. One can infer from this that either E2F binding site number 3 or the cluster of binding sites 2, 3, and 4 as a whole are of particular importance for the transcriptional activation of TAp73.

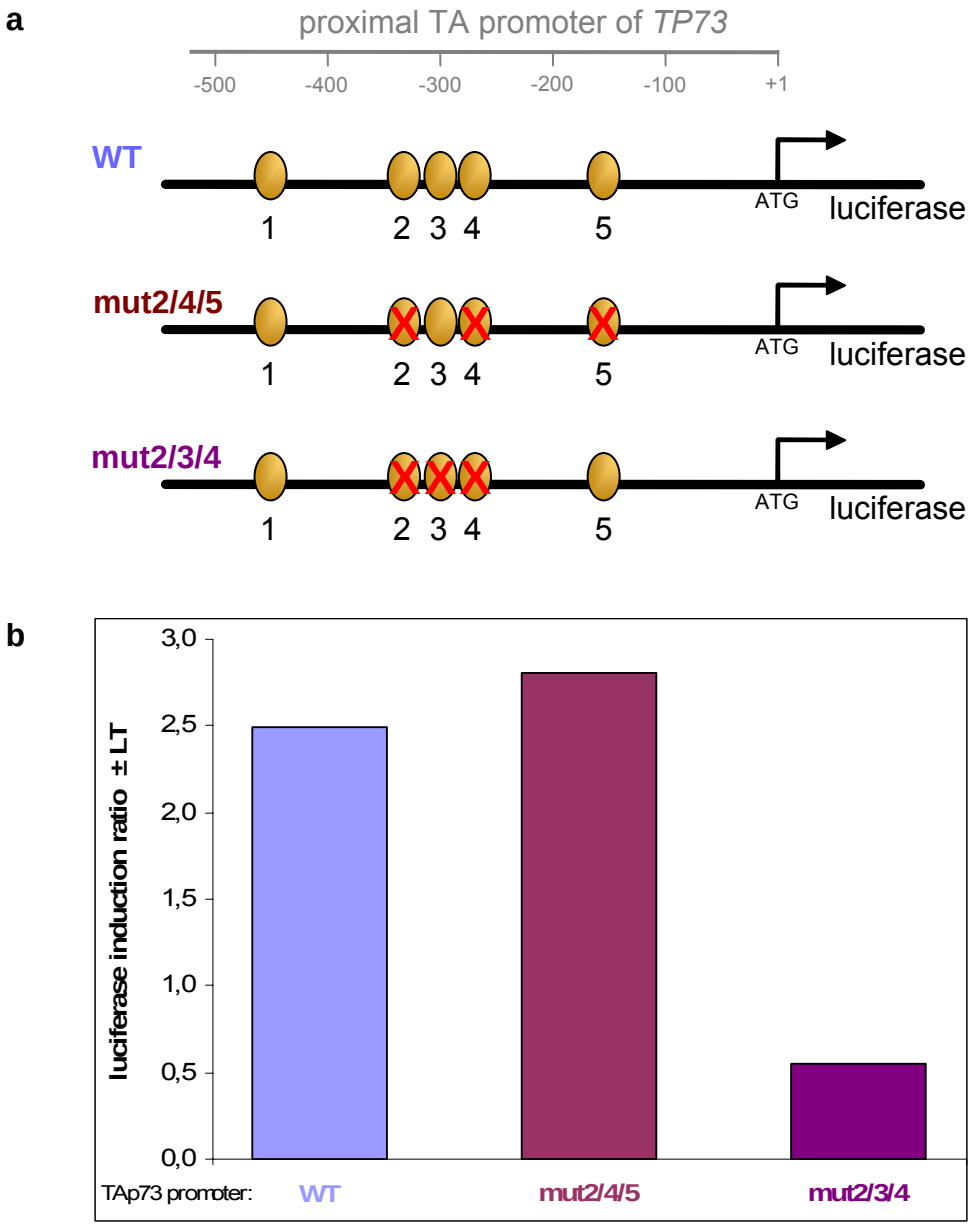

Fig. 23 Luciferase assays with three different variants of the TA promoter of the TP73 gene. (**a**) Schematic representation of the promoter region of the reporter plasmids. Five putative E2F binding sites are indicated by yellow ovals and crossed out if mutated. They are drawn approximately to scale with respect to their distance to the start codon (ATG). The exact positions are -437(?)bp/ E2F1 site #1; -308bp/ #2; -300bp/ #3; -288bp/ #4; -161bp/ #5. (**b**) Representative result of one luciferase assay. Shown is the ratio of luciferase induction in presence over absence of LT. While WT and mut2/4/5 promoters result in a 2.5x induction, there is no transactivation with the mut2/3/4 construct.

3.2.4. Working hypothesis

TAp73 protein level is clearly increased in TE cells but drops sharply in TER cells back down to wild type levels (confer **Fig. 16**). This observation has led us to formulate the following hypothesis. TAp73 is activated in TE cells as a response to oncogenic insult through the SV40 LT. TAp73 acts in its function as a tumor suppressor and presents a block on the way to full transformation. For cells to achieve this stage, the p73 block must be overcome. The

introduction of H-RasV12 is sufficient to surmount that obstacle and confers tumor-like properties on TER cells.

3.2.5. BJ-TE cells are more sensitive to adriamycin than BJ-T

A first piece of evidence that up-regulation of TAp73 could be a protective reaction on the introduction of the SV40 ER was the result of a cytotoxicity assay with adriamycin. This drug, also known as doxorubicin, is a cytotoxic anthracycline antibiotic isolated from cultures of *Streptomyces peucetius*. It induces apoptosis by a number of different ways. Due to the existence of lipophilic-planar as well as hydrophilic regions and its amphoteric character, the molecule is able to bind to a wide range of cellular molecules. The crucial interactions of adriamycin with respect to its cytotoxic effects are intercalation with DNA, blocking DNA RNA polymerases, and the inhibition of topoisomerase II. Adriamycin also binds to both membrane lipids and soluble proteins and is finally implicated in the generation of reactive oxygen species (ROS), thereby affecting a variety of still other cellular functions (Gewirtz, 1999).

BJ-T and BJ-TE cells were exposed for 1h to increasing concentrations of adriamycin. On the next day the remaining cell viability was measured in a luminometer (BMG) after applying the CellTiter-Glo luminescent cell viability assay kit (Promega). The data were fitted with the GraphPad Prism 4 using the equation for a sigmoid dose-response with variable slope:

$$y = \frac{bottom + (top - bottom)}{1 + 10^{(\log EC_{50} - x) * HillSlope}} \qquad \textbf{equ. 1}$$

The lines of best fit are shown in **Fig. 24**. Inserting the parameters calculated for the BJ-T cell line into equ. 1, the fitted curve is described by

$$y = \frac{3788}{1 + 10^{1.579 + 0.1199x}} \qquad \textbf{equ. 2}$$

With the help of equ. 2, the IC_{50} of adriamycin for BJ-T is calculated to be 2.45µM. The same can be done for BJ-TE:

$$y = \frac{5655}{1 + 10^{1.753 + 0.1788x}} \qquad \textbf{equ. 3},$$

which gives an IC_{50} of 1.66µM adriamycin. The concentration required to kill 50% of all BJ-T cells is therefore 1.5 times (48%) higher than for BJ-TE, a difference that is statistically significant. BJ-TE cells are indeed more sensitive to the apoptogenic drug adriamycin. This result was unexpected, because apoptosis caused by adriamycin is reported to be dependent on p53 (Lowe and Ruley, 1993). Since p53 in BJ-TE is deactivated by binding to LT, these cells should be more resistant to the drug. This discrepancy may be interpreted as an effect of the

much higher p73 level (see Discussion). Concerning the relevance of this discovery it should be kept in mind that TE cells carry in contrast to the T cell line the viral oncogenes st and LT antigen. It can be argued that a greater propensity to apoptosis is one mechanism by which the elimination of cells in pre-malignant stages (provoked for example by infection with tumor viruses) is facilitated.

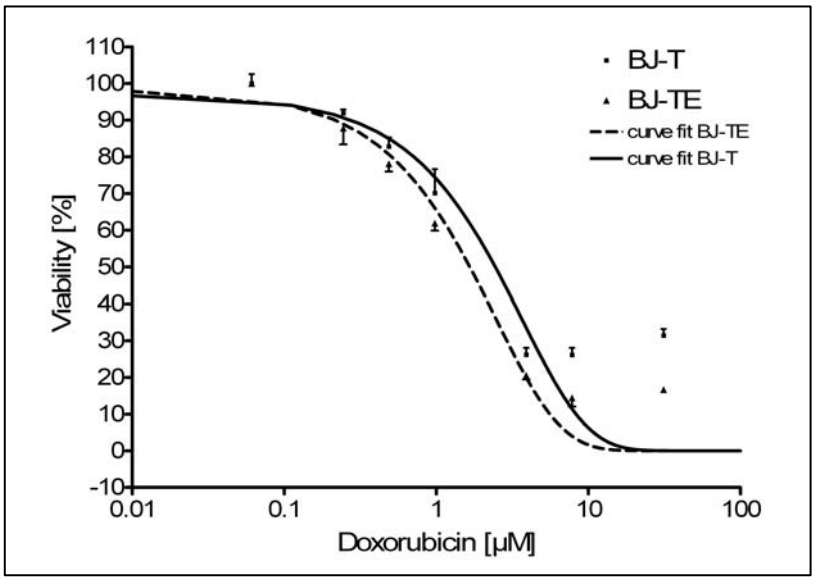

Fig. 24 Dose-response curve for BJ-T and BJ-TE treated with increasing concentrations of doxorubicin/ adriamycin. The curve fit was calculated using the statistical program "GraphPad Prism 4". For details, see main text. According to this analysis of the assay, BJ-TE cells are more sensitive to adriamycin than BJ-T. Their IC_{50} values are 1.66 and 2.45µM adriamycin, respectively. This is a difference of +48%. In other words, the concentration required to kill 50% of all cells is 1.5 times higher for BJ-T. The curves are with statistical significance different ($p<0.05$; Student's t-test, two-tailed, for unpaired samples).

3.2.6. Knockdown of TAp73 results in growth advantage

If high levels of TAp73 indeed suppress tumor-like qualities in TE cells, then an experimental reduction of TAp73 should result in a growth advantage over "normal" BJ-TE with high TAp73. An elegant way to reduce protein levels is the small interfering (si) RNA technology. Short RNA stretches of 20bp are delivered into target cells where they pair with complimentary sequences on the mRNA. Such dsRNA is recognized by the endonuclease and destroyed, effectively diminishing the transcript by up to 90%. A minor drawback of siRNA mediated gene knockdown is that the most effective sequence often has to be determined empirical. For the TAp73 knockdown in VH6-TE cells, three different preparations were tested. The result of a Western immunoblot of lysates from VH6-TE stably transfected with non-silencing (ns; lane 1) or one of the three p73-siRNAs (lanes 2-4) is shown below (**Fig. 25**). It is evident that all three of the siRNAs lead to a clear reduction of TAp73, albeit with different efficiency. Based on these results, VH6-TE>p73si#1 cells were chosen along with VH6-TE>ns for the growth curve experiments to compare their growth kinetics.

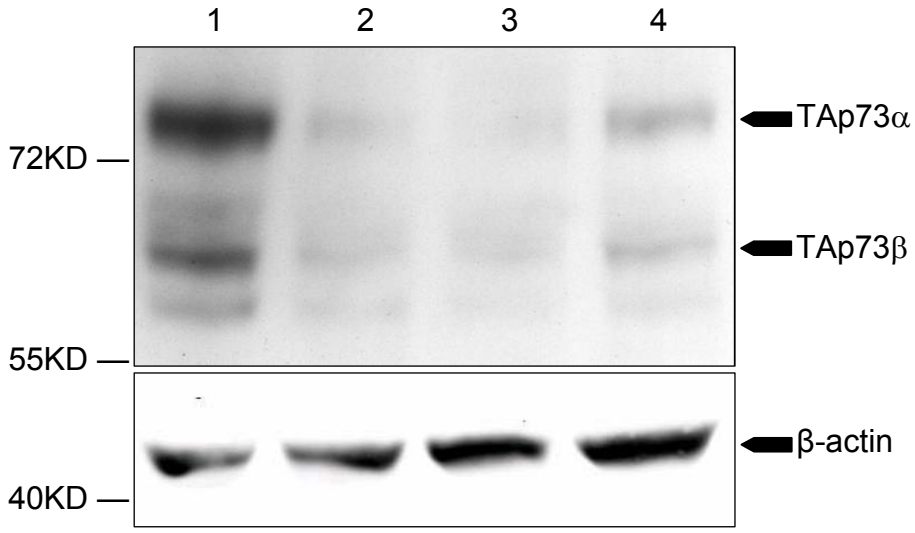

Fig. 25 Western Blot for p73 in VH6-TE cells stably transduced with lentiviruses carrying the following siRNAs: non-silencing (ns; lane 1); p73si#1 (lane 2); p73si#2 (lane 3); p73si#3 (lane 4). Compared with lane 1, all three siRNAs cause a more or less strong reduction of TAp73 expression. Cell line VH6-TE>p73si#1 was chosen for the preparation of growth curves.

The first set of growth curves were generated by seeding $1x10^5$ VH6-TE>ns and VH6-TE>p73si#1 cells separately in a contingent of 60mm plates. Three plates each were counted every 1-2 days. The resulting curves are plotted in **Fig. 26**.

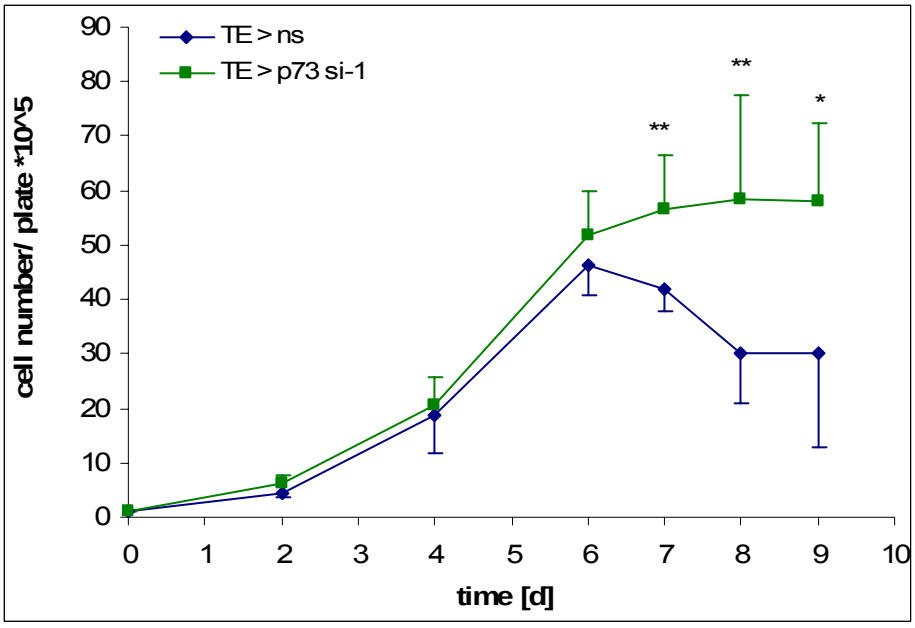

Fig. 26 Growth kinetics in separate cultures of VH6-TE>ns and VH6-TE>p73si#1 cells. $1x10^5$ cells per plate were seeded at day 0 for each line. Total cell numbers were estimated every 1-2 days in a counting chamber. Every time point is the mean of six independent measurements. Statistically significant differences are indicated by asterisks (*: $p<0.05$, **: $p<0.01$; Student's t-test, two-tailed, for unpaired samples). Error bars = standard deviations.

Up to day 6 the growth rate of both lines are indistinguishable. At day 6 however, as the plates have reached full confluence, the curves diverge because the numbers of VH6-TE>ns cells are steadily declining up to day 9, while VH6-TE>p73si#1 slowly continue to increase in number

until they reach a plateau at day 8. The differences between both VH6-TE lines in estimated cell numbers are significantly different for the last three days of the growth curves.

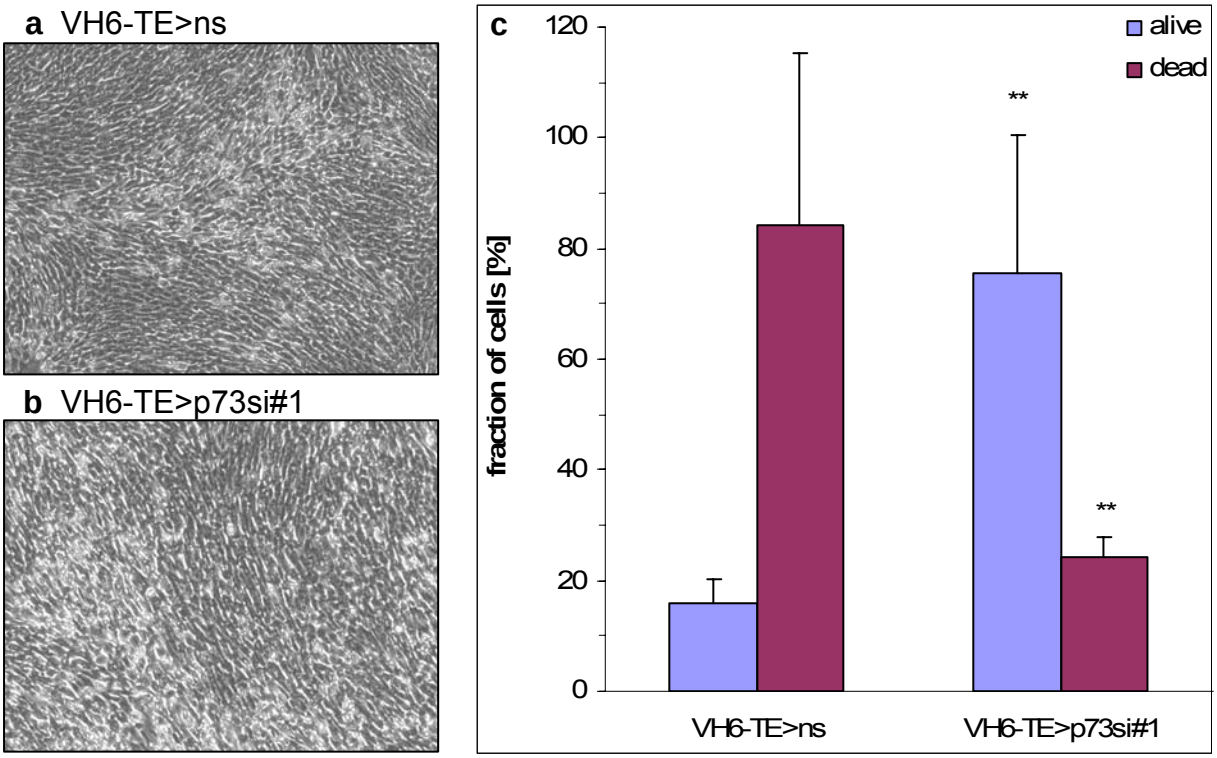

Fig. 27 RNAi mediated TAp73 knockdown results in more resilient cells. VH6-TE>ns and VH6-TE>p73si#1 were trypsinized at day 9, resuspended in a dilution of Trypan blue, and immediately photographed in a counting chamber under a light microscope. Despite similar appearance of both cell types on the plate at that time (**a** and **b**; 50x magnification), the fraction of viable cells is very different (**c**). In VH6-TE>ns only every sixth cell (16%) is still alive, but three quarters (76%) of all VH6-TE>p73si#1 cells. This difference is statistically significant (**: $p<0.01$; Student's t-test, two-tailed, for unpaired samples; n=245 [ns]/ 525 [p73si#1]).

Due to the intrinsic advantages of the RNA interference (RNAi) technology, the two VH6-TE cell lines should be identical with the exception of expression levels of the knockdown target TAp73. From this initial and indirect comparison of these two lines, it can be inferred that the reduction of TAp73 protein does bestow a certain growth advantage on VH6-TE>p73si#1. These cells apparently are able to tolerate the stress of high culture density better than their counterpart VH6-TE>ns. This is also evident from a quantification of trypsinized cells treated with the vitality stain trypan blue (**Fig. 27**). Microscopic images were taken from cells at day 9 of the growth curves, when the viability difference was highest, and the total cells counted. Despite quite similar appearance of the confluent cell layers (**Fig. 27a** and **b**) there was a statistically significant difference in the fraction of viable cells (**Fig. 27c**). While in VH6-TE>ns most cells are in fact dead (viability 16%), the proportion is approximately reversed in VH6-TE>p73si#1 with a viability of 76%.

This result lends support to the conclusion from the growth curve experiment (**Fig. 26**): TAp73 knockdown appears to confer a growth advantage on VH6-TE, as such cells are able to tolerate high culture densities while remaining intact. Control cells not only rapidly drop in numbers after their density peaks; the remaining adherent cells are also mostly non-viable.

This difference in cell viability under stress was a promising finding, yet based on indirect evidence. Hence, the intention was to conduct a co-culture experiment with mixed VH6-TE>ns and VH6-TE>p73si#1 populations. The lentiviral pLVTHM vectors used to produce these cell lines also encode the GFP gene under regulation of the widely used Elongation Factor 1 (EF1-α) promoter. It is therefore possible to discriminate the transduced from the parental VH6-TE cells by optical techniques such as flow cytometry. It is, however, for the same reason not possible to distinguish VH6-TE>ns from VH6-TE>p73si#1 cells, which precluded the actual direct comparison of these two cell lines in co-culture.

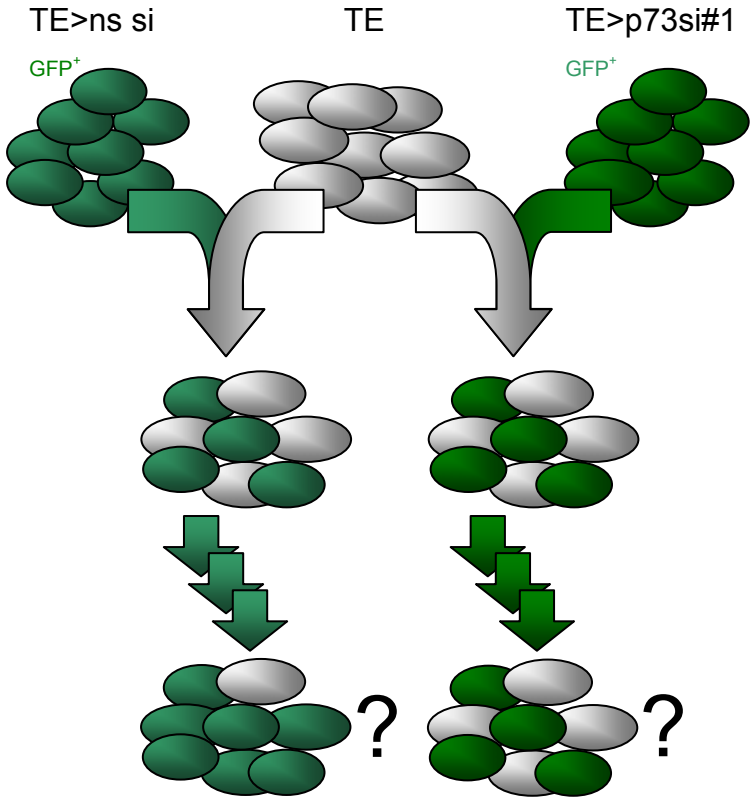

Fig. 28 Concept of the co-culture experiment. At day 0, equal numbers of Vh6-TE and either VH6-TE>ns or VH6-TE>p73si#1 were mixed and plated in quadruplicate on 60mm plates. Plates were trypsinized and counted every 2-3 days, and the cell mix was seeded back at a fixed ratio of 1:4. This scheme was followed for about 3 weeks. The change over time in relative GFP fluorescence in both types of mixes was followed with the help of a flow cytometer.

To test how the two derived cell lines compare to the parental VH6-TE cells in terms of growth kinetics, equal numbers of VH6-TE and either VH6-TE>ns or VH6-TE>p73si#1 were seeded on 60mm plates. Every two days the mixed cultures were trypsinized, subjected to flow cytometry, and seeded back at a fixed ratio (**Fig. 28**). The change of the fraction of green cells

over time was recorded. To ensure that all three cell lines were stable with respect to the level of green fluorescence throughout the course of the co-cultures, they were cultured and measured separately at each time point along with the co-culture samples. **Fig. 29** shows the results of the co-cultures. Both the transduction with non-silencing and p73-siRNA virus evidently confers a growth advantage on VH6-TE cells, since in both mixed cultures the GFP positive cells outgrow the unlabeled ones. This suggests a non-specific effect of the vector or the infection itself. However, there is clearly an additional specific effect of the p73-silencing siRNA, because the inclination of the respective linear curve fit is much steeper than with the ns siRNA. In other words, VH6-TE cells with a stable knockdown of p73 experience a growth advantage as they outgrow parental VH6-TE cells much faster than VH6-TE>ns cells do.

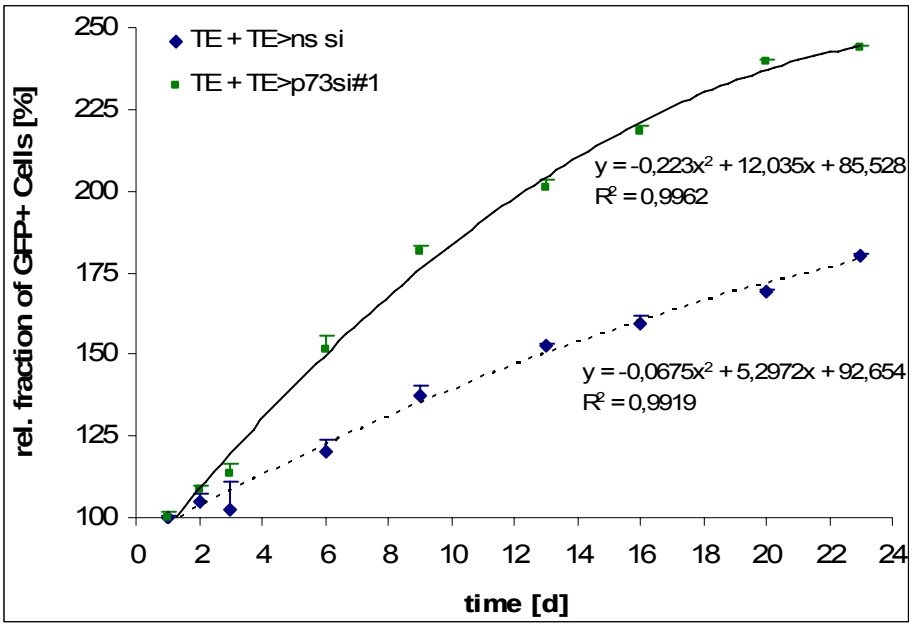

Fig. 29 Co-culture experiment to estimate the growth advantage conferred on VH6-TE cells by p73 knockdown. VH6TE cells were seeded at day 0 together with an equal number of either VH6-TE>ns or VH6-TE>p73si#1 cells, which are green fluorescing. The change of the fraction of GFP positive cells relative to day 1 was followed by flow cytometry. Every time point is the mean of three independent measurements. Second order polynomic curve fits are indicated by the solid lines for the competition of VH6TE with VH6-TE>ns and dotted lines for the VH6TE / VH6-TE>p73si#1 co-culture.

3.2.7. Identification of putative TAp73 targets

The most crucial results presented so far involve the LT-mediated induction of TAp73 in BJ-/VH6-TE cells. We interpreted that as a protective mechanism because TE cells were more sensitive to the apoptosis inducer adriamycin and because reversal of the elevated TAp73 levels with RNAi conferred a growth advantage over control TE cells. Further investigations were dedicated to the characterization of effector pathway(s) of the TAp73 up-regulation. In order to identify candidate key factors it was decided to perform a DNA microarray using the two cell lines VH6-TE>ns and VH6-TE>p73si#1 from the growth kinetic experiments (see sect. 3.2.6).

Cells were harvested at two different densities, proliferating and confluent. This allowed the comparison of transcription profiles from a low and a high TAp73 background (ns vs. p73si) at two clearly distinct, density-dependent stages of TAp73 regulation (compare sect. 3.2.1). Total RNA was extracted from these four samples (RNeasy Mini Kit, Promega). Five µg RNA were loaded on a "GeneChip Human Genome U133A 2.0" array (Affymetrix), which contains 14,500 human genes. Data were then evaluated and analyzed using the GeneSpring GX software (Agilent Technologies).

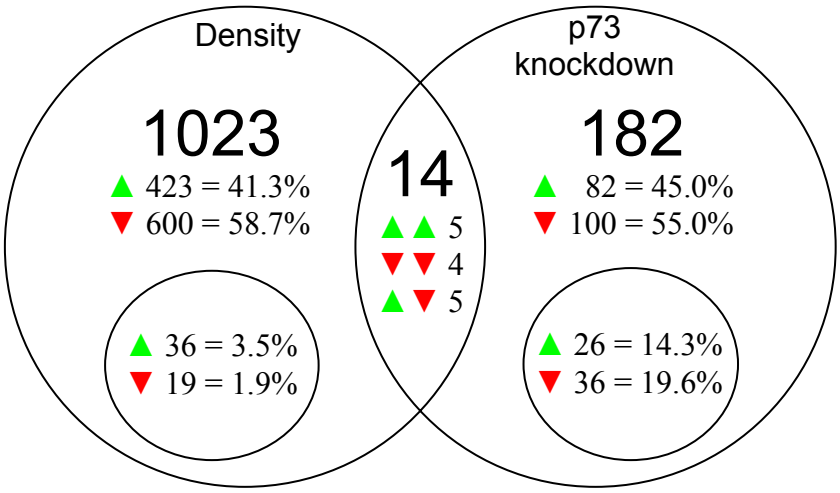

Fig. 30 Numbers of genes which differed at least twofold in their expression levels in VH6-TE>ns and VH6-TE>p73si#1. All in all 1205 of such genes were identified. Of these, 1023 genes were found to be density-dependent regulated and 182 through the knockdown of TAp73. Only 14 genes could be counted to both groups. For each class of genes the absolute and relative amount of targets in each direction of regulation is given. *Small circles* contain the fraction of highly regulated genes (>5fold induction or repression).

Fig. 30 gives an overview of the number of genes that were differentially regulated between two conditions. At least a twofold difference in expression was found in 1205 genes. It is apparent that the majority of these, namely 1023 genes, fall into the category "density dependent regulation". For a complete list see Appendix, **Tab. A-2**. Of these 1023, a total of 423 (31.3%) genes are positively and 600 (58.7%) are negatively regulated. Among these, 36 (3.5%) and 19 (1.9%) show "strong" regulation, i.e. more than five-fold induction or repression, respectively. All genes strongly regulated through cell density are listed in **Tab. 10** (induced genes) and **Tab. 11** (repressed genes). Their functions have been individually determined and categorized and will be analyzed in context with **Fig. 31**. Generally, the 54 genes fall in 15 functional classes: transcription (abbreviated "TC" in the tables below), structural proteins (SP), intracellular signaling (IS), extracellular signaling (ES), receptors (RC), protein degradation (PD), proteases (PR), protease inhibitors (PI), enzymes of cell metabolism (IE), extracellular enzymes (EE),

channels and transporters (CT), cell cycle proteins (CC), angiogenesis (AG), apoptosis (AP), and unknown function (UF).

Tab. 10 From the 1023 density-regulated genes identified the most strongly (>5fold) *induced* genes in proliferating cells are listed below along with their normalized expression levels. The functional class is indicated, preceded by the -fold difference in mRNA levels. All genes exhibit the same direction in VH6-TE>ns and VH6-TE>p73si#1 (not shown).

Position	Gene ID	Accession number	Normalized signal intensity		ratio 100%/40%	Function
			ns 40%	ns 100%		
1	ABCA1	AF285167	0,03	2,73	**97,64**	CT
2	AREG	NM_001657	0,06	2,31	**37,56**	ES
3	ACPP	NM_001099	0,08	1,77	**21,59**	EE
4	AK3	NM_013410	0,36	4,86	**13,61**	IE
5	VEGF	AF022375	0,21	2,18	**10,45**	AG
6	C5orf4	H93077	0,20	2,12	**10,45**	EE
7	NDRG1	NM_006096	0,25	2,34	**9,20**	IS
8	TNFSF10	NM_003810	0,19	1,68	**9,10**	AP
9	DDIT4	NM_019058	0,22	1,99	**9,10**	UF
10	DKFZP586H2123	AI671186	0,21	1,78	**8,57**	PR
11	PTGES	AF010316	0,21	1,76	**8,32**	IE
12	STC1	AI300520	0,28	2,24	**8,04**	ES
13	OAS1	NM_002534	0,08	0,63	**8,03**	IE
14	ZNF395	NM_017606	0,25	1,99	**8,00**	TC
15	OLFML2A	AL050002	0,46	3,53	**7,73**	RC
16	C1RL	NM_016546	0,28	2,04	**7,43**	PR
17	IL1A	M15329	0,30	2,18	**7,30**	ES
18	CCNG2	AW134535	0,28	1,97	**7,12**	CC
19	COLEC12	NM_030781	0,25	1,71	**6,93**	RC
20	LAMA4	NM_002290	0,21	1,42	**6,85**	SP
21	PNRC1	AF279899	0,35	2,39	**6,83**	TC
22		AI004009	0,40	2,68	**6,72**	UF
23	LRP1	BF304759	0,40	2,68	**6,67**	RC
24	BHLHB2	NM_003670	0,31	2,02	**6,61**	TC
25	VNN1	NM_004666	0,25	1,61	**6,40**	IE
26	IL24	NM_006850	0,42	2,62	**6,21**	AP
27	SERPING1	NM_000062	0,35	2,09	**5,98**	PI
28	SLC16A4	NM_004696	0,44	2,64	**5,98**	CT
29	TXNIP	NM_006472	0,36	2,04	**5,72**	IS
30	BTEB1	AI690205	0,31	1,70	**5,51**	TC
31	MYLIP	NM_013262	0,36	1,93	**5,43**	PD
32	SCD	AB032261	0,32	1,67	**5,28**	IE
33	SBLF	BG434174	0,42	2,22	**5,23**	TC
34	CYP1B1	AU154504	0,31	1,60	**5,19**	IE
35	WSB1	BF111821	0,42	2,18	**5,17**	UF
36	SMOX	BC000669	0,33	1,71	**5,16**	IE

Tab. 11 From the 1023 density-regulated genes identified the most strongly (>5fold) *repressed* genes in proliferating cells are listed below along with their normalized expression levels. The functional class is indicated, preceded by the -fold difference in mRNA levels. All genes exhibit the same direction in VH6-TE>ns and VH6-TE>p73si#1 (not shown).

Position	Gene ID	Accession number	Normalized signal intensity		ratio 100%/40%	inverse ratio	Function
			ns 40%	ns 100%			
1	ID1	D13889	1,85	0,16	**0,08**	11,90	TC
2	SPN	X52075	1,18	0,11	**0,09**	11,19	IS
3	DLX2	NM_004405	2,19	0,21	**0,09**	10,68	TC
4	SERPINE1	AL574210	1,77	0,17	**0,10**	10,30	PI
5	ID3	NM_002167	1,78	0,18	**0,10**	10,02	TC
6	SURF2	NM_017503	1,46	0,16	**0,11**	9,15	UF
7	GADD45B	AF087853	2,22	0,28	**0,13**	8,00	CC
8	OXTR	NM_000916	2,41	0,32	**0,13**	7,45	RC
9	HMOX1	NM_002133	1,67	0,24	**0,14**	6,93	IE
10	DKK1	NM_012242	1,99	0,31	**0,15**	6,53	ES
11	CD24	AA761181	2,21	0,34	**0,16**	6,42	IS
12	FGF5	AB016517	1,46	0,24	**0,17**	6,04	ES
13	PODXL	NM_005397	1,66	0,28	**0,17**	6,04	SP
14	CTGF	M92934	1,71	0,29	**0,17**	5,92	ES
15	ID2	NM_002166	2,02	0,36	**0,18**	5,54	TC
16	EDN1	J05008	3,37	0,62	**0,18**	5,42	ES
17		AK000168	2,09	0,40	**0,19**	5,27	UF
18	ADAMTS1	AK023795	2,68	0,52	**0,19**	5,14	PR
19	TNFRSF12A	NM_016639	1,57	0,31	**0,20**	5,02	AG

According to **Fig. 30**, 182 more genes are regulated differently in the VH6-TE strain when TAp73 expression is suppressed by RNAi (attached in full as **Tab. A-3**). The distribution is similar as with the density targets above. A total of 82 (45%) genes are up-, the remaining 100 (55%) are down-regulated; roughly a third of each in turn are strongly regulated. This translates to 26 (14.3%) more than five-fold positively and 36 (19.6%) more than five-fold negatively regulated genes, when p73 expression is suppressed. All these genes are listed in **Tab. 12** (induction) and **Tab. 13** (repression); their functional classification (two-digit abbreviations as stated above) will be analyzed in conjunction with **Fig. 31**. At this point it is evident that the total number of differentially regulated genes is higher when VH6-TE cells become confluent. However, the *proportion* of strongly regulated genes is much larger after p73 knockdown, namely five times higher (28.6% vs. 5.4%). Taken together this might indicate that increasing cell confluence has a more general effect of moderate amplitude while reduction of p73 signaling could be more punctuated both in number and regulation intensity of the affected targets. Definite conclusions have to await a detailed comprehensive analysis of the affected pathways and their interrelation.

Tab. 12 From the 182 genes differentially regulated after p73 knockdown the most strongly (>5fold) induced genes in proliferating cells are listed below along with their normalized expression levels. The functional class is indicated, preceded by the -fold difference in mRNA levels. All genes exhibit the same direction in VH6-TE>ns and VH6-TE>p73si#1.

Position	Gene ID	Accession number	Normalized signal intensity		ratio ns/si	Function
			ns 40%	si 40%		
1	SLC25A30	AL359557	0,05	2,33	**46,99**	CT
2	IL10	NM_000572	0,16	4,04	**24,80**	ES
3	BCMO1	NM_017429	0,17	3,22	**19,54**	IE
4	MGC52019	AI733515	0,19	3,36	**18,05**	UF
5	CXCL11	AF002985	0,10	1,74	**17,99**	ES
6	OAS1	NM_002534	0,08	1,37	**17,62**	IE
7		AL038824	0,11	1,88	**17,12**	UF
8		AL049233	0,13	1,77	**13,34**	UF
9	C6orf103	NM_024694	0,22	2,84	**13,17**	UF
10	UNC93A	AL021331	0,26	3,19	**12,33**	UF
11	KIF1A	NM_004321	0,32	3,29	**10,37**	SP
12	CEACAM1	M69176	0,38	3,84	**10,15**	AG
13	PAP	NM_002580	0,23	2,16	**9,31**	ES
14	HSXIAPAF1	NM_017523	0,15	1,38	**9,30**	TC
15	SLC24A1	AF026132	0,19	1,70	**8,75**	CT
16	ZMYND10	AC002481	0,21	1,67	**8,09**	UF
17	PCDH7	NM_002589	0,16	1,26	**7,96**	SP
18	GLRA3	U93917	0,28	2,20	**7,93**	CT
19	ZFP276	AI983201	0,31	2,40	**7,88**	TC
20	PTGER3	D38298	0,24	1,90	**7,87**	RC
21	FLJ11996	NM_024976	0,36	2,76	**7,77**	UF
22	DYRK1A	Z25423	0,20	1,46	**7,19**	IS
23	BMP10	NM_014482	0,69	4,68	**6,83**	ES
24	GDAP1L1	NM_024034	0,52	3,48	**6,73**	UF
25	DNALI1	NM_003462	0,18	1,13	**6,39**	SP
26	NEU3	AK022450	0,21	1,25	**5,91**	IE

Tab. 13 From the 182 genes differentially regulated after p73 knockdown the most strongly (>5fold) *repressed* genes in proliferating cells are listed below along with their normalized expression levels. The functional class is indicated, preceded by the -fold difference in mRNA levels. All genes exhibit the same direction in VH6-TE>ns and VH6-TE>p73si#1.

Position	Gene ID	Accession number	Normalized signal intensity		ratio ns/si	inverse ratio	Function
			ns 40%	si 40%			
1	GNRH1	NM_000825	0,79	0,02	**0,02**	43,35	ES
2	CENTB2	D26069	1,78	0,05	**0,03**	37,06	IS
3	SPOCK3	BC000460	4,33	0,15	**0,03**	28,85	PI
4	AMOTL2	NM_025017	2,95	0,11	**0,04**	28,13	SP
5	GPLD1	AV699786	1,68	0,07	**0,04**	25,87	EE
6	FLJ23235	NM_024943	2,73	0,16	**0,06**	17,60	UF
7	FLJ11588	NM_024603	3,76	0,24	**0,06**	15,40	UF
8	IGSF3	AB007935	1,03	0,07	**0,07**	14,33	UF
9	ZNF257	AF070651	1,74	0,13	**0,08**	12,97	TC
10	AUTS2	AK025298	1,35	0,11	**0,08**	12,82	PI
11	DCAMKL1	NM_004734	1,85	0,15	**0,08**	12,61	IS
12	KIF5A	NM_004984	2,73	0,24	**0,09**	11,35	SP
13	SOX4	NM_003107	1,05	0,10	**0,10**	10,50	TC
14	FLJ25476	AK021842	0,85	0,09	**0,11**	9,33	TC
15	SORCS3	AB028982	1,88	0,21	**0,11**	8,80	RC

Tab. 13 (continued)

Position	Gene ID	Accession number	Normalized signal intensity		ratio ns/si	inverse ratio	Function
16	SOS2	BF692958	1,64	0,19	**0,11**	8,78	IS
17	KRTHB1	NM_002281	5,77	0,68	**0,12**	8,52	SP
18	EBI2	NM_004951	0,91	0,11	**0,12**	8,46	RC
19		AK000185	2,74	0,34	**0,12**	8,14	UF
20	PIP3-E	AW166711	4,47	0,56	**0,13**	7,94	IE
21	IGSF4	AL519710	1,77	0,22	**0,13**	7,92	SP
22	SIX2	NM_016932	1,83	0,24	**0,13**	7,53	TC
23		AL080315	1,67	0,22	**0,13**	7,48	UF
24	GYG2	U94357	1,30	0,18	**0,13**	7,45	IE
25	JUP	NM_021991	1,33	0,19	**0,14**	7,07	SP
26	MLSTD1	NM_018099	1,37	0,20	**0,14**	7,00	IE
27	DOCK9	BE259050	2,21	0,32	**0,14**	6,97	IS
28	SLC16A10	NM_018593	1,56	0,25	**0,16**	6,31	CT
29	TCF12	AU146580	2,81	0,46	**0,16**	6,15	TC
30	ABAT	AF237813	0,92	0,15	**0,17**	6,03	IE
31	LOC161291	AV691491	1,81	0,32	**0,17**	5,75	UF
32	PPM1H	AB032983	2,08	0,36	**0,17**	5,74	UF
33	ACTG2	NM_001615	2,22	0,41	**0,18**	5,48	SP
34	USP53	AK025301	1,32	0,25	**0,19**	5,32	UF
35	FLJ12895	NM_023926	1,45	0,28	**0,19**	5,21	TC
36	GREB1	NM_014668	0,50	0,10	**0,19**	5,19	UF

As stated above, the number of strongly, more than fivefold regulated genes is almost identical between p73 knockdown and density-dependent regulation (62 and 55, respectively), notwithstanding the fact that with the latter parameter 5.6 times more genes were identified that are least twofold regulated (182 *vs.* 1023). The functional classification for the 118 strongly regulated genes has been carried out individually by consulting their entries in the gene cards and SwissProt databases. Based on the system in Vasseur *et al.* (2003), they were grouped into 15 categories, including "unknown function" (**Fig. 31**).

The distribution of density regulated genes (**Fig. 31a**) is fairly uniform with the notable exception of proteins involved in transcription (both directions), in extracellular signaling (repression), and of enzymes involved in cellular metabolism (induction). The distribution of p73 knockdown-related targets (**Fig. 31b)** is more biased, with many repressed proteins of transcription, structure, intracellular signaling, and metabolism. On the other hand, in following four functional classes no strongly regulated genes were found at all: protein degradation, proteases, cell cycle proteins, and apoptosis. Induction is prominent in extracellular signaling, while the (partial hypothetical) proteins for which no function has yet been reported are by far the single largest category, with 15 genes in total. This is also the most striking difference when comparing **Fig. 31a** and **Fig. 31b**, because the function of all but five of the density-regulated genes is known. Furthermore, if both diagrams are superimposed and all categories are viewed

in combination, the strongest groups by numbers are transcription (17 genes; 7 induced to 10 repressed), cell metabolism (15; 10:5), extracellular signaling (12; 7:5), and structural proteins (11; 4:7). In contrast, six categories include three or less strongly regulated genes (protein degradation, proteases, extracellular enzymes, cell cycle, angiogenesis, apoptosis).

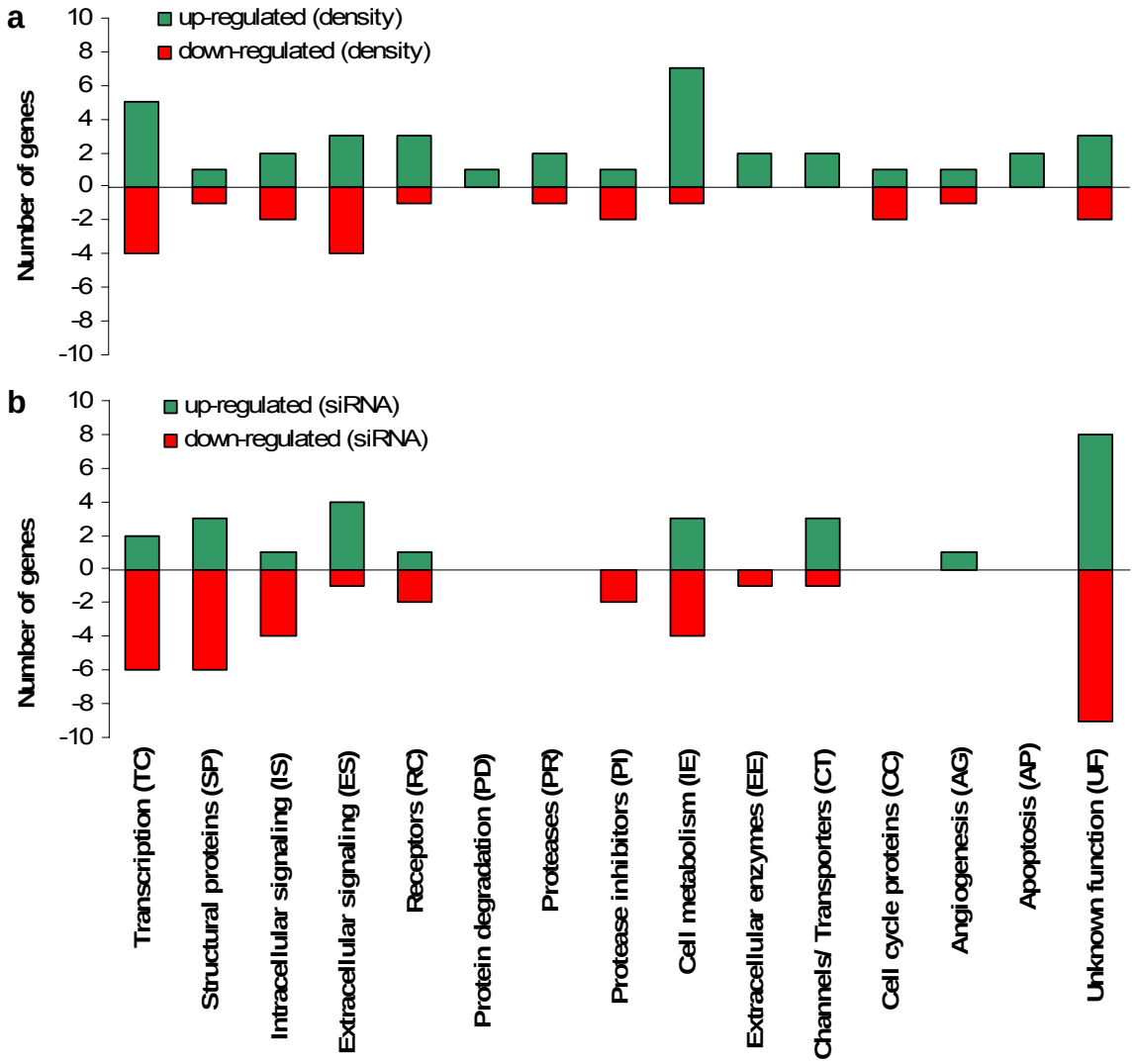

Fig. 31 Functional classification of all genes which were identified to be more than fivefold induced or repressed according to (**a**) density (proliferating *vs.* confluent VH6-TE>ns) or (**b**) 73 knockdown (proliferating VH6-TE>ns *vs.* proliferating VH6-TE>p73si#1). This table represents the census performed on Tab. 10 through Tab. 13. Each gene was assigned only one

It is lastly interesting to see that the three highest induced gene both in the density and knockdown cohort are a transporter (*ABCA1* and *SLC25A30*, respectively), a secreted signal transducer (*AREG, IL10*), and an enzyme (*ACPP, BCMO1*), with ≥20fold up-regulation. There are no outliers for repression among the strongly density-regulated, but there are five genes with more than 20fold repression after p73 knockdown, three of which are again involved either in signal transduction (*GNRH1*, *CENTB2*) or enzymatic conversion (*GPLD1*). The other two are a

gene of a structural protein (*AMOTL2*) and for a protease inhibitor (*SPOCK3*), the latter being of particular interest in the given context.

Finally, among the 1205 genes only 14 could be identified which were regulated differently in VH6-TE>ns and VH6-TE>p73si#1 according to *both* density and p73 level (**Tab. 14**). Nine of these display the same regulation with regard to both parameters, with five targets up- and four down-regulated. The other five genes are up-regulated in confluent cells but down-regulated when cell density and TAp73 levels are low. Interestingly, no gene was found to which the reverse applies.

Tab. 14 Genes that are regulated differently in VH6-TE>ns and VH6-TE>p73si#1 both according to cell density and TAp73 knockdown. The listed values are the normalized expression levels calculated by the GeneSpring software (Agilent Technologies). Green and red arrows indicate up- or down-regulation, respectively, preceded by the -fold change in expression. *Red*: genes that are regulated in parallel to TAp73 and that are therefore the most likely p73 effectors.

Gene	(putative) Function	1 VH6-TE>ns proliferating	2 VH6-TE>si proliferating	3 VH6-TE>ns confluent	4 VH6-TE>si confluent	Regulation	
						density (column 1 vs. 3)	knockdown (column 1 vs. 2)
C1orf29	Antiviral defense?	0.42	0.98	1.02	3.72	**2.4**▲	**2.3**▲
EDN1	Vasoconstrictor; oncogene	3.37	1.38	0.62	0.11	**0.18**▼	**0.41**▼
FAM38B	*Unknown*	0.92	0.39	2.42	1.08	**2.6**▲	**0.42**▼
IGSF3	*Unknown*	1.03	0.07	2.15	0.97	**2.1**▲	**0.07**▼
IGSF4	Adhesion, signal transduction; tumor suppressor	1.58	0.37	3.25	0.42	**2.1**▲	**0.23**▼
JAG1	Signal transduction; oncogene	3.33	0.77	1.23	0.57	**0.37**▼	**0.23**▼
KCNK1	Potassium channel, cell volume	1.27	0.26	3.11	0.73	**2.4**▲	**0.21**▼
KCTD12	*Unknown*	0.38	0.85	1.15	2.83	**3.0**▲	**2.2**▲
KRTHB1	Structural (hair)	5.77	0.68	1.32	0.14	**0.23**▼	**0.18**▼
MGC8685	Structural (cytoskeleton)	0.84	0.21	3.39	1.16	**4.0**▲	**0.25**▼
MT1H	Heavy metal detoxification; oncogene	0.77	2.36	0.36	1.24	**2.1**▲	**3.1**▲
OAS1	Antiviral defense	0.08	1.37	0.63	3.55	**7.9**▲	**17.1**▲
TGFB2	Cytokine, signal transduction; oncogene	2.71	0.91	1.09	0.48	**0.4**▼	**0.36**▼
TRIM22	Antiviral defense, cell proliferation	0.46	1.05	0.95	2.58	**2.1**▲	**2.3**▲

Concerning the levels of regulation it is remarkable that among the 14 genes, only one (*OAS1*; induced) can be found that is "strongly" regulated according to both parameters. Two more are repressed more than fivefold after only one treatment: *EDN1* in confluent VH6-TE>ns and

KRTHB1 in VH6-TE>si. The other 13 show moderate regulation, i.e., between two-and fivefold repression/ induction.

From these 14 genes, the function of eleven is known at least superficially. All but one (*KCNK1*) can be grouped in only three categories: structural proteins (*KRTHB1*, *MGC8685*), antiviral defense (*C1orf29* (?), *OAS1*, *TRIM11*), and cancer related (*EDN1*, *IGSF4*, *MT1H*, *TGFB2*). The first two groups are less interesting for the objectives of this work. Structural proteins are not typically involved in signaling and are therefore probably not decisive for transformation. The antiviral factors on the other hand are probably artifacts of the transfection with shRNA-lentivectors, since all of the cell lines carry these constructs. Such a link has been established for example for *OAS1* and is due to the presence of dsRNA, normally an indicator of intracellular viral activity (see Discussion). In contrast, further research should focus on the tumor suppressor *IGSF4* and the verified oncogenes *EDN1* and *MT1H*, but most importantly on the remaining genes that are regulated in parallel to TAp73: *KCNK1*, *FAM38B*, *IGSF3*, *MGC8685*.

3.3. Down-regulation of p73 in TER cells

Up-regulation of TAp73 in was specifically observed in TE cells, but not in any of the other three model system cell lines. This means that TAp73 expression is again actively restrained in TER cells. It has been proposed that TAp73 presents a block for transformation that is circumvented in the TER cell line (see sect. 3.2.4).

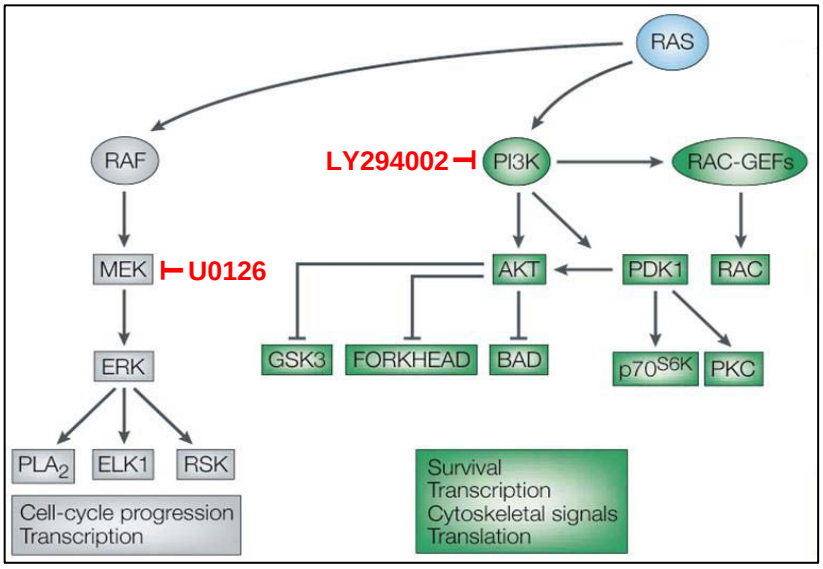

Fig. 32 Overview of the two major Ras signaling pathways involved in transformation. While the Raf/ Mek/ Erk pathway affects cell cycle progression, phosphoinositide 3 kinase (PI3K) is more involved in the control of cell viability (survival and cytoskeletal signals). In addition, both are known to regulate transcription. Targets of the pharmacological inhibitors used here are indicated in red. Modified from Downward (2003).

The final chapter of this work addresses the underlying molecular mechanism of this control evasion. BJ-TER are different from BJ-TE only in their ectopic expression of oncogenic H-RasV12. The 21kDa protein H-Ras belongs to the small GTPase superfamily. It occupies a central role in intracellular signal transduction partly because H-Ras is activated directly at the plasma membrane, placing it high upstream. H-Ras relays receptor-mediated extracellular signals to various signaling pathways in the whole cell (reviewed in Malumbres and Barbacid, 2003). Two of those that are most relevant for transformation are the mitogenic cascade (Raf/ MEK/ ERK) and the phosphoinositide 3 kinase (PI3K) pathway (**Fig. 32**) (Downward, 2003; Joneson *et al.*, 1996; Rodriguez-Viciana *et al.*, 1997).

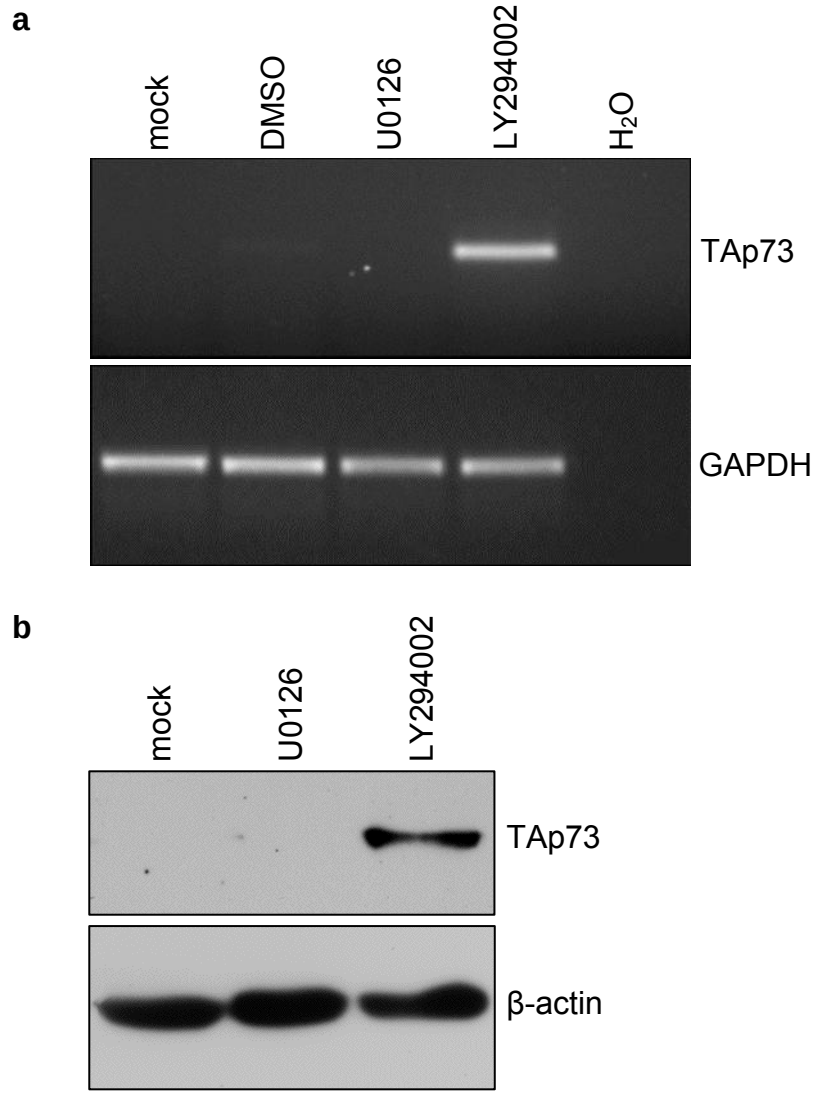

Fig. 33 Inhibition of phosphoinositide 3-kinase (PI3K) raises TAp73 levels in TER cells. (a) Semi-quantitative RT-PCR with BJ-TER cells that were untreated (mock), incubated for 24h with solvent only (DMSO), with the inhibitor of MEK (U0126) or the PI3 kinase (LY294002). (b) Western Blot with lysates from untreated BJ-TER cells (mock) or such with blocked MEK (U0126) or PI3 kinase (LY294002). Only the inhibition of the PI3K pathway could restore higher TAp73 mRNA and protein levels.

To identify which of these two effector pathways triggered the down-regulation of TAp73, we took advantage of the availability of pharmacological inhibitors for key factors. The rationale

behind this approach is straightforward. If the mechanism(s) that cause the decrease of TAp73 in TER are blocked, protein levels should be restored back to what they are in TE cells. The drug U0126 specifically inhibits MEK of the mitogenic cascade, while LY294002 disables the PI3K pathway by blocking PI3K itself. BJ-TER cells were incubated with these drugs or only with the solvents and harvested 24h later. **Fig. 33a** shows the result of a RT-PCR performed with those samples. Only TER cells treated with LY294002 showed a strong PCR signal. This indicates that inhibition of PI3K alone is sufficient to restore transcription of TAp73 in BJ-TER. More importantly, the same is true for the protein level (**Fig. 33b**). These two experiments make a strong case for PI3K being the downstream pathways by which H-Ras achieves down-regulation of TAp73 in TER cells.

3.4. Results: summary

For this project, a published cell culture model of the malignant transformation in human cells was established. It comprises four stages of BJ or VH6 human fibroblasts starting with the wild type, followed by three cell lines with increasing tumor-like properties. -T cells are immortalized by hTERT, -TE carries in addition the SV40 ER, and -TER are fully transformed by the introduction of oncogenic H-RasV12. The validity of the cell lines was proven in immunoblots, cytometric and in soft agar assays.

When investigating the p73 status of the four lines in Real Time PCR, RT-PCR and Western Blot, it was discovered that full length TAp73 was selectively up-regulated in -TE cells. The SV40 Large T antigen was found to cause this, probably by deactivating Rb or its family members p105/ p130 by sequestration and promoting this way E2F1-dependent TAp73 transcription. We proposed a model according to which TAp73 fulfills its role as a tumor suppressor in -TE cells and blocks the progression of transformation. This was supported by finding a significantly higher sensibility in -TE cells towards adriamycin, an apoptosis inducing drug. A knockdown of TAp73 by siRNA resulted in a growth advantage over normal -TE, emphasizing again a restraining role of the protein. Potential mediators conveying such signals downstream of p73 were identified by comparing in DNA microarrays the transcriptom of -TE (VH6-TE>ns, high p73) with that of p73-depleted -TE cells (VH6-TE>p73si#1, low p73).

Complete transformation could only be achieved after the transduction with H-RasV12 to create -TER cells, which express TAp73 again at low, wild type-like levels. There is pharmacological evidence that the observed low level of TAp73 in those is mediated by H-Ras through the phosphoinositide 3-kinase (PI3K) pathway.

4. Discussion

A number of approaches have been developed to unravel the complex changes accompanying the multistage conversion of a normal into a tumor cell. Many publications deal with the description of alterations found in the biopsies tumors or in tumor-derived, established cell lines. In contrast, some groups have recently begun to follow a synthetic strategy. Normal mammalian cells are stepwise genetically manipulated to elicit increasingly cancer-like attributes (reviewed in Rhim, 2000), reflecting the polygenic nature of the disease (Balmain *et al.*, 2003). In this way, the contribution of the genetic alteration or more precisely, of the effected pathway(s) towards transformation can be determined. Another advantage is the versatility of such an approach. It can be adapted to suit different conditions or questions by varying experimental parameters such as the parental cell line or the targeted pathways.

Principal concerns with this kind of reductionist model have been raised as well. They are said to be too simplistic for the clinical reality for they disregard two important aspect of in situ tumor biology, increasing genetic heterogeneity in advanced tumor and failures in tumor-stroma interaction. In other words, such models may fail to appreciate that tumorigenesis is a disease of the whole organism, not a defect of single cells (Sporn, 1996). Nevertheless, the benefit of cell culture models for basic research is invaluable because once established, it allows the rapid identification of novel candidate genes which may be important for the transformation process in a given setup. Subsequent target validation in a physiological environment would then help to determine clinical relevance.

An elegant cell culture model for the transformation of human fibroblasts has been described by the group of Robert Weinberg (Hahn *et al.*, 1999; Hahn *et al.*, 2002). The serial introduction of hTERT, the SV40 Early Region (ER) and H-RasV12 rendered these cells tumorigenic in nude mice. Since it is well-characterized in various publications and due to its relative simplicity, this model system was selected to better characterize the role and regulation of the p73 tumor suppressor during the transformation of normal human cells.

4.1. Validation of the model system

4.1.1. Western Blot

Normal diploid fibroblasts of the BJ strain were transduced sequentially with retroviruses carrying the genes for human telomerase (hTERT), the SV40 small t and Large T antigen (st and LT; encoded by the SV40 ER), and a constitutively active form of H-Ras (HRASV12). The presence of LT and Hras could be demonstrated by Western Blot where expected. BJ-TE and

BJ-TER show high and comparable levels, while high expression of H-Ras is restricted to BJ-TER cells. The antibody used (C-20, Santa Cruz) is of rabbit polyclonal origin and therefore detects all forms of H-Ras, including endogenous wild type protein. Its signal was actually observed in some H-Ras blots in the other three BJ lines as faint bands, but is not visible in the blot shown in **Fig. 5** probably because the levels were below detection limit under the experimental conditions.

Three different mouse monoclonal antibodies were used to probe cell samples for the SV40 st: Ab419 (lab generated, courtesy Dr. A. Chestukhin), Pab 108 (Santa Cruz), and Ab-3 (Calbiochem). The first two were raised against the entire SV40 ER and thus also detect LT, while the latter antibody is specific for st. However, despite continued and extensive effort it was not possible to directly demonstrate the presence of the st antigen. Even samples with high LT content did not show any trace of the 21kDa protein. We favor the explanation that in our hands, all antibodies lacked the required sensitivity. This notion is supported by several lines of evidence. Firstly, sequencing of the expression vector revealed no alterations in the part of the SV40 ER which codes for st, therefore there is no reason to believe the co-expression of LT and st should be disturbed. Secondly, in keeping with the previous observation, the transcript of st was readily detectable with RT-PCR. Thirdly, William Hahn and co-workers state that "LT is expressed much more abundantly than ST" (Hahn *et al.*, 2002). In the blots shown in this publication, the exposure time for st was 30min to produce a signal as strong as that of LT (exposed only one minunte). It should be noted that the same antibodies against the small t antigen (Pab 419 and Pab 108) were used in that study, albeit from a different vendor. Finally and most importantly, the robust formation of large colonies from single BJ-TER cells in soft agar testifies to the presence of st protein, because it was demonstrated to be an absolute requirement for anchorage independent growth in BJ and other cell lines (Chen *et al.*, 2004; Hahn *et al.*, 2002).

Failure to detect hTERT in immunoblots remains unexplained as well, while hTERT mRNA was abundantly present as demonstrated by RT-PCR. Therefore, the same reasons like for the lack of st protein signal could be cited. However, the presence of increased telomerase activity could be functionally demonstrated by quantitative Real Time TRAP.

4.1.2. Real time TRAP

It has been pointed out that one precondition for cells to become immortal is telomere maintenance, otherwise they enter replicative senescence. This is achieved in most tumors as well as in cell culture by the stable expression of telomerase. TRAP (telomeric repeat amplification protocol) is an assay to measure telomerase activity. The basic principle is the

quantification of the amount of synthesized telomeric repeat (in humans: TTAGGG). Originally, the samples were analyzed for the typical six-base product ladder pattern on a DNA gel (Kim *et al.*, 1994; Kim and Wu, 1997). In this work a version of TRAP adapted for Real Time PCR by Wege *et al.* (2003) was employed, which allows a faster yet more precise quantification and better comparability.

Indeed, BJ-T cell lysate harbored high telomerase activity while the heat inactivated preparation as well as wild type BJ cell lysate showed only background telomerase activity. This finding is in agreement with the general consensus that differentiated somatic cells do not maintain appreciable levels of hTERT activity due to down-regulation and sequestration.

To put the results into a broader context, lysates from several telomerase-positive cancer cell lines with equal protein contents were measured as well. Using a standard curve generated from a BJ-T lysate dilution series, it was established that BJ-T have 6, 10, 10, and 29 times more telomerase activity than MCF7, H1299, DU145, and SAOS cells, respectively. While Wege *et al.* also worked with a dilution series and expressed telomerase activity as a percentage of the undiluted lysate, their results cannot be directly compared to the ones above. Wege *et al.* used HEK 293T cells as a standard and their unit of measure was the cell number. This is probably a better choice than total amount of protein when comparing cell lines of various origins, because cell types may vary in protein content. However, the qualitative information derived from the Real Time TRAP is sufficient to conclude that their high telomerase levels render BJ-T cells a very solid platform for the BJ-TE and BJ-TER cells.

4.1.3. Soft agar test

When dealing with newly transformed cells, their cancer-like properties need to be formally proven with appropriate methods. Various methods have been developed and refined to assess defining "macroscopic" features such as anchorage independent growth, tumor formation in animals, or invasiveness. The so-called soft agar test is quite popular to assay unrestrained growth that requires no substrate. Single cells are suspended in a semi-solid matrix that does not provide anchorage signals like the basal lamina in tissues or the surface of cell culture plates. Only fully transformed cells are able to form colonies, for they are independent from external growth stimuli due to constitutive mitogenic signals (in this case a mutant allele of H-RAS). The experimental findings nicely confirm this assertion, since only fully transformed BJ-TER readily formed large colonies. Of minor concern were sporadic colonies observed with TE cells. These appeared preferably when cells were seeded at higher densities. A probable explanation therefore is that cells were imperfectly separated and served as growth substrate for each other. It should also be kept in mind that these cells are nearly fully transformed as they already carry

the LT and st antigen. A manifestation thereof and a possible further reason for the appearance of occasional colonies is the genomic instability of BJ-TE cells (compare **Fig. 8**). In addition, st was shown to be essential for anchorage independent growth in HEK and BJ cells (Chen *et al.*, 2004; Hahn *et al.*, 2002). Small, abortive colonies in normal human cells expressing LT+H-Ras or hTERT+LT have been observed by others and were considered "one manifestation of replicative mortality that occurs in the absence of telomere maintenance" (Elenbaas *et al.*, 2001; Hahn *et al.*, 1999).

Another, perhaps graver concern is the failure to demonstrate tumorigenicity in nude mice (Blair *et al.*, 1982; Fasano *et al.*, 1984). Analogous to the soft agar test results, tumor formation in these animals was expected with the subcutaneous injection of BJ-TER cells. This observation remained elusive, though, despite numerous modifications in the experimental strategy such as increased cell number and concentration; admixing with Matrigel™, a complex soluble preparation which mimics the growth-promoting effect of the extracellular matrix; and usage of new-born nude mice to circumvent neutralizing reactions of the remaining innate immune system (A. Berns, pers. comm.).

Reasons for the inability of TER cells to induce tumor formation could be manifold. In principle, a positive soft agar test and tumor formation in animals do not necessarily correlate (Brookes *et al.*, 2002; LaMontagne *et al.*, 2000). It may also be argued that the microenvironment of the mouse skin lacks certain cell types or growth factors to permit human fibroblasts to thrive. However, these general points can be dismissed since it has been already demonstrated that TER cells form tumors in mice, without showing the additional phenotypes of invasiveness or metastatic ability (Hahn *et al.*, 1999; Hahn *et al.*, 2002). This leaves only shortcomings in the experimental design. Long latency can probably be excluded, since the injected mice were kept under observation for at least two month. A possible explanation is that for tumorgenicity assays, immuno-compromised (irradiated or athymic) mice are often used (Blair *et al.*, 1982; Fasano *et al.*, 1984), which were not available in this work. However, the best support for flawed experiments, as opposed to faulty cell lines, comes from tests with the “original” BJ-TER. We were able to procure some of the cell lines used in the works cited above (courtesy William Hahn). Even with their fully transformed strain we could not induce tumor growth in our animals.

It is concluded that the cell culture model for the transformation of normal human cells by Hahn and co-workers was successfully established. All four introduced genes could be detected either directly (LT, H-Ras) or in functional assays (st, hTERT, H-Ras).

4.1.4. Cell cycle analysis

Increased proliferation rate, immortality and genomic instability are three hallmarks of cancer cells (Hanahan and Weinberg, 2000) which are accessible by cell cycle analysis. The contribution of the three introduced genetic elements towards these attributes is very different and will be briefly reiterated here.

The main function of telomerase is clearly immortalization. hTERT protects the telomeric ends of chromosomes, thereby also counteracting genomic instability, which is in part inflicted on cells by end-to-end fusions or degradation of uncapped chromosomes (Blackburn, 2001). Moreover, stable expression of telomerase does not increase proliferation in human cells (Morales *et al.*, 1999), which has led some to suggest it should not be considered an oncogene at all (Harley, 2002), leaving the status of hTERT somewhat debatable at this time.

The process of immortalization is on its own insufficient to create a fully transformed, tumorigenic cell, and requires the additional introduction of an oncogene such as *Ras* (Hahn *et al.*, 1999; Jiang *et al.*, 1999). The family of *Ras* oncogenes promotes the initiation of tumor growth by stimulating tumor cell proliferation, but also ensures tumor progression by stimulating tumor-associated angiogenesis (Kranenburg *et al.*, 2004). Interestingly, the introduction of H-Ras alone in normal or immortalized mammalian cells leads to the opposite: it triggers senescence (which is different from the senescence induced by short telomeres; see Introduction). Several investigations have made it clear that two functions of LT, neutralizing both p53 and Rb, are necessary for cells to tolerate persistently high levels of H-Ras (Hahn *et al.*, 1999; Srinivasan *et al.*, 1997; Zhu *et al.*, 1992).

Yet these functions combined are still not sufficient to fully convert normal into tumor cells (Morales *et al.*, 1999). As it has been pointed out above, disruption of PP2A signaling by st is necessary and sufficient to finally confer properties like anchorage-independent growth on cells previously transfected with hTERT, LT, and H-Ras (Chen *et al.*, 2005; Chen *et al.*, 2004; Hahn *et al.*, 2002).

In contrast to the general proliferation-stimulating effect of H-Ras, Hahn *et al.* (1999) note that "oncogenic ras led to clear morphological transformation […] but had only a minor effect on the growth rate in monolayers of BJ Fibroblasts expressing both large-T and hTERT". This is in good agreement with my observations, since the onset of proliferation increases already with the introduction of the SV40 ER. In keeping with this it has been found that the cell cycle time of st-expressing BJ or HEK cells is one third shorter compared to control cells (Hahn *et al.*, 2002), an effect that could be attributed to inhibition of PP2A-B56γ complexes by st (Chen *et al.*, 2004). Reports from the same sources of st-mediated, enhanced ability to proliferate in low-

nutrient conditions could also be nicely demonstrated. In contrast to wild type and T cells, TE and TER had almost identical S-phase indices in medium containing 0.1% or 10% FCS. A surprise was the finding that T cells in 10% FCS already had a significantly higher S-phase index than the wild type, if not quite as much as TE and TER. This contradicts the notion that hTERT alone does not increase proliferation. In fact, T grew in cell culture at a similar rate like low-passage wild type, while TE(R) had to be split more often. It is therefore conceivable that the wild type cells used for this particular experiment showed beginning senescence. Their proliferation rate may have slowed down already and could not be raised significantly by serum addition either.

A further notable difference between in the cell cycle profiles is the notable sub-G_1 population in BJ-/ VH6-TE(R) cells. Like the increased S-phase index, this fraction of apoptotic cells is interpreted as a response to the high levels of viral proteins and is reflected by markedly increased debris in cell culture dishes of BJ-/ VH6-TE(R).

4.2. Up-regulation of p73 in TE cells

After having successfully established the fibroblast *in vitro* system of tumorigenesis, the regulation of TAp73 in its four stages was determined. One of the first and most important results of this work was the discovery of SV40 LT-mediated up-regulation of TAp73 in confluent BJ-TE cells. It was further shown that TER cells have again low TAp73 levels. It is therefore suggested that TAp73 presents a roadblock on the way to full transformation in this model system of tumorigenesis, in agreement with the apparent main function of full-length p73 as a tumor suppressor.

4.2.1. TAp73 is up-regulated in confluent BJ-TE cells

Density-dependent elevated levels of TAp73 have been confirmed on RNA level -an effect which is probably universal and not tissue-specific- as well as in protein form. After it was shown to be caused by the SV40 LT alone, the question of the underlying mechanism needed to be answered. According to the current state of research, TAp73 gene expression can be induced by DNA damage, which is sufficient to trigger apoptosis in a p53-independent fashion (Agami *et al.*, 1999; Gong *et al.*, 1999). While p53 is activated by all known forms of DNA-damage, effective inducers of TAp73 include genotoxic drugs like doxorubicin, taxol, cisplatin, or etoposide (Bergamaschi *et al.*, 2003; Irwin *et al.*, 2003) as well as ionizing radiation, but not, for example, UV light (Davis and Dowdy, 2001; Kaghad *et al.*, 1997). Certain oncogenes such as c-Myc, adenoviral E4-orf6/7 and adenoviral E1A are known to directly activate p73 transcription (Flinterman *et al.*, 2005; Shapiro *et al.*, 2006; Zaika *et al.*, 2001).

Results from numerous studies emphasize the central role of E2F1 in the transactivation of TAp73 (Irwin *et al.*, 2000; Pediconi *et al.*, 2003; Rodicker *et al.*, 2001; Stanelle *et al.*, 2003; Stiewe and Putzer, 2000). Repression, for example by TGFβ or C-EBPα (Irwin *et al.*, 2000; Marabese *et al.*, 2003), as well as activation of TAp73 transcription often converge on E2F1. It binds to E2F response elements within the TA promoter and enables in cooperation with other factors the transcription of full-length p73 (Irwin *et al.*, 2000; Stiewe and Putzer, 2000). E2F1 is a major switch in the regulation of the cell cycle, and therefore found very often de-regulated in cancer (Bell and Ryan, 2004). E2F1-dependent gene activation is efficiently suppressed most of the time by the Rb protein (see Introduction). There is but a small time window where E2F is permitted to act. That is the G1/S-phase transition, where Rb becomes deactivated by hyperphosphorylation through cyclin D+CDK4/6 and cyclin E+CDK2 signaling (Harbour *et al.*, 1999).

In this work, the high level of TAp73 in LT-transformed cells has been demonstrated to correlate with the cell density. The mere presence of LT is apparently not sufficient to trigger the same level of p73 expression in sparse, proliferating cells as in (near-) confluent ones. A possible explanation is the following. It is a well-established fact that E2F1 is also regulated by phosphorylation and acetylation (Lin *et al.*, 2001; Martinez-Balbas *et al.*, 2000). In particular, Pediconi *et al.* (2003) have shown that drug-induced DNA damage leads to acetylation of E2F1 at certain lysine residues. These modifications increase its ability to bind to the TAp73 promoter and to activate TAp73 transcription. The authors discuss that stimuli other than DNA damage may also cause E2F1 acetylation and TAp73 up-regulation. It is possible that high cell density is such an additional stress signal, and it might cooperate in the fibroblast model system with the LT-mediated relase of E2F1-inhibition to achieve the observed strong induction of TAp73.

There is evidence that p53 is activated in normal fibroblasts in a cell density-dependent manner, leading to cell cycle arrest (Meerson *et al.*, 2004). The situation with p73 is less clear. To the best of my knowledge, there is only one report which actually investigated the relationship between TAp73 levels and density of cultured cells. The group of Matthias Dobbelstein observed a marked increase in both mRNA and protein level when confluent HaCat immortalized keratinocytes were re-seeded at low density (Waltermann *et al.*, 2003). The authors propose that this effect is due to increased E2F activity in cells that resume cycling. It is not easy to see why the relation of p73 level and density in this work are found inverted for BJ-TE, BJ-TER, and HA1E cells. Cultured cells do shift their expression profile in response to increasing density. Underlying causes include changes in nutrition availability, accumulating metabolic products (acidosis), and last not least due to signaling related to cell-cell contacts,

resulting in phenomena like contact inhibition (Lieberman and Glaser, 1981). However, such general effects can be probably ruled out as TAp73 levels in BJ and BJ-T behaved like described by Waltermann *et al.*, at least regarding transcription. Most likely the altered regulation of TAp73 in the LT-bearing cell types according to cell density can be ascribed to the presence of this viral oncoprotein just like the general elevation; details remain to be elucidated.

4.2.2. SV40 LT, not st, leads to elevated levels of p73 in TE cells

The SV40 Large T antigen was found solely responsible for the high levels of TAp73. While LT comprises several functional domains and is known to effect a considerable number of cellular processes, its role in transforming human cells is fully accounted for by the direct binding of p53 and Rb (Hahn *et al.*, 2002). The working hypothesis of this project envisions a displacement of active Rb from its repressor complex with E2F1, releasing the transcriptional block on the TA promoter of the p73 gene and resulting in the observed accumulation of TAp73 protein. Interference of the LT protein with TAp73 transcription, translation, protein stability or protein degradation was not investigated here, because there is strong evidence in the literature against such a direct mode of regulation. It is a peculiar feature of the p53 family that viral proteins in general tend to interact differently with its members, indicating p53, p63 and p73 might have different effects on viral replication and transformation (Das *et al.*, 2003; Marin *et al.*, 1998; Roth and Dobbelstein, 1999; Steegenga *et al.*, 1999; Wienzek *et al.*, 2000). Importantly, while LT binds and inhibits p53, there is no direct interaction detectable for LT and p63 (Kojima *et al.*, 2001) or p73 (Dobbelstein and Roth, 1998; Higashino *et al.*, 1998; Marin *et al.*, 1998; Reichelt *et al.*, 1999). Moreover, not a single investigation to date reports an indirect link between LT and p73, resulting in an accumulation of TAp73 like observed here.

4.2.3. Transcriptional regulation of TAp73

For initial luciferase assays, three published LT mutants were generated with point mutations abolishing Hsp70 binding (Y34A), Rb binding (E107K; also called K1) and antiapoptotic properties (M528S). From this limited set only the J domain mutant led to a loss of TAp73 transactivation. This is not surprising, considering various reports which demonstrate the J domain to be important for transformation (Srinivasan *et al.*, 1997; Zalvide *et al.*, 1998; Zhu *et al.*, 1992). A review by Lee & Cho (2002) gives a very detailed account of the biochemical and structural background of the mechanism by which LT displaces Rb from its repressor complex with E2F. Briefly, both the N-terminal J domain and the LxCxE motif in large T antigen must act together to inactivate Rb (Campbell *et al.*, 1997; Harris *et al.*, 1998; Srinivasan *et al.*, 1997; Zalvide *et al.*, 1998). SV40 LT, Rb, and E2F form a transient complex to which a co-chaperon

called hsc70 is recruited. Binding to a conserved motif in the LT J domain induces a conformational change in hsc70, stimulating ATP hydrolysis. This in turn induces a further conformational change in Hsp70 which is thought to drive the dissociation of the whole assembly.

Since Rb binding by LT is required to lift the transcriptional block from the TA promoter of p73, it is very surprising that no effect was seen in the luciferase assay with the LT K1 mutant. At face value this would suggest no involvement of Rb in the up-regulation of TAp73 caused by LT, would it not be for the clear drop of p73 induction with the J domain mutant. Closer investigation with more LT mutants is clearly required here. The involvement of the other members of the small pocket family, p107 and p130, was not addressed in this project and should also be looked into, since they are known to be involved in LT-facilitated transformation (Mitchell *et al.*, 2003; Zalvide *et al.*, 1998). Finally, it is important to state that the SV40 LT-pocket protein interactions cited above were mainly investigated in rat or mouse embryonic fibroblasts. In contrast, Hahn and co-workers found an intact LT J domain dispensable for immortalization, growth in soft agar, or the formation of tumors in human cells (Hahn *et al.*, 2002). While it is unclear why these differences between rodents and humans exist, this observation actually supports the notion that a functional J domain might have protective, rather than oncogenic, effects in human cells by activating a tumor suppressor like p73.

LT mutant M528S was initially chosen to serve as a p53-binding deficient LT form. It was later discovered that residue 528 is actually located within the BH1-like domain, which protects host cells from apoptosis *independent* from p53 binding and inactivation (Conzen *et al.*, 1997). As a result, any influence of p53 neutralization by LT was not investigated in this project and cannot formally be excluded as a factor in the LT-p73 relationship. The same is true for the other functional domains found in LT, some of which might be relevant for transformation as well (reviewed in Ali and DeCaprio, 2001; reviewed in Moens *et al.*, 1997), like binding of the transcription co-activators p300, p400, and CBP (Eckner *et al.*, 1996; Lill *et al.*, 1997; Yaciuk *et al.*, 1991). Evaluating these LT activities in light of TAp73 upregulation presents another possible aspect for future research.

The TA promoter of the p73 gene has been subjected previously to detailed computational and biochemical analysis (Ding *et al.*, 1999; Irwin *et al.*, 2000; Seelan *et al.*, 2002; Stiewe and Putzer, 2000). Of the at least five E2F-binding sites present upstream of the start codon, site number three was found in this study to be decisive for p73 induction. While a mutation of site three (at -288bp) resulted in a significant reduction of promoter activity, this data should be treated with caution. The effect was observed reproducibly, but due to the available

constellations of mutated binding sites (2/4/5 and 2/3/4) no definite conclusion can be drawn about the relevance of site one or the other putative E2F binding sites present further upstream as well as downstream of exon 1 (Stiewe and Putzer, 2000). Direct binding of the E2F1 complex should also be demonstrated, for instance by gel shift analysis, to verify the presence of E2F1. Furthermore, in partial contrast to my findings, Seelan *et al.* (2002) identified the highest promoter activity with between -217bp and -113bp, specifically at E2F sites starting at -155bp and -132bp, corresponding to the stretch between -370bp and -266bp from the ATG and what is called here site number 2 and 4, respectively. Site number 1 did bind E2F1 but had a negligible effect on overall activity. The different result might be explained by system specific differences. The experiments of this study were performed in absence and presence of Large T, while Seelan *et al.* looked directly at E2F1 (and its inhibition by increasing levels of Rb). The different origin of the cell lines are probably of greater importance since p73 is known to be tissue specific regulated in the adult organism, with maximal expression in brain, prostate, kidney, placenta, colon, heart, liver, spleen, sceletal muscle, thymus, and pancreas (SwissProt entry O15350). Liu and co-workers used HeLa (cervix carcinoma) and SaOs (osteosarcoma) cells, this study T98G (glioblastoma) and H1299 (lung carcinoma). For this same reason Ding *et al.* (1999) may have pinpointed in MCF7 epithelial breast cancer cells most of the basal p73 promoter activity further downstream than Seelan *et al.*, between -272bp and -134bp, relative to the ATG.

It remains to be seen if the influence of the SV40 LT on p73 transcription regulation also extends to the turnover of the protein. It cannot be formally excluded that LT in some indirect way enhances TAp73 protein stability or blocks its degradation, even though there is no experimental or published evidence to support this notion.

4.2.4. BJ-TE cells are more sensitive to adriamycin than BJ-T

The results above provoke the question what the functional relevance or consequence of the high TAp73 levels for BJ-TE cells is. It was suggested here that this up-regulation presents a block on the road to transformation, perhaps a backup system under conditions where p53 is limited or not available.

As a matter of fact, both full-length and oncogenic ΔN forms of p73 have been repeatedly implicated as determinants of chemosensitivity and therefore of the outcome of cancer chemotherapy, albeit with opposing prefixes (Muller *et al.*, 2005; Tuve *et al.*, 2006). Mutant p53 appears to be a singularly important modulator of the outcome of chemically induced p73 expression (Bergamaschi *et al.*, 2003; Concin *et al.*, 2005; Irwin *et al.*, 2003). Furthermore,

several groups report ties between p73, induction of apoptosis, and DNA mismatch-repair (Gong *et al.*, 1999; Shimodaira *et al.*, 2003).

Defects in apoptosis are frequently found in both drug resistant and cancer cells (Johnstone *et al.*, 2002), linking apoptosis with chemosensitivity. Programmed cell death is a well-characterized outcome of TAp73 activity in certain contexts (reviewed in Dobbelstein *et al.*, 2005; reviewed in Stiewe and Putzer, 2001). Upon genotoxic insult such as cisplatin exposure or gamma irradiation, p73 binds to the non-receptor tyrosine kinase c-Abl, leading to phosphorylation, accumulation, and increased apoptogenic potential of p73 (Agami *et al.*, 1999; Gong *et al.*, 1999). Apoptosis is then triggered by a growing number of different pathways (reviewed in Ramadan *et al.*, 2005), involving the transactivation of scotin, PUMA, and possibly the death receptor CD95.

The fact that BJ-TE cells are significantly more sensitive than BJ-T was unexpected. The mode of action of adriamycin relies on functional p53 (Lowe and Ruley, 1993), which is inhibited in BJ-TE cells due to the abundant presence of the SV40 LT antigen, but should be normally available in BJ-T cells. A solution of this conundrum may be offered through the combination of the apoptotic properties and the elevated levels of TAp73 in BJ-TE. Indeed, BJ-TE cell populations show a substantial sub-G_1 population. However, attempts to quantify the rate of apoptosis by other methods such as Annexin V staining, TUNEL assay, or immunoblots for cleaved PARP and effector caspases were futile because they delivered inconclusive results. Without proper quantification it remains speculative if the increased TAp73 levels account for all or even part of the observed sub-G_1 cells for two main reasons. First, a sub-G1 peak was also seen with TER cells, which have low p73. Second, in extension to the first point it can be argued that the presence of such multi-functional as well as noxious proteins like Large T and H-Ras provokes cell death in different ways, despite their anti-apoptotic properties.

On the other hand, it is known that doxorubicin/ adriamycin itself leads to an induction of p73 (Bergamaschi *et al.*, 2003; Irwin *et al.*, 2003). It stands to reason that the cellular response to the drug is not solely reliant on p53, as suggested by Lowe and Ruley in 1993 (at that time p73 was not yet discovered). For a definite answer on the contribution of p73-mediated apoptosis to the response to genotoxic insults the levels of TAp73 in the cells under adriamycin or similar agents should be determined, under inclusion of the TER line.

4.2.5. Knockdown of TAp73 results in growth advantage

Knockdown of TAp73 in BJ-TE cells and its effect on cell growth kinetics appears to confirm the interpretations of the cytotoxicity assay. Normal cells experience a growth arrest when they become confluent, that is, when they are surrounded by neighboring cells. This effect was

intensely studied in cultured fibroblasts and was termed "contact inhibition" (Lieberman and Glaser, 1981). Conversely, tumor cells lose this regulatory mechanism early in their genesis due to dysfunctions in proliferative signaling and the presence of intrinsic growth stimuli (Hanahan and Weinberg, 2000).

One report on the effect of cell density on p73 levels has been discussed above (Waltermann *et al.*, 2003). As far as I know, the work presented here is the first investigation of the reverse: the effect of p73 levels on the density regulation of cultured cells. An efficient knockdown of TAp73 in VH6-TE resulted in cells that were able to perfectly tolerate confluence, unlike control cells which immediately started to die upon reaching their maximal density. From experience with these cells it was known that adherent cells do not always equal living cells. Therefore cell viability from the last time point of the previous growth curve was quantified by virtue of a vitality staining. In this experiment the difference in remaining live cells was indeed even more pronounced (76% with p73 knockdown vs. 16% in control). Finally, in a direct co-culture test it was established that cells with little TAp73 also grow more dynamical than their controls, when each line was cultured in presence of the parental TE strain.

Taken together, the results from the experiments above strongly argue for the up-regulation of TAp73 as a specific protective response in a p53-deficient context. The cytotoxicity assays showed that upon oncogenic challenge cells are rendered more susceptible to toxins which are known to exert their cytostatic effect through p53 family members. Conversely, a reversion of the high TAp73 levels in TE cells by means of RNAi-mediated knockdown conferred cancer-like properties, specifically reduced contact inhibition, much higher density-related stress tolerance, and more competitive growth kinetics.

4.2.6. Identification of putative TAp73 targets

After some of the effects of altered TAp73 levels in the fibroblast model were delineated, the question of the underlying molecular mechanisms was pursued. To begin answering it, the expression profile of cell lines with high and low TAp73 level at high and low density was determined in microarrays. This grid of two by two yielded a total of 1205 differentially regulated (i.e., at least 2fold up- or downregulated) genes, 1023 according to density and 182 according to p73 knockdown. The "strongly" (more than five-fold) regulated genes are listed in **Tab. 10** (density- induction), **Tab. 11** (density- repression), **Tab. 12** (p73 knockdown-induction), and **Tab. 13** (p73 knockdown- repression) and were further classified into 15 functional categories. For more details see Results. This section will focus on the small group of 14 genes that were differently regulated according to *both* parameters. Out of these 14 human genes, only the five that are regulated like TAp73 (up with density, repressed with p73

knockdown) are briefly characterized in the following. In a concluding summary, their possible significance for tumorigenesis is discussed.

FAM38B

Hypothetical protein FLJ23403; 62.5kDa/ 544 aa protein of unknown function. Highly expressed in heart and lung. Four putative transmembrane domains, therefore probably located in membranes (SwissProt entry #Q9H5I5).

IGSF3

Immunoglobulin superfamily, member 3; maps to chr1p13, related to V7 (a human leukocyte surface protein) but has eight Ig domains; highly expressed in placenta, kidney, lung, and present also in many other tissues (but not peripheral blood lymphocytes). Expression pattern implies IGSF3 is not involved in an immune function (Saupe *et al.*, 1998).

IGSF4*/TSLC1/NECL-2*

Immunoglobulin superfamily member 4; mediates cell-to-cell adhesion (three extracellular Ig loops) and transmits the signals towards the cytoskeleton organization; expressed in brain, lung, testes, and most other tissues; has a tumor suppressive function, because it is inactivated in 30-60% of various cancer, including non-small cell lung cancer, liver, pancreatic, and prostate cancers (reviewed in Murakami, 2005). Loss of heterozygosity is in particular observed in advanced, aggressive forms of these diseases. Very highly conserved in evolution, male *Igsf4*$^{-/-}$ mice are infertile due to defects in spermatogenesis (Yamada *et al.*, 2006).

KCNK1

Potassium channel, subfamily K, member 1; cloned first in 1996, this gene was mapped to chr. 1q42-q43 and codes for TWIK-1, an unusual 337aa potassium channel with four transmembrane segments and two pore regions (Lesage *et al.*, 1996a; Lesage *et al.*, 1996b). These two features define the most recently discovered group of low conductance potassium channels called K_{2p} channels, to which TWIK-1 (tandem of P domains in a weak inward rectifying K^+ channel) is counted (reviewed in Lesage and Lazdunski, 2000). K_{2p} channels are widely expressed in rodent and human tissues. They are insensitive to typical inhibitors, function at all membrane potentials, do not show activating/ inactivating kinetics, therefore are quasi-constitutively active and provide background K^+ flux, regulating the cell volume and in excitable cells, the resting potential (Lesage and Lazdunski, 2000). The highest expression of TWIK-1 in humans was found in brain, placenta, and kidney. Significant levels are also expressed in heart, pancreas, lung, liver, and ovary.

MGC8685*/ TUBB2B*

Tubulin, beta polypeptide paralog; tubulin, beta 2B. Maps to 6p25.2 (GeneCards entry #GC06M003172). The soluble form of tubulin is a heterodimer of an alpha and beta chain. There are currently six known isotypes of α-tubulin and seven of β-tubulin (including β 2B). The heterodimer polymerizes into protofilaments that, arrayed in a hollow cylinder, form the backbone of microtubules. Tubulin is therefore important for mitosis (formation of mitotic spindle), but also in interphase cells (transport of organelles, receptors, etc.). The dynamics of microtubule turnover are the disrupted by a large number of popular and novel cancer drugs, most prominently vinca alkaloids and taxanes. Their main effect is thought to be interference with mitotic spindle formation, which prevents proper chromosome segregation into daughter cells, leads to mitotic arrest and eventually to apoptosis. In addition, microtubule interphase functions seem to be affected (Attard *et al.*, 2006).

A widely recognized but rarely acknowledged basic problem in siRNA use and its downstream applications, in particular expression profiling, is a bias for genes normally involved in antiviral defense. The common denominator is probably the molecular machinery processing vector-based shRNA, such as the RNase III endonuclease Dicer, but which evolved as a weapon against intruding viruses (Waterhouse *et al.*, 2001). A typical example is the up-regulated *OAS1* gene because it is a factor in interferon-mediated cellular responses which in turn are often seen in virus-infected cells but also in those which overexpress siRNA (McManus *et al.*, 2002). *C1orf29/ IFI44L* and *TRIM22/ Staf50* might fall as well into this special category of false positives because of their reported antiviral function. However, *TRIM22/ Staf50* was already demonstrated to be transactivated by p53 and p73 in leukemia cells, suggesting it may be involved in the regulation of their proliferation and/or differentiation (Obad *et al.*, 2004). Why *TRIM22/ Staf50* is up-regulated in the absence of p53 or p73 remains unexplained, though. At any rate it is very hard to tell just from the involvement in virus response if a candidate gene is differentially regulated due to the presence of siRNA vectors or not. Therefore it was decided not to correct for this possible bias and accept a few false positives.

Concerning the direction of regulation in VH6-TE>p73si#1, one would expect to see an up-regulation of oncogenes (i.e., of *EDN1*, *MT1H*, *TGFB2*) and a repression of genes like *IGSF4*. Interestingly, these expectations are fulfilled for only half of these target genes: *MT1H* and *TGFB2* are indeed induced (by both conditions). The reason why *EDN1* and *IGSF4* deviate from expectations might be because the action of certain cancer related factors is determined by the molecular circumstances, just like with p73 or *TGFB2*, and can head one direction or the other, towards tumor suppression or progression.

From the 14 double-regulated genes, the observed slight down-regulation of *TGFB2* with both parameters is of particular relevance because a cross-talk between TGF-β signaling and the p53 network is known to exist (reviewed in Dupont *et al.*, 2004). Specifically, p53/ p63/ p73 were shown to modulate the already very intricate TGF-β activities by cooperating with activated SMAD complexes, thereby enhancing the induction of transcription in different cellular and developmental settings (Cordenonsi *et al.*, 2003). The regulation of gene expression also works the other way. TGF-ß represses E2F1-driven transcription, thus preventing (among other effects) the transcription of p73, thereby creating a negative feedback loop of its modulator. Published signal transduction relationships like this one, which could be reproduced with the microarrays, serve to validate the array data as a whole.

4.3. Downregulation of p73 in TER cells

H-Ras itself is rarely mutated in sarcomas (Bos, 1989). On these grounds it has been argued that the choice of H-RasV12 as the constitutive, intrinsic growth signal is inappropriate for the transformation of fibroblasts (Skinner *et al.*, 2004). A more physiological solution would be for instance to target direct upstream activators of Ras like the receptor tyrosine kinase HER2/neu, frequently overexpressed in Wilm's tumor, bladder, pancreatic, and breast carcinoma (Menard *et al.*, 2001).

The group of William Hahn however has clearly established that H-Ras, while not sufficient, is necessary to fully transform primary human cells. Without Ras, no anchorage-independent growth or tumor formation in nude mice was observed (Hahn *et al.*, 1999). However, the introduction of at least LT was necessary to render the cells permissive for the high levels of mutant H-RasV12. It was later shown that two transforming functions of LT, the binding and inactivation of p53 and Rb, are required for the tolerance of activated H-Ras (Hahn *et al.*, 2002). Tumorgenicity was dependent on the Ras expression levels, and fully transformed human cells consistently had 10-20 times more Ras than tumor samples (Elenbaas *et al.*, 2001; also compare Hingorani and Tuveson, 2003; Tuveson *et al.*, 2004). The Ras protein level found in the TER cells of this work are probably quite comparable (see **Fig. 5**). The authors argued that intense Ras signaling in cells of the model systems may switch on additional effector pathways, possibly to compensate for alterations occurring in "natural" tumors or merely to enable the rapid outgrowth of in mice implanted cells to tumors in a matter of weeks (Elenbaas *et al.*, 2001; Hahn *et al.*, 2002).

Among the complex network of Ras signaling, four principal pathways of clinical relevance have been identified: the Raf/MEK/ERK, PI3 kinase, RALGDS, and PLCε cascades (reviewed in Downward, 2003). Of these, the first two have been reported to be of special importance for

transformation (Joneson *et al.*, 1996; Rodriguez-Viciana *et al.*, 1997). Indeed, results presented in this work support the conclusion that the decisive pathway is the PI3K cascade alone. This would be in contrast to the consideration by the Hahn group, that multiple effectors of H-Ras might be triggered by its high concentration.

In summary, two avenues should be pursued from here to uncover the players downstream of H-Ras which are responsible for the downregulation of TAp73. Firstly, it has to be formally excluded that any of the other principle Ras effector pathways (in particular RALGDS and PLCε) are involved. Secondly, a "bottom up" strategy should be followed to identify the relevant factors downstream of PI3K.

4.4. Summary: role and regulation of p73 in the transformation of normal human fibroblasts

Transformation or the conversion of normal into cancer cells is an exceedingly complex process involving the change of expression of hundreds of genes in dozens of pathways. All positions of even the most prominent factors in this scheme are not found yet. The full-length product of the *TP73* gene, TAp73, is known to play an important role in the prevention of certain cancers and to influence the outcome of their cytostatic therapy. While the signaling in the p73-mediated cancer defense is understood now at least in its outlines, it is considerably less clear how emerging tumors evade protective mechanisms like apoptosis.

This work addressed this question by employing an established cell culture model of tumorigenesis. The four human fibroblast cell lines wild type (VH6 or BJ strain), -T, -TE, and -TER were analysed for their TAp73 status (**Fig 34)**. The fact that its mRNA and protein levels rise sharply in the last non-tumorigenic line (-TE), then drop to near-wild type level in –TER re-emphasize a role for TAp73 in tumor suppression. The molecular basis for the increase of TAp73 in -TE cells seems to lie in the well-documented deactivation of the Rb protein by LT (high cell density probably also contributes). This activity of LT in itself favors transformation as it removes an important master regulator of the cell cycle, leading to increased and quasi-unrestrained proliferation. This is partly accomplished by the release of E2F1 inhibition, which transactivates a number of pro-proliferative targets. However, since E2F1 is also one of the most important activators of TAp73, it appears plausible that this coupling of oncogenic with growth-suppressing signals might represent an inherent safety catch. Strong support comes from various assays in which the robustness under chemical and physical stress of -T and -TE-based cell lines was tested. They unanimously demonstrated that despite their LT, -TE cells (much

TAp73) are actually less stress tolerant and less drug resitant than control cells with low TAp73 levels.

The elimination of TAp73 on the introduction of H-Ras in -TER seems to be achieved through one of the effector pathways of PI3 kinase, itself directly activated by H-Ras. Preliminary results see a selective up-regulation of the oncogenic ΔNp73 in -TER. This would be in agreement with the reported anti-apoptotic, oncogenic function of the truncatd p73 isoforms and nicely complements the picture of the two-faced p73 gene and its role in the transformation of normal human fibroblasts.

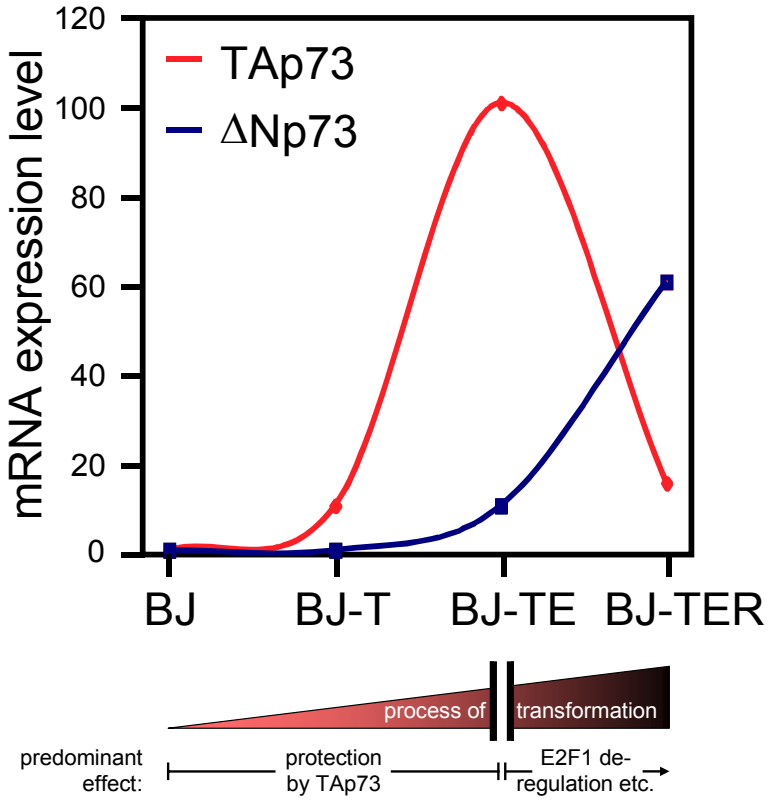

Fig. 34 Model of the function and regulation of p73 in the transformation of normal human fibroblasts. TAp73 mRNA (red line) rises sharply in non-tumorigenic BJ-TE, while fully transformed BJ-TER contain again low levels of TAp73 mRNA and protein. The behaviour up to BJ-TE is therefore dominanted by the protective effect of TAp73, which presents a block for transformation. In BJ-TE this block is enforced by the LT-mediated deactivation of Rb and the subsequent E2F1 deregulation. BJ-TER cells are fully transformed because they carry in addition the mutant H-RasV12 allele. H-Ras seems to suppress TAp73 through a yet to be identified PI3 kinase pathway. Preliminary results indicate a selective increase of ΔNp73 message in BJ-TER and suggest an opposing, anti-apoptotic effect of these transactivation-deficient p73 forms.

Further details on the regulation *of* TAp73 will come from the detailed investigation of the pathways downstream of Ras. The gene regulation *by* TAp73 during transformation is being unraveled by the ongoing analysis and validation of DNA microarrays performed with dense and sparse -TE cells with high and low TAp73 levels.

5. Acknowledgements

First and foremost I am indebted to Thorsten Stiewe for his skillful, patient guidance and for never running out of ideas. I'm grateful to all members of the Stiewe lab, past and present, for making it a fun place to work. In particular I thank Stefano Gaburro (down-regulation by H-ras), Heidi Griesmann, Nicole first-Kirchhof-then-Hüttinger (both mouse experiments) and Christof Burek (AG Rosenwald, Institute of Pathology, University of Würzburg; mircroarrays) for their contributions to this work. Extra special thanks go to Michaela Beitzinger for her patient and proficient help (down-regulation by H-ras; microarray), and last not least to

my parents for support in every way possible

Marina for giving me our daughter Laura!

6. Appendix

6.1. Abbreviations

Tab. A-1 Abbreviations

Abbreviation	Meaning
ALT	alternative lengthening of telomeres
bp	base pairs
(BJ- or VH6-)T	BJ or VH6 cells expressing hTERT
(BJ- or VH6-)TE	BJ or VH6 cells expressing hTERT & SV40 ER
(BJ- or VH6-)TER	BJ or VH6 cells hTERT, SV40 ER & H-Ras V12
BrdU	bromodeoxyuracil
cDNA	complementary DNA
CIAP	calf intestine phosphatase [protein]
CPE	cytopathic effect
DAPI	4',6-diamidino-2-phenylindole
DCC	deleted in colorectal cancer [protein]
DMEM	Dulbecco's minimal essential medium
DMSO	dimethyl sulfoxide
dNTP	desoxynucleotide triphosphate
ECL	enhanced chemoluminescence
EDTA	ethylene diamine tetraacetic acid
EGTA	ethylene glycol tetraacetic acid
ERK	extracellular signal-regulated kinase [protein]
FAP	familial adenomatous polyposis [protein]
FCS	fetal calf serum
GAP	GTPase activating proteins
GAPDH	glyceraldehyde 3-phosphate dehydrogenase [protein]
GDP	guanine diphosphate
GEF	guanine nucleotide exchange factors
GFP	green fluorescent protein
GTP	guanine triphosphate
h	hours
HDM2	human homolog of mouse double minute 2 [protein]
HEK	human embryonic kidney cells
HI	heat inactivated
HMEC	human mammary epithelial cells
HPLC	high performance liquid chromatography
HPV	human papilloma virus
HRP	horse radish peroxidase [protein]
hTERT	human telomerase reverse transcriptase [protein]
IC_{50}	concentration to inhibit 50% [here: of cell growth]
i.e.	id est (that is)

Tab. A-1 (continued)

Abbreviation	Meaning
KAc	potassium acetate
kDa	kilodalton
MDM2	transformed 3T3 cell double minute 2 [protein]
min	minutes
mm	millimeter
nd	not determined
ns	non-silencing *or* not significant
OD	optical density
PBS	phosphate-buffered saline
PCR	polymerase chain reaction
PD	population doublings
PEI	polyethylenimine
PI3K	Phosphoinositide 3-kinase [protein]
PP2A	protein phosphatase 2A [protein]
Rb	retinoblastoma protein
RNAi	RNA interference
ROS	reactive oxygen species
RT	room temperature
RT-PCR	reverse transcription PCR ["Real Time PCR" is not abbreviated]
SD	standard deviation
SDS(-PAGE)	sodium dodecyl sulfate (polyacrylamide gel electrophoresis)
shRNA	small hairpin RNA
siRNA	small interfering RNA
SV40	Simian virus 40
(SV40) ER	Early Region of SV40
(SV40) LT	Large T antigen of SV40
(SV40) st	small t antigen of SV40
TAp63/ TAp73	transactivating (full length) p63/ p73
TRAP	telomeric repeat amplification protocol
U	units
UV	ultraviolet
vs.	versus
wt/ WT	wild type
ΔNp63/ ΔNp73	N-terminally truncated p63/ p73

6.2. Figure index

6.3. Table index

6.4. Additional tables

Tab. A-2 Complete list of 1023 density-regulated genes which differed at least twofold in their mRNA levels in VH6-TE>ns and/or VH6-TE>si cells (proliferating vs. confluent). Gene lists were compiled with the GeneSpring GX software from expression data obtained with an Affymetric GeneChip Human Genome U133A 2.0 microarray. Genes are sorted alphabetically according to their accession numbers.

Gene ID	Accession number	Norm. signal intensity				Gene name
		40%		100%		
		ns	si	ns	si	
TRIM22	AA083478	0,46	1,05	0,95	2,58	tripartite motif-containing 22
KIAA1277	AA127623	0,42	0,58	1,42	1,72	KIAA1277
C10orf56	AA131324	0,56	0,70	1,30	1,31	hypothetical protein FLJ90798
NOL7	AA191426	1,34	1,28	0,55	0,72	nucleolar protein 7, 27kDa
DGCR8	AA203219	1,27	1,41	0,55	0,74	DiGeorge syndrome critical region gene 8
MYL6	AA419227	1,91	1,04	0,91	0,96	myosin, light polypeptide 6, alkali, smooth muscle and non-muscle
SLC7A11	AA488687	2,22	1,49	0,51	0,42	solute carrier family 7, (cationic amino acid transporter, y+ system) member 11
JMJD1A	AA524505	0,45	0,52	1,64	1,48	jumonji domain containing 1
KCTD12	AA551075	0,38	0,85	1,15	2,83	potassium channel tetramerisation domain containing 12
BBX	AA573805	0,64	0,72	1,40	1,28	bobby sox homolog (Drosophila)
MRPS12	AA587905	1,32	1,48	0,63	0,68	mitochondrial ribosomal protein S12
MARS	AA621558	1,67	1,17	0,71	0,83	methionine-tRNA synthetase
GNAS	AA650558	0,59	0,75	1,25	1,62	nt02g10.s1 NCI_CGAP_Lym3 Homo sapiens cDNA clone IMAGE:1192002 3' similar to gb:X56009 GUANINE NUCLEOTIDE-BINDING PROTEIN G(S), ALPHA SUBUNIT (HUMAN);, mRNA sequence.
SCD	AA678241	0,64	0,63	1,36	1,99	stearoyl-CoA desaturase (delta-9-desaturase)
POLYDOM	AA716107	0,47	0,64	1,42	1,36	MRNA full length insert cDNA clone EUROIMAGE 248114
IFRD1	AA747426	2,54	1,13	0,87	0,72	interferon-related developmental regulator 1
IFITM1	AA749101	0,33	0,70	1,30	2,42	interferon induced transmembrane protein 1 (9-27)
PSME3	AA758755	1,70	1,48	0,50	0,52	proteasome (prosome, macropain) activator subunit 3 (PA28 gamma; Ki)
PSME3	AA758755	1,34	1,53	0,46	0,67	proteasome (prosome, macropain) activator subunit 3 (PA28 gamma; Ki)
CD24	AA761181	2,21	1,66	0,34	0,31	nz09g03.s1 NCI_CGAP_GCB1 Homo sapiens cDNA clone IMAGE:1287316 3' similar to gb:M57627 INTERLEUKIN-10 PRECURSOR (HUMAN);, mRNA sequence.
POLR2L	AA772747	1,43	2,08	0,57	0,13	polymerase (RNA) II (DNA directed) polypeptide L, 7.6kDa
MAP2K3	AA780381	1,36	1,71	0,56	0,64	mitogen-activated protein kinase kinase 3
MAP2K3	AA780381	1,42	1,59	0,59	0,53	mitogen-activated protein kinase kinase 3
ING4	AA887083	0,65	0,84	1,42	1,16	inhibitor of growth family, member 4
HSPA9B	AA927701	1,47	1,27	0,70	0,73	heat shock 70kDa protein 9B (mortalin-2)
ZNF292	AA972711	0,63	0,45	1,54	1,37	zinc finger protein 292
KIAA0446	AB007915	1,56	1,23	0,77	0,70	KIAA0446 gene product
IGSF3	AB007935	1,03	0,07	2,15	0,97	immunoglobulin superfamily, member 3
KIAA0582	AB011154	0,76	0,67	1,69	1,24	KIAA0582 protein
ATP9A	AB014511	0,45	0,72	1,33	1,28	ATPase, Class II, type 9A
FGF5	AB016517	1,46	1,79	0,24	0,54	fibroblast growth factor 5
COPEB	AB017493	1,39	1,53	0,61	0,58	core promoter element binding protein
CHST3	AB017915	1,39	1,33	0,67	0,57	carbohydrate (chondroitin 6) sulfotransferase 3
SLC7A5	AB018009	1,48	1,59	0,52	0,49	solute carrier family 7 (cationic amino acid transporter, y+ system), member 5
SIK2	AB018324	0,43	1,06	1,51	0,94	salt-inducible serine/threonine kinase 2
KIAA0795	AB018338	1,28	1,73	0,61	0,72	KIAA0795 protein

AKR1C3	AB018580	0,44	0,64	1,36	1,98	aldo-keto reductase family 1, member C3 (3-alpha hydroxysteroid dehydrogenase, type II)
TXNRD2	AB019695	1,32	2,21	0,64	0,68	thioredoxin reductase 2
C20orf36	AB028973	0,51	0,59	1,66	1,41	Homo sapiens mRNA for KIAA1050 protein, partial cds.
USP24	AB028980	2,62	0,87	1,00	1,00	ubiquitin specific protease 24
EST1B	AB029012	1,55	1,32	0,51	0,68	Est1p-like protein B
KIAA1109	AB029032	0,64	0,54	1,36	1,46	hypothetical protein KIAA1109
SCD	AB032261	0,32	0,33	1,67	1,82	stearoyl-CoA desaturase (delta-9-desaturase)
KIAA1199	AB033025	0,83	0,61	1,93	1,18	KIAA1199 protein
HSPA8	AB034951	1,25	1,61	0,62	0,75	heat shock 70kDa protein 8
SLC7A11	AB040875	1,59	2,03	0,41	0,38	solute carrier family 7, (cationic amino acid transporter, y+ system) member 11
BHLHB3	AB044088	0,64	0,78	1,55	1,22	basic helix-loop-helix domain containing, class B, 3
AMIGO2	AC004010	1,69	1,34	0,66	0,32	Homo sapiens BAC clone GS1-99H8 from 12, complete sequence
NOLA2	AC004079	1,33	1,24	0,65	0,76	
7h3	AC004794	1,30	1,69	0,54	0,70	
FARSLA	AD000092	1,35	1,29	0,65	0,71	
CYR61	AF003114	2,08	1,58	0,42	0,36	cysteine-rich, angiogenic inducer, 61
RTN2	AF004222	0,53	0,56	1,83	1,44	reticulon 2
JARID1A	AF007135	0,70	0,62	1,50	1,30	Jumonji, AT rich interactive domain 1A (RBBP2-like)
GART	AF008655	2,32	1,03	0,72	0,98	phosphoribosylglycinamide formyltransferase, phosphoribosylglycinamide synthetase, phosphoribosylaminoimidazole synthetase
ENC1	AF010314	1,35	1,51	0,54	0,65	ectodermal-neural cortex (with BTB-like domain)
PTGES	AF010316	0,21	0,27	1,76	1,73	prostaglandin E synthase
SH3BP4	AF015043	1,52	1,27	0,73	0,67	SH3-domain binding protein 4
SFRP1	AF017987	0,56	0,66	1,34	1,35	secreted frizzled-related protein 1
SFRP1	AF017987	0,50	0,53	1,47	1,61	secreted frizzled-related protein 1
SFRP1	AF017987	0,36	0,28	1,64	2,10	secreted frizzled-related protein 1
HBP1	AF019214	0,60	0,68	1,51	1,32	HMG-box transcription factor 1
VEGF	AF022375	0,21	0,19	2,18	1,79	vascular endothelial growth factor
SHOX2	AF022654	0,61	0,69	1,31	1,47	short stature homeobox 2
TIMM44	AF026030	1,33	1,56	0,54	0,67	translocase of inner mitochondrial membrane 44 homolog (yeast)
TAPBP	AF029750	0,57	0,72	1,28	1,31	TAP binding protein (tapasin)
PRKCA	AF035594	1,69	1,40	0,54	0,60	protein kinase C, alpha
DIAPH1	AF051782	1,22	1,45	0,61	0,78	diaphanous homolog 1 (Drosophila)
POLR3K	AF060223	1,35	1,62	0,54	0,66	polymerase (RNA) III (DNA directed) polypeptide K, 12.3 kDa
	AF060511	1,29	1,61	0,61	0,71	Homo sapiens clone 016b10 My016 protein mRNA, complete cds.
SMTN	AF064238	1,52	1,59	0,48	0,48	smoothelin
ADSL	AF067854	1,17	1,40	0,54	0,83	adenylosuccinate lyase
DEAF1	AF068892	0,71	0,95	1,45	1,05	deformed epidermal autoregulatory factor 1 (Drosophila)
MGC14376	AF070569	1,34	1,42	0,57	0,66	hypothetical protein MGC14376
RGS20	AF074979	1,75	1,57	0,36	0,43	regulator of G-protein signalling 20
DDX52	AF077033	1,52	1,27	0,73	0,66	DEAD (Asp-Glu-Ala-Asp) box polypeptide 52
TAF9L	AF077053	1,41	1,34	0,66	0,62	TAF9-like RNA polymerase II, TATA box binding protein (TBP)-associated factor, 31kDa
GADD45B	AF078077	1,71	1,97	0,29	0,29	growth arrest and DNA-damage-inducible, beta
EED	AF080227	1,31	1,11	0,65	0,89	embryonic ectoderm development
TTF2	AF080255	2,04	0,96	0,95	1,04	transcription termination factor, RNA polymerase II
AATF	AF083208	1,28	1,28	0,64	0,73	apoptosis antagonizing transcription factor
JARID1B	AF087481	0,68	0,58	1,63	1,32	Jumonji, AT rich interactive domain 1B (RBP2-like)
GADD45B	AF087853	2,22	1,53	0,28	0,47	growth arrest and DNA-damage-inducible, beta
VEGF	AF091352	0,25	0,63	1,37	1,51	vascular endothelial growth factor

PSIP1	AF098482	0,82	0,74	1,71	1,18	PC4 and SFRS1 interacting protein 1
FHL1	AF098518	1,90	1,37	0,63	0,63	four and a half LIM domains 1
HFE	AF115264	0,57	0,78	1,22	1,55	hemochromatosis
PTPN11	AF119855	1,37	1,24	0,68	0,77	predicted protein of HQ1847; Homo sapiens PRO1847 mRNA, complete cds.
GFER	AF124604	1,44	1,86	0,54	0,56	growth factor, augmenter of liver regeneration (ERV1 homolog, S. cerevisiae)
	AF130082	0,62	0,42	1,73	1,38	predicted protein of HQ3121; Homo sapiens clone FLC1492 PRO3121 mRNA, complete cds.
KIAA0830	AF131747	1,76	1,14	0,84	0,87	KIAA0830 protein
P8	AF135266	1,93	1,07	0,93	0,78	p8 protein (candidate of metastasis 1)
DCN	AF138300	0,36	0,37	1,68	1,63	decorin
DCN	AF138302	0,39	0,40	1,78	1,60	decorin
DCN	AF138303	0,37	0,37	1,63	1,63	decorin
MYO9B	AF143684	1,78	1,14	0,86	0,72	myosin IXB
GOLGIN-67	AF164622	0,53	0,91	1,55	1,09	MRNA; cDNA DKFZp686O038 (from clone DKFZp686O038)
FGF5	AF171928	1,45	2,16	0,55	0,56	fibroblast growth factor 5
IFI16	AF208043	0,63	0,59	1,38	1,78	interferon, gamma-inducible protein 16
FHL1	AF220153	1,57	1,47	0,47	0,53	four and a half LIM domains 1
HLA-C	AF226990	0,48	0,79	1,21	1,31	HLA-G histocompatibility antigen, class I, G
GOSR2	AF229796	1,36	1,53	0,64	0,58	golgi SNAP receptor complex member 2
MPZL1	AF239756	1,52	1,46	0,54	0,54	myelin protein zero-like 1
DKFZp564I1922	AF245505	0,66	0,65	1,34	1,45	adlican
HT007	AF246240	1,38	1,11	0,67	0,89	uncharacterized hypothalamus protein HT007
NPD014	AF247168	0,49	0,73	1,41	1,27	hypothetical protein dJ465N24.2.1
MTHFS	AF249277	1,13	1,37	0,56	0,87	hypothetical protein LOC283687
GEMIN4	AF258545	1,24	1,61	0,54	0,76	Homo sapiens chromosome 17 clone PAC P579 HC90, HC71AC, HC6 and HC56 genes, complete sequence.
DLEU2	AF264787	2,18	1,28	0,70	0,72	deleted in lymphocytic leukemia, 2
WDR1	AF274954	1,42	1,33	0,65	0,67	WD repeat domain 1
PNRC1	AF279899	0,35	0,22	2,39	1,65	proline-rich nuclear receptor coactivator 1
ABCA1	AF285167	0,03	0,27	2,73	1,73	ATP-binding cassette, sub-family A (ABC1), member 1
ABCA1	AF285167	0,29	0,35	1,65	2,00	ATP-binding cassette, sub-family A (ABC1), member 1
APG5L	AF293841	1,57	1,27	0,67	0,73	APG5 autophagy 5-like (S. cerevisiae)
GNB5	AF300650	0,51	0,99	1,27	1,01	guanine nucleotide binding protein (G protein), beta 5
FKSG17	AF315951	0,50	0,65	1,90	1,35	FKSG17
MT1H	AF333388	0,77	2,36	0,36	1,24	MT-1H-like protein; mutant as compared to wild-type sequence MT-1H in GenBank Accession Number X64834; Homo sapiens metallothionein 1H-like protein mRNA, complete cds.
GRWD1	AF337808	1,92	1,27	0,47	0,74	glutamate-rich WD repeat containing 1
LOC56902	AF349314	1,72	1,44	0,56	0,53	putatative 28 kDa protein
KCNE4	AI002715	1,28	1,77	0,59	0,72	potassium voltage-gated channel, Isk-related family, member 4
	AI004009	0,40	0,34	2,68	1,60	Transcribed sequence with weak similarity to protein ref:NP_060312.1 (H.sapiens) hypothetical protein FLJ20489 [Homo sapiens]
NCOA2	AI040324	0,72	0,78	1,48	1,22	nuclear receptor coactivator 2
COH1	AI052003	0,49	0,52	1,85	1,48	Cohen syndrome 1
GTPBP4	AI081107	2,54	1,07	0,85	0,93	GTP binding protein 4
KIAA1277	AI131051	0,66	0,62	1,65	1,34	KIAA1277
PDCD4	AI185160	0,57	0,46	1,65	1,43	programmed cell death 4 (neoplastic transformation inhibitor)
TPM4	AI214061	1,32	1,66	0,60	0,68	tropomyosin 4
	AI220627	1,29	1,40	0,61	0,71	tuftelin interacting protein 11
RHOB	AI263909	1,70	1,31	0,69	0,49	ras homolog gene family, member B
LOC400451	AI279819	0,40	0,94	1,45	1,06	Clone IMAGE:4816940, mRNA
STC1	AI300520	0,28	0,31	2,24	1,69	stanniocalcin 1
FZD7	AI333651	1,63	1,22	0,78	0,71	frizzled homolog 7 (Drosophila)
ITGB5	AI335208	0,85	0,87	2,25	1,13	integrin, beta 5

ZRF1	AI338837	1,36	1,20	0,68	0,80	zuotin related factor 1
CDC25A	AI343459	1,93	1,41	0,59	0,49	cell division cycle 25A
TCEB3	AI344128	1,13	1,40	0,53	0,87	transcription elongation factor B (SIII), polypeptide 3 (110kDa, elongin A)
	AI348009	1,25	1,36	0,60	0,75	Clone IMAGE:3605655, mRNA
NOLC1	AI355279	1,49	1,23	0,70	0,77	nucleolar and coiled-body phosphoprotein 1
LYN	AI356412	1,93	1,22	0,67	0,78	v-yes-1 Yamaguchi sarcoma viral related oncogene homolog
TMEM23	AI377497	1,89	1,15	0,85	0,80	mob protein
RRAS2	AI431643	1,74	1,22	0,78	0,68	related RAS viral (r-ras) oncogene homolog 2
AXL	AI467916	1,78	1,15	0,85	0,72	AXL receptor tyrosine kinase
ARHGDIA	AI571798	2,31	1,20	0,55	0,80	Rho GDP dissociation inhibitor (GDI) alpha
SNAI2	AI572079	1,40	1,36	0,64	0,63	snail homolog 2 (Drosophila)
LOC161527	AI632181	0,84	0,85	2,00	1,15	Transcribed sequence with weak similarity to protein ref:NP_061122.1 (H.sapiens) golgin-like protein [Homo sapiens]
	AI638771	1,42	1,23	0,68	0,77	CDNA FLJ26328 fis, clone HRT01493
BCAT1	AI652662	1,56	1,33	0,61	0,67	branched chain aminotransferase 1, cytosolic
TTC3	AI652848	0,65	0,59	1,35	1,36	tetratricopeptide repeat domain 3
SRRM2	AI655799	0,50	0,82	1,19	1,18	serine/arginine repetitive matrix 2
SART3	AI656011	1,26	1,05	0,57	0,95	squamous cell carcinoma antigen recognised by T cells 3
SNX11	AI668643	2,02	1,07	0,50	0,94	sorting nexin 11
DKFZP586H2123	AI671186	0,21	0,40	1,78	1,60	DKFZP586H2123 protein
FLJ40452	AI679213	1,33	1,24	0,50	0,76	hypothetical protein FLJ40452
BTEB1	AI690205	0,31	0,29	1,70	1,69	basic transcription element binding protein 1
FLJ14001	AI694303	0,61	1,03	1,47	0,97	hypothetical protein FLJ14001
LOC113251	AI743740	1,50	1,19	0,49	0,81	c-Mpl binding protein
CDC42EP3	AI754416	1,25	1,40	0,58	0,75	CDC42 effector protein (Rho GTPase binding) 3
HK2	AI761561	0,70	0,81	1,43	1,19	hexokinase 2
PTPRF	AI762627	0,58	1,02	1,18	0,98	protein tyrosine phosphatase, receptor type, F
LOC400451	AI801973	0,58	0,38	1,53	1,42	Clone IMAGE:4816940, mRNA
COL8A2	AI806793	0,86	0,08	1,94	1,14	collagen, type VIII, alpha 2
ZNF278	AI807017	1,60	1,36	0,64	0,56	zinc finger protein 278
	AI810767	0,60	0,32	1,45	1,40	Transcribed sequence with strong similarity to protein ref:NP_003610.1 (H.sapiens) protease, serine, 12
THBS1	AI812030	1,56	1,80	0,44	0,37	thrombospondin 1
MINA	AI823896	1,62	1,34	0,59	0,66	MYC induced nuclear antigen
MINA	AI823896	1,42	1,34	0,60	0,66	MYC induced nuclear antigen
HOMER3	AI871287	1,26	1,30	0,59	0,74	homer homolog 3 (Drosophila)
TPT1	AI888178	0,63	0,73	1,27	1,31	tumor protein, translationally-controlled 1
MBD4	AI913365	0,66	0,74	2,34	1,26	methyl-CpG binding domain protein 4
ERCC2	AI918117	1,38	1,35	0,64	0,65	excision repair cross-complementing rodent repair deficiency, complementation group 2 (xeroderma pigmentosum D)
TCF4	AI927067	0,57	0,76	1,24	1,53	transcription factor 4
DKFZP564D172	AI927701	0,65	0,78	1,35	1,22	hypothetical protein DKFZp564D172
FLJ10618	AI927944	0,75	0,74	1,62	1,25	hypothetical protein FLJ10618
JTV1	AI928526	1,31	1,46	0,49	0,69	heme-regulated initiation factor 2-alpha kinase
PBXIP1	AI935162	0,48	0,65	1,76	1,36	pre-B-cell leukemia transcription factor interacting protein 1
TOX	AI961231	1,60	1,33	0,68	0,51	thymus high mobility group box protein TOX
PSME4	AI972268	1,19	1,43	0,48	0,82	proteasome (prosome, macropain) activator subunit 4
SLC30A1	AI972416	2,75	1,32	0,68	0,65	solute carrier family 30 (zinc transporter), member 1
CLU	AI982754	0,58	0,86	1,54	1,14	clusterin (complement lysis inhibitor, SP-40,40, sulfated glycoprotein 2, testosterone-repressed prostate message 2, apolipoprotein J)
LTBP1	AI986120	0,53	0,48	2,18	1,47	latent transforming growth factor beta binding protein 1
LTBP1	AI986120	0,74	0,72	1,56	1,26	latent transforming growth factor beta binding protein 1
HSPG2	AI991033	0,47	1,00	1,39	1,00	heparan sulfate proteoglycan 2 (perlecan)
DSCR3	AJ001867	1,14	1,53	0,55	0,86	Down syndrome critical region gene 3
DKC1	AJ010395	1,41	1,47	0,55	0,59	Homo sapiens DKC1 gene, exons 1 to 11.

PPM1B	AJ271832	0,73	0,68	1,51	1,27	protein phosphatase 1B (formerly 2C), magnesium-dependent, beta isoform
	AK000168	2,09	1,60	0,40	0,36	Homo sapiens cDNA FLJ20161 fis, clone COL09252, highly similar to L33930 Homo sapiens CD24 signal transducer mRNA.
UPLC1	AK000253	0,59	0,35	1,41	1,53	up-regulated in liver cancer 1
KIAA0690	AK021460	1,52	1,64	0,48	0,28	KIAA0690
KIAA0971	AK021557	1,15	1,26	0,57	0,85	KIAA0971 protein
DAAM1	AK021890	0,84	0,41	1,73	1,16	dishevelled associated activator of morphogenesis 1
DUSP10	AK022513	1,70	1,42	0,50	0,58	dual specificity phosphatase 10
TIMM17A	AK023063	1,35	1,48	0,62	0,65	translocase of inner mitochondrial membrane 17 homolog A (yeast)
SPAG9	AK023512	0,58	0,71	1,29	1,66	sperm associated antigen 9
BM039	AK023669	1,34	1,48	0,62	0,66	uncharacterized bone marrow protein BM039
ADAMTS1	AK023795	2,68	1,48	0,52	0,33	a disintegrin-like and metalloprotease (reprolysin type) with thrombospondin type 1 motif, 1
MOAP1	AK024029	0,64	0,79	1,39	1,21	modulator of apoptosis 1
H6PD	AK024548	0,52	0,68	1,62	1,32	hexose-6-phosphate dehydrogenase (glucose 1-dehydrogenase)
C10orf56	AK024784	0,66	0,58	1,34	1,35	hypothetical protein FLJ90798
BOP1	AK024840	1,36	1,97	0,57	0,64	block of proliferation 1
FLJ13220	AK025248	1,73	1,29	0,65	0,71	hypothetical protein FLJ13220
PRO1855	AK025328	1,30	1,49	0,59	0,70	hypothetical protein PRO1855
C14orf32	AK025580	1,30	1,62	0,52	0,71	chromosome 14 open reading frame 32
APG4A	AL031177	1,38	1,11	0,63	0,90	
EIF3S1	AL031313	1,86	1,19	0,51	0,81	Human DNA sequence from clone RP4-581F12 on chromosome Xq21, complete sequence.
TRMT1	AL031588	1,56	1,29	0,63	0,71	
TNS	AL046979	0,62	0,56	1,38	1,52	tensin
TNS	AL046979	0,61	0,49	1,44	1,39	tensin
DUSP3	AL048503	1,14	1,57	0,56	0,86	DKFZp586M1524_s1 586 (synonym: hute1) Homo sapiens cDNA clone DKFZp586M1524, mRNA sequence.
CHRDL1	AL049176	0,63	0,67	1,33	1,58	Human DNA sequence from clone RP6-141H5 on chromosome Xq22.1-23 Contains the 3' end of the gene for a novel protein with von Willebrand factor type C domains, complete sequence.
FLJ10618	AL049246	0,79	0,49	1,60	1,21	hypothetical protein FLJ10618
	AL049285	0,37	0,91	1,09	1,40	MRNA; cDNA DKFZp564M193 (from clone DKFZp564M193)
DSCR1	AL049369	1,36	1,33	0,67	0,64	Down syndrome critical region gene 1
PBX1	AL049381	0,70	0,48	2,02	1,30	pre-B-cell leukemia transcription factor 1
	AL049435	0,58	0,30	1,53	1,43	MRNA; cDNA DKFZp586B0220 (from clone DKFZp586B0220)
ME1	AL049699	1,85	1,11	0,89	0,77	
OLFML2A	AL050002	0,46	0,24	3,53	1,54	hypothetical protein LOC169611
BRMS1	AL050008	1,34	1,50	0,67	0,62	breast cancer metastasis suppressor 1
DKFZp566C0424	AL050028	1,38	1,51	0,59	0,62	putative MAPK activating protein PM20,PM21
UMPS	AL080099	1,57	1,36	0,52	0,64	uridine monophosphate synthetase (orotate phosphoribosyl transferase and orotidine-5'-decarboxylase)
INSIG2	AL080184	0,58	0,59	1,61	1,41	insulin induced gene 2
UBE2N	AL109622	1,42	1,12	0,48	0,88	Human DNA sequence from clone RP3-526F5 on chromosome Xq26.3-28, complete sequence.
FLJ10737	AL109978	1,33	1,43	0,64	0,67	hypothetical protein FLJ10737
COX4I2	AL117381	1,07	1,38	0,49	0,93	
SAMD4	AL117523	1,27	2,34	0,54	0,73	sterile alpha motif domain containing 4
KPNA3	AL120704	1,39	1,36	0,63	0,64	karyopherin alpha 3 (importin alpha 4)
BNIP3L	AL132665	0,60	0,46	1,47	1,40	BCL2/adenovirus E1B 19kDa interacting protein 3-like
BNIP3L	AL132665	0,59	0,43	1,66	1,41	BCL2/adenovirus E1B 19kDa interacting protein 3-like
SSPN	AL136756	0,55	0,81	1,66	1,19	sarcospan (Kras oncogene-associated gene)
TBC1D3	AL136860	0,46	1,10	1,34	0,90	TBC1 domain family, member 3
DR1	AL137673	1,62	1,25	0,69	0,75	down-regulator of transcription 1, TBP-binding (negative cofactor 2)
ISYNA1	AL137749	0,63	0,60	1,61	1,37	myo-inositol 1-phosphate synthase A1
LLT1	AL353580	2,64	1,06	0,94	0,91	

HIST1H2BD	AL353759	1,69	1,04	0,79	0,96	
ARPC5	AL516350	1,34	1,48	0,65	0,66	actin related protein 2/3 complex, subunit 5, 16kDa
MGC8685	AL533838	0,84	0,21	3,39	1,16	tubulin, beta polypeptide paralog
DNAJA1	AL534104	1,30	1,27	0,60	0,73	DnaJ (Hsp40) homolog, subfamily A, member 1
PLCB4	AL535113	1,73	1,40	0,60	0,47	phospholipase C, beta 4
BTG1	AL535380	0,64	0,69	1,32	1,31	B-cell translocation gene 1, anti-proliferative
GRPEL1	AL542571	1,34	1,76	0,63	0,66	GrpE-like 1, mitochondrial (E. coli)
CCT2	AL545982	1,31	1,44	0,61	0,69	chaperonin containing TCP1, subunit 2 (beta)
GATA2	AL563460	1,47	1,30	0,71	0,62	GATA binding protein 2
LOC90355	AL565741	1,44	1,34	0,58	0,66	hypothetical gene supported by AF038182; BC009203
TIA1	AL567227	0,69	0,53	1,54	1,31	AL567227 Homo sapiens FETAL BRAIN Homo sapiens cDNA clone CS0DF027YA11 3-PRIME, mRNA sequence.
Sep 06	AL568374	0,53	0,55	1,46	1,54	septin 6
C1R	AL573058	0,40	0,56	1,44	2,42	complement component 1, r subcomponent
TFPI2	AL574096	0,49	0,73	1,28	2,12	tissue factor pathway inhibitor 2
SERPINE1	AL574210	1,77	1,92	0,17	0,23	serine (or cysteine) proteinase inhibitor, clade E (nexin, plasminogen activator inhibitor type 1), member 1
G6PC3	AL583123	1,20	1,00	0,55	1,00	glucose-6-phosphatase catalytic subunit 3
COL3A1	AU144167	0,67	0,48	1,34	1,33	collagen, type III, alpha 1 (Ehlers-Danlos syndrome type IV, autosomal dominant)
ZNF451	AU144775	0,61	0,57	1,74	1,39	zinc finger protein 451
CYP1B1	AU144855	0,35	0,53	1,47	1,82	cytochrome P450, family 1, subfamily B, polypeptide 1
FBXL7	AU145127	0,54	0,76	1,33	1,25	F-box and leucine-rich repeat protein 7
LRRC15	AU147799	1,25	1,66	0,54	0,75	leucine rich repeat containing 15
C1QBP	AU151801	1,46	1,38	0,59	0,62	complement component 1, q subcomponent binding protein
SSX2IP	AU152583	1,55	1,15	0,75	0,85	synovial sarcoma, X breakpoint 2 interacting protein
CYP1B1	AU154504	0,31	0,40	1,60	1,68	cytochrome P450, family 1, subfamily B, polypeptide 1
DKFZP586L0724	AU158148	1,47	1,33	0,60	0,67	DKFZP586L0724 protein
CD44	AV700298	1,52	1,18	0,60	0,82	AV700298 GKC Homo sapiens cDNA clone GKCBVGO5 3', mRNA sequence.
LOC54103	AV700415	0,44	1,02	1,08	0,98	Transcribed sequences
SEC13L	AV701173	1,69	1,16	0,84	0,74	sec13-like protein
PRNP	AV725328	1,38	1,60	0,58	0,62	prion protein (p27-30) (Creutzfeld-Jakob disease, Gerstmann-Strausler-Scheinker syndrome, fatal familial insomnia)
ITGA6	AV733308	1,68	1,26	0,74	0,72	integrin, alpha 6
STMN1	AV756729	0,33	1,23	1,14	0,86	stathmin 1/oncoprotein 18
NPAS2	AW000928	0,42	0,68	1,32	1,42	neuronal PAS domain protein 2
KPNA1	AW051311	1,32	1,24	0,65	0,76	karyopherin alpha 1 (importin alpha 5)
C6orf111	AW081113	0,66	0,60	1,48	1,34	chromosome 6 open reading frame 111
PFAAP5	AW084068	0,60	0,45	1,86	1,40	xc26c06.x1 NCI_CGAP_Co18 Homo sapiens cDNA clone IMAGE:2585386 3' similar to contains element OFR repetitive element ;, mRNA sequence.
MGC87042	AW129021	1,30	1,66	0,56	0,70	similar to Six transmembrane epithelial antigen of prostate
CCNG2	AW134535	0,28	0,21	1,97	1,72	cyclin G2
MARCKS	AW163148	0,55	0,80	1,20	1,44	myristoylated alanine-rich protein kinase C substrate
TNFAIP6	AW188198	0,48	0,51	1,49	1,85	tumor necrosis factor, alpha-induced protein 6
PDLIM7	AW206786	1,43	1,31	0,69	0,68	PDZ and LIM domain 7 (enigma)
SCA1	AW235612	0,83	0,75	1,81	1,17	spinocerebellar ataxia 1 (olivopontocerebellar ataxia 1, autosomal dominant, ataxin 1)
JMJD2B	AW237172	0,55	0,70	1,62	1,30	jumonji domain containing 2B
JMJD2B	AW237172	0,36	0,45	1,58	1,55	jumonji domain containing 2B
GCSH	AW237404	1,33	1,18	0,65	0,82	glycine cleavage system protein H (aminomethyl carrier)
YARS	AW245400	1,35	1,38	0,65	0,64	tyrosyl-tRNA synthetase
EIF4E	AW268640	1,45	1,21	0,58	0,79	eukaryotic translation initiation factor 4E
FAM38B	AW269818	0,92	0,39	2,42	1,08	hypothetical protein FLJ23403
TMPO	AW272611	1,99	0,99	0,96	1,01	thymopoietin
KIAA0974	AW300504	0,65	0,91	1,83	1,09	KIAA0974 mRNA
PLEKHC1	AW469573	1,48	1,26	0,74	0,55	pleckstrin homology domain containing, family C (with FERM

						domain) member 1
DR1	AW516932	1,50	1,35	0,64	0,65	down-regulator of transcription 1, TBP-binding (negative cofactor 2)
MGC13024	AW517464	0,47	0,68	1,33	1,32	hypothetical protein MGC13024
MGC48332	AW593996	1,32	1,40	0,59	0,68	hypothetical protein MGC48332
ALDH6A1	AW612403	0,53	0,42	1,87	1,47	chromosome 14 open reading frame 45
ALDH6A1	AW612403	0,46	0,53	1,50	1,47	chromosome 14 open reading frame 45
TRA2A	AW978896	0,57	0,82	1,18	1,30	transformer-2 alpha
USF2	AY007087	1,29	1,29	0,58	0,71	upstream transcription factor 2, c-fos interacting
SMURF2	AY014180	1,42	1,47	0,52	0,58	E3 ubiquitin ligase SMURF2
CCND1	BC000076	1,64	1,28	0,72	0,61	cyclin D1 (PRAD1: parathyroid adenomatosis 1)
GDF15	BC000529	0,82	0,31	1,66	1,18	growth differentiation factor 15
PPAN	BC000535	1,23	2,15	0,48	0,77	peter pan homolog (Drosophila)
MGC70863	BC000596	1,80	1,05	0,90	0,95	ribosomal protein L23a pseudogene 7
SMOX	BC000669	0,33	0,50	1,71	1,50	spermine oxidase
C6orf80	BC000758	0,60	0,69	1,31	1,47	chromosome 6 open reading frame 80
C19orf24	BC000890	1,30	1,55	0,57	0,70	hypothetical protein FLJ20640
NQO1	BC000906	1,33	1,46	0,65	0,67	NAD(P)H dehydrogenase, quinone 1
CA12	BC001012	0,52	0,77	1,45	1,23	carbonic anhydrase XII
LGALS3	BC001120	0,52	0,62	1,38	1,44	lectin, galactoside-binding, soluble, 3 (galectin 3)
UTP14A	BC001149	1,30	1,24	0,65	0,76	serologically defined colon cancer antigen 16
TFRC	BC001188	1,50	1,29	0,71	0,63	transferrin receptor (p90, CD71)
HMGN4	BC001282	0,60	0,98	1,25	1,02	high mobility group nucleosomal binding domain 4
IFRD2	BC001327	1,38	1,64	0,62	0,57	interferon-related developmental regulator 2
PSME3	BC001423	1,31	1,72	0,47	0,69	proteasome (prosome, macropain) activator subunit 3 (PA28 gamma; Ki)
PSME3	BC001423	1,28	1,44	0,64	0,72	proteasome (prosome, macropain) activator subunit 3 (PA28 gamma; Ki)
SKP2	BC001441	1,61	1,25	0,68	0,75	S-phase kinase-associated protein 2 (p45)
PRPS1	BC001605	1,34	1,60	0,59	0,66	phosphoribosyl pyrophosphate synthetase 1
MRPS12	BC001617	1,48	2,02	0,44	0,53	mitochondrial ribosomal protein S12
CDCA8	BC001651	1,35	1,53	0,62	0,65	cell division cycle associated 8
ABCF2	BC001661	1,28	1,72	0,57	0,72	ATP-binding cassette, sub-family F (GCN20), member 2
GAS2L1	BC001782	1,24	1,48	0,47	0,76	growth arrest-specific 2 like 1
RRS1	BC001811	1,51	1,49	0,51	0,49	RRS1 ribosome biogenesis regulator homolog (S. cerevisiae)
ZYX	BC002323	1,65	1,57	0,43	0,39	zyxin
CORO1C	BC002342	1,41	1,79	0,59	0,60	coronin, actin binding protein, 1C
PEA15	BC002426	1,37	1,43	0,63	0,60	phosphoprotein enriched in astrocytes 15
FLJ20244	BC002492	1,49	1,38	0,53	0,62	hypothetical protein FLJ20244
GATA2	BC002557	1,29	1,57	0,58	0,71	GATA binding protein 2
EIF3S1	BC002719	1,56	1,28	0,71	0,72	eukaryotic translation initiation factor 3, subunit 1 alpha, 35kDa
BTN3A2	BC002832	0,61	0,58	1,41	1,40	butyrophilin, subfamily 3, member A2
HSA9761	BC002841	1,33	1,25	0,66	0,76	putative dimethyladenosine transferase
UMPK	BC002906	1,34	1,54	0,66	0,62	uridine monophosphate kinase
DUSP6	BC003143	0,46	0,92	1,08	1,49	dual specificity phosphatase 6
DUSP6	BC003143	0,67	0,71	1,43	1,29	dual specificity phosphatase 6
DUSP6	BC003143	0,61	0,67	1,33	1,64	dual specificity phosphatase 6
LAMA5	BC003355	0,59	0,14	2,01	1,41	synonym: KIAA1907; Homo sapiens laminin, alpha 5, mRNA (cDNA clone IMAGE:2900097), complete cds.
C2orf6	BC003398	1,34	1,27	0,67	0,73	chromosome 2 open reading frame 6
POLR2F	BC003582	1,32	1,39	0,51	0,69	polymerase (RNA) II (DNA directed) polypeptide F
DDIT3	BC003637	1,31	1,51	0,64	0,69	methionine-tRNA synthetase
SARA1	BC003658	1,42	1,30	0,70	0,69	SAR1a gene homolog 1 (S. cerevisiae)
C16orf35	BC004185	1,26	1,28	0,62	0,74	chromosome 16 open reading frame 35
MGC3248	BC004191	1,37	1,40	0,63	0,59	dynactin 4
RANBP3	BC004349	1,11	1,38	0,43	0,89	RAN binding protein 3

POLR2E	BC004441	1,19	1,20	0,58	0,81	polymerase (RNA) II (DNA directed) polypeptide E, 25kDa
HLA-C	BC004489	0,50	0,91	1,09	1,19	major histocompatibility complex, class I, C
PPIF	BC005020	1,26	2,04	0,54	0,74	peptidylprolyl isomerase F (cyclophilin F)
CYCS	BC005299	1,67	1,28	0,65	0,72	cytochrome c, somatic
DCN	BC005322	0,38	0,39	1,65	1,61	decorin
GMFB	BC005359	1,48	1,28	0,72	0,60	glia maturation factor, beta
SCD	BC005807	0,63	0,50	1,37	1,93	stearoyl-CoA desaturase (delta-9-desaturase)
ARHGDIA	BC005851	1,31	1,81	0,64	0,69	Rho GDP dissociation inhibitor (GDI) alpha
PTN	BC005916	0,63	0,59	1,56	1,37	pleiotrophin (heparin binding growth factor 8, neurite growth-promoting factor 1)
FLJ10439	BC006351	1,61	1,38	0,62	0,53	hypothetical protein FLJ10439
CPZ	BC006393	0,50	0,04	2,03	1,50	carboxypeptidase Z
HSPD1	BE256479	1,53	1,14	0,75	0,86	Transcribed sequence with strong similarity to protein pir:A32800 (H.sapiens) A32800 chaperonin GroEL precursor - human
INSIG1	BE300521	0,58	0,50	1,42	1,67	insulin induced gene 1
INSIG1	BE300521	0,44	0,56	1,75	1,44	insulin induced gene 1
HSPC111	BE314601	1,53	1,79	0,47	0,45	hypothetical protein HSPC111
ARTS-1	BE551138	0,49	0,24	1,62	1,51	type 1 tumor necrosis factor receptor shedding aminopeptidase regulator
PVR	BE615277	1,93	1,31	0,69	0,57	poliovirus receptor
PIK3R3	BE622627	1,22	0,95	0,57	1,05	601440792T1 NIH_MGC_72 Homo sapiens cDNA clone IMAGE:3915695 3', mRNA sequence.
MAPRE2	BE671156	0,47	0,72	1,28	1,53	microtubule-associated protein, RP/EB family, member 2
COPEB	BE675435	1,37	1,49	0,63	0,58	core promoter element binding protein
IMP4	BE747342	1,38	1,55	0,61	0,62	U3 snoRNP protein 4 homolog
DKFZp547K1113	BE858194	0,54	0,46	2,67	1,46	hypothetical protein DKFZp547K1113
MET	BE870509	1,49	1,97	0,31	0,51	met proto-oncogene (hepatocyte growth factor receptor)
LOC221810	BE881590	0,33	0,48	1,53	1,97	ets variant gene 1
STIP1	BE886580	1,49	1,17	0,69	0,83	stress-induced-phosphoprotein 1 (Hsp70/Hsp90-organizing protein)
ARPC4	BE891920	1,47	1,66	0,37	0,53	actin related protein 2/3 complex, subunit 4, 20kDa
GALNT10	BE906572	1,43	1,35	0,58	0,65	UDP-N-acetyl-alpha-D-galactosamine:polypeptide N-acetylgalactosaminyltransferase 10 (GalNAc-T10)
MCAM	BE964361	1,67	1,07	0,80	0,93	melanoma cell adhesion molecule
UBE2L3	BE964689	1,25	1,35	0,60	0,75	ubiquitin-conjugating enzyme E2L 3
MICAL2	BE965029	1,73	1,25	0,76	0,74	601658812R1 NIH_MGC_69 Homo sapiens cDNA clone IMAGE:3886131 3', mRNA sequence.
SAT	BE971383	0,45	0,93	1,07	1,14	spermidine/spermine N1-acetyltransferase
PAM	BF038548	0,81	0,64	1,85	1,19	peptidylglycine alpha-amidating monooxygenase
D15Wsu75e	BF057059	1,34	1,65	0,66	0,59	DNA segment, Chr 15, Wayne State University 75, expressed
SCAMP1	BF058944	0,68	0,65	1,48	1,32	secretory carrier membrane protein 1
ETV5	BF060791	0,54	0,78	1,23	1,60	ets variant gene 5 (ets-related molecule)
RIS1	BF062629	0,58	0,60	1,78	1,40	Ras-induced senescence 1
RBL2	BF110947	0,43	0,81	1,47	1,19	retinoblastoma-like 2 (p130)
WSB1	BF111821	0,42	0,28	2,18	1,58	WD repeat and SOCS box-containing 1
PCDH16	BF222893	0,55	0,46	1,57	1,45	protocadherin 16 dachsous-like (Drosophila)
LRP1	BF304759	0,40	0,61	2,68	1,40	low density lipoprotein-related protein 1 (alpha-2-macroglobulin receptor)
IGFBP3	BF340228	1,41	1,57	0,60	0,52	insulin-like growth factor binding protein 3
PBXIP1	BF344265	0,52	0,69	1,39	1,31	pre-B-cell leukemia transcription factor interacting protein 1
TCF4	BF433429	0,50	0,77	1,35	1,23	transcription factor 4
CREBL2	BF438056	0,41	1,29	0,97	1,03	cAMP responsive element binding protein-like 2
PNN	BF508848	1,52	1,25	0,75	0,75	UI-H-BI4-aor-e-06-0-UI.s1 NCI_CGAP_Sub8 Homo sapiens cDNA clone IMAGE:3085907 3', mRNA sequence.
TFPI	BF511231	0,56	0,30	1,45	1,44	tissue factor pathway inhibitor (lipoprotein-associated coagulation inhibitor)
GPR124	BF511315	0,65	0,78	1,53	1,22	G protein-coupled receptor 124
KLF4	BF514079	0,51	0,54	1,46	1,57	Kruppel-like factor 4 (gut)
PTP4A1	BF576710	1,88	1,11	0,89	0,84	602135085F1 NIH_MGC_81 Homo sapiens cDNA clone IMAGE:4290141 5', mRNA sequence.

TCF4	BF592782	0,56	0,73	1,28	1,41	transcription factor 4
TNFRSF5	BF664114	0,54	1,07	1,32	0,93	tumor necrosis factor receptor superfamily, member 5
LIM	BF671400	1,80	1,28	0,73	0,65	LIM protein (similar to rat protein kinase C-binding enigma)
FLJ13910	BF671894	0,77	0,82	1,55	1,18	hypothetical protein FLJ13910
ABCA5	BF693921	0,65	0,59	1,35	1,36	ATP-binding cassette, sub-family A (ABC1), member 5
C6orf68	BF695847	1,63	1,24	0,68	0,76	Similar to hypothetical protein, MGC:7199 (LOC389850), mRNA
NID	BF940043	0,74	0,74	1,71	1,26	nidogen (enactin)
KIAA0153	BF965437	1,27	1,27	0,62	0,73	KIAA0153 protein
PBX1	BF967998	0,79	0,79	1,82	1,21	602269506F1 NIH_MGC_84 Homo sapiens cDNA clone IMAGE:4357777 5', mRNA sequence.
SMAD3	BF971416	0,44	0,98	1,05	1,02	DKFZP586N0721 protein
MEP50	BF975273	1,53	1,51	0,44	0,49	MEP50 protein
MGC52022	BG031677	1,37	1,49	0,61	0,63	musculoskeletal, embryonic nuclear protein 1
C9orf3	BG036668	1,72	1,45	0,43	0,55	chromosome 9 open reading frame 3
LIM	BG054550	1,56	1,23	0,77	0,77	LIM protein (similar to rat protein kinase C-binding enigma)
DKFZp566C0424	BG171020	1,25	1,64	0,56	0,75	602324033F1 NIH_MGC_89 Homo sapiens cDNA clone IMAGE:4427025 5', mRNA sequence.
ANXA11	BG177920	0,53	0,59	1,61	1,42	EST from clone 898903, full insert
	BG251521	0,67	0,60	1,80	1,34	MRNA; cDNA DKFZp586B211 (from clone DKFZp586B211)
	BG251521	0,61	0,54	1,39	1,90	MRNA; cDNA DKFZp586B211 (from clone DKFZp586B211)
H41	BG257762	1,30	1,88	0,63	0,70	hypothetical protein H41
INSIG1	BG292233	0,48	0,43	1,52	1,73	insulin induced gene 1
CD24	BG327863	2,39	1,36	0,64	0,39	CD24 antigen (small cell lung carcinoma cluster 4 antigen)
CD24	BG327863	2,33	1,59	0,41	0,40	CD24 antigen (small cell lung carcinoma cluster 4 antigen)
DKFZp762C186	BG334196	0,38	0,99	1,02	1,37	tangerin
RB1CC1	BG402105	0,64	0,62	1,54	1,36	RB1-inducible coiled-coil 1
KPNA6	BG403834	1,38	1,13	0,64	0,87	karyopherin alpha 6 (importin alpha 7)
SBLF	BG434174	0,42	0,16	2,22	1,58	stoned B-like factor
BOP1	BG491842	1,50	1,68	0,48	0,50	Transcribed sequence with moderate similarity to protein sp:Q14137 (H.sapiens) Y124_HUMAN Hypothetical protein KIAA0124
G3BP	BG500067	1,44	1,28	0,72	0,72	602545874F1 NIH_MGC_60 Homo sapiens cDNA clone IMAGE:4668234 5', mRNA sequence.
RNASEH1	BG534527	1,33	1,47	0,56	0,67	ribonuclease H1
IRAK1BP1	BG545769	0,65	0,61	1,62	1,35	interleukin-1 receptor-associated kinase 1 binding protein 1
ID1	D13889	1,85	1,87	0,16	0,15	inhibitor of DNA binding 1, dominant negative helix-loop-helix protein
KIAA0007	D26488	1,28	1,26	0,55	0,74	KIAA0007 protein
RBMS2	D28483	1,31	1,33	0,62	0,69	RNA binding motif, single stranded interacting protein 2
POP1	D31765	1,47	1,53	0,53	0,48	processing of precursors 1
Sep 06	D50918	0,57	0,65	1,35	1,55	septin 6
ANKRD15	D79994	1,45	1,52	0,56	0,50	ankyrin repeat domain 15
HLA-B	D83043	0,45	0,92	1,08	1,41	major histocompatibility complex, class I, B
HSPH1	D86956	1,43	1,36	0,44	0,64	heat shock 105kDa/110kDa protein 1
KIAA0280	D87470	0,62	0,69	1,31	1,34	KIAA0280 protein
CALD1	D90453	1,29	0,96	0,41	1,04	caldesmon 1
ELOVL1	H93026	1,45	1,23	0,73	0,77	elongation of very long chain fatty acids (FEN1/Elo2, SUR4/Elo3, yeast)-like 1
C5orf4	H93077	0,20	0,37	2,12	1,63	chromosome 5 open reading frame 4
VEGF	H95344	0,23	0,33	1,82	1,67	vascular endothelial growth factor
COL11A1	J04177	0,60	0,45	1,51	1,41	collagen, type XI, alpha 1
EDN1	J05008	3,37	1,38	0,62	0,11	Homo sapiens endothelin-1 (EDN1) gene, complete cds.
C1QBP	L04636	1,53	1,35	0,60	0,65	complement component 1, q subcomponent binding protein
PRDX2	L19185	1,89	0,82	0,72	1,19	Human natural killer cell enhancing factor (NKEFB) mRNA, complete cds.
CD24	L33930	3,04	1,40	0,60	0,50	CD24 antigen (small cell lung carcinoma cluster 4 antigen)
MECP2	L37298	1,33	1,26	0,58	0,74	methyl CpG binding protein 2 (Rett syndrome)
FZD2	L37882	1,37	1,23	0,67	0,77	frizzled homolog 2 (Drosophila)

THBS3	L38969	0,63	0,79	1,29	1,22	thrombospondin 3
TRADD	L41690	0,29	1,08	0,92	1,14	TNFRSF1A-associated via death domain
CCNG2	L49506	0,29	0,56	1,54	1,44	cyclin G2
IL1A	M15329	0,30	0,38	2,18	1,62	interleukin 1, alpha
IL1B	M15330	0,46	0,55	1,45	1,76	interleukin 1, beta
C1S	M18767	0,40	0,64	1,36	1,71	complement component 1, s subcomponent
TGFB2	M19154	2,71	0,91	1,09	0,48	
TPM1	M19267	1,34	1,98	0,66	0,58	tropomyosin; Human tropomyosin mRNA, complete cds.
AMD1	M21154	1,66	1,31	0,57	0,70	adenosylmethionine decarboxylase 1
PIM1	M24779	0,78	0,85	1,65	1,15	pim-1 oncogene
VEGF	M27281	0,40	0,03	1,60	1,61	vascular endothelial growth factor
FGF2	M27968	1,48	1,73	0,41	0,52	fibroblast growth factor 2 (basic)
PSG9	M31125	1,20	1,66	0,51	0,80	pregnancy specific beta-1-glycoprotein 6
IGFBP3	M31159	1,73	1,46	0,52	0,54	insulin-like growth factor binding protein 3
AKR1C1	M33376	1,63	1,36	0,48	0,64	aldo-keto reductase family 1, member C2 (dihydrodiol dehydrogenase 2; bile acid binding protein; 3-alpha hydroxysteroid dehydrogenase, type III)
EPOR	M34986	0,69	0,68	1,54	1,31	erythropoietin receptor
GPR125	M37712	0,94	0,79	1,87	1,07	Homo sapiens p58/GTA protein kinase mRNA, complete cds.
PTN	M57399	0,62	0,63	1,78	1,37	pleiotrophin (heparin binding growth factor 8, neurite growth-promoting factor 1)
DTR	M60278	1,53	1,98	0,47	0,41	diphtheria toxin receptor (heparin-binding epidermal growth factor-like growth factor)
EPOR	M60459	0,55	0,63	1,37	1,38	erythropoietin receptor
HLX1	M60721	1,24	1,58	0,51	0,76	H2.0-like homeo box 1 (Drosophila)
RELA	M62399	1,16	1,56	0,44	0,84	v-rel reticuloendotheliosis viral oncogene homolog A, nuclear factor of kappa light polypeptide gene enhancer in B-cells 3, p65 (avian)
PLA2G4A	M68874	0,64	0,54	1,38	1,36	phospholipase A2, group IVA (cytosolic, calcium-dependent)
SFRS1	M72709	1,35	1,62	0,60	0,65	
CCND1	M73554	2,62	1,34	0,66	0,45	cyclin D1 (PRAD1: parathyroid adenomatosis 1)
LYN	M79321	1,32	1,40	0,60	0,68	v-yes-1 Yamaguchi sarcoma viral related oncogene homolog
CEBPD	M83667	0,33	0,39	1,61	1,89	Human NF-IL6-beta protein mRNA, complete cds.
HLA-G	M90686	0,35	0,85	1,16	1,76	HLA-G histocompatibility antigen, class I, G
CTGF	M92934	1,71	1,80	0,29	0,20	connective tissue growth factor
ACTN1	M95178	1,34	1,43	0,66	0,66	actinin, alpha 1
WSB1	N24643	0,54	0,64	1,57	1,36	WD repeat and SOCS box-containing 1
DAZAP2	N34846	1,51	0,96	0,72	1,04	DAZ associated protein 2
DUSP10	N36770	1,41	1,60	0,59	0,55	dual specificity phosphatase 10
	N53479	0,64	0,46	1,36	1,37	MRNA; cDNA DKFZp686F09142 (from clone DKFZp686F09142)
ASS	NM_000050	0,46	0,56	1,44	1,80	argininosuccinate synthetase
SERPING1	NM_000062	0,35	0,64	2,09	1,36	serine (or cysteine) proteinase inhibitor, clade G (C1 inhibitor), member 1, (angioedema, hereditary)
C3	NM_000064	0,32	0,46	1,55	1,54	complement component 3
COL3A1	NM_000090	0,61	0,52	1,52	1,39	collagen, type III, alpha 1 (Ehlers-Danlos syndrome type IV, autosomal dominant)
CYP1B1	NM_000104	0,40	0,37	1,60	1,68	cytochrome P450, family 1, subfamily B, polypeptide 1
DDB2	NM_000107	0,53	0,75	1,25	1,77	damage-specific DNA binding protein 2, 48kDa
FRDA	NM_000144	1,45	1,22	0,61	0,78	Friedreich ataxia
FUCA1	NM_000147	0,72	0,39	2,11	1,28	fucosidase, alpha-L- 1, tissue
GAA	NM_000152	1,05	0,69	2,14	0,95	glucosidase, alpha; acid (Pompe disease, glycogen storage disease type II)
GK	NM_000167	0,65	0,66	1,34	1,74	glycerol kinase
MET	NM_000245	2,49	1,05	0,95	0,51	synonyms: HGFR, RCCP2; Oncogene MET;Homo sapiens met proto-oncogene (hepatocyte growth factor receptor) (MET), mRNA.
TPM1	NM_000366	1,32	1,67	0,64	0,69	tropomyosin 1 (alpha)
TPM1	NM_000366	1,52	1,92	0,49	0,45	tropomyosin 1 (alpha)
UMPS	NM_000373	1,39	1,41	0,59	0,61	uridine monophosphate synthetase (orotate phosphoribosyl

						transferase and orotidine-5'-decarboxylase)
CDKN1A	NM_000389	0,50	0,49	1,50	1,83	cyclin-dependent kinase inhibitor 1A (p21, Cip1)
GSTM1	NM_000561	0,47	1,04	1,32	0,96	glutathione S-transferase M1
IL1B	NM_000576	0,45	0,46	1,54	1,82	interleukin 1, beta
SERPINE1	NM_000602	1,77	1,94	0,22	0,23	serine (or cysteine) proteinase inhibitor, clade E (nexin, plasminogen activator inhibitor type 1), member 1
BDKRB2	NM_000623	0,38	0,44	1,56	1,91	bradykinin receptor B2
CSF3	NM_000759	0,50	0,50	1,69	1,50	colony stimulating factor 3 (granulocyte)
CYP27A1	NM_000784	0,64	0,40	1,44	1,36	cytochrome P450, family 27, subfamily A, polypeptide 1
CYP27B1	NM_000785	0,59	0,71	1,29	1,53	cytochrome P450, family 27, subfamily B, polypeptide 1
GSTM4	NM_000848	0,44	1,33	1,18	0,82	glutathione S-transferase M2 (muscle)
NQO1	NM_000903	1,57	1,36	0,64	0,55	NAD(P)H dehydrogenase, quinone 1
OXTR	NM_000916	2,41	1,68	0,32	0,22	oxytocin receptor
P4HA1	NM_000917	0,65	0,66	1,66	1,34	procollagen-proline, 2-oxoglutarate 4-dioxygenase (proline 4-hydroxylase), alpha polypeptide I
PLAT	NM_000930	0,71	0,53	1,50	1,29	plasminogen activator, tissue
PPP3R1	NM_000945	1,99	1,38	0,59	0,62	protein phosphatase 3 (formerly 2B), regulatory subunit B, 19kDa, alpha isoform (calcineurin B, type I)
PTGS2	NM_000963	0,85	0,44	1,75	1,15	prostaglandin-endoperoxide synthase 2 (prostaglandin G/H synthase and cyclooxygenase)
SLC12A2	NM_001046	1,56	1,34	0,59	0,66	solute carrier family 12 (sodium/potassium/chloride transporters), member 2
ACPP	NM_001099	0,08	0,23	1,77	2,27	acid phosphatase, prostate
ADAM8	NM_001109	0,48	0,54	2,10	1,46	a disintegrin and metalloproteinase domain 8
ANG	NM_001145	0,40	0,64	1,89	1,36	ribonuclease, RNase A family, 4
ANGPT1	NM_001146	1,72	1,33	0,67	0,59	angiopoietin 1
AOX1	NM_001159	1,21	1,76	0,56	0,79	aldehyde oxidase 1
BIRC2	NM_001166	1,48	1,38	0,58	0,62	baculoviral IAP repeat-containing 2
ARG2	NM_001172	0,59	0,43	1,60	1,41	arginase, type II
ARHGAP6	NM_001174	0,65	0,34	1,35	1,37	Rho GTPase activating protein 6
BACH1	NM_001186	0,75	0,76	1,66	1,24	BTB and CNC homology 1, basic leucine zipper transcription factor 1
CCNA2	NM_001237	1,50	1,21	0,72	0,79	cyclin A2
CDC20	NM_001255	1,27	1,25	0,59	0,75	CDC20 cell division cycle 20 homolog (S. cerevisiae)
CDH13	NM_001257	0,90	0,53	2,62	1,11	cadherin 13, H-cadherin (heart)
AKR1C1	NM_001353	1,28	1,51	0,53	0,72	aldo-keto reductase family 1, member C1 (dihydrodiol dehydrogenase 1; 20-alpha (3-alpha)-hydroxysteroid dehydrogenase)
DKC1	NM_001363	1,40	1,70	0,54	0,60	dyskeratosis congenita 1, dyskerin
FHL2	NM_001450	1,50	1,26	0,74	0,67	four and a half LIM domains 2
ICT1	NM_001545	1,31	1,35	0,57	0,69	immature colon carcinoma transcript 1
CYR61	NM_001554	1,37	1,52	0,63	0,52	cysteine-rich, angiogenic inducer, 61
TNFRSF9	NM_001561	1,20	0,81	2,58	0,76	tumor necrosis factor receptor superfamily, member 9
AREG	NM_001657	0,06	0,38	2,31	1,62	amphiregulin (schwannoma-derived growth factor)
ASNS	NM_001673	2,07	1,27	0,73	0,68	asparagine synthetase
AUH	NM_001698	0,54	0,64	1,36	1,41	AU RNA binding protein/enoyl-Coenzyme A hydratase
BAI2	NM_001703	0,43	0,55	1,45	1,63	brain-specific angiogenesis inhibitor 2
BDNF	NM_001709	1,92	1,35	0,62	0,65	brain-derived neurotrophic factor
BTG1	NM_001731	0,64	0,73	1,41	1,27	B-cell translocation gene 1, anti-proliferative
CDH2	NM_001792	1,35	1,37	0,65	0,46	cadherin 2, type 1, N-cadherin (neuronal)
CEBPG	NM_001806	1,37	1,29	0,56	0,71	CCAAT/enhancer binding protein (C/EBP), gamma
CLTB	NM_001834	1,29	1,53	0,50	0,71	clathrin, light polypeptide (Lcb)
CRABP2	NM_001878	0,37	0,56	1,44	1,86	cellular retinoic acid binding protein 2
CTPS	NM_001905	1,69	1,48	0,43	0,52	CTP synthase
GADD45A	NM_001924	1,69	1,54	0,42	0,46	growth arrest and DNA-damage-inducible, alpha
DPP4	NM_001935	0,59	0,65	1,35	1,80	dipeptidylpeptidase 4 (CD26, adenosine deaminase complexing protein 2)
DPP4	NM_001935	0,61	0,52	1,39	2,13	dipeptidylpeptidase 4 (CD26, adenosine deaminase complexing protein 2)

DR1	NM_001938	1,33	1,37	0,62	0,67	down-regulator of transcription 1, TBP-binding (negative cofactor 2)
DTR	NM_001945	2,35	1,48	0,52	0,35	diphtheria toxin receptor (heparin-binding epidermal growth factor-like growth factor)
EGR1	NM_001964	0,42	0,41	1,60	1,58	early growth response 1
EGR1	NM_001964	0,38	0,32	1,77	1,62	early growth response 1
EIF5	NM_001969	1,38	1,28	0,67	0,72	eukaryotic translation initiation factor 5
ENO2	NM_001975	0,53	0,47	2,24	1,47	enolase 2 (gamma, neuronal)
F3	NM_001993	1,68	1,52	0,48	0,42	coagulation factor III (thromboplastin, tissue factor)
FBLN1	NM_001996	0,62	0,59	1,57	1,38	fibulin 1
FGF2	NM_002006	1,48	1,26	0,53	0,74	fibroblast growth factor 2 (basic)
FKBP4	NM_002014	1,85	1,13	0,80	0,87	FK506 binding protein 4, 59kDa
FKBP4	NM_002014	1,47	1,35	0,65	0,57	FK506 binding protein 4, 59kDa
GABPB2	NM_002041	1,46	1,35	0,66	0,60	GA binding protein transcription factor, beta subunit 2, 47kDa
GAS1	NM_002048	0,64	0,39	1,44	1,36	growth arrest-specific 1
GCLM	NM_002061	1,63	1,42	0,58	0,55	glutamate-cysteine ligase, modifier subunit
GLRX	NM_002064	0,57	0,72	1,37	1,28	glutaredoxin (thioltransferase)
GPC1	NM_002081	1,30	1,48	0,59	0,70	glypican 1
GRK6	NM_002082	1,29	1,30	0,63	0,71	G protein-coupled receptor kinase 6
GYPC	NM_002101	0,53	0,54	1,46	1,47	glycophorin C (Gerbich blood group)
HMOX1	NM_002133	1,67	2,25	0,24	0,33	heme oxygenase (decycling) 1
ID2	NM_002166	1,76	1,63	0,37	0,29	inhibitor of DNA binding 2, dominant negative helix-loop-helix protein
ID2	NM_002166	2,02	1,64	0,36	0,33	inhibitor of DNA binding 2, dominant negative helix-loop-helix protein
ID3	NM_002167	1,78	1,82	0,18	0,22	inhibitor of DNA binding 3, dominant negative helix-loop-helix protein
IGFBP6	NM_002178	0,43	0,42	1,57	1,61	insulin-like growth factor binding protein 6
IL1RAP	NM_002182	0,93	0,47	1,99	1,07	interleukin 1 receptor accessory protein
IL7R	NM_002185	1,55	1,55	0,45	0,42	interleukin 7 receptor
KAI1	NM_002231	0,59	0,68	1,40	1,32	kangai 1 (suppression of tumorigenicity 6, prostate; CD82 antigen (R2 leukocyte antigen, antigen detected by monoclonal and antibody IA4))
KCNK1	NM_002245	1,27	0,26	3,11	0,73	potassium channel, subfamily K, member 1
KRTHB1	NM_002281	5,77	0,68	1,32	0,14	keratin, hair, basic, 1
LAMA4	NM_002290	0,21	0,58	1,42	2,41	laminin, alpha 4
LAMB1	NM_002291	0,64	0,55	1,71	1,36	laminin, beta 1
LIG4	NM_002312	1,40	2,64	0,61	0,41	ligase IV, DNA, ATP-dependent
LUM	NM_002345	0,79	0,21	2,04	1,21	lumican
MAP4	NM_002375	1,40	1,13	0,65	0,87	microtubule-associated protein 4
SLC3A2	NM_002394	1,45	1,95	0,48	0,55	solute carrier family 3 (activators of dibasic and neutral amino acid transport), member 2
MMP3	NM_002422	1,43	1,99	0,40	0,57	matrix metalloproteinase 3 (stromelysin 1, progelatinase)
NGFB	NM_002506	1,33	1,86	0,54	0,67	nerve growth factor, beta polypeptide
NRAS	NM_002524	1,66	1,16	0,73	0,84	neuroblastoma RAS viral (v-ras) oncogene homolog
OAS1	NM_002534	0,08	1,37	0,63	3,55	2',5'-oligoadenylate synthetase 1, 40/46kDa
ODC1	NM_002539	1,56	1,88	0,35	0,44	ornithine decarboxylase 1
SLC22A18	NM_002555	0,44	0,68	1,32	1,54	solute carrier family 22 (organic cation transporter), member 18
FURIN	NM_002569	0,79	0,87	1,84	1,13	furin (paired basic amino acid cleaving enzyme)
PAWR	NM_002583	2,09	1,21	0,79	0,58	PRKC, apoptosis, WT1, regulator
SERPINF1	NM_002615	0,44	0,29	1,99	1,57	serine (or cysteine) proteinase inhibitor, clade F (alpha-2 antiplasmin, pigment epithelium derived factor), member 1
PHB	NM_002634	1,24	1,74	0,60	0,76	prohibitin
PIK3C2B	NM_002646	0,59	0,12	1,49	1,41	phosphoinositide-3-kinase, class 2, beta polypeptide
PRKCM	NM_002742	1,93	1,01	0,95	0,99	protein kinase C, mu
MAP2K3	NM_002756	1,39	1,52	0,57	0,62	mitogen-activated protein kinase kinase 3
PRPS1	NM_002764	1,39	1,33	0,58	0,67	phosphoribosyl pyrophosphate synthetase 1
PSG9	NM_002784	1,65	1,10	0,79	0,90	pregnancy specific beta-1-glycoprotein 9

PTPRF	NM_002840	0,61	0,84	1,47	1,16	protein tyrosine phosphatase, receptor type, F
RANGAP1	NM_002883	1,41	1,80	0,54	0,59	Ran GTPase activating protein 1
RANGAP1	NM_002883	1,41	1,65	0,52	0,59	Ran GTPase activating protein 1
RAP2B	NM_002886	2,00	1,15	0,85	0,78	RAP2B, member of RAS oncogene family
ABCE1	NM_002940	1,30	1,26	0,60	0,74	ATP-binding cassette, sub-family E (OABP), member 1
MRPL12	NM_002949	1,25	1,60	0,55	0,75	mitochondrial ribosomal protein L12
CXCL6	NM_002993	0,53	0,53	1,47	1,58	chemokine (C-X-C motif) ligand 6 (granulocyte chemotactic protein 2)
SRF	NM_003131	1,38	1,32	0,61	0,68	serum response factor (c-fos serum response element-binding transcription factor)
SRM	NM_003132	1,46	1,64	0,48	0,54	spermidine synthase
STC1	NM_003155	0,42	0,47	2,00	1,53	stanniocalcin 1
TCEA2	NM_003195	0,54	0,49	1,46	1,49	transcription elongation factor A (SII), 2
TCEB3	NM_003198	1,41	1,18	0,51	0,82	transcription elongation factor B (SIII), polypeptide 3 (110kDa, elongin A)
TCF7	NM_003202	1,06	1,28	0,45	0,94	transcription factor 7 (T-cell specific, HMG-box)
TFRC	NM_003234	1,47	1,69	0,53	0,47	transferrin receptor (p90, CD71)
TGFB2	NM_003238	2,14	1,46	0,46	0,54	transforming growth factor, beta 2
TGFBR3	NM_003243	0,57	0,66	1,34	2,07	transforming growth factor, beta receptor III (betaglycan, 300kDa)
THBS2	NM_003247	0,57	0,47	1,68	1,43	thrombospondin 2
ICAM5	NM_003259	0,64	0,67	1,41	1,33	intercellular adhesion molecule 5, telencephalin
TLR2	NM_003264	0,48	0,49	1,57	1,51	toll-like receptor 2
TRPC1	NM_003304	0,63	0,69	1,31	1,32	transient receptor potential cation channel, subfamily C, member 1
TXNRD1	NM_003330	1,54	1,52	0,48	0,44	thioredoxin reductase 1
ZYX	NM_003461	1,64	1,47	0,53	0,49	zyxin
SCG2	NM_003469	0,61	0,27	1,58	1,39	secretogranin II (chromogranin C)
ARD1	NM_003491	1,34	1,23	0,63	0,77	ARD1 homolog, N-acetyltransferase (S. cerevisiae)
CXorf12	NM_003492	0,55	0,88	1,16	1,12	chromosome X open reading frame 12
PRSS12	NM_003619	0,57	0,73	1,28	1,38	protease, serine, 12 (neurotrypsin, motopsin)
PARG	NM_003631	0,49	1,01	0,99	1,51	poly (ADP-ribose) glycohydrolase
CNTNAP1	NM_003632	0,52	0,76	1,24	1,44	contactin associated protein 1
ENC1	NM_003633	1,65	1,71	0,34	0,35	ectodermal-neural cortex (with BTB-like domain)
IFITM1	NM_003641	0,46	0,74	1,26	2,36	interferon induced transmembrane protein 1 (9-27)
BHLHB2	NM_003670	0,31	0,37	2,02	1,63	basic helix-loop-helix domain containing, class B, 2
PDLIM4	NM_003687	0,52	0,86	1,14	1,42	PDZ and LIM domain 4
RNASET2	NM_003730	0,64	0,72	1,41	1,28	ribonuclease T2
EIF3S1	NM_003758	1,53	1,26	0,73	0,74	eukaryotic translation initiation factor 3, subunit 1 alpha, 35kDa
SERPINB7	NM_003784	1,47	2,07	0,54	0,46	serine (or cysteine) proteinase inhibitor, clade B (ovalbumin), member 7
TNFSF10	NM_003810	0,19	0,32	1,68	2,21	tumor necrosis factor (ligand) superfamily, member 10
SOCS2	NM_003877	1,61	1,34	0,66	0,60	suppressor of cytokine signaling 2
ZNF259	NM_003904	1,52	1,17	0,57	0,83	zinc finger protein 259
MBD3	NM_003926	1,25	1,88	0,60	0,75	methyl-CpG binding domain protein 3
GENX-3414	NM_003943	1,63	1,16	0,78	0,85	genethonin 1
SELENBP1	NM_003944	0,75	0,43	2,52	1,25	selenium binding protein 1
NPR2	NM_003995	0,56	1,01	1,24	0,99	natriuretic peptide receptor B/guanylate cyclase B (atrionatriuretic peptide receptor B)
OSMR	NM_003999	0,53	0,86	1,41	1,14	oncostatin M receptor
BNIP3	NM_004052	0,55	0,58	1,42	1,42	synonym: NIP3; Nip3 nuclear gene encoding mitochondrial protein, mRNA.
BYSL	NM_004053	1,38	1,53	0,55	0,62	bystin-like
EIF2S1	NM_004094	1,58	1,17	0,72	0,83	eukaryotic translation initiation factor 2, subunit 1 alpha, 35kDa
FCGRT	NM_004107	0,78	0,82	1,65	1,18	Fc fragment of IgG, receptor, transporter, alpha
FDX1	NM_004109	1,51	0,78	0,62	1,22	ferredoxin 1
FDXR	NM_004110	0,56	0,79	1,22	1,56	ferredoxin reductase
GBP2	NM_004120	0,60	0,56	1,47	1,40	guanylate binding protein 2, interferon-inducible

GYG	NM_004130	1,51	1,35	0,65	0,61	glycogenin
SREBF1	NM_004176	0,47	0,60	1,56	1,40	sterol regulatory element binding transcription factor 1
P4HA2	NM_004199	0,64	0,82	1,29	1,18	procollagen-proline, 2-oxoglutarate 4-dioxygenase (proline 4-hydroxylase), alpha polypeptide II
SYNGR3	NM_004209	0,52	0,07	2,12	1,48	synaptogyrin 3
EEF1E1	NM_004280	1,34	1,23	0,63	0,77	eukaryotic translation elongation factor 1 epsilon 1
RNF14	NM_004290	1,45	1,33	0,54	0,67	ring finger protein 14
ARHGDIA	NM_004309	1,30	1,89	0,54	0,71	Rho GDP dissociation inhibitor (GDI) alpha
ARHGDIA	NM_004309	1,38	1,35	0,50	0,65	Rho GDP dissociation inhibitor (GDI) alpha
BCS1L	NM_004328	1,27	1,55	0,58	0,73	BCS1-like (yeast)
CCNG2	NM_004354	0,34	0,38	1,62	1,65	cyclin G2
DLX2	NM_004405	2,19	1,74	0,21	0,26	distal-less homeo box 2
DSCR1	NM_004414	1,62	1,25	0,75	0,71	Down syndrome critical region gene 1
DUSP1	NM_004417	1,90	1,29	0,71	0,60	dual specificity phosphatase 1
ETV5	NM_004454	0,65	0,83	1,38	1,17	ets variant gene 5 (ets-related molecule)
FGF5	NM_004464	1,52	2,36	0,30	0,48	fibroblast growth factor 5
FOXD1	NM_004472	1,45	2,12	0,50	0,56	forkhead box D1
GTF2A2	NM_004492	1,30	1,20	0,63	0,80	general transcription factor IIA, 2, 12kDa
HNRPAB	NM_004499	1,30	1,47	0,56	0,70	heterogeneous nuclear ribonucleoprotein A/B
NFKBIE	NM_004556	0,51	0,86	1,15	1,14	nuclear factor of kappa light polypeptide gene enhancer in B-cells inhibitor, epsilon
PKNOX1	NM_004571	1,34	1,51	0,66	0,53	PBX/knotted 1 homeobox 1
BAP1	NM_004656	1,18	1,04	0,56	0,96	BRCA1 associated protein-1 (ubiquitin carboxy-terminal hydrolase)
VNN1	NM_004666	0,25	0,39	1,61	1,74	vanin 1
SLC16A4	NM_004696	0,44	0,28	2,64	1,56	solute carrier family 16 (monocarboxylic acid transporters), member 4
RNU3IP2	NM_004704	1,38	1,94	0,61	0,62	RNA, U3 small nucleolar interacting protein 2
DDX21	NM_004728	1,35	1,47	0,65	0,59	DEAD (Asp-Glu-Ala-Asp) box polypeptide 21
ETF1	NM_004730	1,49	1,37	0,63	0,63	eukaryotic translation termination factor 1
SLC33A1	NM_004733	1,97	1,02	0,98	0,76	solute carrier family 33 (acetyl-CoA transporter), member 1
NOLC1	NM_004741	1,45	1,54	0,50	0,55	nucleolar and coiled-body phosphoprotein 1
POLR2D	NM_004805	1,24	1,18	0,60	0,82	polymerase (RNA) II (DNA directed) polypeptide D
AIM2	NM_004833	0,51	0,13	1,50	1,49	absent in melanoma 2
AGTR1	NM_004835	1,68	1,34	0,64	0,66	angiotensin II receptor, type 1
IL27RA	NM_004843	0,72	0,72	1,73	1,28	interleukin 27 receptor, alpha
KIF23	NM_004856	1,35	1,28	0,68	0,72	kinesin family member 23
MARS	NM_004990	1,30	1,27	0,61	0,73	methionine-tRNA synthetase
ROR1	NM_005012	1,71	0,98	0,82	1,03	receptor tyrosine kinase-like orphan receptor 1
PMSCL1	NM_005033	1,37	1,55	0,50	0,63	polymyositis/scleroderma autoantigen 1, 75kDa
SFPQ	NM_005066	1,48	1,30	0,58	0,70	splicing factor proline/glutamine rich (polypyrimidine tract binding protein associated)
RCE1	NM_005133	1,33	1,47	0,30	0,67	RCE1 homolog, prenyl protein protease (S. cerevisiae)
ACTC	NM_005159	1,53	1,80	0,44	0,47	actin, alpha, cardiac muscle
ALDOC	NM_005165	0,34	0,37	1,71	1,63	aldolase C, fructose-bisphosphate
BCL3	NM_005178	0,56	0,62	1,38	1,50	B-cell CLL/lymphoma 3
CHES1	NM_005197	0,57	0,94	1,44	1,06	chromosome 14 open reading frame 116
NFIL3	NM_005384	0,55	0,44	1,77	1,45	nuclear factor, interleukin 3 regulated
PODXL	NM_005397	1,66	2,83	0,28	0,34	podocalyxin-like
BCAT1	NM_005504	1,54	1,30	0,66	0,70	branched chain aminotransferase 1, cytosolic
GTF2E1	NM_005513	1,31	1,18	0,60	0,82	general transcription factor IIE, polypeptide 1, alpha 56kDa
HSD11B1	NM_005525	0,40	0,70	1,30	1,99	hydroxysteroid (11-beta) dehydrogenase 1
IDH3A	NM_005530	1,53	1,41	0,51	0,59	isocitrate dehydrogenase 3 (NAD+) alpha
IDH3A	NM_005530	1,50	1,36	0,54	0,64	isocitrate dehydrogenase 3 (NAD+) alpha
LGALS3BP	NM_005567	0,41	0,86	1,14	1,58	lectin, galactoside-binding, soluble, 3 binding protein
SMAD6	NM_005585	1,74	1,27	0,73	0,53	MAD, mothers against decapentaplegic homolog 6 (Drosophila)

ALDH6A1	NM_005589	0,60	0,62	1,43	1,38	aldehyde dehydrogenase 6 family, member A1
RTN2	NM_005619	0,39	0,56	1,70	1,44	reticulon 2
ABCF2	NM_005692	1,32	1,66	0,56	0,68	ATP-binding cassette, sub-family F (GCN20), member 2
TSSC4	NM_005706	1,37	1,76	0,39	0,63	tumor suppressing subtransferable candidate 4
RGS19IP1	NM_005716	1,20	1,36	0,59	0,80	regulator of G-protein signalling 19 interacting protein 1
PPIF	NM_005729	1,46	2,14	0,43	0,54	peptidylprolyl isomerase F (cyclophilin F)
ARL4A	NM_005738	1,42	1,59	0,56	0,59	ADP-ribosylation factor-like 4
MBNL2	NM_005757	1,27	1,34	0,63	0,73	muscleblind-like 2 (Drosophila)
ZNF443	NM_005815	0,73	0,42	1,70	1,28	zinc finger protein 443
LRRC17	NM_005824	0,54	0,34	1,79	1,46	leucine rich repeat containing 17
SLC35B1	NM_005827	1,39	1,37	0,63	0,61	solute carrier family 35, member B1
RAB9P40	NM_005833	1,35	1,29	0,61	0,71	Rab9 effector p40
PURA	NM_005859	1,18	1,54	0,55	0,82	purine-rich element binding protein A
FMNL1	NM_005892	0,83	0,95	1,76	1,05	formin-like 1
SMAD7	NM_005904	1,77	1,25	0,73	0,75	MAD, mothers against decapentaplegic homolog 7 (Drosophila)
MXI1	NM_005962	0,38	0,24	1,87	1,62	MAX interacting protein 1
UCHL3	NM_006002	1,52	1,13	0,70	0,88	ubiquitin carboxyl-terminal esterase L3 (ubiquitin thiolesterase)
WFS1	NM_006005	0,74	0,90	1,59	1,10	Wolfram syndrome 1 (wolframin)
TNIP1	NM_006058	0,48	0,94	1,06	1,12	TNFAIP3 interacting protein 1
TUBB4	NM_006086	1,14	1,07	0,56	0,93	tubulin, beta, 4
NDRG1	NM_006096	0,25	0,26	2,34	1,75	N-myc downstream regulated gene 1
CD2BP2	NM_006110	1,32	1,35	0,48	0,68	CD2 antigen (cytoplasmic tail) binding protein 2
TOMM40	NM_006114	1,39	1,38	0,59	0,62	translocase of outer mitochondrial membrane 40 homolog (yeast)
BMP1	NM_006129	0,58	0,74	1,58	1,26	bone morphogenetic protein 1
NOL1	NM_006170	1,58	1,33	0,67	0,64	HOM-TES-103 tumor antigen-like
PLCD1	NM_006225	0,31	0,68	1,49	1,32	phospholipase C, delta 1
PLTP	NM_006227	0,54	0,77	1,23	1,47	phospholipid transfer protein
CCL7	NM_006273	0,37	0,36	1,63	2,42	chemokine (C-C motif) ligand 7
JTV1	NM_006303	1,37	1,49	0,48	0,63	JTV1 gene
TIMM17A	NM_006335	1,38	1,55	0,59	0,63	translocase of inner mitochondrial membrane 17 homolog A (yeast)
FST	NM_006350	1,83	1,42	0,53	0,58	follistatin
TIMM44	NM_006351	1,27	1,35	0,59	0,73	translocase of inner mitochondrial membrane 44 homolog (yeast)
TRIM38	NM_006355	0,64	0,70	1,30	1,55	tripartite motif-containing 38
NOL5A	NM_006392	1,26	1,37	0,60	0,74	nucleolar protein 5A (56kDa with KKE/D repeat)
POLR3F	NM_006466	2,18	0,80	1,07	0,93	polymerase (RNA) III (DNA directed) polypeptide F, 39 kDa
TXNIP	NM_006472	0,50	0,43	2,21	1,51	thioredoxin interacting protein
TXNIP	NM_006472	0,47	0,37	1,75	1,53	thioredoxin interacting protein
TXNIP	NM_006472	0,36	0,44	2,04	1,56	thioredoxin interacting protein
NCOA3	NM_006534	0,51	0,70	1,31	1,48	nuclear receptor coactivator 3
YKT6	NM_006555	1,40	1,37	0,60	0,63	SNARE protein Ykt6
YKT6	NM_006555	1,61	1,33	0,54	0,67	SNARE protein Ykt6
CUGBP1	NM_006560	1,09	1,25	0,52	0,92	CUG triplet repeat, RNA binding protein 1
CGRRF1	NM_006568	1,47	1,34	0,67	0,66	cell growth regulator with ring finger domain 1
SLC12A7	NM_006598	0,47	1,05	0,95	1,49	solute carrier family 12 (potassium/chloride transporters), member 7
NFAT5	NM_006599	0,55	0,82	1,18	1,27	nuclear factor of activated T-cells 5, tonicity-responsive
JARID1B	NM_006618	0,69	0,60	1,95	1,31	Jumonji, AT rich interactive domain 1B (RBP2-like)
PLK2	NM_006622	1,38	1,43	0,61	0,62	polo-like kinase 2 (Drosophila)
ZMYND11	NM_006624	1,67	1,17	0,83	0,74	adenovirus 5 E1A binding protein
RPP40	NM_006638	1,44	1,76	0,56	0,53	ribonuclease P1
CRA	NM_006697	0,73	0,57	1,65	1,28	cisplatin resistance associated
RNPS1	NM_006711	1,61	1,14	0,77	0,86	RNA binding protein S1, serine-rich domain
C1orf29	NM_006820	0,42	0,98	1,02	3,72	chromosome 1 open reading frame 29
EBNA1BP2	NM_006824	1,22	1,52	0,59	0,78	EBNA1 binding protein 2

RAB32	NM_006834	1,37	1,73	0,58	0,63	RAB32, member RAS oncogene family
IL24	NM_006850	0,42	0,44	2,62	1,56	interleukin 24
RAB35	NM_006861	1,13	1,52	0,50	0,87	RAB35, member RAS oncogene family
RBPMS	NM_006867	0,56	0,93	1,22	1,08	RNA binding protein with multiple splicing
ELF2	NM_006874	0,56	0,77	1,40	1,23	E74-like factor 2 (ets domain transcription factor)
B3GNT6	NM_006876	0,55	0,74	1,26	1,46	UDP-GlcNAc:betaGal beta-1,3-N-acetylglucosaminyltransferase 6
HNMT	NM_006895	0,83	0,61	2,12	1,17	histamine N-methyltransferase
SLC2A3	NM_006931	0,71	0,67	1,50	1,29	solute carrier family 2 (facilitated glucose transporter), member 3
SMTN	NM_006932	1,39	1,53	0,61	0,59	smoothelin
BTN3A3	NM_006994	0,48	0,38	1,59	1,52	butyrophilin, subfamily 3, member A3
BTN3A3	NM_006994	0,62	0,54	1,38	1,42	butyrophilin, subfamily 3, member A3
DUSP14	NM_007026	1,36	1,40	0,54	0,64	dual specificity phosphatase 14
DNAJB4	NM_007034	1,71	1,48	0,52	0,48	DnaJ (Hsp40) homolog, subfamily B, member 4
CDC42EP1	NM_007061	1,42	1,64	0,58	0,53	CDC42 effector protein (Rho GTPase binding) 1
TBC1D8	NM_007063	0,55	0,48	1,45	1,73	TBC1 domain family, member 8 (with GRAM domain)
LSM6	NM_007080	1,32	1,21	0,63	0,79	LSM6 homolog, U6 small nuclear RNA associated (S. cerevisiae)
TNFAIP6	NM_007115	0,53	0,64	1,36	1,67	tumor necrosis factor, alpha-induced protein 6
MME	NM_007287	0,64	0,59	1,36	1,54	membrane metallo-endopeptidase (neutral endopeptidase, enkephalinase, CALLA, CD10)
MME	NM_007287	0,66	0,66	1,34	1,49	membrane metallo-endopeptidase (neutral endopeptidase, enkephalinase, CALLA, CD10)
PHLDA1	NM_007350	0,65	0,57	1,47	1,35	pleckstrin homology-like domain, family A, member 1
NID2	NM_007361	0,74	0,60	1,75	1,26	nidogen 2 (osteonidogen)
ELL2	NM_012081	1,42	1,43	0,58	0,44	elongation factor, RNA polymerase II, 2
ASE-1	NM_012099	1,39	1,60	0,61	0,44	CD3-epsilon-associated protein; antisense to ERCC-1
CHORDC1	NM_012124	1,71	1,25	0,75	0,73	cysteine and histidine-rich domain (CHORD)-containing, zinc binding protein 1
GCA	NM_012198	0,50	0,68	1,39	1,33	grancalcin, EF-hand calcium binding protein
DKK1	NM_012242	1,99	1,70	0,31	0,28	dickkopf homolog 1 (Xenopus laevis)
RRAS2	NM_012250	1,58	1,32	0,68	0,57	related RAS viral (r-ras) oncogene homolog 2
HSPBP1	NM_012267	1,26	1,40	0,61	0,74	hsp70-interacting protein
MAPRE1	NM_012325	1,36	1,31	0,59	0,69	microtubule-associated protein, RP/EB family, member 1
MMD	NM_012329	0,62	0,68	1,32	1,32	monocyte to macrophage differentiation-associated
GTPBP4	NM_012341	1,68	1,31	0,69	0,63	GTP binding protein 4
GTPBP4	NM_012341	1,82	1,42	0,58	0,49	GTP binding protein 4
BAMBI	NM_012342	1,38	1,50	0,62	0,50	BMP and activin membrane-bound inhibitor homolog (Xenopus laevis)
STEAP	NM_012449	1,26	1,37	0,51	0,74	six transmembrane epithelial antigen of the prostate
TIMM10	NM_012456	1,35	2,35	0,56	0,65	translocase of inner mitochondrial membrane 10 homolog (yeast)
FLRT2	NM_013231	0,56	0,84	1,16	1,96	fibronectin leucine rich transmembrane protein 2
STK39	NM_013233	1,72	1,20	0,81	0,72	serine threonine kinase 39 (STE20/SPS1 homolog, yeast)
VPS4A	NM_013245	1,35	1,33	0,54	0,67	vacuolar protein sorting 4A (yeast)
MYLIP	NM_013262	0,36	0,56	1,93	1,44	myosin regulatory light chain interacting protein
TRA2A	NM_013293	1,48	1,29	0,70	0,71	transformer-2 alpha
SEC61A1	NM_013336	1,37	1,26	0,67	0,74	Sec61 alpha 1 subunit (S. cerevisiae)
GREM1	NM_013372	1,45	1,31	0,69	0,42	cysteine knot superfamily 1, BMP antagonist 1
GREM1	NM_013372	1,73	1,26	0,74	0,44	cysteine knot superfamily 1, BMP antagonist 1
FST	NM_013409	1,49	1,64	0,48	0,51	follistatin
AK3	NM_013410	0,36	0,25	4,86	1,64	adenylate kinase 3
NRG1	NM_013959	2,52	1,47	0,53	0,36	neuregulin 1
BNIP1	NM_013979	1,18	1,27	0,54	0,82	BCL2/adenovirus E1B 19kDa interacting protein 1
DEXI	NM_014015	1,25	0,96	0,62	1,04	dexamethasone-induced transcript
SSX2IP	NM_014021	1,66	1,33	0,67	0,54	synovial sarcoma, X breakpoint 2 interacting protein
DKFZP586A0522	NM_014033	0,38	0,37	1,62	1,65	DKFZP586A0522 protein
C6orf66	NM_014165	1,58	1,39	0,61	0,58	chromosome 6 open reading frame 66

C14orf123	NM_014169	1,54	1,17	0,75	0,83	chromosome 14 open reading frame 123
MRPL15	NM_014175	1,42	1,33	0,67	0,67	mitochondrial ribosomal protein L15
STXBP6	NM_014178	1,40	1,33	0,48	0,67	syntaxin binding protein 6 (amisyn)
EVI2A	NM_014210	1,62	1,23	0,77	0,68	ecotropic viral integration site 2A
IMPA2	NM_014214	0,58	0,73	1,39	1,27	inositol(myo)-1(or 4)-monophosphatase 2
SLC25A15	NM_014252	1,64	1,14	0,73	0,86	solute carrier family 25 (mitochondrial carrier; ornithine transporter) member 15
IGSF4	NM_014333	1,58	0,37	3,25	0,42	immunoglobulin superfamily, member 4
E2IG5	NM_014367	0,70	0,66	1,45	1,30	growth and transformation-dependent protein
HSA9761	NM_014473	1,25	1,20	0,55	0,80	putative dimethyladenosine transferase
UBE2S	NM_014501	1,26	1,68	0,53	0,74	ubiquitin-conjugating enzyme E2S
EVC	NM_014556	0,64	0,48	1,40	1,36	Ellis van Creveld syndrome
S100A6	NM_014624	0,49	0,98	1,02	1,14	S100 calcium binding protein A6 (calcyclin)
MTSS1	NM_014751	0,54	0,84	1,16	1,28	metastasis suppressor 1
PTDSS1	NM_014754	1,46	1,30	0,69	0,70	phosphatidylserine synthase 1
KIAA0133	NM_014777	1,44	1,77	0,56	0,52	
KIAA0669	NM_014779	1,25	1,25	0,59	0,75	go_function: transcription factor activity [goid 0003700]regulation of transcription, DNA-dependent [goid 0006355] [evidence IEA]; Homo sapiens KIAA0669
CUL7	NM_014780	0,56	0,88	1,21	1,12	KIAA0076
TRIM14	NM_014788	1,06	1,28	0,48	0,94	tripartite motif-containing 14
ZBTB24	NM_014797	1,48	1,22	0,57	0,78	
p44S10	NM_014814	1,35	1,28	0,67	0,72	proteasome regulatory particle subunit p44S10
KIAA0469	NM_014851	1,80	1,38	0,62	0,57	
KIAA0020	NM_014878	1,47	1,33	0,61	0,67	KIAA0020
FAM13A1	NM_014883	0,62	0,76	1,24	1,44	
DOC1	NM_014890	1,43	1,22	0,66	0,78	downregulated in ovarian cancer 1
NAV3	NM_014903	1,39	1,39	0,52	0,61	neuron navigator 3
RAB21	NM_014999	1,59	1,21	0,79	0,76	RAB21, member RAS oncogene family
SYNE2	NM_015180	0,53	0,52	1,99	1,47	spectrin repeat containing, nuclear envelope 2
EFA6R	NM_015310	0,41	0,80	1,33	1,20	ADP-ribosylation factor guanine nucleotide factor 6
KIAA0409	NM_015324	1,47	1,19	0,69	0,81	KIAA0409 protein
TAZ	NM_015472	0,67	0,47	1,43	1,33	transcriptional co-activator with PDZ-binding motif (TAZ)
ZNF288	NM_015642	0,61	0,78	1,25	1,22	zinc finger protein 288
DKFZP564C186	NM_015658	1,36	1,51	0,62	0,64	DKFZP564C186 protein
GADD45B	NM_015675	1,78	1,52	0,35	0,49	growth arrest and DNA-damage-inducible, beta
CGI-96	NM_015703	1,35	1,49	0,63	0,65	CGI-96 protein
MBD1	NM_015845	1,48	1,18	0,68	0,82	methyl-CpG binding domain protein 1
PIASY	NM_015897	1,15	1,41	0,54	0,85	protein inhibitor of activated STAT protein PIASy
CGI-01	NM_015935	1,31	1,30	0,53	0,70	CGI-01 protein
CGI-14	NM_015944	1,38	2,12	0,60	0,63	CGI-14 protein
CUTC	NM_015960	1,28	1,19	0,53	0,81	CGI-32 protein
MRPS7	NM_015971	1,24	1,68	0,58	0,77	mitochondrial ribosomal protein S7
ABHD5	NM_016006	1,57	1,31	0,60	0,70	abhydrolase domain containing 5
UCHL5	NM_016017	1,94	1,05	0,95	0,95	synonyms: UCH37, CGI-70; ubiquitin carboxyl-terminal esterase L5; go_component: cytosol [goid 0005829] [evidence IEA]; go_component: intracellular [goid 0005622] [evidence IEA]; go_function: ubiquitin thiolesterase activity [goid 0004221] [evidence IEA]; go_function: hydrolase activity [goid 0016787] [evidence IEA]; go_process: ubiquitin-dependent protein catabolism [goid 0006511] [evidence IEA]; Homo sapiens ubiquitin carboxyl-terminal hydrolase L5 (UCHL5), mRNA.
CGI-115	NM_016052	1,66	1,39	0,58	0,61	CGI-115 protein
CGI-127	NM_016061	0,59	0,55	1,42	1,41	yippee protein
GLRX2	NM_016066	1,23	1,56	0,61	0,77	glutaredoxin 2
Magmas	NM_016069	1,35	1,76	0,62	0,66	mitochondria-associated protein involved in granulocyte-macrophage colony-stimulating factor signal transduction
KIAA0992	NM_016081	1,49	1,33	0,65	0,67	palladin

CGI-37	NM_016101	1,63	1,27	0,63	0,73	comparative gene identification transcript 37
TAO1	NM_016151	1,61	1,15	0,75	0,85	Prostate derived STE20-like kinase PSK (PSK), mRNA
ING4	NM_016162	0,45	0,87	1,62	1,13	inhibitor of growth family, member 4
C1orf33	NM_016183	1,38	1,51	0,53	0,62	chromosome 1 open reading frame 33
KLF2	NM_016270	1,46	1,21	0,70	0,79	Kruppel-like factor 2 (lung)
EVL	NM_016337	0,58	0,58	1,44	1,42	Enah/Vasp-like
SLCO4A1	NM_016354	0,37	0,91	1,12	1,09	solute carrier organic anion transporter family, member 4A1
C9orf114	NM_016390	1,54	1,19	0,54	0,81	hypothetical protein HSPC109
HSPC111	NM_016391	1,76	1,47	0,45	0,53	hypothetical protein HSPC111
HYPK	NM_016400	1,35	1,48	0,58	0,65	Huntingtin interacting protein K
TUBG2	NM_016437	0,50	0,92	1,28	1,08	tubulin, gamma 2
CRIM1	NM_016441	1,67	1,24	0,76	0,58	cysteine-rich motor neuron 1
C1RL	NM_016546	0,28	0,21	2,04	1,73	complement component 1, r subcomponent-like
E2IG2	NM_016565	1,32	1,44	0,54	0,68	E2IG2 protein
MRPL35	NM_016622	1,30	1,46	0,62	0,70	mitochondrial ribosomal protein L35
TNFRSF12A	NM_016639	1,57	1,81	0,31	0,43	tumor necrosis factor receptor superfamily, member 12A
LOC51337	NM_016647	0,66	0,81	1,44	1,19	mesenchymal stem cell protein DSCD75
OGG1	NM_016820	1,77	1,15	0,80	0,85	8-oxoguanine DNA glycosylase
ADD3	NM_016824	0,61	0,74	1,26	1,44	adducin 3 (gamma)
SURF2	NM_017503	1,46	1,94	0,16	0,54	surfeit 2
ZNF395	NM_017606	0,25	0,27	1,99	1,73	hypothetical protein DKFZp434K1210
BNC2	NM_017637	0,67	0,81	1,37	1,19	
FLJ20186	NM_017702	1,22	1,19	0,56	0,81	hypothetical protein FLJ20186
FLJ20244	NM_017722	1,32	1,49	0,61	0,68	hypothetical protein FLJ20244
FLJ20272	NM_017735	1,63	1,21	0,72	0,79	hypothetical protein FLJ20272
FLJ20298	NM_017752	0,58	0,30	1,42	1,44	FLJ20298 protein
FLJ20457	NM_017832	1,53	0,99	0,55	1,01	hypothetical protein FLJ20457
COMMD8	NM_017845	1,44	1,26	0,72	0,74	COMM domain containing 8
RNF126	NM_017876	1,34	1,33	0,67	0,61	ring finger protein 126
TPCN1	NM_017901	0,56	0,62	1,45	1,38	two pore segment channel 1
PAK1IP1	NM_017906	2,32	1,02	0,89	0,98	PAK1 interacting protein 1
NOL8	NM_017948	1,27	1,16	0,56	0,84	nucleolar protein 8
MRPL20	NM_017971	1,29	1,19	0,55	0,81	mitochondrial ribosomal protein L20
FLJ10134	NM_018004	0,62	0,58	1,59	1,38	hypothetical protein FLJ10134
SLC38A4	NM_018018	2,65	0,53	1,25	0,75	solute carrier family 38, member 4
HELLS	NM_018063	0,62	0,63	1,49	1,37	helicase, lymphoid-specific
FLJ10374	NM_018074	1,37	1,42	0,62	0,63	hypothetical protein FLJ10374
POLR3B	NM_018082	1,50	1,27	0,59	0,73	RNA polymerase III subunit RPC2
FLJ10415	NM_018089	0,66	0,78	1,35	1,22	hypothetical protein FLJ10415
FLJ10439	NM_018093	1,97	1,15	0,71	0,85	hypothetical protein FLJ10439
KBTBD4	NM_018095	1,31	1,06	0,62	0,94	kelch repeat and BTB (POZ) domain containing 4
FLJ10504	NM_018116	1,41	1,30	0,60	0,70	misato
FLJ10525	NM_018126	1,99	1,04	0,96	0,72	hypothetical protein FLJ10525
FLJ10546	NM_018133	1,67	1,24	0,63	0,76	hypothetical protein FLJ10546
C14orf104	NM_018139	1,59	0,99	0,64	1,01	chromosome 14 open reading frame 104
FLJ10618	NM_018155	0,63	0,61	1,37	1,51	hypothetical protein FLJ10618
NAV2	NM_018162	0,57	0,79	1,49	1,21	
ATAD3A	NM_018188	1,40	1,42	0,60	0,55	hypothetical protein FLJ10709
WDR12	NM_018256	1,25	1,44	0,62	0,75	WD repeat domain 12
CWF19L1	NM_018294	1,30	1,91	0,64	0,70	CWF19-like 1, cell cycle control (S. pombe)
BRF2	NM_018310	1,40	1,34	0,48	0,66	BRF2, subunit of RNA polymerase III transcription initiation factor, BRF1-like
BRIX	NM_018321	2,02	1,13	0,87	0,71	BRIX
LIN7C	NM_018362	1,30	1,28	0,64	0,72	lin-7 homolog C (C. elegans)

FLJ11336	NM_018393	1,66	1,15	0,64	0,85	hypothetical protein FLJ11336
EFA6R	NM_018422	0,61	0,57	1,40	1,45	hypothetical protein DKFZp761K1423
C14orf116	NM_018589	0,74	0,61	1,52	1,26	chromosome 14 open reading frame 116
WSB2	NM_018639	1,73	1,24	0,76	0,70	WD repeat and SOCS box-containing 2
ZNF395	NM_018660	0,37	0,30	1,63	1,68	papillomavirus regulatory factor PRF-1
HCA127	NM_018684	0,53	0,81	1,19	1,39	hepatocellular carcinoma-associated antigen 127
LANCL2	NM_018697	1,36	1,59	0,64	0,61	LanC lantibiotic synthetase component C-like 2 (bacterial)
TOLLIP	NM_019009	1,43	1,35	0,65	0,59	toll interacting protein
DDIT4	NM_019058	0,22	0,27	1,99	1,73	DNA-damage-inducible transcript 4
HOXA5	NM_019102	0,86	0,35	1,86	1,15	homeo box A5
TUFT1	NM_020127	1,70	1,24	0,76	0,62	tuftelin 1
LOC56902	NM_020143	1,65	1,54	0,36	0,46	putatative 28 kDa protein
C21orf7	NM_020152	0,73	0,39	1,94	1,28	chromosome 21 open reading frame 7
LXN	NM_020169	0,57	0,57	1,43	1,54	latexin protein
C14orf132	NM_020215	0,46	0,45	1,74	1,54	chromosome 14 open reading frame 132
CTNNBIP1	NM_020248	0,49	0,97	1,25	1,03	catenin, beta interacting protein 1
PLSCR4	NM_020353	0,63	0,50	1,45	1,37	phospholipid scramblase 4
AVEN	NM_020371	1,40	1,37	0,63	0,62	apoptosis, caspase activation inhibitor
C12orf4	NM_020374	1,43	1,32	0,62	0,68	chromosome 12 open reading frame 4
PCDH9	NM_020403	1,49	2,54	0,49	0,51	protocadherin 9
MCOLN1	NM_020533	1,92	1,05	0,70	0,95	mucolipin 1
LTBP3	NM_021070	0,40	0,63	1,38	1,46	latent transforming growth factor beta binding protein 3
SLC5A6	NM_021095	1,61	1,34	0,55	0,66	solute carrier family 5 (sodium-dependent vitamin transporter), member 6
PMAIP1	NM_021127	0,59	0,81	1,21	1,19	phorbol-12-myristate-13-acetate-induced protein 1
PSAT1	NM_021154	2,14	1,41	0,45	0,60	phosphoserine aminotransferase 1
POLD4	NM_021173	0,61	0,87	1,36	1,13	polymerase (DNA-directed), delta 4
C6orf47	NM_021184	1,29	1,25	0,42	0,75	apolipoprotein M
SRPRB	NM_021203	1,47	1,37	0,63	0,55	signal recognition particle receptor, B subunit
JAM2	NM_021219	0,58	0,60	1,40	1,98	junctional adhesion molecule 2
ARHGAP22	NM_021226	1,30	1,22	0,55	0,79	Rho GTPase activating protein 22
TRIB2	NM_021643	0,34	0,45	1,70	1,55	tribbles homolog 2
PEO1	NM_021830	1,31	1,37	0,59	0,69	progressive external ophthalmoplegia 1
FANCE	NM_021922	1,31	1,49	0,59	0,69	Fanconi anemia, complementation group E
FLJ22649	NM_021928	1,42	1,31	0,69	0,69	hypothetical protein FLJ22649 similar to signal peptidase SPC22/23
FLJ12438	NM_021933	1,24	1,06	0,51	0,94	hypothetical protein FLJ12438
GMPPB	NM_021971	1,45	1,38	0,63	0,59	GDP-mannose pyrophosphorylase B
SPHK1	NM_021972	1,44	1,98	0,51	0,56	sphingosine kinase 1
SDF2L1	NM_022044	1,34	1,33	0,52	0,67	stromal cell-derived factor 2-like 1
SH2D4A	NM_022071	1,37	1,97	0,59	0,63	hypothetical protein FLJ20967
FLJ12455	NM_022078	1,27	1,16	0,59	0,84	hypothetical protein FLJ12455
LOC63920	NM_022090	0,66	0,69	1,34	1,31	Homo sapiens transposon-derived Buster3 transposase-like (LOC63920), mRNA.
PP3111	NM_022156	1,51	1,24	0,70	0,76	PP3111 protein
POPDC3	NM_022361	1,33	1,49	0,61	0,67	popeye domain containing 3
TFB2M	NM_022366	1,89	1,10	0,90	0,87	transcription factor B2, mitochondrial
C10orf117	NM_022451	1,55	1,25	0,59	0,75	AD24 protein
RNF25	NM_022453	1,28	1,29	0,53	0,72	ring finger protein 25
MPP5	NM_022474	1,50	1,39	0,60	0,61	membrane protein, palmitoylated 5 (MAGUK p55 subfamily member 5)
COPS7B	NM_022730	1,20	1,35	0,36	0,80	COP9 constitutive photomorphogenic homolog subunit 7B (Arabidopsis)
FLJ12484	NM_022767	1,38	1,51	0,55	0,62	hypothetical protein FLJ12484
DDX31	NM_022779	1,25	1,28	0,45	0,75	DEAD (Asp-Glu-Ala-Asp) box polypeptide 31
CDCP1	NM_022842	0,68	0,46	1,38	1,32	CUB domain-containing protein 1

NOL6	NM_022917	1,47	1,63	0,50	0,53	nucleolar protein family 6 (RNA-associated)
ANKRA2	NM_023039	0,55	0,52	1,65	1,45	ankyrin repeat, family A (RFXANK-like), 2
FLJ12439	NM_023077	1,50	1,33	0,58	0,67	hypothetical protein FLJ12439
PYCRL	NM_023078	1,44	2,28	0,47	0,56	hypothetical protein FLJ13852
MOSPD3	NM_023948	0,58	0,98	1,23	1,02	motile sperm domain containing 3
LRFN4	NM_024036	1,37	1,33	0,58	0,67	leucine rich repeat and fibronectin type III domain containing 4
MGC2603	NM_024037	1,52	1,05	0,76	0,95	hypothetical protein MGC2603
NUDT9	NM_024047	1,23	1,27	0,53	0,77	nudix (nucleoside diphosphate linked moiety X)-type motif 9
PCIA1	NM_024050	1,35	1,32	0,55	0,68	hypothetical protein MGC2594
PDCL3	NM_024065	1,70	1,25	0,75	0,74	phosducin-like 3
MGC3162	NM_024078	1,37	1,32	0,68	0,40	hypothetical protein MGC3162
MGC2574	NM_024098	1,47	1,67	0,47	0,53	hypothetical protein MGC2574
MGC3731	NM_024313	1,53	1,17	0,65	0,83	hypothetical protein MGC3731
C20orf121	NM_024331	1,22	1,27	0,61	0,78	chromosome 20 open reading frame 121
PCDH16	NM_024542	0,63	0,75	1,25	1,32	
FLJ22709	NM_024578	0,67	0,79	1,94	1,21	hypothetical protein FLJ22709
FLJ23221	NM_024579	0,52	0,45	1,61	1,48	hypothetical protein FLJ23221
FLJ23548	NM_024590	1,87	1,10	0,90	0,89	hypothetical protein FLJ23548
FLJ12666	NM_024595	1,16	1,07	0,54	0,93	hypothetical protein FLJ12666
FLJ12649	NM_024597	1,55	1,45	0,55	0,55	
FLJ21125	NM_024627	1,48	1,81	0,53	0,52	hypothetical protein FLJ21125
FLJ11506	NM_024666	1,25	1,27	0,60	0,75	hypothetical protein FLJ11506
TBC1D17	NM_024682	0,60	0,67	1,33	1,33	TBC1 domain family, member 17
FLJ22729	NM_024683	1,32	1,22	0,56	0,78	hypothetical protein FLJ22729
SLC25A22	NM_024698	1,29	1,61	0,64	0,71	solute carrier family 25 (mitochondrial carrier: glutamate), member 22
FLJ13479	NM_024706	1,05	1,84	0,45	0,95	hypothetical protein FLJ13479
FLJ12649	NM_024765	1,83	1,05	0,91	0,95	
GEMIN6	NM_024775	1,24	1,43	0,59	0,77	gem (nuclear organelle) associated protein 6
FLJ14154	NM_024845	1,43	1,22	0,70	0,78	hypothetical protein FLJ14154
FLJ20920	NM_025149	0,66	0,77	1,66	1,23	hypothetical protein FLJ20920
PUS1	NM_025215	1,44	1,58	0,43	0,56	pseudouridylate synthase 1
PDCD1LG2	NM_025239	1,52	1,82	0,48	0,41	programmed cell death 1 ligand 2
MGC2776	NM_025265	1,77	1,11	0,66	0,89	hypothetical protein MGC2776
WNT5B	NM_030775	1,35	1,92	0,51	0,65	wingless-type MMTV integration site family, member 5B
MFTC	NM_030780	1,49	1,27	0,73	0,69	mitochondrial folate transporter/carrier
COLEC12	NM_030781	0,25	0,29	1,71	2,80	collectin sub-family member 12
SYNCOILIN	NM_030786	1,39	1,32	0,65	0,68	intermediate filament protein syncoilin
DKFZP434F0318	NM_030817	0,62	0,59	1,39	1,84	hypothetical protein DKFZp434F0318
	NM_030892	0,86	0,79	1,81	1,14	
SNX27	NM_030918	0,54	0,81	1,19	1,20	sorting nexin family member 27
ARPC5L	NM_030978	1,34	1,56	0,57	0,66	actin related protein 2/3 complex, subunit 5-like
CDCA3	NM_031299	1,21	1,28	0,58	0,79	cell division cycle associated 3
PSG3	R32065	1,86	1,34	0,66	0,64	pregnancy specific beta-1-glycoprotein 3
AKR1C1	S68290	1,28	1,57	0,51	0,72	aldo-keto reductase family 1, member C1 (dihydrodiol dehydrogenase 1; 20-alpha (3-alpha)-hydroxysteroid dehydrogenase)
CCL2	S69738	0,49	0,36	1,51	2,09	chemokine (C-C motif) ligand 2
UAP1	S73498	1,74	1,34	0,66	0,61	UDP-N-acteylglucosamine pyrophosphorylase 1
NF2	S73854	1,37	1,48	0,49	0,63	neurofibromin 2 (bilateral acoustic neuroma)
DKFZp564A176	T16388	0,66	0,66	1,34	1,42	hypothetical protein DKFZp564A176
DKFZp564A176	T16388	1,37	1,02	0,63	0,98	hypothetical protein DKFZp564A176
AKR1C1	U05598	1,25	1,49	0,50	0,75	aldo-keto reductase family 1, member C2 (dihydrodiol dehydrogenase 2; bile acid binding protein; 3-alpha hydroxysteroid dehydrogenase, type III)
CYB561	U06715	0,63	1,02	1,32	0,98	Human cytochrome B561, HCYTO B561, mRNA, partial cds.

CASP1	U13699	0,45	0,83	1,17	1,58	caspase 1, apoptosis-related cysteine protease (interleukin 1, beta, convertase)
BNIP3	U15174	0,54	0,51	1,75	1,46	Homo sapiens BCL2/adenovirus E1B 19kD-interacting protein 3 (BNIP3) mRNA, complete cds.
GLIPR1	U16307	1,39	1,33	0,68	0,64	GLI pathogenesis-related 1 (glioma)
MET	U19348	1,54	1,47	0,53	0,44	Human (tpr-met fusion) oncogene mRNA, complete cds.
CXCL12	U19495	1,33	1,42	0,56	0,67	chemokine (C-X-C motif) ligand 12 (stromal cell-derived factor 1)
EIF2B5	U23028	1,23	1,18	0,60	0,82	eukaryotic translation initiation factor 2B, subunit 5 epsilon, 82kDa
CBLB	U26710	0,56	0,59	1,53	1,41	Cas-Br-M (murine) ecotropic retroviral transforming sequence b
FHL1	U29538	2,31	1,29	0,62	0,71	four and a half LIM domains 1
SMG1	U32581	0,62	0,31	1,42	1,38	PI-3-kinase-related kinase SMG-1
RAB27A	U38654	0,52	0,71	1,34	1,29	RAB27A, member RAS oncogene family
NUP98	U41815	1,54	1,30	0,57	0,71	nucleoporin 98kDa
STC1	U46768	0,33	0,36	1,75	1,64	stanniocalcin 1
RABGGTB	U49245	1,51	1,24	0,69	0,76	Rab geranylgeranyltransferase, beta subunit
LEPR	U50748	0,55	0,40	1,63	1,45	leptin receptor
PWP2H	U56085	1,37	1,49	0,63	0,59	PWP2 periodic tryptophan protein homolog (yeast)
DKC1	U59151	1,45	1,42	0,58	0,57	dyskeratosis congenita 1, dyskerin
DDX17	U59321	0,54	0,83	1,17	1,22	DEAD (Asp-Glu-Ala-Asp) box polypeptide 17
TEAD4	U63824	1,30	1,23	0,54	0,77	TEA domain family member 4
LEPR	U66495	0,66	0,65	1,34	1,88	leptin receptor
JAG1	U73936	3,33	0,77	1,23	0,57	jagged 1 (Alagille syndrome)
RABIF	U74324	1,40	1,29	0,63	0,71	RAB interacting factor
RABIF	U74324	1,63	1,28	0,68	0,72	RAB interacting factor
FAP	U76833	0,43	0,74	1,26	1,44	fibroblast activation protein, alpha
JAG1	U77914	2,92	0,84	1,16	0,76	jagged 1 (Alagille syndrome)
ANGPT1	U83508	1,56	1,40	0,60	0,55	angiopoietin 1
ADAM17	U86755	0,71	0,91	1,91	1,09	a disintegrin and metalloproteinase domain 17 (tumor necrosis factor, alpha, converting enzyme)
BTN3A3	U90548	0,70	0,42	1,53	1,30	butyrophilin, subfamily 3, member A3
BTN3A1	U90552	0,54	0,74	1,26	1,58	butyrophilin, subfamily 3, member A1
KPNA4	U93240	1,37	1,40	0,55	0,63	karyopherin alpha 4 (importin alpha 3)
JARID1B	W02593	0,61	0,57	1,50	1,39	za51e06.r1 Soares fetal liver spleen 1NFLS Homo sapiens cDNA clone IMAGE:296098 5', mRNA sequence.
RGS10	W19676	0,61	1,46	1,23	0,77	zb36h07.r1 Soares_parathyroid_tumor_NbHPA Homo sapiens cDNA clone IMAGE:305725 5', mRNA sequence.
TTC4	W22690	1,34	1,32	0,66	0,68	71G4 Human retina cDNA Tsp509I-cleaved sublibrary Homo sapiens cDNA not directional
HNRPD	W74620	0,72	0,60	1,51	1,28	heterogeneous nuclear ribonucleoprotein D (AU-rich element RNA binding protein 1, 37kDa)
	W85912	0,67	0,81	1,50	1,19	Clone 23872 mRNA sequence
HF1	X04697	0,60	0,73	1,31	1,27	H factor 1 (complement)
SPN	X52075	1,18	1,09	0,11	0,91	Human gene for sialophorin (CD43).
HFL1	X56210	0,64	0,43	1,36	1,65	H factor (complement)-like 1
RAP1GDS1	X63465	1,36	1,43	0,62	0,64	RAP1, GTP-GDP dissociation stimulator 1
PLEKHC1	Z24725	1,54	1,27	0,73	0,68	pleckstrin homology domain containing, family C (with FERM domain) member 1

Tab. A-3 Complete list of 182 genes which differed at least twofold in their mRNA levels in proliferating and/or confluent cells (VH6-TE>ns vs. VH6-TE>si). Gene lists were compiled with the GeneSpring GX software from expression data obtained with an Affymetric GeneChip Human Genome U133A 2.0 microarray. Genes are sorted alphabetically according to their accession numbers.

Gene ID	Accession number	Norm. signal intensity				Gene name
		40%		100%		
		ns	si	ns	si	
TRIM22	AA083478	0,46	1,05	0,95	2,58	tripartite motif-containing 22
KCTD12	AA551075	0,38	0,85	1,15	2,83	potassium channel tetramerisation domain containing 12
	AA731709	0,35	0,15	3,33	1,28	Similar to seven transmembrane helix receptor (LOC401428), mRNA
CALCB	AA747379	0,99	2,06	0,37	1,01	calcitonin-related polypeptide, beta
FBXW3	AA845710	1,36	0,64	1,37	0,23	breakpoint cluster region
IGSF3	AB007935	1,03	0,07	2,15	0,97	immunoglobulin superfamily, member 3
MLLT4	AB016898	0,58	0,12	5,70	1,42	myeloid/lymphoid or mixed-lineage leukemia (trithorax homolog, Drosophila); translocated to, 4
KIAA0746	AB018289	0,90	2,64	0,44	1,10	KIAA0746 protein
GARNL1	AB020691	0,84	1,74	0,39	1,16	GTPase activating RANGAP domain-like 1
SORCS3	AB028982	1,88	0,21	1,15	0,19	VPS10 domain receptor protein SORCS 3
PPM1H	AB032983	2,08	0,36	1,64	0,19	ras homolog gene family, member C like 1
B3GALT3	AB050855	1,97	0,66	1,34	0,28	UDP-Gal:betaGlcNAc beta 1,3-galactosyltransferase, polypeptide 3
ZMYND10	AC002481	0,21	1,67	0,33	2,36	
CXCL11	AF002985	0,10	1,74	0,60	1,40	chemokine (C-X-C motif) ligand 11
PDE4D	AF012074	2,87	1,25	0,75	0,05	phosphodiesterase 4D, cAMP-specific (phosphodiesterase E3 dunce homolog, Drosophila)
SLC24A1	AF026132	0,19	1,70	0,30	1,96	solute carrier family 24 (sodium/potassium/calcium exchanger), member 1
CXCL11	AF030514	0,52	1,72	0,30	1,48	chemokine (C-X-C motif) ligand 11
OLR1	AF035776	2,33	0,78	1,22	0,52	oxidised low density lipoprotein (lectin-like) receptor 1
ZNF257	AF070651	1,74	0,13	1,53	0,47	zinc finger protein 257
IGSF4	AF132811	1,28	0,43	2,26	0,72	immunoglobulin superfamily, member 4
LIMK1	AF134379	1,70	0,69	1,31	0,59	LIM domain kinase 1
SERPINB13	AF169949	1,25	2,71	0,04	0,75	serine (or cysteine) proteinase inhibitor, clade B (ovalbumin), member 13
ABAT	AF237813	0,92	0,15	2,51	0,38	4-aminobutyrate aminotransferase
ATP6AP2	AF248966	0,58	1,83	0,57	1,42	ATPase, H+ transporting, lysosomal accessory protein 2
MT1H	AF333388	0,77	2,36	0,36	1,24	MT-1H-like protein; mutant as compared to wild-type sequence MT-1H in GenBank Accession Number X64834; Homo sapiens metallothionein 1H-like protein mRNA, complete cds.
KMO	AI074145	0,73	2,07	0,37	1,27	kynurenine 3-monooxygenase (kynurenine 3-hydroxylase)
HOXA9	AI246769	2,18	0,64	1,36	0,55	homeo box A9
FLJ12895	AI375002	1,59	0,41	2,22	0,09	hypothetical protein FLJ12895
MGC52019	AI733515	0,19	3,36	0,06	1,39	hypothetical protein MGC52019
ZFP276	AI983201	0,31	2,40	0,12	1,70	Fanconi anemia, complementation group A
GK	AJ252550	0,41	1,18	0,82	1,88	
	AK000185	2,74	0,34	1,66	0,26	CDNA FLJ20178 fis, clone COL09990
ZNF236	AK000847	1,36	3,95	0,22	0,64	zinc finger protein 236
FLJ25476	AK021842	0,85	0,09	2,40	1,15	FLJ25476 protein
PROSC	AK021923	0,31	1,37	0,65	1,35	proline synthetase co-transcribed homolog (bacterial)
NEU3	AK022450	0,21	1,25	0,75	1,72	sialidase 3 (membrane sialidase)
SBNO1	AK024128	0,63	1,37	0,48	2,00	sno, strawberry notch homolog 1 (Drosophila)
	AK024527	0,89	2,17	0,21	1,11	Homo sapiens cDNA: FLJ20874 fis, clone ADKA02818.
	AK025206	1,94	0,73	1,27	0,53	Homo sapiens cDNA: FLJ21553 fis, clone COL06329.
AUTS2	AK025298	1,35	0,11	1,45	0,65	autism susceptibility candidate 2

USP53	AK025301	1,32	0,25	1,82	0,68	ubiquitin specific protease 53
TP53I11	AK026607	1,05	0,44	6,75	0,95	tumor protein p53 inducible protein 11
LOC159110	AK026667	1,17	0,36	2,16	0,49	LOC389919 (LOC389919), mRNA
LAMA4	AK027151	0,66	1,68	0,45	1,34	laminin, alpha 4
UNC93A	AL021331	0,26	3,19	0,10	0,96	
	AL038824	0,11	1,88	0,40	1,60	CDNA FLJ44891 fis, clone BRAMY2044686
	AL049233	0,13	1,77	0,66	1,34	MRNA; cDNA DKFZp564A023 (from clone DKFZp564A023)
FLJ13236	AL049983	1,06	0,45	1,81	0,56	Homo sapiens mRNA; cDNA DKFZp564D042 (from clone DKFZp564D042).
	AL050335	0,59	1,71	0,37	1,41	
	AL080315	1,67	0,22	1,66	0,34	
LOC283687	AL109714	1,37	0,45	1,59	0,63	hypothetical protein LOC283687
SRPUL	AL110206	0,93	2,75	0,40	1,08	sushi-repeat protein
ANKRD26	AL137351	1,63	0,75	1,25	0,58	ankyrin repeat domain 26
SLC25A30	AL359557	0,05	2,33	0,44	1,56	hypothetical protein LOC253512
RGS4	AL514445	2,08	1,03	0,97	0,39	AL514445 Homo sapiens NEUROBLASTOMA Homo sapiens cDNA clone CL0BB010ZF08 3-PRIME, mRNA sequence.
IGSF4	AL519710	1,77	0,22	3,50	0,23	immunoglobulin superfamily, member 4
MGC8685	AL533838	0,84	0,21	3,39	1,16	tubulin, beta polypeptide paralog
PI4KII	AL561930	0,87	2,30	0,25	1,13	phosphatidylinositol 4-kinase type II
PKNOX1	AP001748	1,09	0,26	1,90	0,92	
TCF12	AU146580	2,81	0,46	1,54	0,16	transcription factor 12 (HTF4, helix-loop-helix transcription factors 4)
	AU147800	2,07	0,88	1,12	0,16	AU147800 MAMMA1 Homo sapiens cDNA clone MAMMA1001745 3', mRNA sequence.
LOC161291	AV691491	1,81	0,32	1,69	0,17	hypothetical protein LOC161291
GPLD1	AV699786	1,68	0,07	0,59	0,05	glycosylphosphatidylinositol specific phospholipase D1
IGFBP5	AW007532	1,29	0,33	2,26	0,71	ws52h07.x1 NCI_CGAP_Brn25 Homo sapiens cDNA clone IMAGE:2500861 3', mRNA sequence.
PRKCM	AW085172	0,52	2,13	0,06	1,48	protein kinase C, mu
RPLP2	AW149827	0,86	3,34	0,41	1,14	xf42g03.x1 NCI_CGAP_Brn50 Homo sapiens cDNA clone IMAGE:2620756 3' similar to contains Alu repetitive element;, mRNA sequence.
PIP3-E	AW166711	4,47	0,56	1,44	0,47	Transcribed sequences
REPS1	AW166925	1,13	0,49	1,98	0,88	RALBP1 associated Eps domain containing 1
IMAGE:4215339	AW182303	1,96	0,67	1,33	0,55	hypothetical protein IMAGE:4215339
CLCN7	AW190208	1,01	2,39	0,45	0,99	chloride channel 7
FAM38B	AW269818	0,92	0,39	2,42	1,08	hypothetical protein FLJ23403
HIPK3	AW291829	0,66	2,12	0,19	1,34	homeodomain interacting protein kinase 3
CYB561	BC000021	1,13	0,46	2,16	0,87	cytochrome b-561
SPOCK3	BC000460	4,33	0,15	0,77	0,27	sparc/osteonectin, cwcv and kazal-like domains proteoglycan (testican) 3
HPCA	BC001777	0,39	1,73	0,39	1,61	hippocalcin
XRCC4	BC005259	0,39	1,63	0,13	1,61	X-ray repair complementing defective repair in Chinese hamster cells 4
ZNF339	BC006148	0,33	1,26	0,74	2,46	zinc finger protein 339
	BE046461	0,56	1,44	0,54	1,50	Clone 24628 mRNA sequence
DOCK9	BE259050	2,21	0,32	1,68	0,25	dedicator of cytokinesis 9
	BE892698	1,35	0,65	1,60	0,46	CDNA FLJ16360 fis, clone THYMU2028942, moderately similar to ZINC FINGER PROTEIN 132
YT521	BF592058	1,34	0,62	1,66	0,66	splicing factor YT521-B
SOS2	BF692958	1,64	0,19	2,63	0,36	son of sevenless homolog 2 (Drosophila)
FLJ21687	BG413572	0,30	0,08	2,69	0,51	PDZ domain containing, X chromosome
CENTB2	D26069	1,78	0,05	1,39	0,61	centaurin, beta 2
PTGER3	D38298	0,24	1,90	0,63	1,37	prostaglandin E receptor 3 (subtype EP3)
SLC5A5	D87920	0,74	1,76	0,51	1,26	solute carrier family 5 (sodium iodide symporter), member 5

FLJ13910	H65865	1,74	0,61	1,39	0,20	hypothetical protein FLJ13910
LCP1	J02923	1,69	0,52	1,44	0,56	lymphocyte cytosolic protein 1 (L-plastin)
EDN1	J05008	3,37	1,38	0,62	0,11	Homo sapiens endothelin-1 (EDN1) gene, complete cds.
	M14087	3,46	0,98	1,02	0,16	beta-galactoside-binding lectin; Human HL14 gene encoding beta-galactoside-binding lectin, 3' end, clone 2.
TGFB2	M19154	2,71	0,91	1,09	0,48	
POLR2A	M21610	0,77	0,19	1,99	0,28	polymerase (RNA) II (DNA directed) polypeptide A, 220kDa
ANXA2P1	M62895	0,57	1,16	0,84	2,01	Human lipocortin (LIP) 2 pseudogene mRNA, complete cds-like region.
IGFBP5	M65062	1,46	0,58	1,35	0,65	insulin-like growth factor binding protein 5
CEACAM1	M69176	0,38	3,84	0,14	1,62	
KIAA0339	N30342	0,68	1,53	0,37	1,32	KIAA0339 gene product
KAL1	NM_000216	1,30	0,50	2,18	0,71	Kallmann syndrome 1 sequence
IL10	NM_000572	0,16	4,04	0,08	0,18	interleukin 10
GNRH1	NM_000825	0,79	0,02	2,79	1,21	gonadotropin-releasing hormone 1 (leutinizing-releasing hormone)
GRM1	NM_000838	1,15	0,44	2,03	0,08	glutamate receptor, metabotropic 1
DAZL	NM_001351	0,66	1,76	0,14	1,35	deleted in azoospermia-like
IL12RB2	NM_001559	3,18	0,93	1,07	0,21	interleukin 12 receptor, beta 2
ACRV1	NM_001612	0,84	3,28	0,57	1,16	acrosomal vesicle protein 1
ACTG2	NM_001615	2,22	0,41	1,59	0,27	actin, gamma 2, smooth muscle, enteric
CPA3	NM_001870	1,61	0,39	3,77	0,13	carboxypeptidase A3 (mast cell)
EPIM	NM_001980	1,50	0,51	1,54	0,15	epimorphin
KCNK1	NM_002245	1,27	0,26	3,11	0,73	potassium channel, subfamily K, member 1
KRTHB1	NM_002281	5,77	0,68	1,32	0,14	keratin, hair, basic, 1
MX1	NM_002462	0,65	1,35	0,58	2,36	myxovirus (influenza virus) resistance 1, interferon-inducible protein p78 (mouse)
MX2	NM_002463	0,42	1,27	0,74	1,57	myxovirus (influenza virus) resistance 2 (mouse)
NTRK3	NM_002530	0,40	1,35	0,65	2,42	neurotrophic tyrosine kinase, receptor, type 3
OAS1	NM_002534	0,08	1,37	0,63	3,55	2',5'-oligoadenylate synthetase 1, 40/46kDa
PAP	NM_002580	0,23	2,16	0,36	1,64	pancreatitis-associated protein
PCDH7	NM_002589	0,16	1,26	0,74	1,50	BH-protocadherin (brain-heart)
SOX4	NM_003107	1,05	0,10	1,99	0,95	SRY (sex determining region Y)-box 4
DNALI1	NM_003462	0,18	1,13	0,88	2,15	dynein, axonemal, light intermediate polypeptide 1
CHN2	NM_004067	0,83	1,90	0,04	1,17	chimerin (chimaerin) 2
KIF1A	NM_004321	0,32	3,29	0,16	1,50	kinesin family member 1A
DACH1	NM_004392	0,12	0,53	1,47	3,37	dachshund homolog (Drosophila)
KCNQ3	NM_004519	2,81	0,69	1,32	0,17	potassium voltage-gated channel, KQT-like subfamily, member 3
PKP2	NM_004572	1,92	0,78	1,22	0,47	plakophilin 2
DCAMKL1	NM_004734	1,85	0,15	1,92	0,04	doublecortin and CaM kinase-like 1
EBI2	NM_004951	0,91	0,11	2,59	1,10	Epstein-Barr virus induced gene 2 (lymphocyte-specific G protein-coupled receptor)
KIF5A	NM_004984	2,73	0,24	1,76	0,19	kinesin family member 5A
KRAS2	NM_004985	2,44	0,61	1,38	0,62	v-Ki-ras2 Kirsten rat sarcoma 2 viral oncogene homolog
TPD52	NM_005079	1,36	0,64	1,80	0,12	tumor protein D52
SLC17A4	NM_005495	2,82	1,28	0,72	0,20	solute carrier family 17 (sodium phosphate), member 4
HFL3	NM_005666	0,29	1,16	0,84	1,86	H factor (complement)-like 3
TLR6	NM_006068	1,45	0,39	1,55	0,55	toll-like receptor 6
PRKAA2	NM_006252	0,25	1,04	0,96	2,04	protein kinase, AMP-activated, alpha 2 catalytic subunit
C1orf29	NM_006820	0,42	0,98	1,02	3,72	chromosome 1 open reading frame 29
SOX12	NM_006943	0,52	1,48	0,52	1,53	SRY (sex determining region Y)-box 12
DELGEF	NM_012139	0,37	1,35	0,65	1,38	deafness locus associated putative guanine nucleotide exchange factor
EDG7	NM_012152	0,96	2,15	0,52	1,04	endothelial differentiation, lysophosphatidic acid G-protein-coupled receptor, 7
SLCO3A1	NM_013272	1,50	0,50	1,91	0,15	solute carrier organic anion transporter family, member 3A1

YPEL1	NM_013313	0,77	0,21	4,12	1,24	yippee-like 1 (Drosophila)
IGSF4	NM_014333	1,58	0,37	3,25	0,42	immunoglobulin superfamily, member 4
BMP10	NM_014482	0,69	4,68	0,29	1,21	bone morphogenetic protein 10
GREB1	NM_014668	0,50	0,10	1,12	0,20	GREB1 protein
RIPX	NM_014961	1,37	0,63	1,39	0,63	rap2 interacting protein x
KLK13	NM_015596	1,10	0,33	2,02	0,90	kallikrein 13
MYO15A	NM_016239	0,57	2,78	0,20	1,43	myosin XVA
ATP8A2	NM_016529	0,75	1,62	0,31	1,25	ATPase, aminophospholipid transporter-like, Class I, type 8A, member 2
OAS1	NM_016816	0,53	1,27	0,73	3,68	2',5'-oligoadenylate synthetase 1, 40/46kDa
SIX2	NM_016932	1,83	0,24	1,34	0,66	sine oculis homeobox homolog 2 (Drosophila)
PARD6A	NM_016948	0,40	1,38	0,65	1,35	par-6 partitioning defective 6 homolog alpha (C.elegans)
BCMO1	NM_017429	0,17	3,22	0,18	0,80	beta-carotene 15,15'-monooxygenase 1
HSXIAPAF1	NM_017523	0,15	1,38	0,62	1,77	synonym: XAF1; isoform 1 is encoded by transcript variant 1; go_function: zinc ion binding [goid 0008270] [evidence IEA]; Homo sapiens XIAP associated factor-1 (HSXIAPAF1), transcript variant 1, mRNA.
HSAJ2425	NM_017532	0,34	0,95	1,05	3,13	
FLJ20694	NM_017928	0,64	2,28	0,07	1,36	hypothetical protein FLJ20694
MLSTD1	NM_018099	1,37	0,20	1,44	0,63	male sterility domain containing 1
THEDC1	NM_018324	1,39	0,36	1,35	0,65	hypothetical protein FLJ11106
SLCO4C1	NM_018515	0,44	2,05	0,64	1,36	synonyms: OATPX, OATP-H, OATP-M1, OATP4C1, PRO2176, SLC21A20; Homo sapiens solute carrier organic anion transporter family, member 4C1 (SLCO4C1), mRNA.
SLC16A10	NM_018593	1,56	0,25	1,50	0,50	solute carrier family 16 (monocarboxylic acid transporters), member 10
A2BP1	NM_018723	1,95	0,74	1,26	0,35	ataxin 2-binding protein 1
C8orf4	NM_020130	1,91	0,46	1,42	0,58	chromosome 8 open reading frame 4
SBZF3	NM_020394	0,95	2,30	0,19	1,05	zinc finger protein SBZF3
FXYD2	NM_021603	1,99	0,87	1,13	0,38	FXYD domain containing ion transport regulator 2
JUP	NM_021991	1,33	0,19	3,58	0,67	junction plakoglobin
FLJ14011	NM_022103	0,37	0,14	3,86	0,97	hypothetical zinc finger protein FLJ14011
FLJ12895	NM_023926	1,45	0,28	1,66	0,55	hypothetical protein FLJ12895
MS4A4A	NM_024021	1,53	0,55	1,45	0,04	membrane-spanning 4-domains, subfamily A, member 4
GDAP1L1	NM_024034	0,52	3,48	0,27	1,48	ganglioside-induced differentiation-associated protein 1-like 1
FLJ11588	NM_024603	3,76	0,24	0,32	0,13	hypothetical protein FLJ11588
C6orf103	NM_024694	0,22	2,84	0,38	1,34	
FLJ13840	NM_024746	0,76	3,49	0,18	1,25	hypothetical protein FLJ13840
FLJ14075	NM_024894	1,08	2,16	0,40	0,92	hypothetical protein FLJ14075
FLJ23235	NM_024943	2,73	0,16	0,90	0,27	hypothetical protein FLJ23235
	NM_024964	0,51	1,49	0,05	1,72	
FLJ11996	NM_024976	0,36	2,76	0,12	1,19	
AMOTL2	NM_025017	2,95	0,11	1,58	0,42	
CXXC4	NM_025212	2,32	0,59	1,41	0,56	CXXC finger 4
CNOT4	R64001	1,72	0,75	1,25	0,12	CCR4-NOT transcription complex, subunit 4
IGFBP5	R73554	1,56	0,71	1,29	0,60	insulin-like growth factor binding protein 5
BIRC4	U32974	0,76	1,69	0,49	1,24	baculoviral IAP repeat-containing 4
FABP3	U72237	0,47	1,53	0,26	3,65	fatty acid-binding protein; Homo sapiens fatty acid-binding protein (FABP3-ps) pseudogene, complete cds.
JAG1	U73936	3,33	0,77	1,23	0,57	jagged 1 (Alagille syndrome)
GLRA3	U93917	0,28	2,20	0,12	1,72	glycine receptor, alpha 3
GYG2	U94357	1,30	0,18	3,04	0,70	glycogenin 2
PTPRC	Y00062	0,74	0,36	3,23	1,26	protein tyrosine phosphatase, receptor type, C
STK3	Z25422	1,88	0,82	1,18	0,38	serine/threonine kinase 3 (STE20 homolog, yeast)
DYRK1A	Z25423	0,20	1,46	0,54	1,68	dual-specificity tyrosine-(Y)-phosphorylation regulated kinase 1A

6.5. Lebenslauf

Lars Hofmann
Geb. 12.03.1976 in Aschaffenburg/ M.
Ledig, 1 Kind

Berufliche Laufbahn	
seit 01 / 2007	Wissenschaftl. Außendienst bei Clontech/ Takara Bio Europe
Akademische Ausbildung	
2006	Fortbildungskurse bei der ATV GmbH, Würzburg o Betriebswirtschaftslehre und Management o Marketing- und Vertriebsmanagement
2002– 2006	Promotion am Rudolf-Virchow-Zentrum für experimentelle Biomedizin, Würzburg (Graduiertenkolleg Life Sciences, Schule Biomedizin) Thema: „Role of the p53-homolog p73 in the malignant transformation“
11 / 2002	Diplomprüfung (Note: gut)
2000 – 2001	Akademisches Jahr als Austauschstudent an der State University of New York at Albany, NY (USA) Dort Anfertigung der Diplomarbeit: „Role of the lysosomes in the methotrexate resistance of a breast cancer cell line“
10 / 1998	Vordiplomprüfung (Note: gut)
1996 – 2002	Studium Biologie (Dipl.) an der Julius-Maximilians-Universität Würzburg
Wehr- oder Zivildienst	
1995 – 1996	Zivildienst beim Sozialdienst für Personen mit besonderen Schwierigkeiten von Caritas und Diakonie, Offenbach/ M.
Schulbildung	
06 / 1995	Abitur (Durchschnittsnote: 1,9)
1986 – 1995	Franziskaner-Gymnasium Kreuzburg, Großkrotzenburg

6.6. Own publications

Marshall LA, Rhee MS, **Hofmann L**, Khodjakov A, Schneider E: "Increased lysosomal uptake of methotrexate polyglutamates in two methotrexate-resistant cell lines with distinct mechanisms of resistance". 2005. Biochem Pharmacol. 71(1-2): 203-213.

Hofmann L, Beinoraviciute-Kellner R, Stiewe T: "p73: ein Protein auf der Gratwanderung zwischen Tumorsuppressor und Onkogen" [German]. 2005. Bioforum 28(10): 74-75.

Hüttinger N, Cam H, Griesmann H, **Hofmann L**, Beitzinger M, Schmauser B, Stiewe T: "The p53 family inhibitor ΔNp73 interferes with multiple developmental programs". 2005. Cell Death Differ 13: 174-177.

Cam H, Griesmann H, **Hofmann L**, Hüttinger-Kirchhof N, Oswald C, Friedl P, Gattenlöhner S, Burek C, Rosenwald A, Stiewe T: "p53 family members in myogenic differentiation and rhabdomyosarcoma development". 2006. Cancer Cell 10: 281-293.

Pütz S, **Hofmann L**, Stiewe T, Sickmann A: "Differential 2D-PAGE of four different fibroblast cell lines containing the genetic elements hTERT, SV40 ER and H-rasV12". 2007. Manuscript in prep.

Beitzinger M, **Hofmann L**, Bretz AC, Sauer M, Burek C, Rosenwald A, Stiewe T: “p73 poses a barrier to malignant transformation by limiting anchorage-independent growth”. 2007. Submitted.

7. References

Agami R, Blandino G, Oren M, Shaul Y. 1999. Interaction of c-Abl and p73alpha and their collaboration to induce apoptosis. Nature 399(6738):809-813.

Ali SH, DeCaprio JA. 2001. Cellular transformation by SV40 large T antigen: interaction with host proteins. Semin Cancer Biol 11(1):15-23.

Argilla D, Chin K, Singh M, Hodgson JG, Bosenberg M, de Solorzano CO, Lockett S, DePinho RA, Gray J, Hanahan D. 2004. Absence of telomerase and shortened telomeres have minimal effects on skin and pancreatic carcinogenesis elicited by viral oncogenes. Cancer Cell 6(4):373-385.

Attard G, Greystoke A, Kaye S, De Bono J. 2006. Update on tubulin-binding agents. Pathol Biol (Paris) 54(2):72-84.

Balmain A. 2001. Cancer genetics: from Boveri and Mendel to microarrays. Nat Rev Cancer 1(1):77-82.

Balmain A. 2002. Cancer as a complex genetic trait: tumor susceptibility in humans and mouse models. Cell 108(2):145-152.

Balmain A, Gray J, Ponder B. 2003. The genetics and genomics of cancer. Nat Genet 33 Suppl:238-244.

Bell LA, Ryan KM. 2004. Life and death decisions by E2F-1. Cell Death Differ 11(2):137-142.

Bergamaschi D, Gasco M, Hiller L, Sullivan A, Syed N, Trigiante G, Yulug I, Merlano M, Numico G, Comino A, Attard M, Reelfs O, Gusterson B, Bell AK, Heath V, Tavassoli M, Farrell PJ, Smith P, Lu X, Crook T. 2003. p53 polymorphism influences response in cancer chemotherapy via modulation of p73-dependent apoptosis. Cancer Cell 3(4):387-402.

Berns A, van Lohuizen M, Verbeek S, Domen J, Saris C. 1991. Transgenic mice as a model system to study synergism between oncogenes. In: Brugge J, Curran T, Harlow E, McCormick F, editors. Origins of Human Cancers: A Comprehensive Review. Plainview, NY: Cold Spring Harbor Laboratory Press. p 791-801.

Blackburn EH. 2001. Switching and signaling at the telomere. Cell 106(6):661-673.

Blair DG, Cooper CS, Oskarsson MK, Eader LA, Vande Woude GF. 1982. New method for detecting cellular transforming genes. Science 218(4577):1122-1125.

Bodnar AG, Ouellette M, Frolkis M, Holt SE, Chiu CP, Morin GB, Harley CB, Shay JW, Lichtsteiner S, Wright WE. 1998. Extension of life-span by introduction of telomerase into normal human cells. Science 279(5349):349-352.

Bos JL. 1989. ras oncogenes in human cancer: a review. Cancer Res 49(17):4682-4689.

Boveri T. 1914. Zur Frage der Entstehung maligner Tumoren. Jena: Gustav Fischer.

Boyle P. 1999. Cancer epidemiology. In: Pollock RE, editor. Manual of clinical oncology. 7th ed. New York: Wiley-Liss.

Bradford MM. 1976. A rapid and sensitive method for the quantitation of microgram quantities of protein utilizing the principle of protein-dye binding. Anal Biochem 72:248-254.

Brookes S, Rowe J, Ruas M, Llanos S, Clark PA, Lomax M, James MC, Vatcheva R, Bates S, Vousden KH, Parry D, Gruis N, Smit N, Bergman W, Peters G. 2002. INK4a-deficient human diploid fibroblasts are resistant to RAS-induced senescence. Embo J 21(12):2936-2945.

Bryan TM, Englezou A, Dalla-Pozza L, Dunham MA, Reddel RR. 1997. Evidence for an alternative mechanism for maintaining telomere length in human tumors and tumor-derived cell lines. Nat Med 3(11):1271-1274.

Campbell KS, Mullane KP, Aksoy IA, Stubdal H, Zalvide J, Pipas JM, Silver PA, Roberts TM, Schaffhausen BS, DeCaprio JA. 1997. DnaJ/hsp40 chaperone domain of SV40 large T antigen promotes efficient viral DNA replication. Genes Dev 11(9):1098-1110.

Casciano I, Mazzocco K, Boni L, Pagnan G, Banelli B, Allemanni G, Ponzoni M, Tonini GP, Romani M. 2002. Expression of DeltaNp73 is a molecular marker for adverse outcome in neuroblastoma patients. Cell Death Differ 9(3):246-251.

Cerone MA, Autexier C, Londono-Vallejo JA, Bacchetti S. 2005. A human cell line that maintains telomeres in the absence of telomerase and of key markers of ALT. Oncogene 24(53):7893-7901.

Chen W, Arroyo JD, Timmons JC, Possemato R, Hahn WC. 2005. Cancer-associated PP2A Aalpha subunits induce functional haploinsufficiency and tumorigenicity. Cancer Res 65(18):8183-8192.

Chen W, Possemato R, Campbell KT, Plattner CA, Pallas DC, Hahn WC. 2004. Identification of specific PP2A complexes involved in human cell transformation. Cancer Cell 5(2):127-136.

Cho US, Morrone S, Sablina AA, Arroyo JD, Hahn WC, Xu W. 2007. Structural basis of PP2A inhibition by small t antigen. PLoS Biol 5(8):e202.

Concin N, Becker K, Slade N, Erster S, Mueller-Holzner E, Ulmer H, Daxenbichler G, Zeimet A, Zeillinger R, Marth C, Moll UM. 2004. Transdominant DeltaTAp73 isoforms are frequently up-regulated in ovarian cancer. Evidence for their role as epigenetic p53 inhibitors in vivo. Cancer Res 64(7):2449-2460.

Concin N, Hofstetter G, Berger A, Gehmacher A, Reimer D, Watrowski R, Tong D, Schuster E, Hefler L, Heim K, Mueller-Holzner E, Marth C, Moll UM, Zeimet AG, Zeillinger R. 2005. Clinical relevance of dominant-

negative p73 isoforms for responsiveness to chemotherapy and survival in ovarian cancer: evidence for a crucial p53-p73 cross-talk in vivo. Clin Cancer Res 11(23):8372-8383.
Conzen SD, Cole CN. 1995. The three transforming regions of SV40 T antigen are required for immortalization of primary mouse embryo fibroblasts. Oncogene 11(11):2295-2302.
Conzen SD, Snay CA, Cole CN. 1997. Identification of a novel antiapoptotic functional domain in simian virus 40 large T antigen. J Virol 71(6):4536-4543.
Cordenonsi M, Dupont S, Maretto S, Insinga A, Imbriano C, Piccolo S. 2003. Links between tumor suppressors: p53 is required for TGF-beta gene responses by cooperating with Smads. Cell 113(3):301-314.
Costanzo A, Merlo P, Pediconi N, Fulco M, Sartorelli V, Cole PA, Fontemaggi G, Fanciulli M, Schiltz L, Blandino G, Balsano C, Levrero M. 2002. DNA damage-dependent acetylation of p73 dictates the selective activation of apoptotic target genes. Mol Cell 9(1):175-186.
Counter CM, Hahn WC, Wei W, Caddle SD, Beijersbergen RL, Lansdorp PM, Sedivy JM, Weinberg RA. 1998. Dissociation among in vitro telomerase activity, telomere maintenance, and cellular immortalization. Proc Natl Acad Sci U S A 95(25):14723-14728.
Das S, El-Deiry WS, Somasundaram K. 2003. Efficient growth inhibition of HPV 16 E6-expressing cells by an adenovirus-expressing p53 homologue p73beta. Oncogene 22(52):8394-8402.
Davis PK, Dowdy SF. 2001. p73. Int J Biochem Cell Biol 33(10):935-939.
Dimri GP, Lee X, Basile G, Acosta M, Scott G, Roskelley C, Medrano EE, Linskens M, Rubelj I, Pereira-Smith O, et al. 1995. A biomarker that identifies senescent human cells in culture and in aging skin in vivo. Proc Natl Acad Sci U S A 92(20):9363-9367.
Ding Y, Inoue T, Kamiyama J, Tamura Y, Ohtani-Fujita N, Igata E, Sakai T. 1999. Molecular cloning and functional characterization of the upstream promoter region of the human p73 gene. DNA Res 6(5):347-351.
Dix D. 1989. The role of aging in cancer incidence: an epidemiological study. J Gerontol 44(6):10-18.
Dobbelstein M, Roth J. 1998. The large T antigen of simian virus 40 binds and inactivates p53 but not p73. J Gen Virol 79 (Pt 12):3079-3083.
Dobbelstein M, Strano S, Roth J, Blandino G. 2005. p73-induced apoptosis: a question of compartments and cooperation. Biochem Biophys Res Commun 331(3):688-693.
Donehower LA, Harvey M, Slagle BL, McArthur MJ, Montgomery CA, Jr., Butel JS, Bradley A. 1992. Mice deficient for p53 are developmentally normal but susceptible to spontaneous tumours. Nature 356(6366):215-221.
Downward J. 2003. Targeting RAS signalling pathways in cancer therapy. Nat Rev Cancer 3(1):11-22.
Dupont S, Zacchigna L, Adorno M, Soligo S, Volpin D, Piccolo S, Cordenonsi M. 2004. Convergence of p53 and TGF-beta signaling networks. Cancer Lett 213(2):129-138.
Eckner R, Ludlow JW, Lill NL, Oldread E, Arany Z, Modjtahedi N, DeCaprio JA, Livingston DM, Morgan JA. 1996. Association of p300 and CBP with simian virus 40 large T antigen. Mol Cell Biol 16(7):3454-3464.
Elenbaas B, Spirio L, Koerner F, Fleming MD, Zimonjic DB, Donaher JL, Popescu NC, Hahn WC, Weinberg RA. 2001. Human breast cancer cells generated by oncogenic transformation of primary mammary epithelial cells. Genes Dev 15(1):50-65.
Fasano O, Birnbaum D, Edlund L, Fogh J, Wigler M. 1984. New human transforming genes detected by a tumorigenicity assay. Mol Cell Biol 4(9):1695-1705.
Fearon ER, Vogelstein B. 1990. A genetic model for colorectal tumorigenesis. Cell 61(5):759-767.
Flinterman M, Guelen L, Ezzati-Nik S, Killick R, Melino G, Tominaga K, Mymryk JS, Gaken J, Tavassoli M. 2005. E1A activates transcription of p73 and Noxa to induce apoptosis. J Biol Chem 280(7):5945-5959.
Flores ER, Sengupta S, Miller JB, Newman JJ, Bronson R, Crowley D, Yang A, McKeon F, Jacks T. 2005. Tumor predisposition in mice mutant for p63 and p73: evidence for broader tumor suppressor functions for the p53 family. Cancer Cell 7(4):363-373.
Flores ER, Tsai KY, Crowley D, Sengupta S, Yang A, McKeon F, Jacks T. 2002. p63 and p73 are required for p53-dependent apoptosis in response to DNA damage. Nature 416(6880):560-564.
Fontemaggi G, Kela I, Amariglio N, Rechavi G, Krishnamurthy J, Strano S, Sacchi A, Givol D, Blandino G. 2002. Identification of direct p73 target genes combining DNA microarray and chromatin immunoprecipitation analyses. J Biol Chem 277(45):43359-43368.
Fridman JS, Lowe SW. 2003. Control of apoptosis by p53. Oncogene 22(56):9030-9040.
Gewirtz DA. 1999. A critical evaluation of the mechanisms of action proposed for the antitumor effects of the anthracycline antibiotics adriamycin and daunorubicin. Biochem Pharmacol 57(7):727-741.
Goldstein S. 1990. Replicative senescence: the human fibroblast comes of age. Science 249(4973):1129-1133.
Gong JG, Costanzo A, Yang HQ, Melino G, Kaelin WG, Jr., Levrero M, Wang JY. 1999. The tyrosine kinase c-Abl regulates p73 in apoptotic response to cisplatin-induced DNA damage. Nature 399(6738):806-809.
Granger MP, Wright WE, Shay JW. 2002. Telomerase in cancer and aging. Crit Rev Oncol Hematol 41(1):29-40.
Hahn WC, Counter CM, Lundberg AS, Beijersbergen RL, Brooks MW, Weinberg RA. 1999. Creation of human tumour cells with defined genetic elements. Nature 400(6743):464-468.

Hahn WC, Dessain SK, Brooks MW, King JE, Elenbaas B, Sabatini DM, DeCaprio JA, Weinberg RA. 2002. Enumeration of the simian virus 40 early region elements necessary for human cell transformation. Mol Cell Biol 22(7):2111-2123.

Hahn WC, Weinberg RA. 2002a. Modelling the molecular circuitry of cancer. Nat Rev Cancer 2(5):331-341.

Hahn WC, Weinberg RA. 2002b. Rules for making human tumor cells. N Engl J Med 347(20):1593-1603.

Hamad NM, Elconin JH, Karnoub AE, Bai W, Rich JN, Abraham RT, Der CJ, Counter CM. 2002. Distinct requirements for Ras oncogenesis in human versus mouse cells. Genes Dev 16(16):2045-2057.

Hanahan D, Weinberg RA. 2000. The hallmarks of cancer. Cell 100(1):57-70.

Harbour JW, Luo RX, Dei Santi A, Postigo AA, Dean DC. 1999. Cdk phosphorylation triggers sequential intramolecular interactions that progressively block Rb functions as cells move through G1. Cell 98(6):859-869.

Harrington L, Zhou W, McPhail T, Oulton R, Yeung DS, Mar V, Bass MB, Robinson MO. 1997. Human telomerase contains evolutionarily conserved catalytic and structural subunits. Genes Dev 11(23):3109-3115.

Harris KF, Christensen JB, Radany EH, Imperiale MJ. 1998. Novel mechanisms of E2F induction by BK virus large-T antigen: requirement of both the pRb-binding and the J domains. Mol Cell Biol 18(3):1746-1756.

Higashino F, Pipas JM, Shenk T. 1998. Adenovirus E4orf6 oncoprotein modulates the function of the p53-related protein, p73. Proc Natl Acad Sci U S A 95(26):15683-15687.

Hingorani SR, Tuveson DA. 2003. Ras redux: rethinking how and where Ras acts. Curr Opin Genet Dev 13(1):6-13

Irwin M, Marin MC, Phillips AC, Seelan RS, Smith DI, Liu W, Flores ER, Tsai KY, Jacks T, Vousden KH, Kaelin WG, Jr. 2000. Role for the p53 homologue p73 in E2F-1-induced apoptosis. Nature 407(6804):645-648.

Irwin MS, Kaelin WG. 2001a. p53 family update: p73 and p63 develop their own identities. Cell Growth Differ 12(7):337-349.

Irwin MS, Kaelin WG, Jr. 2001b. Role of the newer p53 family proteins in malignancy. Apoptosis 6(1-2):17-29.

Irwin MS, Kondo K, Marin MC, Cheng LS, Hahn WC, Kaelin WG, Jr. 2003. Chemosensitivity linked to p73 function. Cancer Cell 3(4):403-410.

Jat PS, Cepko CL, Mulligan RC, Sharp PA. 1986. Recombinant retroviruses encoding simian virus 40 large T antigen and polyomavirus large and middle T antigens. Mol Cell Biol 6(4):1204-1217.

Jiang XR, Jimenez G, Chang E, Frolkis M, Kusler B, Sage M, Beeche M, Bodnar AG, Wahl GM, Tlsty TD, Chiu CP. 1999. Telomerase expression in human somatic cells does not induce changes associated with a transformed phenotype. Nat Genet 21(1):111-114.

Johnstone RW, Ruefli AA, Lowe SW. 2002. Apoptosis: a link between cancer genetics and chemotherapy. Cell 108(2):153-164.

Joneson T, White MA, Wigler MH, Bar-Sagi D. 1996. Stimulation of membrane ruffling and MAP kinase activation by distinct effectors of RAS. Science 271(5250):810-812.

Kaghad M, Bonnet H, Yang A, Creancier L, Biscan JC, Valent A, Minty A, Chalon P, Lelias JM, Dumont X, Ferrara P, McKeon F, Caput D. 1997. Monoallelically expressed gene related to p53 at 1p36, a region frequently deleted in neuroblastoma and other human cancers. Cell 90(4):809-819.

Kamijo T, Zindy F, Roussel MF, Quelle DE, Downing JR, Ashmun RA, Grosveld G, Sherr CJ. 1997. Tumor suppression at the mouse INK4a locus mediated by the alternative reading frame product p19ARF. Cell 91(5):649-659.

Kim NW, Piatyszek MA, Prowse KR, Harley CB, West MD, Ho PL, Coviello GM, Wright WE, Weinrich SL, Shay JW. 1994. Specific association of human telomerase activity with immortal cells and cancer. Science 266(5193):2011-2015.

Kim NW, Wu F. 1997. Advances in quantification and characterization of telomerase activity by the telomeric repeat amplification protocol (TRAP). Nucleic Acids Res 25(13):2595-2597.

Kipling D, Cooke HJ. 1990. Hypervariable ultra-long telomeres in mice. Nature 347(6291):400-402.

Knudson AG. 2001. Two genetic hits (more or less) to cancer. Nat Rev Cancer 1(2):157-162.

Knudson AG, Jr. 1971. Mutation and cancer: statistical study of retinoblastoma. Proc Natl Acad Sci U S A 68(4):820-823.

Knudson AG, Jr. 1983. Model hereditary cancers of man. Prog Nucleic Acid Res Mol Biol 29:17-25.

Knudson AG, Jr. 1985. Hereditary cancer, oncogenes, and antioncogenes. Cancer Res 45(4):1437-1443.

Kojima T, Ikawa Y, Katoh I. 2001. Analysis of molecular interactions of the p53-family p51(p63) gene products in a yeast two-hybrid system: homotypic and heterotypic interactions and association with p53-regulatory factors. Biochem Biophys Res Commun 281(5):1170-1175.

Komarova NL, Wodarz D. 2004. The optimal rate of chromosome loss for the inactivation of tumor suppressor genes in cancer. Proc Natl Acad Sci U S A 101(18):7017-7021.

Kovalev S, Marchenko N, Swendeman S, LaQuaglia M, Moll UM. 1998. Expression level, allelic origin, and mutation analysis of the p73 gene in neuroblastoma tumors and cell lines. Cell Growth Differ 9(11):897-903.

Kranenburg O, Gebbink MF, Voest EE. 2004. Stimulation of angiogenesis by Ras proteins. Biochim Biophys Acta 1654(1):23-37.

LaMontagne KR, Jr., Moses MA, Wiederschain D, Mahajan S, Holden J, Ghazizadeh H, Frank DA, Arbiser JL. 2000. Inhibition of MAP kinase kinase causes morphological reversion and dissociation between soft agar growth and in vivo tumorigenesis in angiosarcoma cells. Am J Pathol 157(6):1937-1945.

Land H, Parada LF, Weinberg RA. 1983. Tumorigenic conversion of primary embryo fibroblasts requires at least two cooperating oncogenes. Nature 304(5927):596-602.

Lane DP, Crawford LV. 1979. T antigen is bound to a host protein in SV40-transformed cells. Nature 278(5701):261-263.

Lau LM, Nugent JK, Zhao X, Irwin MS. 2007. HDM2 antagonist Nutlin-3 disrupts p73-HDM2 binding and enhances p73 function. Oncogene.

Lee C, Cho Y. 2002. Interactions of SV40 large T antigen and other viral proteins with retinoblastoma tumour suppressor. Rev Med Virol 12(2):81-92.

Lee CW, La Thangue NB. 1999. Promoter specificity and stability control of the p53-related protein p73. Oncogene 18(29):4171-4181.

Lesage F, Guillemare E, Fink M, Duprat F, Lazdunski M, Romey G, Barhanin J. 1996a. TWIK-1, a ubiquitous human weakly inward rectifying K+ channel with a novel structure. Embo J 15(5):1004-1011.

Lesage F, Lazdunski M. 2000. Molecular and functional properties of two-pore-domain potassium channels. Am J Physiol Renal Physiol 279(5):F793-801.

Lesage F, Mattei M, Fink M, Barhanin J, Lazdunski M. 1996b. Assignment of the human weak inward rectifier K+ channel TWIK-1 gene to chromosome 1q42-q43. Genomics 34(1):153-155.

Lieberman MA, Glaser L. 1981. Density-dependent regulation of cell growth: an example of a cell-cell recognition phenomenon. J Membr Biol 63(1-2):1-11.

Lill NL, Tevethia MJ, Eckner R, Livingston DM, Modjtahedi N. 1997. p300 family members associate with the carboxyl terminus of simian virus 40 large tumor antigen. J Virol 71(1):129-137.

Lin WC, Lin FT, Nevins JR. 2001. Selective induction of E2F1 in response to DNA damage, mediated by ATM-dependent phosphorylation. Genes Dev 15(14):1833-1844.

Linzer DI, Levine AJ. 1979. Characterization of a 54K dalton cellular SV40 tumor antigen present in SV40-transformed cells and uninfected embryonal carcinoma cells. Cell 17(1):43-52.

Lowe SW, Cepero E, Evan G. 2004. Intrinsic tumour suppression. Nature 432(7015):307-315.

Lowe SW, Ruley HE. 1993. Stabilization of the p53 tumor suppressor is induced by adenovirus 5 E1A and accompanies apoptosis. Genes Dev 7(4):535-545.

Malumbres M, Barbacid M. 2003. RAS oncogenes: the first 30 years. Nat Rev Cancer 3(6):459-465.

Marabese M, Vikhanskaya F, Rainelli C, Sakai T, Broggini M. 2003. DNA damage induces transcriptional activation of p73 by removing C-EBPalpha repression on E2F1. Nucleic Acids Res 31(22):6624-6632.

Marin MC, Jost CA, Irwin MS, DeCaprio JA, Caput D, Kaelin WG, Jr. 1998. Viral oncoproteins discriminate between p53 and the p53 homolog p73. Mol Cell Biol 18(11):6316-6324.

Martinez-Balbas MA, Bauer UM, Nielsen SJ, Brehm A, Kouzarides T. 2000. Regulation of E2F1 activity by acetylation. Embo J 19(4):662-671.

Masutomi K, Hahn WC. 2003. Telomerase and tumorigenesis. Cancer Lett 194(2):163-172.

McManus MT, Petersen CP, Haines BB, Chen J, Sharp PA. 2002. Gene silencing using micro-RNA designed hairpins. Rna 8(6):842-850.

Meerson A, Milyavsky M, Rotter V. 2004. p53 mediates density-dependent growth arrest. FEBS Lett 559(1-3):152-158.

Melino G, De Laurenzi V, Vousden KH. 2002. p73: Friend or foe in tumorigenesis. Nat Rev Cancer 2(8):605-615.

Menard S, Casalini P, Campiglio M, Pupa S, Agresti R, Tagliabue E. 2001. HER2 overexpression in various tumor types, focussing on its relationship to the development of invasive breast cancer. Ann Oncol 12 Suppl 1:S15-19.

Metz T, Harris AW, Adams JM. 1995. Absence of p53 allows direct immortalization of hematopoietic cells by the myc and raf oncogenes. Cell 82(1):29-36.

Meyerson M, Counter CM, Eaton EN, Ellisen LW, Steiner P, Caddle SD, Ziaugra L, Beijersbergen RL, Davidoff MJ, Liu Q, Bacchetti S, Haber DA, Weinberg RA. 1997. hEST2, the putative human telomerase catalytic subunit gene, is up-regulated in tumor cells and during immortalization. Cell 90(4):785-795.

Miller AD, Chen F. 1996. Retrovirus packaging cells based on 10A1 murine leukemia virus for production of vectors that use multiple receptors for cell entry. J Virol 70(8):5564-5571.

Mills AA. 2006. p63: oncogene or tumor suppressor? Curr Opin Genet Dev 16(1):38-44.

Mills AA, Zheng B, Wang XJ, Vogel H, Roop DR, Bradley A. 1999. p63 is a p53 homologue required for limb and epidermal morphogenesis. Nature 398(6729):708-713.

Millward TA, Zolnierowicz S, Hemmings BA. 1999. Regulation of protein kinase cascades by protein phosphatase 2A. Trends Biochem Sci 24(5):186-191.

Mitchell PJ, Perez-Nadales E, Malcolm DS, Lloyd AC. 2003. Dissecting the contribution of p16(INK4A) and the Rb family to the Ras transformed phenotype. Mol Cell Biol 23(7):2530-2542.

Moens U, Seternes OM, Johansen B, Rekvig OP. 1997. Mechanisms of transcriptional regulation of cellular genes by SV40 large T- and small T-antigens. Virus Genes 15(2):135-154.

Morales CP, Holt SE, Ouellette M, Kaur KJ, Yan Y, Wilson KS, White MA, Wright WE, Shay JW. 1999. Absence of cancer-associated changes in human fibroblasts immortalized with telomerase. Nat Genet 21(1):115-118.

Morgenstern JP, Land H. 1990. Advanced mammalian gene transfer: high titre retroviral vectors with multiple drug selection markers and a complementary helper-free packaging cell line. Nucleic Acids Res 18(12):3587-3596.

Morgunkova AA. 2005. The p53 Gene Family: Control of Cell Proliferation and Developmental Programs. Biochemistry (Mosc) 70(9):955-971.

Muller M, Schilling T, Sayan AE, Kairat A, Lorenz K, Schulze-Bergkamen H, Oren M, Koch A, Tannapfel A, Stremmel W, Melino G, Krammer PH. 2005. TAp73/DeltaNp73 influences apoptotic response, chemosensitivity and prognosis in hepatocellular carcinoma. Cell Death Differ.

Murakami Y. 2005. Involvement of a cell adhesion molecule, TSLC1/IGSF4, in human oncogenesis. Cancer Sci 96(9):543-552.

Nakamura TM, Morin GB, Chapman KB, Weinrich SL, Andrews WH, Lingner J, Harley CB, Cech TR. 1997. Telomerase catalytic subunit homologs from fission yeast and human. Science 277(5328):955-959.

Obad S, Brunnstrom H, Vallon-Christersson J, Borg A, Drott K, Gullberg U. 2004. Staf50 is a novel p53 target gene conferring reduced clonogenic growth of leukemic U-937 cells. Oncogene 23(23):4050-4059.

Osada M, Ohba M, Kawahara C, Ishioka C, Kanamaru R, Katoh I, Ikawa Y, Nimura Y, Nakagawara A, Obinata M, Ikawa S. 1998. Cloning and functional analysis of human p51, which structurally and functionally resembles p53. Nat Med 4(7):839-843.

Ozaki T, Nakagawara A. 2005. p73, a sophisticated p53 family member in the cancer world. Cancer Sci 96(11):729-737.

Pediconi N, Ianari A, Costanzo A, Belloni L, Gallo R, Cimino L, Porcellini A, Screpanti I, Balsano C, Alesse E, Gulino A, Levrero M. 2003. Differential regulation of E2F1 apoptotic target genes in response to DNA damage. Nat Cell Biol 5(6):552-558.

Peto R, Roe FJ, Lee PN, Levy L, Clack J. 1975. Cancer and ageing in mice and men. Br J Cancer 32(4):411-426.

Petrenko O, Zaika A, Moll UM. 2003. deltaNp73 facilitates cell immortalization and cooperates with oncogenic Ras in cellular transformation in vivo. Mol Cell Biol 23(16):5540-5555.

Phillips AC, Vousden KH. 2001. E2F-1 induced apoptosis. Apoptosis 6(3):173-182.

Prowse KR, Greider CW. 1995. Developmental and tissue-specific regulation of mouse telomerase and telomere length. Proc Natl Acad Sci U S A 92(11):4818-4822.

Radloff R, Bauer W, Vinograd J. 1967. A dye-buoyant-density method for the detection and isolation of closed circular duplex DNA: the closed circular DNA in HeLa cells. Proc Natl Acad Sci U S A 57(5):1514-1521.

Ramadan S, Terrinoni A, Catani MV, Sayan AE, Knight RA, Mueller M, Krammer PH, Melino G, Candi E. 2005. p73 induces apoptosis by different mechanisms. Biochem Biophys Res Commun 331(3):713-717.

Rangarajan A, Hong SJ, Gifford A, Weinberg RA. 2004. Species- and cell type-specific requirements for cellular transformation. Cancer Cell 6(2):171-183.

Rangarajan A, Weinberg RA. 2003. Opinion: Comparative biology of mouse versus human cells: modelling human cancer in mice. Nat Rev Cancer 3(12):952-959.

Reichelt M, Zang KD, Seifert M, Welter C, Ruffing T. 1999. The yeast two-hybrid system reveals no interaction between p73 alpha and SV40 large T-antigen. Arch Virol 144(3):621-626.

Rhim JS. 2000. Development of human cell lines from multiple organs. Ann N Y Acad Sci 919:16-25.

Rodicker F, Stiewe T, Zimmermann S, Putzer BM. 2001. Therapeutic efficacy of E2F1 in pancreatic cancer correlates with TP73 induction. Cancer Res 61(19):7052-7055.

Rodriguez-Viciana P, Warne PH, Khwaja A, Marte BM, Pappin D, Das P, Waterfield MD, Ridley A, Downward J. 1997. Role of phosphoinositide 3-OH kinase in cell transformation and control of the actin cytoskeleton by Ras. Cell 89(3):457-467.

Rossi M, De Laurenzi V, Munarriz E, Green DR, Liu YC, Vousden KH, Cesareni G, Melino G. 2005. The ubiquitin-protein ligase Itch regulates p73 stability. Embo J 24(4):836-848.

Roth J, Dobbelstein M. 1999. Failure of viral oncoproteins to target the p53-homologue p51A. J Gen Virol 80 (Pt 12):3251-3255.

Rundell K, Parakati R. 2001. The role of the SV40 ST antigen in cell growth promotion and transformation. Semin Cancer Biol 11(1):5-13.

Rundquist I. 1993. Equilibrium binding of DAPI and 7-aminoactinomycin D to chromatin of cultured cells. Cytometry 14(6):610-617.

Saenz-Robles MT, Sullivan CS, Pipas JM. 2001. Transforming functions of Simian Virus 40. Oncogene 20(54):7899-7907.

Saupe S, Roizes G, Peter M, Boyle S, Gardiner K, De Sario A. 1998. Molecular cloning of a human cDNA IGSF3 encoding an immunoglobulin-like membrane protein: expression and mapping to chromosome band 1p13. Genomics 52(3):305-311.

Sawai ET, Butel JS. 1989. Association of a cellular heat shock protein with simian virus 40 large T antigen in transformed cells. J Virol 63(9):3961-3973.

Scheffzek K, Lautwein A, Scherer A, Franken S, Wittinghofer A. 1997. Crystallization and preliminary X-ray crystallographic study of the Ras-GTPase-activating domain of human p120GAP. Proteins 27(2):315-318.

Schmale H, Bamberger C. 1997. A novel protein with strong homology to the tumor suppressor p53. Oncogene 15(11):1363-1367.

Seelan RS, Irwin M, van der Stoop P, Qian C, Kaelin WG, Jr., Liu W. 2002. The human p73 promoter: characterization and identification of functional E2F binding sites. Neoplasia 4(3):195-203.

Seger YR, Garci, a-Cao M, Piccinin S, Cunsolo CL, Doglioni C, Blasco MA, Hannon GJ, Maestro R. 2002. Transformation of normal human cells in the absence of telomerase activation. Cancer Cell 2(5):401-413.

Senoo M, Manis JP, Alt FW, McKeon F. 2004. p63 and p73 are not required for the development and p53-dependent apoptosis of T cells. Cancer Cell 6(1):85-89.

Serrano M, Lin AW, McCurrach ME, Beach D, Lowe SW. 1997. Oncogenic ras provokes premature cell senescence associated with accumulation of p53 and p16INK4a. Cell 88(5):593-602.

Shapiro GS, Van Peursem C, Ornelles DA, Schaack J, DeGregori J. 2006. Recombinant adenoviral vectors can induce expression of p73 via the E4-orf6/7 protein. J Virol 80(11):5349-5360.

Shay JW, Wright WE. 1989. Quantitation of the frequency of immortalization of normal human diploid fibroblasts by SV40 large T-antigen. Exp Cell Res 184(1):109-118.

Sherr CJ. 2004. Principles of tumor suppression. Cell 116(2):235-246.

Shields JM, Pruitt K, McFall A, Shaub A, Der CJ. 2000. Understanding Ras: 'it ain't over 'til it's over'. Trends Cell Biol 10(4):147-154.

Shimodaira H, Yoshioka-Yamashita A, Kolodner RD, Wang JY. 2003. Interaction of mismatch repair protein PMS2 and the p53-related transcription factor p73 in apoptosis response to cisplatin. Proc Natl Acad Sci U S A 100(5):2420-2425.

Skinner J, Bounacer A, Bond JA, Haughton MF, deMicco C, Wynford-Thomas D. 2004. Opposing effects of mutant ras oncoprotein on human fibroblast and epithelial cell proliferation: implications for models of human tumorigenesis. Oncogene 23(35):5994-5999.

Sonoda Y, Ozawa T, Aldape KD, Deen DF, Berger MS, Pieper RO. 2001. Akt pathway activation converts anaplastic astrocytoma to glioblastoma multiforme in a human astrocyte model of glioma. Cancer Res 61(18):6674-6678.

Sporn MB. 1996. The war on cancer. Lancet 347(9012):1377-1381.

Srinivasan A, McClellan AJ, Vartikar J, Marks I, Cantalupo P, Li Y, Whyte P, Rundell K, Brodsky JL, Pipas JM. 1997. The amino-terminal transforming region of simian virus 40 large T and small t antigens functions as a J domain. Mol Cell Biol 17(8):4761-4773.

Stanelle J, Stiewe T, Rodicker F, Kohler K, Theseling C, Putzer BM. 2003. Mechanism of E2F1-induced apoptosis in primary vascular smooth muscle cells. Cardiovasc Res 59(2):512-519.

Steegenga WT, Shvarts A, Riteco N, Bos JL, Jochemsen AG. 1999. Distinct regulation of p53 and p73 activity by adenovirus E1A, E1B, and E4orf6 proteins. Mol Cell Biol 19(5):3885-3894.

Stiewe T, Putzer BM. 2000. Role of the p53-homologue p73 in E2F1-induced apoptosis. Nat Genet 26(4):464-469.

Stiewe T, Putzer BM. 2001. p73 in apoptosis. Apoptosis 6(6):447-452.

Stiewe T, Putzer BM. 2002. Role of p73 in malignancy: tumor suppressor or oncogene? Cell Death Differ 9(3):237-245.

Stiewe T, Theseling CC, Putzer BM. 2002a. Transactivation-deficient Delta TA-p73 inhibits p53 by direct competition for DNA binding: implications for tumorigenesis. J Biol Chem 277(16):14177-14185.

Stiewe T, Tuve S, Peter M, Tannapfel A, Elmaagacli AH, Putzer BM. 2004. Quantitative TP73 transcript analysis in hepatocellular carcinomas. Clin Cancer Res 10(2):626-633.

Stiewe T, Zimmermann S, Frilling A, Esche H, Putzer BM. 2002b. Transactivation-deficient DeltaTA-p73 acts as an oncogene. Cancer Res 62(13):3598-3602.

Strano S, Monti O, Pediconi N, Baccarini A, Fontemaggi G, Lapi E, Mantovani F, Damalas A, Citro G, Sacchi A, Del Sal G, Levrero M, Blandino G. 2005. The transcriptional coactivator Yes-associated protein drives p73 gene-target specificity in response to DNA Damage. Mol Cell 18(4):447-459.

Sullivan CS, Cantalupo P, Pipas JM. 2000. The molecular chaperone activity of simian virus 40 large T antigen is required to disrupt Rb-E2F family complexes by an ATP-dependent mechanism. Mol Cell Biol 20(17):6233-6243.

Tuve S, Racek T, Niemetz A, Schultz J, Soengas MS, Putzer BM. 2006. Adenovirus-mediated TA-p73beta gene transfer increases chemosensitivity of human malignant melanomas. Apoptosis 11(2):235-243.

Tuveson DA, Shaw AT, Willis NA, Silver DP, Jackson EL, Chang S, Mercer KL, Grochow R, Hock H, Crowley D, Hingorani SR, Zaks T, King C, Jacobetz MA, Wang L, Bronson RT, Orkin SH, DePinho RA, Jacks T. 2004. Endogenous oncogenic K-ras(G12D) stimulates proliferation and widespread neoplastic and developmental defects. Cancer Cell 5(4):375-387.

Vasseur S, Malicet C, Calvo EL, Labrie C, Berthezene P, Dagorn JC, Iovanna JL. 2003. Gene expression profiling by DNA microarray analysis in mouse embryonic fibroblasts transformed by rasV12 mutated protein and the E1A oncogene. Mol Cancer 2(1):19.

Vogelstein B, Fearon ER, Hamilton SR, Kern SE, Preisinger AC, Leppert M, Nakamura Y, White R, Smits AM, Bos JL. 1988. Genetic alterations during colorectal-tumor development. N Engl J Med 319(9):525-532.

Vogelstein B, Lane D, Levine AJ. 2000. Surfing the p53 network. Nature 408(6810):307-310.

Waltermann A, Kartasheva NN, Dobbelstein M. 2003. Differential regulation of p63 and p73 expression. Oncogene 22(36):5686-5693.

Waring MJ. 1966. Structural requirements for the binding of ethidium to nucleic acids. Biochim Biophys Acta 114(2):234-244.

Waterhouse PM, Wang MB, Lough T. 2001. Gene silencing as an adaptive defence against viruses. Nature 411(6839):834-842.

Wege H, Chui MS, Le HT, Tran JM, Zern MA. 2003. SYBR Green real-time telomeric repeat amplification protocol for the rapid quantification of telomerase activity. Nucleic Acids Res 31(2):E3-3.

Weinberg RA. 1991. Oncogenes, tumor suppressor genes, and cell transformation: trying to put it all together. In: Brugge J, Curran T, Harlow E, McCormick F, editors. Origins of Human Cancers: A Comprehensive Review. Plainview, NY: Cold Spring Harbor Laboratory Press. p 1-16.

Weinberg RA. 1997. The cat and mouse games that genes, viruses, and cells play. Cell 88(5):573-575.

Wienzek S, Roth J, Dobbelstein M. 2000. E1B 55-kilodalton oncoproteins of adenovirus types 5 and 12 inactivate and relocalize p53, but not p51 or p73, and cooperate with E4orf6 proteins to destabilize p53. J Virol 74(1):193-202.

Yaciuk P, Carter MC, Pipas JM, Moran E. 1991. Simian virus 40 large-T antigen expresses a biological activity complementary to the p300-associated transforming function of the adenovirus E1A gene products. Mol Cell Biol 11(4):2116-2124.

Yamada D, Yoshida M, Williams YN, Fukami T, Kikuchi S, Masuda M, Maruyama T, Ohta T, Nakae D, Maekawa A, Kitamura T, Murakami Y. 2006. Disruption of spermatogenic cell adhesion and male infertility in mice lacking TSLC1/IGSF4, an immunoglobulin superfamily cell adhesion molecule. Mol Cell Biol 26(9):3610-3624.

Yang A, Kaghad M, Caput D, McKeon F. 2002. On the shoulders of giants: p63, p73 and the rise of p53. Trends Genet 18(2):90-95.

Yang A, Kaghad M, Wang Y, Gillett E, Fleming MD, Dotsch V, Andrews NC, Caput D, McKeon F. 1998. p63, a p53 homolog at 3q27-29, encodes multiple products with transactivating, death-inducing, and dominant-negative activities. Mol Cell 2(3):305-316.

Yang A, Schweitzer R, Sun D, Kaghad M, Walker N, Bronson RT, Tabin C, Sharpe A, Caput D, Crum C, McKeon F. 1999. p63 is essential for regenerative proliferation in limb, craniofacial and epithelial development. Nature 398(6729):714-718.

Yang A, Walker N, Bronson R, Kaghad M, Oosterwegel M, Bonnin J, Vagner C, Bonnet H, Dikkes P, Sharpe A, McKeon F, Caput D. 2000. p73-deficient mice have neurological, pheromonal and inflammatory defects but lack spontaneous tumours. Nature 404(6773):99-103.

Zaika A, Irwin M, Sansome C, Moll UM. 2001. Oncogenes induce and activate endogenous p73 protein. J Biol Chem 276(14):11310-11316.

Zaika AI, Kovalev S, Marchenko ND, Moll UM. 1999. Overexpression of the wild type p73 gene in breast cancer tissues and cell lines. Cancer Res 59(13):3257-3263.

Zaika AI, Slade N, Erster SH, Sansome C, Joseph TW, Pearl M, Chalas E, Moll UM. 2002. DeltaNp73, a dominant-negative inhibitor of wild-type p53 and TAp73, is up-regulated in human tumors. J Exp Med 196(6):765-780.

Zalvide J, Stubdal H, DeCaprio JA. 1998. The J domain of simian virus 40 large T antigen is required to functionally inactivate RB family proteins. Mol Cell Biol 18(3):1408-1415.

Zerrahn J, Knippschild U, Winkler T, Deppert W. 1993. Independent expression of the transforming amino-terminal domain of SV40 large I antigen from an alternatively spliced third SV40 early mRNA. Embo J 12(12):4739-4746.

Zhao JJ, Roberts TM, Hahn WC. 2004. Functional genetics and experimental models of human cancer. Trends Mol Med 10(7):344-350.

Zhu J, Jiang J, Zhou W, Chen X. 1998. The potential tumor suppressor p73 differentially regulates cellular p53 target genes. Cancer Res 58(22):5061-5065.

Zhu J, Rice PW, Gorsch L, Abate M, Cole CN. 1992. Transformation of a continuous rat embryo fibroblast cell line requires three separate domains of simian virus 40 large T antigen. J Virol 66(5):2780-2791.